Current Awareness Bulletin

of

SCHOLARLY ARTICLES PUBLISHED BY

Faculty, Students and Alumni

~ January 2013 ~

DELHI TECHNOLOGICAL UNIVERSITY CENTRAL LIBRARY
(formerly Delhi College of Engineering, Bawana Road, DELHI)

PREFACE

This is the First Issue of Current Awareness Bulletin for the year 2013, started by Delhi Technological University Library. The aim of the bulletin is to compile, preserve and disseminate information published by the Faculty, Students and Alumni for mutual benefits. The bulletin also aims to propagate the intellectual contribution of DTU as a whole to the academia. It contains information resources available in the internet in the form of articles, reports, presentation published in international journals, websites, etc. by the faculty and students of Delhi Technological University in the field of science and technology. The publication of Faculty and Students, which are not covered in this bulletin, may be because of the reason that the full text either was not accessible or could not be searched by the search engine used by the library for this purpose. To make the bulletin more comprehensive, the learned faculty and Students may provide their uncovered publication to the library either through email or in CD, etc.

This issue contains the information published during January 2013. The arrangement of the contents is alphabetical wise starting from A-Z. The Full text of the article, which is either subscribed by the University or available in the web, is provided in this Bulletin.

CONTENTS

13. Shear Strength Parameters for Silty-Sand Using Relative Compaction by ***@Sadanand Ojha*** and ****AshutoshTrivedi***.

14. SPV based water pumping system for an academic institution by ***Majid Jamil, Ahmed Sharique Anees*** and ****M. Rizwan***.

15. Subpixel Target Enhancement in Hyperspectral Images by *Manoj K. Arora* and ****K.C. Tiwari***.

16. Synthesis and characterization of nanocrystalline ferroelectric Sr0.8Bi2.2Ta2O9 by conventional and microwave sintering: A comparative study by ****Sugandha*** and **A. K. Jha*.

17. SynthesisandcharacterizationofnovelK2La2 xEuxTi3O10 phosphor for blue chip white LEDs by *Bhaskar Kumar Grandhe, Vengala Rao Bandi* , **** M Jayasimhadri*** , Kiwan Jang , *Ho-Sueb Lee , Dong-Soo Shin , Soung-Soo Yi , Jung-Hyun Jeong.*

18. Voltage mode OTRA MOS-C Single Input Multi Output Biquadratic Universal Filter by ***@Rajeshwari Pandey, @Neeta Pandey***, *Sajal Kumar Paul,* ***@Ajay Singh, @Balamurali Sriram and@, Kaushlendra Trivedi***.

*****	**Faculty**
@	**Students/Research Scholars**
#	**Alumni**

pISSN 1976-913X
eISSN 2092-805X

J Inf Process Syst, Vol.8, No.4, December 2012 http://dx.doi.org/10.3745/JIPS.2012.8.4.621

A Comparative Study of Estimation by Analogy using Data Mining Techniques

Geeta Nagpal*, Moin Uddin** and Arvinder Kaur***

Abstract—Software Estimations provide an inclusive set of directives for software project developers, project managers, and the management in order to produce more realistic estimates based on deficient, uncertain, and noisy data. A range of estimation models are being explored in the industry, as well as in academia, for research purposes but choosing the best model is quite intricate. Estimation by Analogy (EbA) is a form of case based reasoning, which uses fuzzy logic, grey system theory or machine-learning techniques, etc. for optimization. This research compares the estimation accuracy of some conventional data mining models with a hybrid model. Different data mining models are under consideration, including linear regression models like the ordinary least square and ridge regression, and nonlinear models like neural networks, support vector machines, and multivariate adaptive regression splines, etc. A precise and comprehensible predictive model based on the integration of GRA and regression has been introduced and compared. Empirical results have shown that regression when used with GRA gives outstanding results; indicating that the methodology has great potential and can be used as a candidate approach for software effort estimation.

Keywords—Software Estimations, Estimation by Analogy, Grey Relational Analysis, Robust Regression, Data Mining Techniques

1. INTRODUCTION

Software development is a creative process where each person's efficiency is different. It is difficult to plan and estimate at the beginning as most software projects have deficient information and vague associations amongst effort drivers and the required effort. Software developers and researchers are using different methods and are more concerned about accurately predicting the effort of the software product being developed. Even a small enhancement in the prediction accuracy and validity are highly valued by researchers and software developers. During the last couple of years, research on software effort estimation has drifted from formal methods like Cocomo, Cocomo II, Function point and SLIM to Estimation by Analogy (E*b*A). In E*b*A, the effort required to develop a new software project requires the gathering of the particulars of the desired project. The particulars are then compared to a past project from the dataset having approximately the same specifications, but the challenge is the inconsistency in the struc-

※ The authors would like to thank the Promise Repository for providing such valuable datasets for our being able to carry out our research work

Manuscript received April 20, 2012; first revision July 4, 2012; accepted October 8, 2012.

Corresponding Author: Geeta Nagpal

* Dept. of Computer Science and Engineering, National Institute of Technology, Jalandhar (sikkag@gmail.com)

** Delhi Technological University, Delhi , India (prof_moin@yahoo.com)

*** University School of IT, Gurugobind Singh Indraprastha University, Delhi, India (arvinderkaurtakkar@yahoo.com)

ture of the datasets used and in the feature set classification. The motivation behind E*b*A is that comparable software projects have similar costs.

E*b*A methods range from machine learning methods, regression techniques, the Grey System Theory (GST), and soft computing methods to a combination of these. GST is a recently developed system engineering theory that was first established by Deng in 1982 [1-3]. It draws out valuable information by generating and developing the partially known information. It has been applied in different areas of image processing [4], mobile communication [5], machine vision inspection [6], decision making [7], stock price prediction [8], and system control [9]. Some of the research carried out using E*b*A has been discussed. Mukhopadhyay et al. [10] developed ESTOR, which is a CBR tool to estimate project effort. The metrics used by ESTOR are the function point components and inputs to the intermediate COCOMO model. Shepperd et al. [11], developed ANGEL, which is a tool that supports the collection, storage, and identification of the most analogous projects, in order to estimate the effort for a new project. ANGEL uses Euclidean distance as the similarity metric in n dimensional space. Angelis et al. [12] uses a statistical simulation modus operandi to improve estimation by analogy. They investigated the problem of determining the most favourable method parameter configuration before application. The ANALOGY-X [13] tool provides a sound statistical basis for analogy based estimation using the Mantel's correlation randomization test. It removes the need for heuristic search, and greatly improves the algorithmic performance of the model. Baskeles et al., in [14] propose a machine-learning based model for software effort estimation and tested it on three different data sets, namely, NASA, USC, and SoftLab Data Repository (SDR). Idri et al. [15] suggested an approach based on reasoning by analogy, fuzzy sets, and linguistic quantifiers for software effort estimation when the project is described by either categorical or numerical data. Azzeh et al. in [16] integrated an analogy-based estimation with fuzzy numbers to improve the performance of software project effort estimation during its early development stages, using all of the available early data. They proposed a new similarity measure technique based on fuzzy numbers. Shepperd et al. [17] proposed a Grey Relational Analysis based software project effort (GRACE) prediction method, including a feature subset selection. Hsu and Huang [18] integrated six different weighted measures with the GRA method, namely, non-weight, distance-based weight, correlative weight, linear weight, nonlinear weight, and maximal weight, were applied to 127 projects from the ISBSG data set. GRACE^{+}[19] addresses some of the theoretical challenges in applying GRA to outlier detection, feature subset selection, and effort prediction. In [20], Chiu et al. used genetic algorithms to optimize the analogy weights for software effort estimation. In [20], they integrated GA with GRA. Kosti et al.[21] suggested a new algorithm that initiates the notion of distance. It uses the similarity between distributions of distances instead of leaving one out cross validation to find the number of appropriate neighbours to be used for estimating the effort for new projects. AQUA [22] combines ideas from two known analogy-based estimation techniques: case-based reasoning and collaborative filtering. The method is applicable to predict efforts related to any object in the requirements, features, or project levels. In this research study, GRA, which is a technique of GST, utilizes the concept of absolute point-to-point distance between cases [17]. GRA is used to find the number of comparative projects (k) that are closest to the reference project from the total of n projects. The projects are ranked based on their Grey Relational Grade's (GRG). Regression techniques namely, the Ordinary Least Square (OLS), Robust Regression (RR) techniques and Stepwise Regression (SWR) are applied to the k most influential projects in order to estimate the effort of the reference project. The value of k varies

with each reference project. The results obtained have shown an improvement over the conventional data mining techniques and also a significant improvement over GRACE [17], GRACE^{+} [19], and FGRA [23]. A brief literature overview of the various analogy based approaches for software effort estimation is provided in Table 1. The remainder of the paper is organized as follows: Section II is a brief review of GRA and various regression techniques. Section III describes the proposed software effort prediction mechanisms using *GREAT_RM,* the validation and evaluation criteria, and the datasets used in the methodology. Section IV provides the experimental results of *GREAT_RM* and its comparison with some of the conventional data mining methods for software cost estimation along with their statistical significance. Section V provides, comparison of the results with some previously published results. Section VI presents threats to validity. The conclusion and directions for future work are presented in Section VII.

Table 1. Literature Overview of the Application of Analogy Based Approaches for Software Effort Estimation

Sr No.	Author/Year	Title	Journal/ Conference	Approach/ Technique	Datasets	Performance							Testing Mode
1.	Srinivasan K, Fisher D, (1995)[24]	Machine Learning Approaches to Estimating Software Development Efforts	***IEEE Transactions on Software Engineering***	ANN, CART	Kemerer, COCOMO-81		**MRE**	**R^2**	**Eqn**				Holdout
						CartX	364	0.83	102.5+0.075x				
						B.Prpgt	70	0.80	78.13+0.88x				
						Func pt	10.3	0.58	-37+0.96x				
						Cocomo	610	0.70	27.7+0.156x				
						Slim	772	0.89	49.9+0.082x				
2.	Shepperd N. Schofield C, (1997)[11]	Estimating Software Project Efforts Using Analogies	***IEEE Transactions on Software Engineering***	OLS, Case based reasoning	Desharnais Finnish Kemerer Mermaid Telecom	**Dataset**	**MMRE (%)**	**Reg1**	**Reg2**	**Pred (25%)**	**Reg1**	**Reg2**	Cross Validation
						Desharnais 1	37	41	41	47	45	45	
						Desharnais 2	29	29	29	47	48	48	
						Desharnais 3	26	36	49	70	30	50	
						Mermaid E	53	62	62	39	27	27	
						Mermaid N	60	--	--	25	--	--	
3.	Witting G, Finnie G., (1997)[25]	Estimating Software Development Efforts with Connectionist Models	***Information and Software Technology***	ANN	Simulated data Desharnais	**ARE**		**%**		**Cum %**			Holdout
						0-10%		40.0		40.0			
						11-25%		36.7		76.7			
						26-50%		20.0		96.7			
						>50%		3.3		100			
4	Burgess C.J., Lefley M., (2001)[26]	Can Genetic Programming Improve Software Effort Estimation? A Comparative Evaluation	***Information and Software Technology***	Genetic Algorithm	Desharnais	**Correlation**				0.752			Random
						AMSE				11.13			
						Pred(25)				4.2			
						Pred(25)%				23.3			
						MMRE				44.55			
						BMMRE				75			
5	Essam *et.al.,* (2002)[27]	Software Project Effort Estimation Using Genetic Programming	***IEEE***	Genetic Algorithm	ISBSG	**MSE**				Tr = 2.90			Random
										Ts = 5.4			
						R^2				Tr = 0.44			
										Ts = 0.40			
						MMRE				Tr = 2.67			
										Ts = 1.91			
						Pred(25%)				Tr = 0.19			
										Ts = 0.21			
						Pred(50%)				Tr = 0.39			
										Ts = 0.40			
6	Idri et al., (2002)[28]	Estimating Software Project Efforts by Analogy Based on Linguistic Values	***Eighth IEEE International Symposium on Software Metrics***	Fuzzy Analogy		**MMRE**				22.5			-
						Pred(25%)				62.14			

Table 1. <Continue>

Sr No.	Author/Year	Title	Journal/ Conference	Approach/ Technique	Datasets	Performance				Testing Mode
7	Huang X, Caretz L.F., and Ren J., (2003)[29]	A Neuro-Fuzzy Model for Software Cost Estimation	***Third International Conference on Quality Software, (QSIC'03)***	Neuro-Fuzzy, COCOMO II	COCOMO'81+ 6 industry projects.	**Pred (20%)**	86			All
						Pred(30%)	92			
8	Song Q., Shepperd M., and Carolyn M, (2005)[17]	Using Grey Relational Analysis to Predict Software Efforts with Small Data Sets	***IEEE International Software Metrics Symposium***	Analogy, Grey Relational Analysis		**MMRE**	**MdMRE**	**Pred (25)%**	**Bias**	Jack Knifing
					Albrecht	60.25	21.35	52.63	-12.13	
					NASA	32.88	28.38	46.67	17.34	
					COCOMO81	76.09	60.52	20.63	-18.89	
					Desharnais	49.83	33.93	30.00	-16.52	
					Kemerer	58.83	46.94	26.67	-7.07	
9	Bohem *et. al., (*2005)[30]	Feature Subset Selection Can Improve Software Cost Estimation Accuracy	***PROMISE'05***	Feature Subset Selection (WRAPPER), COCOMO		**Mean (Pred(30))**		**Median(Pred(30))**		Random
					COCOCMO'81	51.3		7.66		
					NASA60	81.3		7.32		
					Project04	66.7		6.92		
					Project03	55.8		15.65		
					Project02	97.1		15.16		
10	Sentas P, Angelis L, Stamelos I, (2005)[31]	Software Productivity and Effort Prediction with Ordinal Regression	***Information and Software Technology***	OLS regression, Ordinal regression	COCOMO-81, Maxwell, ISBSG R7		**MMRE**	**PRED 20**	**PRED 25**	Holdout
						Fitting accuracy for all 52 projects	33.28%	44.2%	53.8%	
						Fitting accuracy for learning dataset	34.38%	40.5%	50.0%	
						Predictive accuracy for the test data set	45.06%	30.0%	40.0%	
11	Sheta A F, A.(2006)[32]	Estimation of the COCOMO Model Parameters Using Genetic Algorithms for NASA Software Projects	***Journal of Computer Science***	Genetic Algorithm, COCOMO	NASA	**VAF**		96.31		Random
12	Auer M, Trendowicz A, Biffl S, Haunschmid E, Graser B (2006)[33]	Optimal Project Feature Weights in Analogy-Based Cost Estimation: Improvement and Limitations	***IEEE Transactions on Software Engineering***	Case base reasoning	ESA, Desharnais, DPS database, Kemerer, Albrecht	**Dataset**	**MMRE**	**Pred 25**	**VAR_r**	**MFWV**	Cross Validation
						Albrecht	15	20	21	34	
						Desharnais 44	12	11	20	43	
						Desharnais 23	13	19	23	65	
						Desharnais 10	21	20	30	18	
						ESA 29	8	7	1	58	
						ESA 13	3	4	9	29	
						Kemerer 15	2	16	3	34	
						Laturi 12	6	14	3	8	
						Laturi 11	16	25	20	27	
13	Baskeles B Turhan B Bener A, (2007)[14]	Software Effort Estimation Using Machine Learning Models	***22nd International Symposium on Computer and Information Science***	RBF, MLP, SVM, Decision Tree		**MMRE**		**Pred(30)**		-
						22.11		73.25		
						110.94		33		
						25.72		75		
						12.85		83.75		
14	Chiu N, Huang S (2007)[34]	The Adjusted Analogy-Based Software Effort Estimation Based on Similarity Distances	***The Journal of Systems and Software***	OLS regression, artificial neural network, CART, case based reasoning	DPS database, Abran	**Model**		**MMRE**		**MDMRE**		**PRED 0.25**		Cross Validation
								train	test	train	test	train	test	
						Euc Dist	AE	0.96	1.25	0.51	0.58	0.33	0.19	
							AAE	0.60	0.52	0.20	0.36	0.60	0.46	
							Imp %	38	58	61	38	82	126	
						Man Dis	AMH	1.03	1.01	0.59	0.51	0.24	0.29	
							AAMH	0.66	0.49	0.26	0.31	0.52	0.38	
							IMP %	36	52	56	39	117	31	
						Minkowski Dis	AMK	0.99	1.24	0.55	0.55	0.31	0.24	
							AAMK	0.61	0.49	0.29	0.38	0.50	0.38	
							IMP %	37	57	55	36	87	72	
						Mean imp %								

Table 1. <Continue>

Sr No.	Author/Year	Title	Journal/ Conference	Approach/ Technique	Datasets	Performance				Testing Mode
15	Keung J.W, Kitchenham A and Jeffery, D R (2008)[13]	Analogy-X: Providing Statistical Inference to Analogy-Based Software Cost Estimation	***IEEE Transaction on Software Engineering***	Analogy, Jackknife	Desharnais	**Mental' R**	0.440			All
						UCL	0.466			
16	Huang S J, Chiu N H and Chen L W, (2008)[20]	Integration of Grey Relational Analysis with Genetic Algorithm for Software Effort Estimation	***European Journal of Operational Research, Elsevier***	Grey Relational, Genetic Algorithm			**MMRE**	**Pred(0.25)**		Random
					COCOMO	Tr	0.53	0.41		
						Ts	20.69	0.38		
					Albrecht	Tr	0.37	0.49		
						Ts	0.31	0.48		
17	Kiran et.al., (2008)	Software Development Cost Estimation Using Wavelet Neural Networks	***The Journal of Systems and Software***	Wavelet Neural Network		**MMRE**	**Pred(0.25)**	**MdMRE**		Random
					Albrecht	0.121	0.708	0.177		
					Desharnais	0.198	0.666	0.163		
18	Azzeh M, Neagu D, and Cowling P, (2008)[36]	Improving Analogy Software Effort Estimation Using the Fuzzy Feature Subset Selection Algorithm	***PROMISE'08***	Feature Subset Selection, Fuzzy Algorithm		**MMRE**	**MdMRE**	**Pred(25)**		Jack Knifing
					ISBSG	28.7	21.8	54.7		
					Desharnais	40.2	32.4	39.8		
19	Azzeh M, Neagu D and Cowling P I, (2010)[23]	Fuzzy Grey Relational Analysis for Software Effort Estimation	***Empir Software Eng, Springer***	Analogy, Fuzzy Grey Relational		**MMRE**	**MdMRE**	**MMER**	**Pred(0.25)**	Jack Knifing
					ISBSG	33.3	22.0	28.6	55.2	
					Deshrnais	30.6	17.5	34.4	64.7	
					COCOMO'81	23.2	14.8	25.6	66.7	
					Kemerer	36.2	33.2	34.3	52.9	
					Albrecht	51.1	48.0	60.4	28.6	
20	Azzeh M ,.Neagu D and Cowling P I, (2010)[16]	Analogy–Based Software Effort Estimation Using Fuzzy Numbers	***The Journal of Systems and Software***	Analogy, Fuzzy Numbers		**MMRE**	**MdMRE**	**Pred(25)**		Jack Knifing
					ISBSG	28.55	17.80	59.80		
					COCOMO'81	33.37	20.36	62.33		
					Desharnais	26.89	19.32	64.94		
					Albrecht	50.08	30.75	50.00		
					Kemerer	55.65	24.24	53.33		
21	Chaudhary K, (2010)[35]	GA Based Optimization of Software Development Effort Estimation	***IJCSI***	SEL model, Walston-Felix model, COCOMO, Genetic Algorithm	**Effort**					Random
22	.Hari et. al. (2011)[37]	CPN-A Hybrid Model for Software Cost Estimation	***IEEE Explorer***	COCOMO, PSO, Neural Network	COCOMO'81	**MARE**	Tr = 19.49			Random
							Ts = 10.96			
23	Song and Shepperd et al., (2011)[19]	Predicting Software Project Effort: A Grey Relational Analysis Based Method	***Expert System with Applications***	Analogy, Fuzzy Numbers			**MMRE**	**Pred(25)**		-
					Albrecht		26.1	50		
					COCO NASA		24.2	60.3		
					COCOMO'81		49.8	29		
					Desharnais		41.4	45.3		
					Kemerer		19.6	78.6		

2. MODELING TECHNIQUES

2.1 The Grey Relational Analysis

This is comparatively a novel technique in software estimations and can be effectively used for analyzing the relationships between two series. It is a technique of the Grey Systems Theory (GST), which was introduced by Deng [1,2,3]. The term ***Grey*** lies between *Black* (meaning "no information") and *White* (meaning "full information") and it indicates that the information is partially available. It is suitable for unascertained problems with poor information. GRA has the ability to learn from a small number of cases, which is effective in the context of data-starvation [17] The magnetism of GRA is its flexibility to model a complex nonlinear relationship [18,20]. The basic concepts of GRA are as given below:

Factor space:
$\{p(X); Q\}$ is a factor space where $p(X)$ is a theme described by the factor set X, and Q as the influence relation. The factor space $\{p(X); Q\}$ has the following properties[17]:

1. Existence of key factors.
2. The number of factors is limited and countable.
3. Factor independence.
4. Factor expansibility.

Suppose $x_i = \{x_i(1), x_i(2). . . ,x_i(m)\}$, where, $i = 0, 1, 2, . . . , n \in N$; $m \in N$, is a data series.

Comparable series:
The series is *comparable* if, and only if, they are *dimensionless, scaled,* and *polarized*.

Grey relational space:
The factor space is a grey relational space if all the series in a factor space $\{p(X); Q\}$ are comparable. It is denoted as $\{p(X); \Gamma\}$. In a grey relational space $\{p(X); \Gamma\}$, X is a collection of data series $x_i (i = 0, 1, . . . , n)$, in which $x_i = \{x_i(1), x_i(2), . . . , x_i(k)\}$, is the series; and $k = 1, 2, . . . , m$, are the factors. Γ, which is the Grey Relational Map set. It is based on geometrical mathematics and has the following four properties [17]:

Normality $0 \le \Gamma(x_i(k), x_j(k)) \le 1, \forall i, \forall j, \forall k,$
$\Gamma(x_i, x_j) = 1 \Leftrightarrow x_i \equiv x_j ,$
$\Gamma(x_i, x_j) = 0 \Leftrightarrow x_i \cap x_j \in \phi.$

Symmetry $\forall x_i, \forall x_j \in X,$
$\Gamma(x_i, x_j) = \Gamma(x_j, x_i) \Leftrightarrow X = \{x_i, x_j\}.$

Entirety $\forall x_i, \forall x_j \in X = \{x\sigma | \sigma = 0, 1, . . . , n\}, n \ge 2,$
$\Gamma(x_i, x_j)$ *often* $\neq \Gamma(x_j, x_i).$

Proximity $\Gamma(x_i(k), x_j(k))$ *increases as* $\Delta(k) = |x_i(k) - x_j(k)|$ *decrease for* $\forall k \in \{1, 2, . . . , m\}.$

2.1.1 Grey Relational Grade by Deng's Method

GRA is used to measure all the influences of various features and the relationship among data series that is a collection of measurements [1-3]. The steps involved are as listed below.

Data Processing

The first step is the standardization of the various attributes. Every attribute has the same amount of influence, as the data is made dimensionless by using various techniques like upper bound effectiveness, lower bound effectiveness, or moderate effectiveness. The formulas for data processing techniques are as follows:

- Upper-bound effectiveness (i.e., the larger the better)

$$x_i^*(k) = \frac{x_i(k) - \min_i x_i(k)}{\max_i x_i(k) - \min_i x_i(k)} \tag{1}$$

where $i=1,2,...,m$ and $k=1,2,...,n$.

- Lower-bound effectiveness (i.e., the smaller the better)

$$x_i^*(k) = \frac{\max_i x_i(k) - x_i(k)}{\max_i x_i(k) - \min_i x_i(k)} \tag{2}$$

where $i=1,2,...,m$ and $k=1,2,...,n$.

- Moderate effectiveness (i.e., the nominal is the best)

$$x_i^*(k) = 1 - \frac{\left| x_i(k) - x_{ab}(k) \right|}{\max\left\{ \max_i x_i(k) - x_{ab}(k), x_{ab}(k) - \min_i x_i(k) \right\}} \tag{3}$$

where $i=1,2,...,m$ and $k=1,2,...,n$.

$x_i(k)$ represents the value of the k_{th} attribute in the i_{th} series; (k) represents the modified value of the k_{th} attribute in the i_{th} series; $max_i x_i$ represents the maximum of the k_{th} attribute in all series; $min_i x_i$ represents the minimum of the k_{th} attribute in all series, and $x_{ab}(k)$ is the objective value of the k_{th} attribute.

Difference Series

The GRA uses the grey relational coefficient to describe the trend relationship between an objective series and a reference series at a given point in a system.

$$\gamma\left(x_0(k), x_i(k)\right) = \frac{\Delta_{\min} + \zeta\Delta_{\max}}{\Delta_{o,i}(k) + \zeta\Delta_{\max}} \tag{4}$$

where $\Delta_{0,i}(k) = |x_0(k) - x_i(k)|$ is the difference of the absolute value between $x_0(k)$ and $x_i(k)$;
$\Delta_{min} = min_j min_k |x_0(k) - x_j(k)|$ is the smallest value of $\Delta_{0,j}\ \forall j \in \{1, 2, \ldots, n\}$;
$\Delta_{max} = max_j max_k |x_0(k) - x_j(k)|$ is the largest value of $\Delta_{0,j}\ \forall j \in \{1, 2, \ldots, n\}$;
and ζ is the distinguishing coefficient, $\zeta \in (0, 1]$.

The ζ value will change the magnitude of $\gamma(x_0(k), x_i(k))$. In this study the value of ζ has been taken as 0.5 Deng [23].

Grey Relational Grade

The GRG is used to find the overall similarity degree between reference tuple x_o and comparative tuple x_i. When the value of the GRG approaches 1, the two tuples are "more closely similar." When the GRG approaches a value of 0, the two tuples are "more dissimilar." The GRG $\Gamma(x_0, x_i)$ between an objective series x_i and the reference series x_0 was defined by Deng as follows:

$$\Gamma(x_0, x_i) = \frac{1}{n}\sum_{k=1}^{n} \gamma(x_0(k), x_i(k)) \tag{5}$$

2.2 Regression

Regression analysis is a statistical technique for modelling and analysing variables. It is used to study the relationship that exists between a dependent variable and one or more independent variables.

2.2.1 Ordinary Least Square Regression

It is the most popular and widely applied technique to build software cost estimation models. According to the principle of least squares the "best fitting" line is the line which minimizes the deviations of the observed data away from the line. The regression parameters for the least square line, are the estimates of the unknown regression parameters in the model. This is also referred to as multiple linear regression and is given by:

$$y_i = \beta_0 + \beta_1 x_{i,1} + ...\beta_k x_{i,k} + \varepsilon_i \tag{6}$$

where, Y_i is a dependent variable whereas $x_1, x_2, \ldots\ldots x_k$ are k independent variables. β_o is the y intercept, β_1, β_2 are the slope of y, ε_i is the error term. The corresponding prediction equation is given as:

$$\hat{y}_i = \hat{\beta}_0 + \hat{\beta}_1 x_{i,1} + ...\hat{\beta}_k x_{i,k} \tag{7}$$

In this equation $\hat{\beta}_0, \hat{\beta}_1, \ldots\ldots \hat{\beta}_k$ are the least square coefficients and $\hat{y}_i$ is the estimated response for the i^{th} term.

Thus, the response estimated from the regression line minimizes the sum of squared distances between the regression line and the observed response.

2.2.2 Robust Regression

Robust Regression is a type of regression technique, which prevails over the limitations of the ordinary least square. Ordinary least square estimates are extremely non-robust to outliers. Outliers are those observations in the dataset that do not follow the prototype of the other observations. These can inefficiently influence the whole process of fitting. In this study, we evaluated the performance of some well-known robust M-estimators. They are as follows: the "Andrew-estimator" [40], the "Bisquare-estimator," the "Cauchy-estimator," the "Fair-estimator," the "Huber-estimator" [38, 39, 43], the "Logistic-estimator," the "Talwar-estimator," and the "Welsch-estimator," etc. They have been used with their different weight functions [41] for predicting the software effort of the projects.

M-estimators are also called maximum-likelihood estimators, as they try to minimize the weighted sum of residuals. They work on the principle of the Iteratively Reweighted Least Square (IRLS). The least square method tries to minimize $\sum e_i^2$, which is unstable in case there are outliers present in the data, whereas the M-estimators try to minimize the effect of these outliers by substituting the squared residuals e_i, by the function given below.

$$\min \sum_{i=1}^{n} \rho(e_i) \tag{8}$$

The steps involved in IRLS [42] are:

Step 1: In the first iteration, each observation is allocated an equal weight and the coefficients of the model are estimated using OLS.

Step 2: In the second step, after the OLS, residuals are used to find weights. The observation with a larger residual is assigned a lower weight.

Step 3: In the third iteration, the new model parameters and the residuals are recomputed using Weighted Least Squares (WLS).

Step 4: In Step 4, new weights, as per Step 2, are found and the procedure continues until the values of the parameter estimates converge within a specified tolerance.

2.2.3 Stepwise Regression

This is a method for adding and removing terms based on their statistical importance. The forward approach starts with no variables in the model. It tries out the variables one by one and includes them if they are "statistically important." The selection has been used for estimating the effort of the reference project for various similar projects. At each step, a predictor is entered based on partial *F*-tests or *t* test. The procedure continues until more variables can be justifiably entered. The first variable that is put in the stepwise model is the variable having the smallest *t*-test *P*-value (below $\alpha_E = 0.05$). The level of significance (α) is taken to be 5%.

3. PROPOSED ALGORITHM, FOR SOFTWARE ESTIMATION

3.1 Modeling the Grey Relational Effort Analysis Technique with Regression Methods (*GREAT_RM*)

In this methodology, the focus is project selection based on GRA and effort prediction by re-

gression. In the GRA based studies so far, effort is estimated by generating similar projects to the target project and then estimating effort from those most similar projects. *GREAT_RM* uses GRA for generating similar projects to the target project, but effort is calculated by applying regression on those most similar projects. In this study, ten regression techniques have been applied, including OLS, eight robust regression methods, and SWR. The individuality of the work is that the value of *k* varies with each reference project. The basic steps of the methodology are:

Step1: Select the continuous attributes from the dataset.

Step2: Data series construction: The data set consists of series $x_0=\{x_1(1),x_1(2),\ldots,x_1(m)\}$, $x_1=\{x_2(1),x_2(2),\ldots,x_2(m)\}$, $x_2=\{x_3(1),x_3(2),\ldots,x_3(m)\}$ and $x_n=\{x_n(1),x_n(2),\ldots,x_n(m)\}$, x_0 is the reference series whose effort is to be estimated based on the objective series x_1, $x_2,\ldots x_n$.

Step3: Data Preparation: The numerical features are normalized in a specified range so that each feature has the same weight on effort and hence it eases out their comparisons and processing.

Step4: Ranking the k closest projects: This aims at retrieving software projects from the data that exhibits large similarities with projects that are under investigation. The distance $\overline{\Delta}_{o,i}$ between two tuples at the k^{th} feature, is calculated by the formula as shown in Eq. (4).

$$\gamma\left(x_0(k),x_i(k)\right)=\frac{\Delta_{\min}+\zeta\Delta_{\max}}{\Delta_{o,i}(k)+\zeta\Delta_{\max}} \tag{9}$$

For all grey relational grades between the reference project *o* and the i^{th} comparative project, the $\Gamma\ (x_o, x_i)$ values are calculated for each *i* according to Eq. (5). The range of Γ is from 0 to 1 in each case [47]. For more similarity between projects the value of Γ approaches one and for two projects that are completely dissimilar, it approaches zero. The projects that have the higher value on GRG get the greatest opportunity to contribute in the final estimate.

Step5. Effort Prediction by GRA: The effort for GRA is the simple aggregation of the *k* most influential projects [17].

$$\hat{\varepsilon}=\sum_{i=1}^{k} w_i * \varepsilon_i \tag{10}$$

where, ε_i is the effort of the i^{th} most influential project and w_i is the weight given by:

$$w_i=\frac{\tau\left(x_0,x_i\right)}{\sum_{j=1}^{k}\tau\left(x_0,x_i\right)} \tag{11}$$

Step 6. Effort Prediction by Regression: In this step, effort estimate for a given project is cal-

culated by applying various regression techniques on only the *k* most similar projects obtained from Step 4.

3.2 Evaluation criteria

For the purpose of validating and evaluating the new methodology, the basic necessity is to measure how accurate the estimations are. There are various approaches used by researchers to measure the accuracy of effort prediction methods, such as the Mean Magnitude of Relative Error (MMRE), the Median Magnitude of Relative Error (MdMRE), the Magnitude of Relative Error Relative to the Estimate (MMER), the adjusted R-squared or coefficient of determination, and Pred(*n*). In order to measure the accuracy of the software estimation, we have used the four most popularly used evaluation criteria in software engineering, (i.e., MMRE, MdMRE, MMER and Pred(*n*).)

3.2.1 Mean Magnitude of Relative Error (MMRE)

Relative error is the absolute error in the observations divided by its actual value. The magnitude of relative error is the percentage of actual effort for the project and is given as:

$$MRE = \frac{|actual_i - estimated_i|}{actual_i} \tag{12}$$

The MRE for each observation is aggregated over the total number of projects, N, in order to generate the mean MRE (MMRE). MMRE is calculated as:

$$MMRE = \frac{1}{N}\sum_{X=1}^{N} MRE_x \tag{13}$$

MMRE favors models that underestimate, and it is extremely sensitive to small actuals. As MMRE is sensitive to individual predictions with excessively large MREs, we also use the median of MRE's for the n projects. (MdMRE), which is less sensitive to extreme values, is used as another measure for estimation accuracy.

3.2.2 Median MRE (MdMRE)

Median MRE is less sensitive to extreme values as compared to MMRE, so in case of large datasets we prefer using MdMRE as the estimation accuracy criteria and it is given by:

$$MdMRE = median\ (MREx) \tag{14}$$

A higher score for both MMRE and MdMRE means worse prediction accuracy.

3.2.3 Magnitude of Relative Error relative to the Estimate (MMER):

Another measure akin to MRE is MER. It is more preferable to MRE since it measures the error relative to the estimate. MER is given by:

$$MER = \frac{|actual_i - estimated_i|}{estimated_i} \tag{15}$$

We use the notation MMER to denote the mean MER.

$$MMER = \frac{1}{N}\sum_{X=1}^{N} MER_x \tag{16}$$

3.2.4 Pred (n)

It is used as the opposite measure to count the percentage of estimates that fall within less than *n* percent of the actual values. The common used value for Pred(n) is 25% . A low score on MMRE, MdMRE, MMER and a high score on Pred (n) entails better accuracy.

3.3 Data Sources

The data used in the present study comes from the PROMISE repository [44]. Though these datasets are old, they are still extensively being used to assess the comparative accuracy of new techniques. The descriptive statistics of these sets are given below. Five different datasets have been used in the study with the belief that if the model validation is successful with these models then it can also be validated on any other dataset. The descriptive statistics of all the five dataset are given below in Table 2.

Table 2. Descriptive Statistics of the Datasets

	Dataset	*Cases*	*Features*	*Effort Mean*	*Effort Standard Deviation*
1.	Finnish	38	8	7,678.29	7,135.28 (hours)
2.	Desharnais	77	9	4,834	4,188 (hours)
3.	COCOMO-81	63	17	683.52	1,821.51 (hours)
4.	Albrecht	24	8	21,875	28,417 (hours)
5.	Kemerer	15	5	219.25	263 (man hours)

4. EXPERIMENTAL RESULTS

The results obtained using the proposed methods are summarized in Table 3. The table provides the comparison of results obtained using only GRA, GRA and OLS, GRA and RR, and finally GRA and SWR for all of the five datasets. Only the best result obtained using eight robust regression techniques have been produced and put to statistical analysis. This empirical study is carried out using Leave One Out Cross Validation (LOOCV). For each iteration, one project is held out once and the training is performed on (n-1) projects. The accuracy is then measured by aggregating the accuracy of all the sets.

Boxplot of absolute residuals and Wilcoxon signed rank test of residuals are applied in order to study the distribution of residuals and statistical significance of *GREAT_RM* technique.

Table 3. Prediction Accuracy Results of GREAT_RM

	GRA	GRA with OLS	GRA with Robust Regression	GRA with Stepwise
Finnish dataset				
MMRE	11.37	11.88	10.3	58.61
Median (MRE)	2.67	2.19	1.93	27.93
MMER	12	12.88	9.81	40.99
Pred (25)	76.32	89.47	89.47	47.37
Albrecht dataset				
MMRE	46.35	29.83	24.16	32.64
Median (MRE)	4.89	7.47	10	12.39
MMER	17.15	21.72	22.57	24.87
Pred (25)	70.83	70.83	70.83	70.83
COCOMO -81 dataset				
MMRE	30	32.35	25.59	21.04
Median (MRE)	7.07	5.32	4.82	9.42
MMER	26.86	15.71	18.9	48.71
Pred (25)	68.25	76.19	74.6	76.19
Desharnais dataset				
MMRE	34.9	18.19	25.44	16.78
Median (MRE)	5.07	1.51	8.36	7.84
MMER	22.12	8.74	18.97	31.63
Pred (25)	68.83	90.9	79.22	74.02
Kemerer dataset				
MMRE	46.67	35.18	29.63	38.65
Median(MRE)	11.46	21.92	16.56	31.35
MMER	35.58	41.04	27.93	78.8
Pred (25)	60	53.33	60	40

Boxplots represent the results obtained by GRA, GRA+OLS, GRA+RR, and GRA+SWR.

1. The Boxplots in Fig. 1,2,3,4, and 5 show that medians are very close to zero for all the datasets, thus indicating that the spread is tighter towards the minimum value. The box overlays the lower tail for Albrecht, COCOMO-81, Desharnais, and Kemerer datasets, thus presenting an accurate prediction.

2. The range of absolute residuals for the Finnish dataset is large for GRA and GRA+SWR, but because the medians are tilted towards the minimum value, it indicates that the predictions are good.

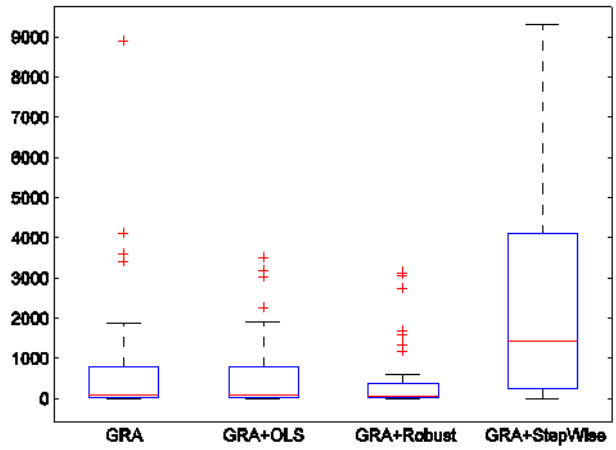

Fig. 1. Boxplot of Absolute Residuals for the Finnish dataset

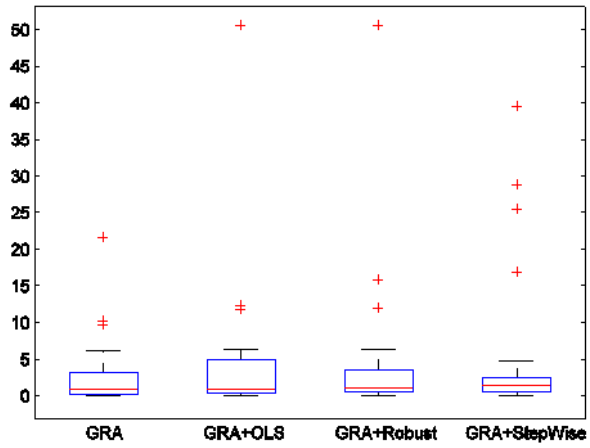

Fig. 2. Boxplot of Absolute Residuals for the Albrecht dataset

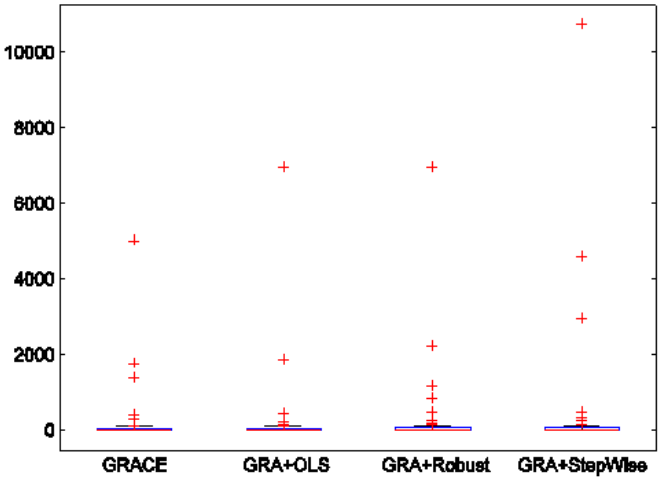

Fig. 3. Boxplot of Absolute Residuals for the COCOMO-81 dataset

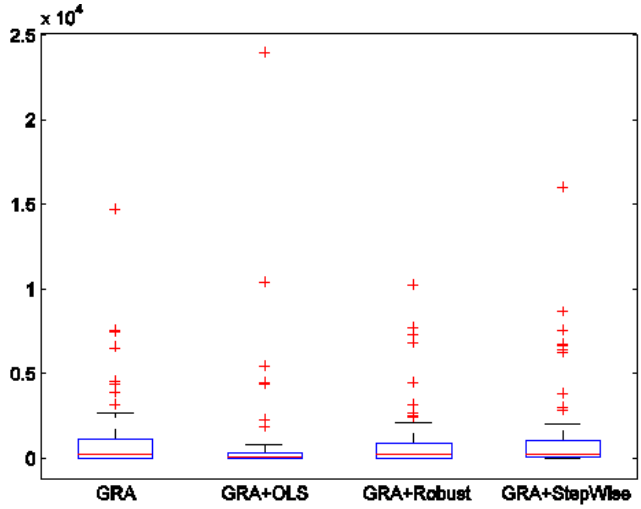

Fig. 4. Boxplot of Absolute Residuals for the Desharnais dataset

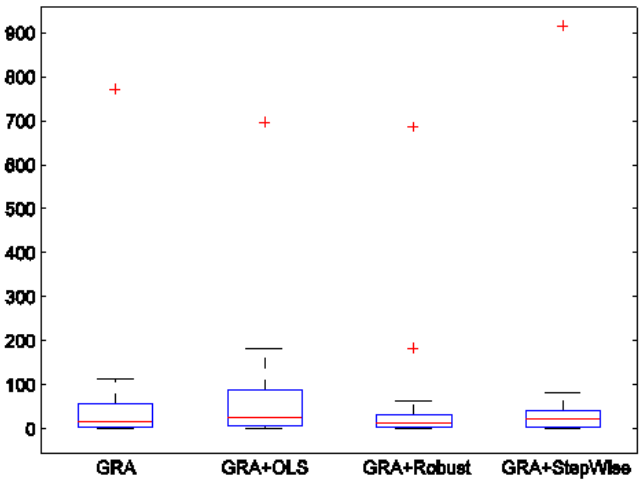

Fig. 5. Boxplot of Absolute Residuals for the Kemerer Dataset

4.1 Comparison of GREAT_RM to Multiple Linear Regression, Ridge Regression, Neural Networks, Support Vector Machine, and Multiple Adaptive Regression Splines

This section presents the results obtained when we compared the *GREAT_RM* model to Multiple Linear Regression (MLR), Ridge Regression (RR), Artificial Neural Networks (ANN), the Support Vector Machine (SVM), and Multiple Adaptive Regression Splines (MARS). We should note here that all the techniques were applied to the same numerical features of the same five datasets. However, in this section we investigate whether these techniques produce equivalent or better results than *GREAT_RM*. We used boxplots of absolute residuals to statistically measure the distribution of residuals. Based on absolute residuals we tested the statistical significance of all the results. All statistical significant tests were obtained using SPSS 19 for Windows.

(1) *Multiple Linear Regression (MLR):* In this work, the MLR uses data collected from historical projects to examine the relationships between independent attributes and dependent attributes and then developed a formal model based on that. This is already explained in Section 2.2.1

(2) *Artificial Neural Network (ANN):* ANNs are very sophisticated modeling and prediction techniques that are capable of modeling extremely complex functions and data relationships. They have the ability to learn by examples, which enables the user to model data and establish accurate rules governing the underlying relationship between various data attributes. They take the sample data, and then invoke *training algorithms,* which can automatically learn the structure of the data. One of the abilities of the neural network is to accurately predict data that is not part of the training dataset, and the process is known as *generalization.* In this work, multilayer perceptrons have been applied. Multilayer perceptrons are supervised feed-forward networks trained with a back propagation algorithm. With training input data and preferred output data, the multilayer perceptrons are trained on how to convert input data into a particular output. Three parameters have a major impact on the accuracy of the network, which should be defined before building the network. They are: number of hidden layers, the number of neurons in each hidden layer, and the type of activation functions [23].

(3) *Ridge Regression (RR):* RR is an alternative regression technique that tries to address the potential problems with OLS that arise due to highly correlated attributes. In regression, the objective is to "explain" the variation in one or more "response variables," by associating this variation with proportional variation in one or more "explanatory variables. However, the problem arises when the explanatory variables vary in similar ways, which reduces their collective power of explanation. This phenomenon is known as ***near collinearity***. As the different variables are correlated the covariance matrix $X^{'}X$ will be nearly singular and as a result the estimates will be unstable. A small variation in error will have a large impact on $\widehat{\beta}$. Ridge regression reduces the sensitivity by adding a number δ to the elements on the diagonal of the matrix that is to be inverted. δ is called the ridge parameter and it yields the following estimator of β.

$$\hat{\beta}_{\delta} = \left(X'X + \delta I_n\right)^{-1}\left(X'e\right) \tag{17}$$

where, I_n represents the identity matrix of rank n.

(4) *Support Vector Machine (SVM):* The regression SVM estimates the functional dependence of the dependent variable y on a set of independent variables x. It assumes, like other regression problems, that the relationship between the independent and dependent variables is given by a deterministic function of f plus the addition of some additive noise.

$$y = f(x) + \text{noise} \tag{18}$$

SVM finds a functional form for f that correctly predicts new cases that are presented to SVM. This is achieved by training the SVM model on a sample set (i.e., training set, a process that involves the sequential optimization of an error function). SVM constructs a hyper plane or set of hyper planes in a high- or infinite-dimensional space, which can be used for regression. A

good separation is achieved by the hyper plane that has the largest distance to the nearest training data point of any class. In general, the larger the margin, the lower the generalization error of the classifier. To construct an optimal hyper plane, SVM employs an iterative training algorithm, which minimizes an error function.

(5) *MAR Splines:* MAR Splines focuses on the development and deployment of accurate and easy-to-understand regression models. The MAR Splines model is designed to predict continuous numeric and high quality probability models. The MAR Splines model is a regression model that automatically generates non-linearities and interactions between variables and is thus a promising technique to be used for software effort estimation. MAR Splines has shown evidences of very high-performance results in forecasting the electricity requirement for power-generating companies, relating customer satisfaction scores to the engineering specifications of products, and presence/absence modeling in Geographical Information Systems (GIS). MAR Splines fits the data in the following equation:

$$e_i = b_0 + \sum_{k=1}^{K} b_k \Pi_{i=1}^{L} h_i\left(x_i(j)\right) \tag{19}$$

In this b_o and b_k are the intercept and slope. Parameters $h_i(x_i(j))$ *are the* hinge functions. They take the form *max (0,* x_i *(j)-b)* where, b is the knot. MAR Splines behaves as a multiple piece wise linear regression by adding multiple hinge functions.

4.2 Comparison of the Finnish Dataset

Table 4 summarizes the accuracy of the respective methods when applied to the Finnish data. From the results we can observe that *GREAT_RM* produced better accuracy than all other models.

The results also revealed that *GREAT_RM*, ANN, and MAR Splines are similar in terms of MMRE, MdMRE, and Pred (25) accuracy. The Boxplot of absolute residuals for the various techniques shows that:

- The box of *GREAT_RM* overlays the lower tail, which implies that the absolute residuals are skewed towards the minimum value and that it also presents a more accurate estimation than all other models.
- The median of *GREAT_RM* is smaller than the median of other models, which revealed that at least half of the predictions are more accurate than other models.

Table 4. Results of the Finnish Dataset

	OLS	RR	ANN	SVM	MAR Splines	GREAT_RM
Finnish Dataset						
MMRE	0.75	0.71	0.06	0.42	0.08	0.103
MdMRE	0.36	0.32	0.02	0.16	0.07	0.193
MMER	0.05	1.3	0.05	0.13	0.09	0.981
Pred (25)	36.84	36.84	92.11	63.15	97.37	89.47

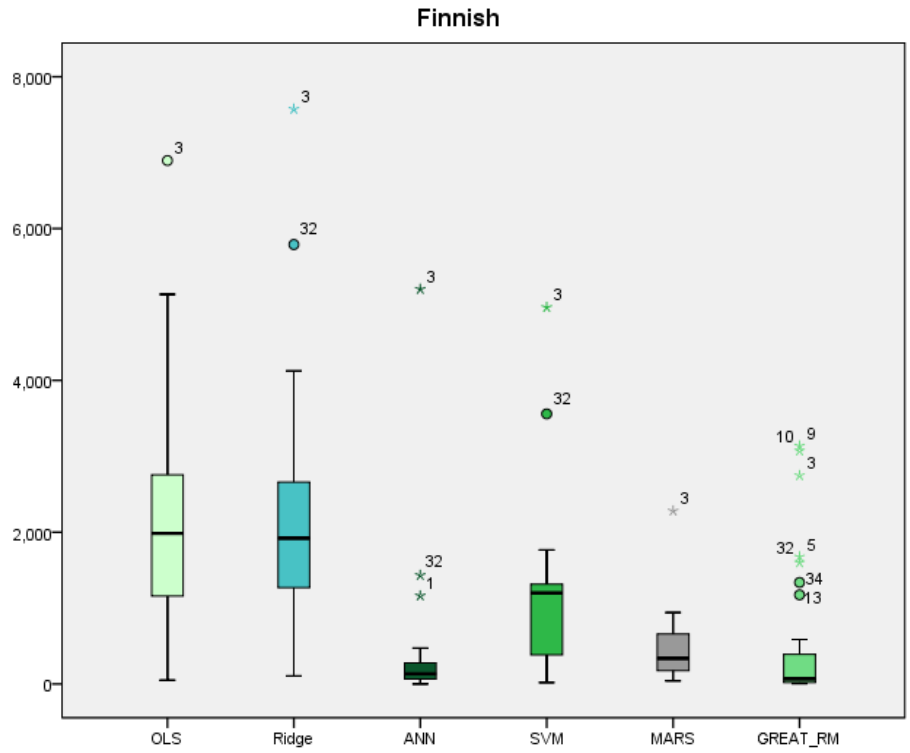

Fig. 6. Boxplot of Absolute Residuals for Finnish data set

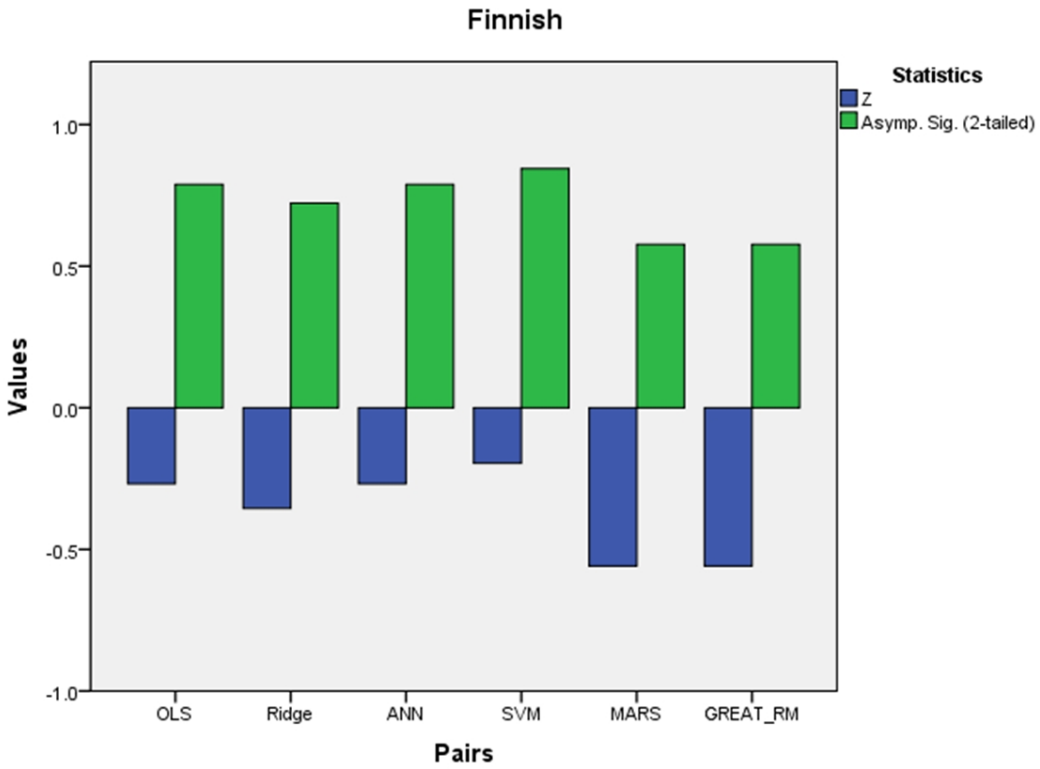

Fig. 7. Bar Graph(WILCOXON Signed Rank Test)

Table 5. Wilcoxon signed rank test (Test Statistics[c])

Finnish Dataset	OLS	Ridge	ANN	SVM	MARS	GREAT_RM
Z	-.268[a]	-.355[a]	-.268[b]	-.196[b]	-.558[a]	-.558[a]
Asymp. Sig. (2-tailed)	.788	.722	.788	.845	.577	.577

a. Based on negative ranks. b. Based on positive ranks. c. Wilcoxon signed rank test

WILCOXON Signed Rank Test:

Step 1: Hypotheses

H_0: μ (*Before*) = μ (*After*) ; H_a: μ (*Before*) > μ (*After*)

(Residual Median) = Hypothetical Median (test value).

Step 2: Significance Level: α= 0.05.

Step 3: Rejection Region: Reject the null hypothesis if p-value <= 0.05.

Step 4: Test Statistic: Wilcoxon signed rank test.

Step 5: Decision.

The p-value in all the cases is greater than 0.05, as shown in Table 5. Thus, we accept the null hypothesis. Consequently, we conclude that the residuals obtained by using all approaches were not significantly different from the test value of zero. As a result, the proposed methods can be used for software effort estimation.

4.3 Comparison of the Albrecht Dataset

On analyzing the Albrecht results, Table 6 summarizes the accuracy of the respective methods. From the results we can observe that GREAT_RM produced better accuracy than OLS, ridge, ANN, SVM, and MAR Splines.

The results also revealed that *GREAT_RM* produced better results of not only MMRE, but also MdMRE, MMER, and Pred (25). Thus, *GREAT_RM* tends to be more accurate than all other models. Amongst the other models, ANN produced better results in the Albrecht dataset. Unsurprisingly, predictions based on the *GREAT_RM* model presented statistically significant accurate estimations, which was also established by the Boxplot of absolute residuals as shown in Fig. 8.

The Boxplot of absolute residuals for the various techniques shows that:

- The box of *GREAT_RM* overlays the lower tail, which shows that the absolute residuals are skewed towards the minimum value and also presents an accurate estimation.
- The range of absolute residuals of *GREAT_RM* and ANN are smaller than the absolute residuals of other models, which implies that the variance is less.

Table 6. Results of the Albrecht Dataset

	OLS	RR	ANN	SVM	MAR Splines	GREAT_RM
Albrecht Dataset						
MMRE	0.9	0.91	0.78	0.51	1.23	0.24
MdMRE	0.43	0.52	0.17	0.33	0.6	0.10
MMER	0.17	0.27	0.28	0.35	0.52	0.23
Pred (25)	37.5	37.5	58.33	45.83	29.17	70.83

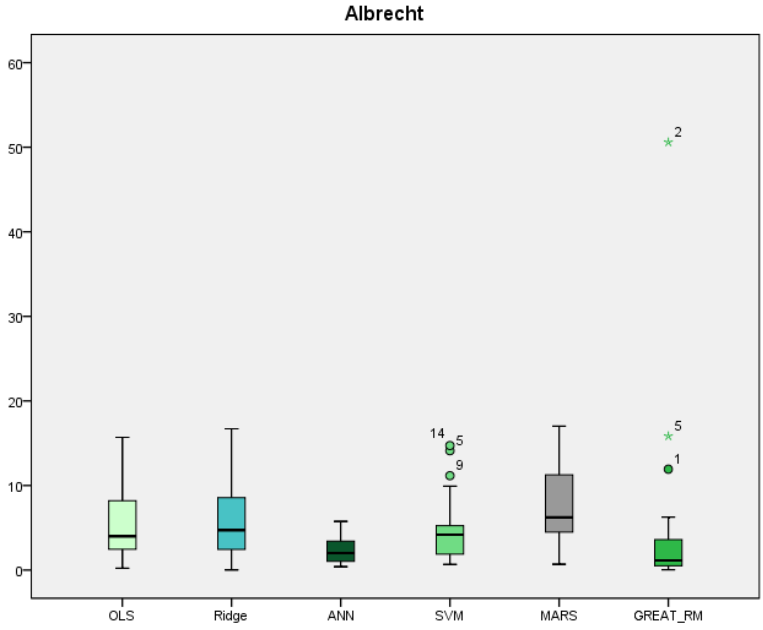

Fig. 8. Boxplot of Absolute Residuals for Albrecht data set

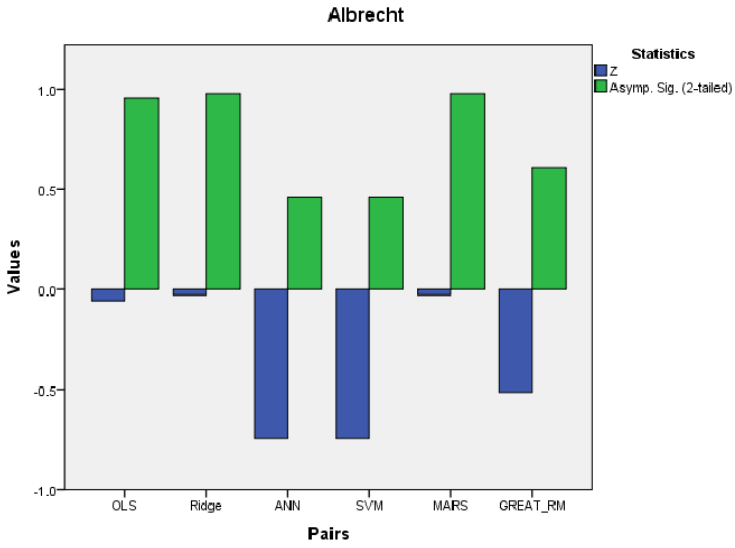

Fig. 9. Bar Graph (WILCOXON Signed Rank Test)

- The median of *GREAT_RM* is smaller than the median of other models, which revealed that at least half of the predictions of FGRA are more accurate than other models.

WILCOXON Signed Rank Test:

The p-value in all the cases is greater than 0.05, as shown in Table 7. Thus, we accept the null hypothesis. Consequently, we conclude that the residuals obtained by using all approaches were not significantly different from the test value of zero. As a result, the proposed methods can be used for software effort estimation.

Table 7. Wilcoxon signed rank test (Test Statistics[c])

Albrecht Dataset	OLS	Ridge	ANN	SVM	MARS	GREAT_RM
Z	-.057[a]	-.029[a]	-.743[a]	-.743[b]	-.029[b]	-.514[a]
Asymp. Sig. (2-tailed)	.954	.977	.458	.458	.977	.607

a. Based on positive ranks. b. Based on negative ranks. c. Wilcoxon signed rank test

4.4 Comparison of the COCOMO-81 Dataset

Table 8 summarizes the accuracy of the various models in the COCOMO_81 dataset. From the results we can observe that *GREAT_RM* performed significantly better than all of the other models. The results also revealed that *GREAT_RM* produced credible results in terms of not only MMRE but also MdMRE, MMER, and Pred (25).

The Boxplot of absolute residuals for the various techniques shows that:

Predictions based on the *GREAT_RM* model presented statistically significant accurate estimations, measured using absolute residuals, and was confirmed by the results of the Boxplot of absolute residuals, as shown in Fig. 10.

- The box of *GREAT_RM* has been minimized as can be seen in Fig. 10, which shows that

Table 8. Results of the COCOMO_81 Dataset

	OLS	RR	ANN	SVM	MAR Splines	GREAT_RM
COCOMO-81 Dataset						
MMRE	14.77	12.73	2.67	11.25	16.79	0.25
MdMRE	3.72	3.56	0.88	2.39	2.73	0.482
MMER	0.33	0.52	1.77	0.18	15.87	0.189
Pred (25)	11.11	12.69	25.39	12.69	0.02	74.6

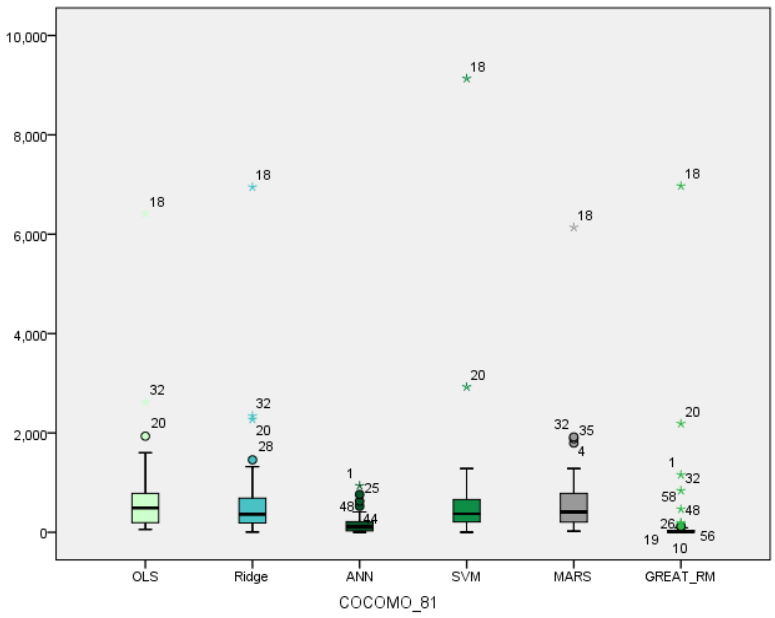

Fig. 10. Boxplot of Absolute Residuals for the COCOMO_81 Dataset

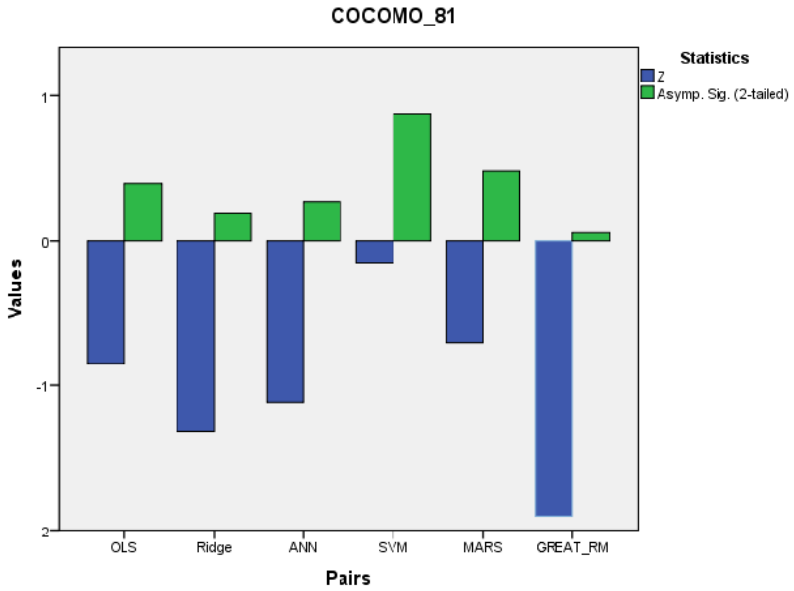

Fig. 11. Bar Graph (WILCOXON Signed Rank Test)

Table 9. Wilcoxon signed rank test (Test Statistics)

COCOMO_81 Dataset	OLS	Ridge	ANN	SVM	MARS	GREAT_RM
Z	-.849[a]	-1.321[a]	-1.116[a]	-.157[a]	-.705[a]	-1.903[a]
Asymp. Sig. (2-tailed)	.396	.186	.264	.875	.481	.057

a. Based on positive ranks. b. Wilcoxon signed rank test

the absolute residuals are skewed towards the minimum value and thus presents a more accurate estimation than the other five models.

- The range of absolute residuals of *GREAT_RM* is smaller than the absolute residuals of others.
- The median of *GREAT_RM* is approaching zero, which revealed that at least half of the predictions of FGRA are more accurate than other models.
- On the other hand, the range of absolute residual values for OLS, Ridge, SVM, and MARS produced the worst individual estimation.

WILCOXON Signed Rank Test:

The p-value in all the cases is greater than 0.05, as shown in Table 9. Thus, we accept the null hypothesis. Consequently, we conclude that the residuals obtained by using all approaches are not significantly different from the test value of zero. As a result, all the proposed methods can be used for software effort estimation.

4.5 Comparison of the Desharnais Dataset

Table 10 summarizes the accuracy of the various models in the Desharnais dataset. From the results we can observe that *GREAT_RM* performed significantly better than all of the other models. The results also revealed that *GREAT_RM* produced credible results in terms of not

Table 10. Wilcoxon Signed Rank Test

	OLS	RR	ANN	SVM	MAR Splines	GREAT_RM
Desharnais Dataset						
MMRE	0.5	0.47	0.47	0.48	0.51	0.16
MdMRE	0.31	0.3	0.31	0.31	0.32	0.078
MMER	0.40	0.41	0.35	0.16	0.40	0.31
Pred (25)	35.06	41.56	31.63	40.26	35.06	74.19

only MMRE but also MdMRE and Pred (25).

The Boxplot of absolute residuals for the various techniques shows that:

- Predictions based on the *GREAT_RM* model presented statistically significant accurate estimations, measured using absolute residuals, and was confirmed by the results of the boxplot of absolute residuals, as shown in Fig 12.
- The medians for the *GREAT_RM* techniques applied to the Desharnais dataset are very close to zero, as is clear from the values on the Y-axis, indicating that the estimates were closer to the minimum value.
- The range of absolute residuals of *GREAT_RM* is smaller.
- On the other hand, the range of absolute residual values for OLS, Ridge, ANN, SVM, and MARS produced the worst individual estimations.
- Extreme values presented in other models affected the estimation process.

WILCOXON Signed Rank Test:

The p-value in all the cases is greater than 0.05, as shown in Table 11. Thus, the proposed methods are statistically significant. As a result, all of the proposed methods can be used for software effort estimation.

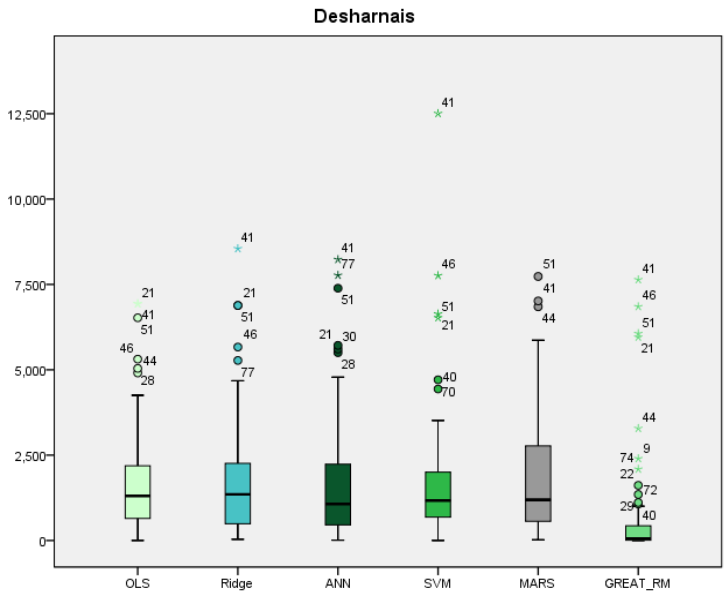

Fig. 12. Boxplot of Absolute Residuals for the Desharnais Dataset

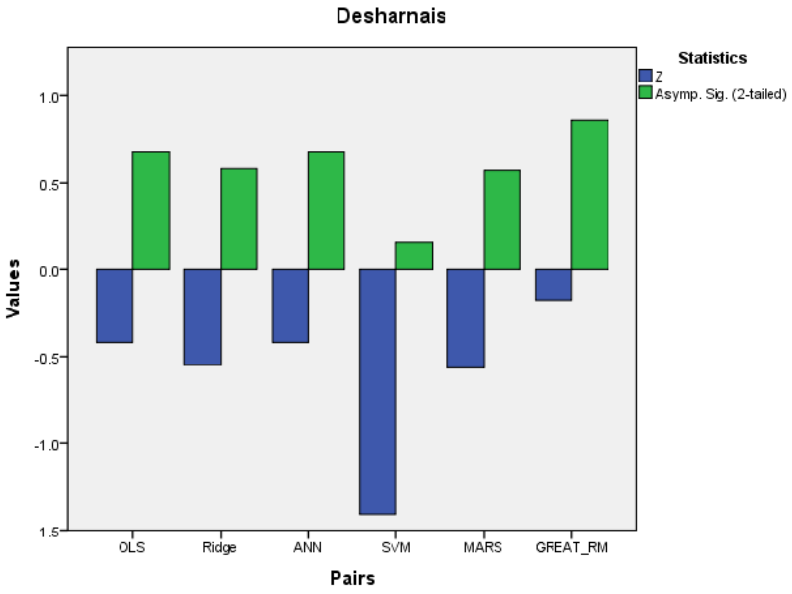

Fig. 13. Bar graph(WILCOXON Signed Rank Test)

Table 11. Wilcoxon Signed Rank Test (Test Statistics[c])

Desharnais Dataset	OLS	Ridge	ANN	SVM	MARS	GREAT_RM
Z	-.419[a]	-.551[a]	-.419[a]	-1.409[a]	-.566[a]	-.175[b]
Asymp. Sig. (2-tailed)	.675	.582	.675	.159	.571	.861
a. Based on positive ranks. b. Based on negative ranks. c. Wilcoxon Signed Rank Test						

4.6 Comparison of the Kemerer Dataset

Table 12 summarizes the accuracy of the various models in the Kemerer dataset. From the results we can observe that *GREAT_RM* and ANN performed significantly better than all other models. The results also revealed that both the techniques produced credible results in terms of not only MMRE but also MdMRE, MMER, and Pred (25).

The Boxplot of absolute residuals for the various techniques shows that:

- Predictions based on the *GREAT_RM* model presented statistically significant accurate estimations, measured using absolute residuals, and was confirmed by the results of boxplot of absolute residuals, as shown in Fig 14.

Table 12. Wilcoxon signed rank test

	OLS	RR	ANN	SVM	MAR Splines	GREAT_RM
Kemerer Dataset						
MMRE	0.74	0.68	0.31	0.003	1.05	0.296
MdMRE	0.54	0.37	0.12	0.0012	0.65	0.16
MMER	0.028	0.04	0.37	8.47	0.25	0.28
Pred (25)	26.67	20	66.67	100	3.33	60

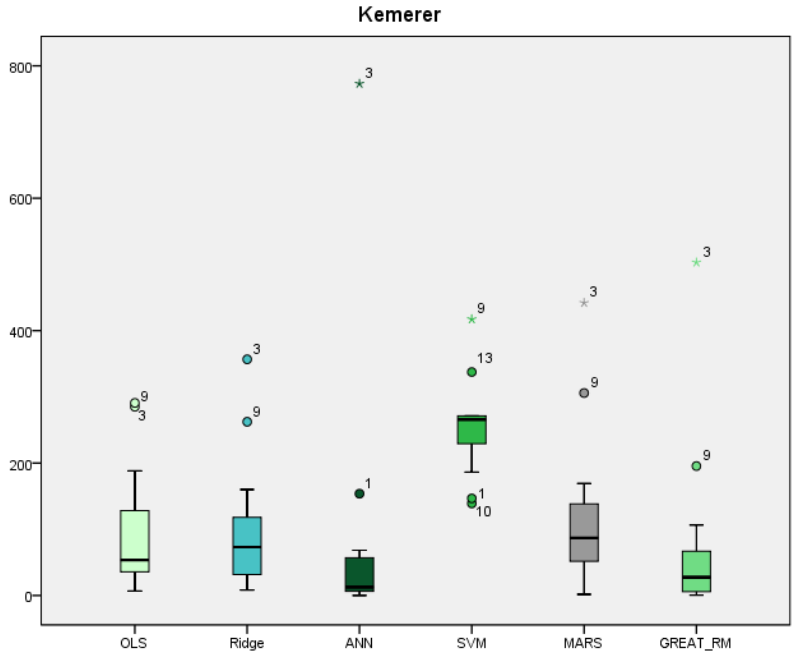

Fig. 14. Boxplot of Absolute Residuals for Kemerer Dataset

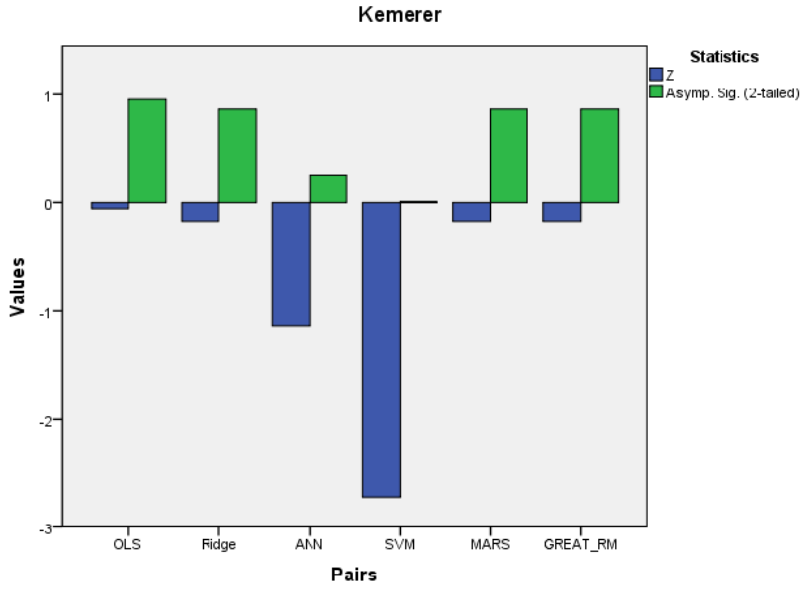

Fig. 15. Bar graph(WILCOXON Signed Rank Test)

- The medians for the *GREAT_RM* techniques applied to the Kemerer dataset are very close to the median, as is clear from the values on the Y-axis, indicating that the estimates were closer to the minimum value.
- The range of absolute residuals of *GREAT_RM* is smaller than the absolute residuals of others.
- On the other hand, the range of absolute residual values for SVM produced the worst individual estimations.

Table 13. Wilcoxon signed rank test (Test Statistics[c])

Kemerer Dataset	OLS	Ridge	ANN	SVM	MARS	GREAT_RM
Z	-.419[a]	-.551[a]	-.419[a]	-1.409[a]	-.566[a]	-.175[b]
Asymp. Sig. (2-tailed)	.675	.582	.675	.159	.571	.861

a. Based on positive ranks. b. Based on negative ranks. c. Wilcoxon signed ranks test

WILCOXON Signed Rank Test:

The p-value in all of the cases is greater than 0.05, as shown in Table 13. Thus, the proposed methods are statistically significant.

5. COMPARISON OF *GREAT_RM* WITH OTHER ESTIMATION METHODS

To ensure impartial assessment between our model and previous available results we have taken only those results for comparison that possess the same: (1) validation procedure, (2) number of projects, (3) number of features, and (4) treatment to missing values.

5.1 Comparison for the Finnish Dataset

The best results have been achieved with the Finnish dataset, with an MMRE of 10.03% and a Pred (25) accuracy of 89.47%, with the Fair M-estimator. The lower edge of the boxplot for all cases overlaps the lower whisker. This shows that the data is probably skewed towards the lower end of the scale. The smaller sizes of the box with the robust estimator indicate a reduced variability of absolute residuals.

5.2 Comparison for the Albrecht Dataset

On using the proposed methodology with the Albrecht dataset, the best MMRE = 24.16% and Pred (25) accuracy = 70.83% with the Huber M-estimator is obtained. This is an MMRE improvement of 36.09% over the GRACE technique [17], 26.94% over FGRA [23], and 1.94% over GRACE+[19]. The prediction accuracy has also been remarkable. There has been an improvement of 18.2% over GRACE, 20.83% over GRACE+ and an improvement of 42.23% over FGRA. In the study, carried out by Shepperd and Schofield [11], that made comparison between regression and analogy estimation models using the Albrecht dataset. The regression model resulted in MMRE=90% and Pred=33%, while analogy obtained MMRE=62% and Pred=33%. Thus, the results achieved by GREAT_RM are significantly better than other estimation methodologies. The results of MdMRE and MMER obtained by the GREAT_RM methodology are mentioned in Table 14.

Table 14. Comparison for the Albrecht Dataset

Albrecht Dataset				
	MMRE	Median MRE	Pred(25)	MMER
GREAT_RM	24.16	10	70.83	22.57
GRACE+	26.1	24.2	50	
FGRA	51.1	48	28.6	60.4
GRACE	60.25	21.35	52.63	

5.3 Comparison for the COCOMO-81 Dataset

GRACE [17] used GRA and stepwise regression on the COCOMO 81 dataset. The results obtained using GRA were MMRE =76.09% and Pred (25)= 20.63%. The results obtained based on regression were MMRE=1540.84% and Pred(25)=6.67%. Dolado [45] used regression and genetic programming and achieved MMRE=113% and Pred(25)=17% with regression, whereas, MMRE=23.2% and Pred(25)=15% was obtained using genetic programming. GRACE^{+} [19] used GRA and obtained MMRE=49.8% and Pred(25)=29%, whereas, the best results of MMRE=23.2% and Pred(25)=66.7% have been achieved by Azzeh et al. on using Fuzzy GRA [23]. Using the proposed hybrid analogy technique the finest results were obtained on integrating GRA with stepwise regression. Thus, the result obtained demonstrate its applicability for the COCOMO-81 dataset, as it yielded better results than Song et al.[17, 19], Dolado [45], and Azzeh et al.[23]. The results obtained for MdMRE and MMER using the *GREAT_RM* methodology are also mentioned in Table 15.

Table 15. Comparison for the COCOMO-81 Dataset

COCOMO 81				
	MMRE	Median MRE	Pred(25)	MMER
GREAT_RM	21.04	9.42	76.19	48.71
GRACE+	49.8	55.2	29	-
FGRA	23.2	14.8	66.7	25.6
GRACE	76.09	60.52	20.63	-

5.4 Comparison for the Desharnais Dataset

The Desharnais dataset has been extensively used for testing models based on software estimations. GRACE by Song et al. [17] obtained an MMRE of 49.83% with a Pred (25) accuracy of 30% with the Desharnais dataset. Mair et al. [46] also used analogy and obtained MMRE=57%. Shepperd [11] on using the Desahrnais dataset achieved MMRE=64% and Pred (25)=36%. Mair and Shepperd [46], however, used the hold out strategy, whereas, Song et al. and Azzeh used the jackknifing technique for GRACE^{+}[19] by Song et al. and obtained MMRE=49.83% and Pred(25)=30%. The finest results so far have been by Azzeh et al. [23] with using Fuzzy GRA and they obtained the lowest MMRE=30% and a Pred (25) as high as 64.7. The results obtained by using the *GREAT_RM* techniques have been superior to all the results mentioned above with an MMRE as low as 16.78% and Pred (25) as high as 74.02% when using GRA with stepwise regression. The GRA, when applied with OLS, also produced good results, as shown in Table 1. Thus, the result obtained demonstrates its applicability for the Deshanais dataset, yielding better results than those by Song et al. [17] and Azzeh et al. [23].

Table 16. Comparison for the Desharnais Dataset

Desharnais Dataset				
	MMRE	Median MRE	Pred(25)	MMER
GREAT_RM	16.78	7.84	74.02	31.63
GRACE+	41.4	29.2	45.3	-
FGRA	30.6	17.5	64.7	34.4
GRACE	49.83	33.93	30	-

With the OLS method, applied to the GRA, the dataset obtained equally good results with an MMRE of 18.19% with a Pred (25) of 90.9% . This is an MMRE improvement of 31.64 % over GRACE, 12.41 over FGRA, and 23.21 over GRACE^{+}. The results of MdMRE and MMER obtained by the *GREAT_RM* methodology are also mentioned in Table 16.

5.5 Comparison for the Kemerer Dataset

For the Kemerer dataset, the FairM-estimator obtained the best results when used with GRA. MMRE of 29.63 % and a Pred (25) accuracy of 60 % is an MMRE improvement of 29.2% over GRACE [17], 6.57% over FGRA [23], and with a Pred (25) accuracy improvement of 33.33% over GRACE [17] and 7.1% over FGRA [23]. The results however didn't improve over GRACE^{+}. This may be because of the very small size of the dataset and may also be due to the feature selection process and outlier detection performed by Song et al.[19].

Table 17. Comparison for the Kemerer Dataset

Kemerer Dataset				
	MMRE	Median MRE	Pred(25)	MMER
GREAT_RM	29.63	16.56	60	27.93
GRACE+	19.6	13.8	78.6	-
FGRA	36.2	33.2	52.9	34.3
GRACE	58.83	46.94	26.67	-

6. THREATS TO VALIDITY

There are two types of threats to validity. One is the threat to internal validity and the second is the threat to external validity. The external validity is more crucial with respect to the internal validity as they are related to the generalization ability of the predicted models. For five publicly available datasets it has been cleared that the new proposed model achieved by integrating GRA and regression has improved predictive power, which is better than with the other conventional estimation methods, but we have not analyzed how a smaller or larger dataset than those used in the study would yield consistent results. The results have been shown consistent for sample sizes ranging from 15 to 77 samples. We do not think that increasing the sample size beyond this range would show any inconsistent results. The threats to validity can however be reduced by conducting more studies across varied datasets.

7. CONCLUSION

Producing accurate software estimates has always been a challenge, where no one method has established itself to the fullest to consistently deliver an accurate estimate. Analogy based estimation is still one of the most extensively used methods in the industry. It is based on finding efforts for similar projects from the project repository.

The proposed hybrid *EbA* methodology has certainly improved the estimation process. The results obtained on applying the proposed methodology to five publically available datasets for software effort estimation have been presented in the previous section. The results obtained are compared to various types of linear regression models like OLS, ridge regression, etc., and to

nonlinear models like neural networks, support vector machines, and Multivariate Adaptive Regression Splines (MAR Splines), etc. The results obtained using *GREAT_RM* are not only better but are also encouraging with a lower MMRE, MdMRE, MMER, and higher Pred (25) for five publicly available datasets. The results are also significant when compared to three well known estimation models of GRACE, FGRA, and GRACE^{+} .The results based on the Wilcoxon signed rank test for residuals illustrates that most of the models using *GREAT_RM* produced statistically accurate predictions as their medians are not statistically different from the hypothesized median.

The empirical evaluations have revealed that the *GREAT_RM* techniques can certainly enhance the estimation process and hence can be used as an alternative technique for early stage software estimation where the data is uncertain. The results obtained are also finer over our previous results wherein the value of *k* was fixed for each reference project [48].

This methodology can further be explored on some other large datasets with resampling methods in order to further enhance the validity of the produced results. This methodology can be worked out using other robust regression techniques like S-estimator, Least Trimmed Square or MM-estimator etc. Attribute weighting can also be incorporated along with feature selection, in order to study the impact of individual features on the prediction accuracy.

REFERENCES

[1] J. L. Deng, "Control problems of grey system". *System and Control Letters*, Vol.1, 1982, pp.288-94.

[2] J.Deng,. "Introduction to Grey System theory", *The Journal of Grey System*,Vol.1, No.1, 1989, pp.1-24.

[3] J.Deng, "Grey information space", *The Journal of Grey System* Vol.1, No.1, 1989, pp.103-117.

[4] J. M. Jou, P. Y.Chen, and J. M.Sun, "The grey prediction search algorithm for block motion estimation". *IEEE Transactions on Circuits and Systems for Video Technology*, Vol.9, No.6, 1999, pp.843-848.

[5] S. L. Su, Y. C. Su, and J. F.Huang, "Grey-based power control for DS-CDMA cellular mobile systems". *IEEE Transactions on Vehicular Technology*, Vol.49, No.6,2000, pp.2081-2088.

[6] B.C.Jiang, , S. L.Tasi and C. C.Wang, "Machine vision-based gray relational theory applied to IC marking inspection". *IEEE Transactions on Semiconductor Manufacturing*, Vol.15, No.4, 2002, pp.531-539

[7] R. C.Luo, T. M.Chen, and K. L. Su, "Target tracking using a hierarchical grey-fuzzy motion decision making method". *IEEE Transactions on Systems, Man and Cybernetics, Part A*, Vol.31, No.3, 2001, pp.179-186.

[8] Y. F.Wang, "On-demand forecasting of stock prices using a real-time predictor". *IEEE Transactions on Knowledge and Data Engineering*, Vol.15, No.4, 2003, pp.1033-1037.

[9] S. J.Huang and C. L.Huang, "Control of an inverted pendulum using grey prediction model". *IEEE Transactions on Industry Applications*, Vol.36, No.2, 2000, pp.452-458.

[10] T. Mukhopadhyay, S. Vicinanza and M .J. Prietula, "Examining the feasibility of a case-based reasoning model for software effort estimation", *MIS Quarterly*, Vol.16, No.2, 1992, pp.155-171.

[11] M. J. Shepperd and C.Schofield, "Estimating Software Project Effort Using Analogies", *IEEE Transaction on Software Engineering ,*Vol.23, 1997, pp.736-743.

[12] L. Angelis, I. Stamelo, "A simulation tool for efficient analogy based cost estimation*," Empirical Software Engineering,* Vol.5, 2000, pp.35-68.

[13] J.W. Keung, B. A. Kitchenham, D. R. Jeffery, "Analogy-X:Providing Statistical Inference to Analogy-Based Software Cost Estimation", *IEEE Transactions on Software Engineering,* Vol.34, No.4, 2008.

[14] B. Baskeles, B. Turhan, A. Bener, "Software effort estimation using machine learning methods," *22nd international symposium on Computer and information sciences,* 2007, pp.1-6.

[15] A. Idri, A. Abran, T. M. Khoshgoftaar, "Estimating Software Project Effort by Analogy Based on Linguistic Values,"*, Eighth IEEE International Symposium on Software Metrics (METRICS'02),* 2002, pp.21.

[16] M. Azzeh, D. Neagu and P. I. Cowling, "Analogy-based software effort estimation using Fuzzy numbers". *Journal of Systems and Software,* Vol.84, No.2, 2011, pp.270-284 [doi: 10.1016/j.jss.2010.09.028]

[17] Q.Song, M.Shepperd and C.Mair,"Using Grey Relational Analysis to Predict Software Effort with Small Data Sets". *Proceedings of the 11th International Symposium on Software Metrics* (METRICS'05), 2005, pp.35-45.

[18] C. J. Hsu and C. Y. Huang, "Comparison and Assessment of Improved Grey Relation Analysis for Software Development Effort Estimation," Proceedings of the 3rd International Conference on Management of Innovation and Technology (ICMIT'06), 2006, pp.663-667.

[19] Q.Song and M. J.Shepperd, "Predicting software project effort: A grey relational analysis based method". *Expert Syst. Appl.* Vol.38, No.6, 2011, pp.7302-7316. [doi:10.1016/j.eswa.2010.12.005]

[20] S. J. Huang, N. H. Chiu and L.W. Chen, "Integration of the grey relational analysis with genetic algorithm for software effort estimation". *European Journal of operational and researc*h Vol.188, 2007, pp.898-909. [doi:10.1145/1540438.1540440]

[21] M. V. Kosti, N. Mittas, L. Angelis, " DD-EbA: An algorithm for determining the number of neighbors in cost estimation by analogy using distance distributions", *3d Artificial Intelligence Techniques in Software Engineering Workshop,*7 October, 2010, Larnaca, Cyprus.

[22] G. Li, J.Ruhe, A. Al-Emran and M.M.Richter, "A flexible method for software effort estimation by analogy", *Empirical Software Engineering*, Vol.12, No.65, 2007, pp.106. [doi:10.1007/s10664-006-7552-4]

[23] M. Azzeh, D. Neagu and P. I. Cowling, "Fuzzy grey relational analysis for software effort estimation", *Journal of Empirical software Engineering,* Vol.15, No.1, 2010. [doi:10.1007/s10664-009-9113-0]

[24] K. Srinivasan and D. Fisher, "Machine Learning Approaches to Estimating Software Development Effort," *IEEE Trans. Software Eng*., Vol.21, No.2, 1995, pp.126-137.

[25] G. Wittig and G. Finnie, "Estimating Software Development Effort with Connectionist Models," Information and Software Technology, Vol.39, No.7, 1997, pp.469-476.

[26] C. Burgess and M. Lefley, "Can Genetic Programming Improve Software Effort Estimation? A Comparative Evaluation," *Information and Software Technology*, Vol.43, 2001, pp.863-873.

[27] Y. Shan, R.J. McKay, C. J. Lokan and D.L. Essam, "Software Project Effort Estimation Using Genetic Programming", IEEE, Available at: http://www.isbsg.org.au, 2002.

[28] A.Idri, A. Abran and T. M. Khoshgoftaar, "Estimating Software Project Effort by Analogy Based on Linguistic Values", Eighth IEEE International Symposium on Software Metrics (METRICS'02), 2002.

[29] X. Huang, L. F. Capretz and J. Ren, "A Neuro Fuzzy Model for Software Cost Estimation", Proceedings of the third International Conference on Quality Software (QSIC'03) 0-7695 2015-4/03, IEEE, 2003.

[30] Z. Chen, T. Menzies, D. Port, and B. Boehm, "Feature Subset Selection Can Improve Software Cost Estimation Accuracy," *ACM SIGSOFT Software Eng. Notes*, Vol.30, No.4, 2005, pp.1-6

[31] P. Sentas, L. Angelis, I. Stamelos, and G. Bleris, "Software Productivity and Effort Prediction with Ordinal Regression," *Information and Software Technology,* Vol.47, 2005, pp.17-29.

[32] A. F. Sheta, "Estimation of the COCOMO Model Parameters Using Genetic Algorithms for NASA Software Projects", *Journal of Computer Science* 2 (2): 118-123, ISSN 1549-3636, 2006.

[33] M. Auer, A. Trendowicz, B. Graser, E. Haunschmid, and S. Biffl,"Optimal Project Feature Selection Weigths in Analogy-Based Cost Estimation: Improvement and Limitations," *IEEE Trans.Software Eng.,* Vol.32, No.2, 2006, pp.83-92.

[34] N.-H. Chiu and S.-J. Huang, "The Adjusted Analogy-Based Software Effort Estimation Based on Similarity Distances," *The J. Systems and Software*, Vol.80, 2007, pp.628-640.

[35] K. Chaudhary, "GA Based Optimization of Software Development Effort Estimation", GA Based Optimization of Software Effort Estimation*, IJCSI*, Vol.1, 2010, pp.38-40.

[36] M. Azzeh, D. Neagu and P. Cowling, "Improving Analogy Software Effort Estimation using Fuzzy Feature Subset Selection Algorithm", PROMISE'08 ,Leipzig, Germany, 2008.

[37] V. Ch, M.K. Hari, T. S. Sethi, B. S. S. Kaushal and A. Sharma, "CPN-A Hybrid Model for Software Cost Estimation", 978-1-4244-9477-4/11, IEEE, 2011.

[38] P. J. Huber, "Robust Estimation of a Location Parameter". *Annals of Mathematical Statistics*, Vol.35, 1964, pp.73-101.
[39] P. J. Huber, Robust regression: Asymptotics, conjectures and Monte Carlo, *The Annals of Statistics*, Vol.1, 1981, pp.799-821.
[40] D.F.Andrews, P.J. Bickel, F. R. Hampel, P.J. Huber, W.H. Rogers and J. W.Tukey, *Robust Estimates of Location: Survey and Advances*. Princeton University Press, Princeton, New Jersey,1972.
[41] MATLAB® Documentation, http://www.mathworks.com/help/techdoc/
[42] G.A.N.Mbamalu and M.E.El. Hawary, "Load Forecasting via Suboptimal Seasonal Autoregressive models and Iteratively Reweighted Least Squares Estimation" *IEEE Transactions on Power Systems*,Vol.8, No.1, 1993, pp.343-347.
[43] V.Verardi, and C. Croux, "Robust regression in Stata", *Stata Journal*, StataCorp LP, Vol.9, No.3, 2009, pp.439-453.
[44] PROMISE Repository of empirical software engineering data http://promisedata.org/ repository
[45] Dolado JJ (2001) "On the problem of the software cost function". *Journal of Information and Software Technology,* Vol.43, pp.61-72.
[46] Mair C, Kadoda G, Lefley M, Phalp K, Schofield C, Shepperd M, Webster S , "An investigation of machine learning based prediction systems". *J Syst Software*, Vol.53, 2000, pp.23-29.
[47] G. Nagpal, M. Uddin and A. Kaur, "A hybrid technique using Grey Relational analysis and Regression for Software Effort Estimation using Feature Selection" *International Journal of Soft Computing and Engineering (IJSCE)*, Vol.1, No.6, 2012.

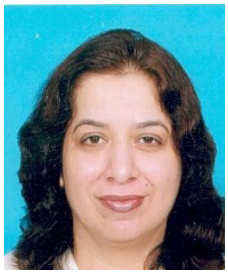

Geeta Nagpal

Geeta Nagpal, pursuing Ph D programme in the Department of Computer Science and Engineering, National Institute of Technology, Jalandhar, INDIA. She completed her Master's degree in Computer Science from Punjab Agricultural University, Ludhiana. She is presently working as Associate Professor in the Department of Computer Science and Engineering at National Institute of Technology, Jalandhar. Her research interests are Software Engineering, Databases and Data mining.

Prof. Moin Uddin

Prof. Moin Uddin, Pro Vice Chancellor, Delhi Technological University, Delhi , INDIA. He obtained his B.Sc. Engineering and M.Sc. Engineering (Electrical) from AMU, Aligarh in 1972 and 1978 respectively. He obtained hid Ph. D degree from University of Roorkee, Roorkee in 1994. Before Joining as the Pro Vice Chancellor of Delhi Technological University, he was the Director of NIT, Jalandhar for five years. He has worked as Head Electrical Engineering Department and Dean Faculty of Engineering and Technology at Jamia Millia Islamia (Central University) NewDelhi. He supervised 14 Ph. D thesis and more than 30 M.Tech dissertations. He has published more than 40 research papers in reputed journals and conferences. Prof. Moin Uddin holds membership of many professional bodies. He is a Senior Member of IEEE.

Dr. Arvinder Kaur

Dr. Arvinder Kaur, Associate Professor, University School of IT, Guru Gobind Singh Indraprastha University,Delhi, India. She completed her masters degree in Computer Science from Thapar Institute of Engineering and Technology and Ph D from Guru Gobind Singh Indraprastha University,Delhi. Prior to joining the school, she worked with Dr. B. R. Ambedkar Regional Engineering College, Jalandhar and Thapar Institute of Engineering and Technology. Her research interests include Software Engineering, Object-Oriented Software Engineering, Software Metrics, Microprocessors, Operating Systems, Artificial Intelligence, and Computer networks. She is a lifetime member of ISTE and CSI. She is also a member of ACM. She has published 45 research papers in national and international journals and conferences. Her paper titled, “Analysis of object oriented Metrics”was published as a chapter in the book Innovations in Software Measurement (Shaker-Verlag, Aachen 2005).

Achieving Second Green Revolution through Nanotechnology in India

Dr. Seema Singh*

Abstract

Initial spurt in agricultural growth rate as a result of the "First Green Revolution" has experienced distinct slow-down in recent years. There is urgent need to enhance productivity through technological as Nanotechnology, intervention. It is one of the emerging technologies with enormous agricultural application, which can be effectively applied in the development and design of methods and instrumentation for enhancing quantity and quality of food products and managing environment in better way. The paper discusses feasibility of achieving Second Green Revolution in India through nanotechnological application in agriculture in India.

Key word: Agricultural Growth, Nanotechnology, Market forces, Subsistence Agriculture.

1. Introduction

The 'First Green Revolution' witnessed during early 70's culminated in tremendous yield increase through four basic elements of production system viz. semi-dwarf high yielding varieties of rice and wheat, extensive use of irrigation, fertilizers and agro-chemicals. However, after tremendous growth, there has been a distinct slowdown in the agricultural growth rate since the mid-1990s. The agricultural production is experiencing a plateau, which has adversely affected the livelihood base of the farming community at large. As the availability of arable land for agriculture would reduce in future due to urbanisation, the only way out could be expected through productivity route. In fact, the country needs a 'Second Green Revolution' (Thakur, 2009). In this background, this paper tries to investigate whether nanotechnology can be used as a catalyst to initiate 'Second Green Revolution' in India?

Nanotechnology[1] is the latest buzzword in the engineering, and technological field and if believed the experts, it is going to make drastic changes in almost every aspect of economic life of 21st century. In general parlance, nanotechnology[2] is a science of miniature. Contrary of bulk material, nano-materials are 5,000 to 50,000 times smaller than the diameter of a human hair. These light but strong, transparent materials are very active and aggressive in any chemical reaction. Nano-materials can be mixed with any other materials to make them thousand times stronger and more efficient. The paper discusses feasibility of achieving 'Second Green Revolution' through nanotechnology in India. Second section of the paper discusses myriad agricultural application of Nanotechnology which can be effectively applied in the development of new functional material, product development, and design of methods and instrumentation for enhancing productivity, food safety and bio-security. Third section discusses present state of Indian agriculture. Challenges associated with Nanotechnological application in agriculture in India and India's preparedness to face them have been discussed in fourth section. Last section concludes the discussion.

2. Application of Nanotechnology in Agriculture

The recent UN Millenium Project Report, task force on Science, Technology and Innovation, puts forward the idea that nanotechnology will be important to the developing world because it harbours the potential to transform minimal work, land and maintenance inputs into highly productive and cheap outputs; and it requires only modest quantities of material and energy to do so (see Invernizzi and Foladori, 2005). It has wide range of agricultural application also. Some of them have been discussed as follows :

2.1 Agrinfortronics

Agriculture is seasonal in nature and depends on many variables such as soil, crops, weather etc. Sensing, acquisition, manipulation, storage and transfer of reliable and accurate data about the plant/animal and production-handling environment is therefore crucial in managing this variability to optimise both inputs and outputs and reduce impacts on the environment to meet the demand for high and good quality products. This requires successful fusion of ICT and mechatronics for agricultural applications. Based on advances in nanotechnology research, it was recently reported that the development of a new scanning-probe-based data-storage concept called "millipede" that combines ultrahigh density, terabit capacity, small form factor, and high data rate. Other developments include nanosensors to monitor the health of crops and farm animals and magnetic nonoparticles to remove soil contaminants. Dispersed throughout fields, a network of nano-sensors would relay detailed data about crops and soils. The sensors will be able to monitor plant conditions, such as the presence of plant viruses or the level of soil nutrient. Nanoparticles or nanocapsules could provide a more efficient means to distribute pesticide and fertilizers,

*Associate Professor in Economics, Delhi Technological University Delhi -110 042 seemasinghdtu@gmail.com

reducing the quantitites of chemicals released into the environment. Livestock may be identified and tracked using implanted nanochips (Holden and Ortiz, 2003).

2.2 Integration of Agricultural Biotechnology, Bioengineering and Nanobiology

Agriculture is an integral part of the wider biological industry. Given that the world of biology is at the scale of microns and below region where the sphere of nanotechnology resides, the convergence of biotechnology, bioengineering and nanobiology to solve practical problems facing agricultural is logical. Just like advances in modern agricultural biotechnology have separately created staggering possibilities in crop and animal production through genetic manipulation of species, development in nanobiology are bound to impact on future agricultural technologies. For instance, it was reported that the successful arrangement of control proteins on DNA within a cell. These advances open up tremendous scope for nanofabrication in modern molecular biology or agricultural biotechnology of plants and animals. Nanoscience is leading to the development of a range of inexpensive nanotech applications to increase fertility and crop production. Furthermore, nanofabricated devices offer the scope for their injection into plants and animals to detect tissue parts affected by rare phenomena such as diseases, nutrient deficiency and developmental abnormalities (Opara, 2004).

2.3 Agricultural Diagnostics and Drug Delivery with Nanotubes

Progress in nano material sciences and technology has resulted in the development of several devices which have potential applications in agricultural and related biological industries. For instance, nanotube devices can be integrated with other chemical, mechanical, or biological system, and can be excellent candidates for electrical sensing of individual bio molecules. Nanotube electronic devices have been shown to function very well under certain extreme biological conditions such as saline (salty) water and have dimension comparable to typical bio-molecules (e.g. DNA, whose width is approx. 2nm). Despite the practical difficulties in achieving reliable, rapid and reproducible nanofabrication of complex arrays of nanotubes, such devices have the potential to revolutionise site-specific and process exact diagnosis, drug delivery and in livestock disease and health management as well as in the identification and site-specific control of plant pests and diseases. Nanotech materials are being developed for slow release and efficient dosages of fertilizers for plant and nutrients and medicines for livestock (Opara, 2004).

2.4 Particle farming

It is an example of harvesting nanoparticles for industrial use, by growing plants in specially prepared soils. For example, research has shown that alfalfa plants grown in gold rich soil absorb gold nanoparticles through their tissues. The gold particles can be mechanically separated from the plant tissue (http://knowledge.cta.int/en/layout/set/print/Dossiers/S-TIssues-in-Perspectie/Nanotechnology).

2.5 Nanobots

Nanobots (miniature/micro robots the size of human blood cells or even smaller) which can be deployed by billion, could explore every capillary and even by guiding in for close-up inspections of neutral details in animals during breeding and special on-farm diagnostic. Using high-speed wireless connections, the nanobots would communicate with one another and with other computers that are compiling the scan database (Roco & Bainbridge, 2002).

2.6 Nanostructures

Nanostructures (such as smart nano-cards that collect and store data about products and process history) which can be implanted into plants and animals during growth and development to collect and transmit vital real-time data such as growth rates and physiological activities that provide clues on performance, productivity and exposure to environmental, chemical and physical hazards. Such smart nano-cards will further facilitate integrated supply chain traceability and management (Opara, 2004).

2.7 Nanotechnology and Food Processing

The application of Nanotechnology in the food industry has become more apparent with the initiation of consortia for better and safe food along with increased coverage in the media. Nanotechnology food application includes: smart packaging, on-demand preservation, and interactive foods which allows consumers to modify food, depending on their own nutritional needs and tastes. The concept is that thousands of nano-capsules containing flavour or colour enhancers or added nutritional elements (such as vitamins), would remain dormant in the food and will only be released when triggered by the consumer (http://knowledge.cta.int/en/layout/set/iprint/Dossiers/S-T Issues- in-Perspectie/Nanotechnology). Nanoparticles may also deliver growth hormone or vaccine to livestock, or DNA for genetic engineering of plants (Phoenix, 2009). A nanocomposite coating process could improve food packing by placing anti microbial agents directly on the surface of the coated film. Nanocomposites could increase or decrease gas permeability of different fillers as is needed for different products. They can also improve the mechanical and heat-resistance properties and lower the oxygen transmission rate. Research is being performed to apply nanotechnology to the detection of chemical and biological substances for sensing biochemical changes in foods (Dept. of Electronics, 2007/08).

2.8 Electricity

In India, there has not been much effort to link the technology's potential with development in agriculture and addressing the needs of people in rural areas, which form the backbone of India's economy, according to Anil Rajvanshi, Director of the Nambkar Agricultural Research Institute, Maharashtra. For example, nanomaterials could help improve solar cells and biogas reactors, said Rajvanshi (*http://www.scidev.net/en/news/india-must-regulate-nanotechnology-urgently.html*). which can be used for mechanization and electrification of agricultural processes. It is a challenge before Indian researchers and scientists to innovate and adapt Nanotechnological application for Indian agriculture.

3. Present State of Indian Agriculture[3]

Indian agriculture may be discussed form two point of view i.e. supply side and demand side. From supply side, even though, there is high levels of aggregate growth over the last two decades, the Indian economy still remains predominantly an agrarian economy in terms of livelihood activities of people. The share of employment in agriculture (UPSS) in 2004-05 was as high as 52.1% but its share in GDP was 15.7 in 2008-09 (Economic Survey, 2010). The growth of agriculture in terms of both gross product and output has visibly decelerated during the post-reform period compared to the 1980s. For example, the growth rate of agricultural GDP decelerated from 3.08 per cent during 1980-1 to 1990-1 to 2.57 per cent during 1992-3 to 2005-6. The growth rate for all crop taken together decelerated to 1.96 per cent during 1990-1 to 2000-1, compared with a growth rate of 3.19 per cent during 1980-1 to 1990-1. The cause for concern is not merely the decline in the rate of growth of agricultural production, but also the decline in the growth rate of foodgrains, which fell from 2.85 per cent in the 1980s to 1.16 per cent in the 1990s, lower than the rate of growth of population of 1.9 per cent during the latter period. The 1990s were thus the first decade since the 1970s in which the rate of growth of food production fell below the population growth rate. This was essentially due to the gradual decline in the growth of yield levels, especially of some food crops. While the annual yield growth rate for all crops taken together declined from 2.56 per cent during the 1980s to 1.09 per cent during the later period, for rice it decelerated from 3.47 per cent to 0.92 per cent, and for wheat from 3.10 per cent to 2.21 per cent. There is increasing evidence that there can not be rural development, even in relatively prosperous regions like A.P. and Punjab without high agricultural growth (Singh & Pal, 2010). Some of the significant features of the deceleration in Indian agricultural growth have been discussed below:

3.1. Resource Stress in Indian Agriculture

Unequal availability of irrigation across the country, and increasing stress on available irrigation resources are one of the major reason for deceleration in agricultural growth. The recent trends in irrigation show the distortion in the development and utilization of water resources for agricultural purposes. It is well known that one of the major areas of public investment in post-Independence India has been the investment on major and medium irrigation projects, which contributed to a substantial expansion of areas irrigated. In the post-reform period, however, there has been a net decline in the area irrigated under canals. The Plan era also showed neglect of minor surface irrigation sources such as tanks, leading to decay and disuse of these water bodies. The only source that has been continuously on the increase, which by 2003-4 accounted for almost two-thirds of the net irrigated area in the country, is groundwater exploitation through wells and borewells, though the rate of growth of even this resource is slowing down because of increasing risks and limits to the potential in certain regions. The extension of Green Revolution technology to rain fed and dry regions, the neglect of small surface water harvesting system such as tanks, and decline in public investment in irrigation in the 1990s have together contributed to the growing reliance on ground water resources. Dependence on groundwater has emerged as the single largest source of irrigation, with all its accompanying problems of serious risks to farmers' investment and degradation of environment. There has been over exploitation in the dry regions, leading to serious and unstoppable depletion in these regions. The existing irrigated areas have been displaying serious water stress as both reservoir and groundwater resource are depleting in many parts of the country (Reddy and Mishra, 2009). Fertilizer and pesticide which was one of the key factor for productivity improvement during first green revolution has also losing its shine. Effectiveness of pesticide is declining. One of the important reasons may be pest resistance (Bhalla, 2007).

Another crucial input for agricultural growth is electricity which is not available in sufficient amount as well as quality of electricity is also not good. As a support, farmers prefer to have diesel run generators which ultimately increases cost of cultivation.

3.2 Environmental Stress

A serious source of environmental footprint of agriculture is increasing pollution of river and canal water. Many of the rivers and lakes are getting contaminated from industrial effluents and agricultural run-off, with toxic chemicals and heavy metals, which are hard to remove from drinking water with standard purification facilities. Irrigation undertaken by polluted water can also seriously contaminate crops such as vegetables and fruits with toxic elements. Soil erosion is the most serious cause of land degradation in India. Estimation shows that around 130 million hectares of land (45 per cent of total geographical area) is affected by serious soil erosion through ravine and

gully, cultivation of wastelands, water logging, shifting cultivation, etc. It is also estimated that India loses about 5310 million tonnes of soil annually. According to estimates of the National Remote Sensing Agency (NRSA), the degraded land increased in the 980s by 7 million hectares from 11.31 per cent to 18 per cent of cultivable area (Chand 2006). These accumulation of salts and alkaline affects the productivity of agricultural lands in arid and semi-arid regions that are under irrigation. The magnitude of waterlogging in irrigated command is estimated at 2.46 million hectares (Pingali, 2005). Besides, 3.4 million hectares suffers from surface water stagnation. Injudicious use of canal water causes water logging and a rise in the water-table, which, if left uncorrected, eventually leads to salination. Although irrigation and drainage should go hand in hand, the drainage aspect has not been given due attention in major and medium irrigation projects in the country. There has been water logging associated with many of the large reservoirs since their inception (Government of lndia, Ninth Five Year Plan). Another area of concern, which is adding to land degradation, is over and unbalanced use of chemicals and fertilisers, which are important inputs for increasing agricultural production. Their use has increased significantly from the mid-1960s due to the Green Revolution technology. Over and unbalanced use of these chemicals is fraught with danger. Serious problems have arisen in the Indo-Gangetic Plain (IGP) because of the distorted ratio of application of nitrogen, phosphorus and potassium (NPK). There has been excessive use of nitrogen with adverse effects on soil fertility (Venugopal, 2004). This partly is the result of price differentials and partly due to lack of knowledge among farmers about the need for balanced fertilizer use. The consequence is soil nutrient depletion that is a major cause of the stagnation of rice yields. This is especially true is areas that make concentrated use of fertilizers and pesticides (Reddy and Mishra, 2009).

Climate change is also intensifying the strain on crops such as rice, corn and wheat. Poor long-term growing conditions such as drought, saline soils and heat, cold or extreme weather phenomenon cause billions of rupees of damage to agriculture every year (Bayer Crop Science, 09).

3.3 Human Stress

There are two type of human stress on Indian agriculture. As it has already been that almost half of the working population is dependent on agriculture and most of them are illiterate. After liberalisation and globalisation, they have been exposed to the global market without having proper information about them. Second type of human stress is about large agricultural dependant population is landless and resource starved.

3.4 Demand Side Perspective of Agriculture

India ranked 65 out of 84 countries in the Global Hunger Index of 2004, in the 'alarming' category, below countries including North Korea, Sudan and Zimbabwe. China was 60 places higher than India, in 5th place. Only 57 per cent of Indian men and 52 per cent of women are at a healthy weight for their height. 43.5 per cent of Indian children under the age of five are underweight for their age, compared to 7 per cent in China (Williams, 2005-06). The situation is quite alarming and if food security has to be realised, the agricultural output must has to increase, not only in terms of quantity but it needs to have more nutritional value[4] also. Along with the existing problems of food insecurity, growing prosperity and threshold market has changed the eating habits. Global agriculture in the 21st century has undergone a remarkable paradigm shift to emphasis on quality and traceability. Consumers are increasingly demanding for steady supply of consistent quality extending from organoleptic attributes to meeting their specific health and nutritional needs. Measuring and predicting quality reliability is therefore an important challenge in postharvest engineering of agri-foods (Opara, 2004). There is increasing demand of non vegetarian food "meat" which means more and better food is not only required for human being but for animals also. Then, there is increasing demand of non-food agricultural products also which creates a lot of stress on the available natural resources.

4. Challenges associated with Nanotechnological Application in Agriculture in India and India's Preparedness to Face Them

As U. N. Millennium Project Report, task force on Science, Technology and Innovation discussed the benefits of nanotechnology to make millennium goal into more achievable goal, several developing countries have launched nanotechnology initiatives. Countries like Argentina, Brazil, Chile, China, Mexico, Philippines, South Africa and Thailand are all involved in this frontier science. More precisely, there are 44 countries working on Nanotechnology in the food and agriculture field. But most of the activities are in the early stage (http:// www.nanoindia.com/printphp?news id=766). The Indian Government has also taken plunge to develop human resource and their capability in the emerging technology[5]. Impetus for developing a plan stems from fears that India has fallen behind China, Japan, the United States and the United Kingdom, which all have launched Nanotechnology programme over the past several years and are investing heavily in R&D. Though Nanotechnology as a branch of study is not very old, Indian universities and R&D centres have taken Nanotechnological research very aggressively[6]. Along with the government other stake holders are also taking interest in the development of the area. Sabir Bhatita, co-founder of Hotmail, plans to build a multibillion dollar "Nano city" in Chandigarh, Northern India, envisioned as the "Silicon Valley" of India. In the United states, Indian-American have already begun to show their support for a National Nanotechnology initiative in India though a

programme dubbed the "Indus Nanotechnology Association" which hopes to provide a common platform for researchers, entrepreneurs, technologists and investors of Indian origin seeking to leverage the emerging nanotechnology industry (Krishnidas, 2007).

The Indian government is looking towards nanotechnology as a means of boosting agricultural productivity in the country. A report released in April'08, Planning Commission of India has recommended that Nanotechnology research and development (R&D) should become one of the six areas of investment. The report says that Nanotechnology such as nano-sensors and nano-based smart delivery systems could help to ensure natural resources like water, nutrients and chemicals are used efficiently in agriculture. Nano-barcodes and nano-processing could also help monitor the quality of agricultural produce. The report proposes a national consortium on nanotechnology R&D, to include the proposed national institute and Indian institutions that are already actively researching nanotechnology. The report suggests ways to harness nanotechnology, biotechnology and bioinformatics to transform Indian agriculture, including creating a National Institute of Nanotechnology in Agriculture (Sreelata M, 2008).

The road map for development of Nanotechnological application in agriculture is very logical. The government took initiative which was the first level. At second level, R&D work was carried out aggressively at the universities and R&D centres. The second stage is at present going on. At third level, successful R&D need to be commercially produced[7]. Despite explosion in nanotechnology R&D, realisation of those R&D still lies ahead in the near future. Most of the R&D is being carried out in government research institutions (e.g. universities, research institutions) and private sector companies. This means that much of the knowledge arising from these laboratories will be tied up to intellectual property rights of the funding organisations and this implies that it would take much longer time than anticipated to see agriculture nano-machine in farms and food handling/processing centres (Opara, 2004). Not only that, as they are tied with IPR, it is difficult to get full access to research materials[8]. Another aspect is commercial feasibility of successful R&D. At the development stage, researchers hardly takes care of the economic aspect. India has the example of successful model of Information, and communication technology[9] which can be replicated for Nanotechnology also. However, in case of Nanotechnology, while there is still not coherent international approach to determining if and what risks are posed by what kind of nanotechnology materials (Maynard, 2006). A lack of standard. definition[10] makes these early investigations hard to compare and sometimes they even contradict each other, a situation that is especially confusing in risk assessments of carbon nanotubes. It has been discusses by many that nanoparticles are more toxic than their bulk counterparts which may enter in our body through membrane (Anbrecht et.al., 2006) and ultimately, it could be critical to biodiversity and ecosystem health[11]. Nematodes are pretty much at the bottom of the food chain and if they are capable of absorbing nanoparticles then another point of great interest and concern is the possible transfer and accumulation of nanoparticles through the food chain (Berger, 2009).

The broad implication of Nanotechnology for society can be grouped into two categories, namely environmental, health and safety implications and societal & economic dimensions. Responsible development of Nanotechnology entails along with aggressive R&D towards agricultural application of Nanotechnology, research must be carried out towards understanding the public health and safety of all those who are producing and will consume them. Another important issue associated with Nanotechnological application in agriculture is the prospect for improving environmental quality. It is predictable that widespread adoption of Nanoagriculture in the future may be induced by environmental regulation to promote sustainable agriculture. Research is warranted to determine the application of nanotechnology in environmental management. Channels of communication should be established with relevant stakeholders, in terms of providing information and seeking input. Second is the cost and benefit aspect, especially in context of socio economic milieu of the majority of the Indian farmer and size of the majority of the land holding[12]. Adoption of Nanotechnological application in agriculture depends on its ability to create employment and increase wage rate[13]. However, even now, there are more than 700 nano products which are already in the market. Some of them are used in agriculture also as pesticides (Syngenta), Food additive (nano-carorenoids, BASF) etc. (Wetter, 2005). Under such circumstances, there is high probabilities that the benefit of nanotechnology will only be experienced by rich people but its side effect will be experienced by all as nanoparticle present in pesticide may go into water body. It will create further gap between rich and poor.

Technological advances have always been a two-edged sword; offering a two-edged sword; offering both upsides and downsides. Sometimes, even when technology has been used for good, it has had unexpected negative results. But the history of human progress is the story of our ability to exploit the benefits(http:// knowledge.cta.int/en/layout/set/print/Dossiers/S-T Issues-in-Perspective/Nanotechnology). So, onus is on the government, scientific community and social activists to discuss at different platform and inform the farming community about the pros and cons of nanotechnological application in agriculture[14]. It will create a well inform farming community to be able to judge about its adoption.

5. Conclusion

India is basically an agrarian economy and has experience production boost during First Green Revolution. But the agricultural growth rate is experiencing a plateau and there is immediate need for enhancing agricultural productivity for maintaining self sufficiency in agriculture. Nanotechnology is the latest buzz word in the field of engineering and technology which can play as a catalyst for enhancing agricultural growth rate. Nanotechnology has myriad agricultural application across the spectrum which includes both on-farm as Nanosensors which may detect plant disease and off-farm which include nano packaging or nano coating which increases self life of the food products. At least, forty four countries of the world including India are pursuing R&D for Nanotechnological application in agriculture for alleviating malnutrition and to achieve Second Green Revolution. So far, it has been done mainly for developed countries only and now it is up to the Indian researchers and scientists to innovate and adapt them to suit the socio-economic milieu. Successful R&D should be commercially produced which means taking care of financial and regulation aspects. The broad implication of Nanotechnology for society can be grouped into two categories, namely environmental, health and safety implication and societal dimensions. Responsible development of Nanotechnology entails along with aggressive R&D towards agricultural application of Nanotechnology, research must be carried out towards understanding the public health and safety of all those who are producing and will consume them. Research is warranted to determine the its effect on environmental management. Even if India does not adopt nanotechnological initiative in agriculture, there are chances that they will come in the Indian market due to liberalization and opening up of the economy. In those circumstances, farmers need a lot of counselling and guidance regarding pros cons of adoption. Channels of communication need to be established with relevant stake holders, in terms of providing information and seeking input from them.

Notes:

1. Nano in Greak means dwarf. Nanometer (nm) is a unit of measurement used to measure very small particles like atoms and molecules. One nanometer = one-billionth (10^{-9}) of a meter.
2. Nanotechnology can be defined as the application of science, engineering and technology to develop novel materials and devices in different fields in the nanorange.
3. This section has been largely borrowed from "chapter one-Agriculture in the Reforms Regime" by Reddy D. Narsimha and Srijit Mishra in their edited book entitled *Agrarian Crisis in India*, Oxford University Press, New Delhi, pp. 03-43.
4. According to scientist nearly 30 per cent of the Indian population suffers from malnutrition especially due to lack of iron, zink and vitamin A (*www.newindpress.com*).
5. India formed a Vision Group consisting of about a dozen researcher from academia, industry and research spheres to develop a national nanotechnology. The vision group was headed by Prof. C.N.R. Rao.
6. Nanotechnology is being taught at many engineering institutions at post graduate level and Ph.D. is being carried out in different form at almost all universities of India. Data presented by NISTADS scientist Vinod Kumar Gupta shows Indian publications in nanotechnology rose from none in 1990 to about 2200 in 2007, totalling nearly 21,000 at the end of 2007-an almost exponential growth. The number of patent was negligible until 2001, after which it climbed steadily to 35 in 2007. Gupta said almost half- 48 per cent—of the publication came from universities, while government research and development institute contributed 28 per cent. He said that emergence of Indian universities as centres for the generation of nanotechnology knowledge was "encouraging". Even some relatively poorly funded colleges were publishing in international journal (Padma, 2009).
7. India is not far behind the world in nanoscience. The difference is of five to seven years, said V. Srivastava, co-founder of QTech Nanosystem. There are 30 nanotechnology start-ups. Now, India needs a dedicated venture capital fund for nanotechnology (Krishnadas, 2008).
8. In 2009, an anonymous public statement was signed and submitted to the US Environment Protection Agency (EPA) by 26 leading scientists, entomologists who work with insects that infect com. It stated that scientists are unable to conduct independent research on GM crops as patents prevent full access to research materials and the ability to grow and study their plants. As a consequence, the scientists stated, the data that the scientific advisory panel of the EPA has available to it is unduly limited. Some of the scientists who signed the statement said that they were not opposed to genetic engineering per se, but were simply interested in researching these crops (Byravan, 2010).
9. The boom in information and communication technology (ICT) has been largely driven private sector funding - though the initial impetus came from the government. Within the telecom sector, the government, for instance, set up a specialised

regulatory body to address the concerns relating to pricing, efficiency and competition aspect of supplying and consuming telecom products and services (Chowdhury, 2006).

10. Experts like davies and Maynard have contended that it is the latter two—i.e. nano materials and product containing such materials that need to be regulated (Chowdhury, 2006).

11. In a paper, published in the December 9, 2008 online edition of Environmental Pollution addresses if metal oxide nanoparticles are more toxic than their bulk counterparts to C. Elegans, especially to their reproductive capability, and further explains that the observed toxicity was not simple due to dissolved metal ions.

12. An analysis of landholding structure reveals that (i) there has been a general tendency of increase in the share of households and the area cultivated by small and marginal farmers, (ii) there has been reduction in the share of land holding as well as the area cultivated by the large farms, and (iii) the average size of holdings in all size classes is on the decline (Reddy, 2006).

13. The advent of new agricultural technology (NAT) in India is often a source of controversy regarding its impact on various aspects of farm societies. One of the major controversies is its horizontal as well as vertical diffusion in terms of its adoption, income generation potential, etc. In the absence of proper diffusion of benefits of NAT, its contribution to growth and equity will be limited and may jeopardize the overall economic development. It has been effectively argued that if the adoption of NAT is confined to a few region (horizontal diffusion) to a few large farmers (vertical diffusion), the aggregate supply of food and the aggregate demand for labour will not shift appreciably. If the new technology is landsque, its adoption is expected to contribute to a favourable distribution in the agricultural sector through higher intensity of labour and other linked inputs. Conversely, a labour saving and land using technology in the Hickksian sense would result in aggravating the rural inequalities (V. Ratna Reddy, 1994).

14. When the first green revolution was launched, it was carried out like a symphony in unison by scientists, policy makers, state agriculture departments, marketing agencies and farmers. Over the years, with the monstrous growth of the administration and multiple ministers handling farm issues at the centre and state levels, the delivery mechanism has collapsed. As a result, implementation of various agricultural policies remained on paper, Swaminathan lamented. On the prospect of ushering in a second green revolution as advocated by the Prime Minister Dr. Manmohan Singh in his Science Congress inaugural address, Swaminathan said that more than technology and government support, there was a need to empower panchayats and to give greater importance to women in farming activities (Balaji, 2008).

REFERENCES

Albrecht Mathhew A., Cameron W. Evans and Colin L. Raston (2006), "Green Chemistry and the health Implications of Nanoparticles" http:// www.filterair.info/library files/l-2009aa.pdf down loaded on 11-5-2011.

Balaji Fakir (2008), "India needs special agricultural zones: swaminathan" //http://twocircles.net/node/35320 down loaded on 18-3-2009

Bayer Crop Science (2009), "Research for the Second Green Revolution" *http:* www.research.bayer. com/ edition-20/safe harvests worldwide aspx down loaded on 11-07-2009.

Berger Michael (2009), "Investigating Potential Nanotechnology risks at the bottom of the Food Chain" (http://www.nanowerk. com/spot light/ spotid=8774.php) down loaded on 28-2-2009.

Byravan Sujatha (2010), "The Inter-Academy Report on Genetically Engineered Crops: Is It Making a Farce od Science?" Economic and Political Weekly, XLV no. 43, pp 14-16.

Chand, R. (2006), "India's Agricultural Challenge and their Implications for Growth and Equity," paper presented at Silver Jubilee Seminar on Perspective on Equitable Development: International Experiences and Can India Learn? Centre for Economic and Social Studies, Hyderabad as mentioned in Reddy and Mishra (2009).

Chowary Npur (2006), "Regulatory Supervision of Emerging Technologies", Economic and Political Weekly, Vo141, No. 46, http://beta.epw.in/newsltem/ comment/63159/down/loaded on 05-02-2011.

Dept. of Electronics (2007-08), "Nanotechnology Application", IED0060, TTU, http://www.elin. ttu.ee/eldes/LOENGUD/NANOEL/IED0060 nano applic.pdf down loaded on 11-05-2011.

Holden N. M. And M.C. Ortiz (Prepared) (2003) "Agometeological Aspects of Organic farming, Urban Agriculture, Indoor Agricultural and Precision Agriculture", CAgM Report No. 90.

http://www.wamis.org/agm/pubs/CAGMRep/CAGM90.pdf downloaded on 2011. http:// knowledge.cta.int/ en/layout/ set/print/Dossiers/ S-T Issues-in-Perspectise Nano-technology down loaded on 28th February, 2009.

(http://www.scidev.net/en/news/india-must-regulate-nanotechnology-urgently .html) down loaded on 17th January' 2009. http://vww.nanoindia. com/ print. php?news id=766 down loaded on 17th January' 2009.

Invernizzi Noela and Guillermo Foladori (2205), "Nanotechnology and the Developing World: Will Nanotechnology overcome Poverty or Widen Disparities?" Nanotechnology, Law and Business Journal, Vol 2 Issue 3 *http:// estudiosdeldesarrollo.net/administracion/ docentes/ documentos personales/11947LBJ. p df downloaded on 10-5-2011.*

Krishnadas, K.C. (2007), "India Rolls Out Nanotech Initiative" EE Times *http://www.eetimes. com/ news/semi/showArticle.jhtml? articleID=204-701839* down loaded on 06-12 2007.

.....(2008), "India forms vision group to draft nanotech policy" EE Times, *http://www. eetindia.co.in/ART 8800496199 1800007 NT fc00a257.HTM* downloaded on 28-2-2009.

MS Swaminathan Research Foundation (2008), "Crop biofortification to fight malnutrition" http:// www.mssrf.org/events conferences/content events/January 2008.scmedia.pdf down loaded on 11-7-2009.

Maynard Andrew D. (2006), "Nanotechnology: A Research Strategy for Addressing Risk" Project for Emerging Nanotechnologies, Woodrow Wilson International Center for Scholars, *http:// www.tinhoahoc.com/Nanoteclnology/Risk Related Research Maynard 7-06- Final. pdf* down loaded on 11-5-2011.

Opara Linus U. (2004), "Emerging Technological Innivation Triad for smart Agriculture in the 21st Century. Part 1 Prospects and Impacts of Nanotechnology in Agriculture", Agricultural Engineering International: the CIGR Journal of Scientific Research & Development, Invited Overview *http:// www.cigrjournal.org/index.php/Ejounral/ article/view/554/548 down loaded on 11-05- 2011.*

Parker Rachel (2008), "Leapfrogging Development through Nanotechnology Investment: Chinese and Indian Science and Technology Policy Starategies" China-India_US Workshop on Science, Technology and Innovation Policy *http:// www.1aw.gmu.edu/nctl/slpp/us china pubs/ china india us workshop/Sec9 young schlors/ Sec9*_item3_parkerpdf downloaded on 11-7-2009.

Phoenix Laurel E. (2009), "Critical Food Issues- Problems and state of the Art Solution WorldWide: Environment, Agriculture and Health Concern", *http://www.scribd.com/doc/37362360/Critical-Food-Issues-2-Volume-Set-Malestrom downloaded on 10-5-2011.*

Reddy D. Narasimha (2006), "Changes in Agrarian Structure and Agricultural Technology: Is Peasant Farming Sustainable under Institutional Retrogression." In R.Radhakrishna, S.K. Rao, S. Mahendra Dev, and K. Subba Rao (eds.), *India in a Globalising World: Some Aspect of Macroeconomy, Agriculture and Poverty*, Essays in Honour of C.H. Hanumantha Rao, Academic Press, New Delhi.

Reddy V. Ratna (1994), "New Agricultural Technology, Increasing Costs and Relative Shares of Labour and Other factors: A Spacio-Temporal Analysis of Andhra Pradesh" The Indian Journal of Labour Economics, Vol 37, No.2. Pp. 215- 227.

Reddy D. Narsimha and Srijit Mishra (2009), "Agriculture in the Reforms Regime" in Reddy D. Narsimha and Srijit Mishra (eds) Agrarian Crisis in India, Oxford University Press, New Delhi, pp. 03-43.

Singh Alka & Suresh Pal, (2010), "The Changing Pattern and Sources of Agricultural Growth in India" Chapter- 11, The Shifting Pattern of Agricultural Production and productivity World wide, The Midwest Agribusiness Trade Research and Informatiom Centre, Iowa State University, Ames, Iowa *http://www.card.iastate. edu/books/ shifting patterns/pdfs/chapter 11. pdf* downloadeed on 10-5-2011.

Sastry R. Kalpana, NH Rao Richard Cahoon and Terry Tucker (2007), "Can Nanotechnology Provide the Innovations for a Second Green Revolution in Indian Agriculture?" http: //www.nseresearch.org/ 2007/overviews/sastry_speaker.doc down loaded on 11-7-2009.

Tamboli P.M. and Y.L. Nene (2009), "Science in India with Special Reference to Agriculture" *http:// www.agri-history.org/Science%20in%20india% 20with%20special%20reference%20to% 20Agriculture. pdf* down loaded on 11.7.2009.

Thakur T.C. (2009), "Technological Advances in Soil Cultivation and Nutrient Management in Rainfed Agriculture", Theme Paper on Engineering Intervention for Sustainable Rainfed Agriculture

of 43rd Annual Convention of Indian Society of Agricultural Engineers held between February 15-17, 2009 at Birsa Agricultural University, Ranchi.

Sreelata M., (2008), "India looks to nanotechnology to boost agriculture" May 16, 2008, *http://www.scidev.net/en/agriculture-and-environment/farming-practices/news/india-looks* down loaded on 23rd February' 09.

Michael R. Taylor (2009), "keynote Address", 1st Annual Conference on Nanotechnology Law, regulation and policy, Food and Drug Law Institute and the Project on Emerging Nanotechnologies, February 28-29, 2008

Padma T.V. (2009), "Exponential rise in Indian nanotech", *http://www.scidev.net/en/new-technologies/nanotechnology/news/exponential-rise-in-india* down loaded on 23-2-2009.

Roco Mihail C & William Sims Bainbridge (eds) (2002), "Converging Technologies for Improving Human Performance", NSF and DoC sponsored report *http://www.scribd.com/doc/11426952/Nsf-Human-Perfomance down loaded on 10-5-2011*

Williams Matthias (compli) (2005-06), "global Huanger Index" WHO, UNICEF, Indian Governments' National Family Health Survey, *http://www.reuters.com/article/2010/04/20/idUSSGE63E0EAdown loaded on 10-05-2011.*

www.newindpress.com (2008), Crop Biofortification to fight malnutrition, *http://www.mssrf.org/events conference/content events/January 2008. scmedia.pdf. down loaded on 11-7-2009.*

Wetter Kathy Jo, ETC Group (2009), "Implication and Challenges of Emerging Technologies for Rural Development: Focus on Agriculture", IMI Workshop: What are the Innovation Challenges for Rural Development? Casa San Bernardo, Rome, 15-17 November .http://www.ifpd.org/innovation/presentation/Wetter.ppt#290.20. s1ide 20.

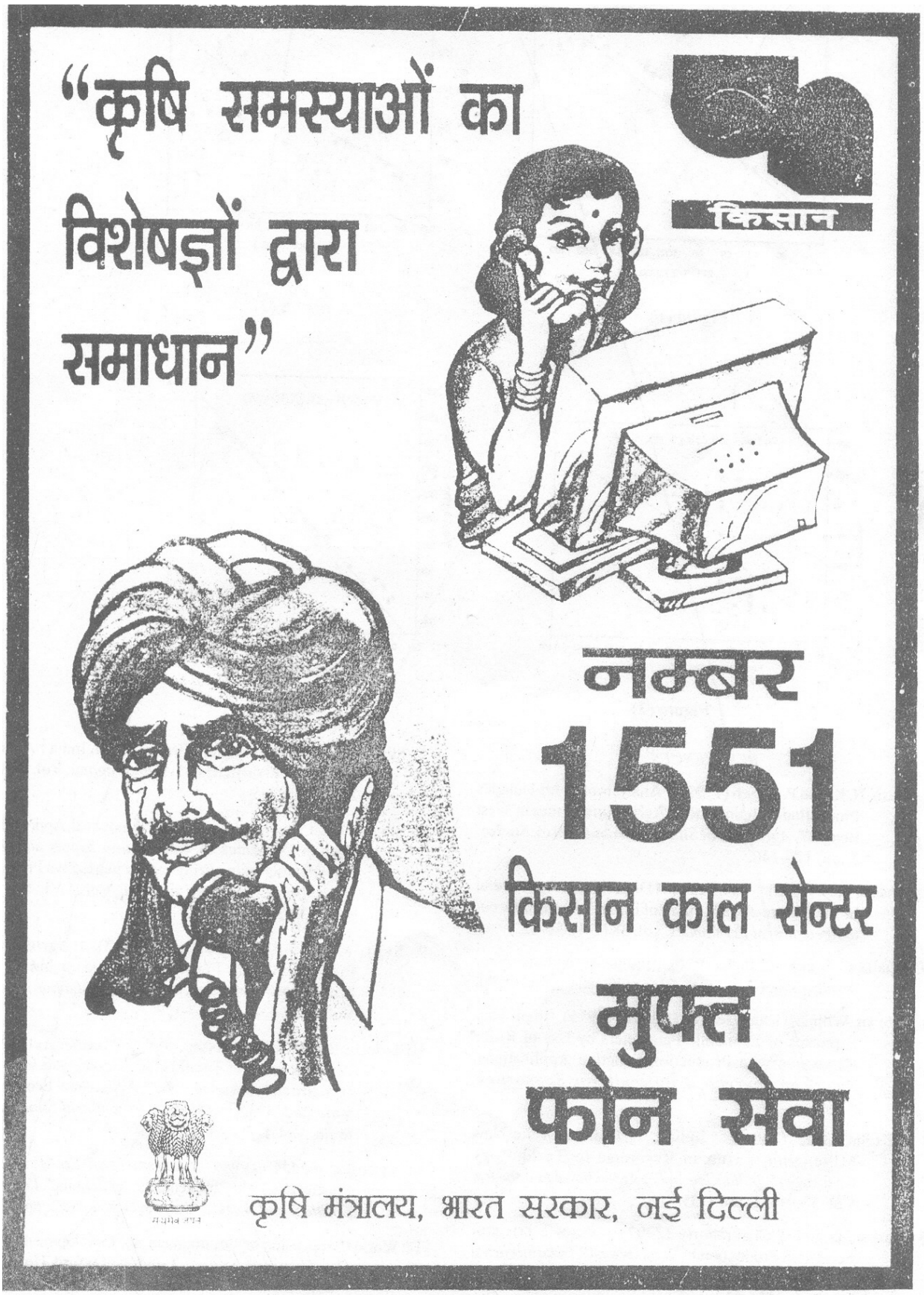
"कृषि समस्याओं का
विशेषज्ञों द्वारा
समाधान"
किसान
नम्बर
1551
किसान काल सेन्टर
मुफ्त
फोन सेवा
कृषि मंत्रालय, भारत सरकार, नई दिल्ली

C. Agro-Economic Research

Economics of Production, Processing and Marketing of Fodder Crops in Punjab*

In Punjab, livestock is one of the important component of the primary sector of the economy; contributing about 14 per cent of the State Domestic Product of the state, which is one-third the share of agriculture. The yield of milch animals, though higher than national average, is not in consonance with the levels attained in developed countries. The dairy sector in the state is facing problems due to less productivity of animals, higher cost of production and marketing of the produce. The fodder availability in the state comes to be 10-12 kg per animal, which is quite lower as compared to the optimum requirement of 40 to 50 kg per animal. Hence, the milch animals are under nourished and it affects their productivity level. About 5.68 lakh hectare area in the state is under fodder cultivation in the state, which comes out to be about 7 per cent of gross cropped area of the state. The present study tries to evaluate the costs and returns analysis for various fodder crops which will be helpful to examine the relative profitability of these crops in the region. The processing and marketing system of these crops were also examined as the farmers will get the remunerative prices for their surplus produce only when the effective and efficient processing and marketing system is in place.

Objectives of the study

1. To estimate the costs of production and returns associated with the cultivation of important fodder crops;
2. To identify the processing and marketing system and to estimate the costs and returns at each link for these fodder crops;
3. To study the problems faced by the producers in production, marketing and processing of these fodder crops.

Methodology

The study was conducted in the Punjab state. In the present study, one most important fodder crop each in the kharif, rabi and summer seasons viz. sorghum, berseem and maize fodder respectively were selected for the in depth analysis. Amongst different districts of the state, three districts with the highest area in the state were selected purposively. Amongst the selected districts, two blocks from each district, one block near and one distant to the periphery of district headquarters were selected randomly to realise the effect of distance factor in the findings. From each block, a cluster of 3 to 5 villages were randomly chosen, Finally, a sample of 25 farmers was selected randomly from each selected cluster, spreading over various farm size categories i.e. marginal (less than one hectare), small (1.2 hectares), semi-medium (2.4 hectares), medium (4-10 hectares) and large (more than 10 hectares) based on the size of the operational holding, making a total sample of 150 farmers. The primary data collection was done by the personal interview method for the reference year 2008-09. At least 10 market functionaries like forwarding agent/ commission agents/chaff cutters/dairy owners/consumers, depending upon the market functionaries involved in the disposal of each crop, were selected from the local markets in the selected blocks for data collection. The detail of sample growers is as follows :

District	Blocks	No. of sample farmers	Total
Ludhiana	Ludhiana-I	25	50
	Machhiwara	25	
Hoshiarpur	Hoshiarpur-II	25	50
	Bhunga	25	
Ferozpur	Ferozpur	25	50
	Zira	25	
Total		150	150

Status of livestock population in the state

The livestock population in the state has been decreasing continuously since 1990 and showed tremendous decrease from about 97 lakh in 1990 to about 71 lakh in 2007, decreasing at the rate of 1.5 per cent per annum over this period (Table 1). The buffalo population showed the

*AERC, Punjab Agricultural University, Ludhiana.

increase in number till 1997 after which it decreased sharply. Presently, Punjab is dominated by the buffalo population, as its share in total livestock population was about 69 per cent in 2007. On the other hand, cattle population has declined from about 28 lakh to about 17 lakh during this period, decreasing at the rate of 2.29 per cent per annum. Ferozpur, Sangrur and Amritsar are the leading districts in terms of bovine population in the state. The population of sheep is reduced almost to one third-while population of goat is reduced almost to half as compared to their population of about 5 lakh in 1990. The share of sheep and goat in total livestock population has reduced to 3 and 4 per cent respectively in 2007. Ferozpur and Bathinda are the leading districts in terms of sheep and goats population in the State.

TABLE 1— NUMBER OF LIVESTOCK, PUNJAB, 1990 -2007

(thousand heads)

Particulars	1990	1997	2003	2007	AAGR (%) 1990-2007
Cattle	2841 (29.26)	2564 (26.66)	1933 (23.63)	1668 (23.54)	–2.29
Buffaloes	5597 (57.64)	6096 (63.37)	5743 (70.22)	4902 (69.17)	–0.69
Horses and ponies	33 (0.34)	33 (0.34)	27 (0.33)	27 (0.38)	–0.99
Donkeys	36 (0.37)	20 (0.21)	5 (0.06)	5 (0.07)	–4.85
Mules	16 (0.16)	17 (0.18)	8 (0.10)	9 (0.13)	–2.26
Sheep	509 (5.24)	378 (3.93)	184 (2.25)	189 (2.67)	–3.49
Goat	538 (5.54)	391 (4.06)	252 (3.08)	260 (3.67)	–2.87
Camels	43 (0.44)	27 (0.28)	3 (0.04)	2 (0.03)	–5.29
Pigs	97 (1.0)	93 (0.97)	24 (0.29)	25 (0.35)	–4.15
Total livestock	**9710 (100.00)**	**9619 (100.00)**	**8179 (100.00)**	**7087 (100.00)**	**–1.50**

Status of fodder crops cultivated in the state

In Punjab, on an average, about 5.83 lakh hectare area was under fodder crops during the period 2005-09, which comes out to be about 7 per cent of gross cropped area of the state. But the area was found to decrease continuously from the level of about 7.8 lakh hectare during 1990-94, which may be due to the decreasing livestock population and increasing productivity of fodder during this period (Table 2). The fodder crops occupied about 2.64 lakh hectare area in the kharif season and about 2.97 lakh hectare during the rabi season. Maize fodder was also cultivated during the summer season covering about 21 thousand hectare area during the season. Sorghum, bajra and guara were the important kharif fodders covering about 24, 14 and 3 per cent of the total area under fodder cultivation in the state during the period 2005-09. Berseem and oats were the important rabi fodders covering about 34 and 12 per cent of the total area under total fodder cultivation in the state. Maize fodder is also cultivated during the summer season covering about 4 per cent of the total area under fodder cultivation in the state during the period 2005-09. During the period 1990-91 to 2008-09, most of the fodder crops showed decrease in area except guara during kharif season and oats during rabi season. During kharif season, maize fodder showed the highest decrease in area (-11.74 per cent per annum) during the period 1990-91 to 2008-09,

while during rabi season, berseem showed the highest decrease in area (-2 per cent per annum) during the same period. Maize fodder recorded increase in area during the recent years (2000-01 to 2008-09), but also showed the highest inter year level of variation in area during this period.

The area under the sorghum crop was found to decrease continuously and declined to 1.37 lakh hectares in the period 2005-09 as compared to the average area of about 2.34 lakh hectares during the period 1990-94. Patiala and Sangrur are the leading districts in terms of area under sorghum cultivation in the state. During the periods, 2000-01 to 2008-09 and 1990-91 to 2008-09, all the districts showed the decrease in area. The area under berseem crop was also found to decrease continuously to average of about 1.95 lakh hectares during the period 2005-09 as compared to the average of about 2.55 lakh hectares during the period

TABLE 2—AVERAGE AREA OF MAJOR FODDER CROPS, PUNJAB, 1990-91 TO 2008-09 (FIVE YEARS AVERAGE)

(Hectares)

Crop	1990-94	1995-99	2000-04	2005-09
Kharif				
Sorghum	234293	205281	182340	137894
	(30.24)	(29.12)	(27.88)	(23.66)
Bajra	93849	96921	108518	83216
	(12.11)	(13.75)	(16.59)	(14.28)
Guara	16315	9138	9881	18946
	(2.11)	(1.30)	(1.51)	(3.25)
Maize	26986	16643	7906	4670
	(3.48)	(2.36)	(1.21)	(3.23)
Others	39658	22132	14505	18799
	(5.12)	(3.140)	(2.22)	(45.22)
Sub-total	411101	350115	323150	263525
	(53.06)	(49.67)	(49.41)	(45.22)
Rabi				
Berseem	255010	227037	220397	195226
	(32.92)	(32.21)	(33.70)	(33.50)
Oats	57010	65725	63984	68279
	(7.36)	(9.32)	(9.78)	(11. 72)
Others	30675	42821	29768	34456
	(3.96)	(6.07)	(4.55)	(5.91)
Sub-total	342695	335583	314149	297961
	(44.23)	(47.60)	(48.04)	(3.64)
Summer				
Maize	20940	19241	16674	21228
	(2.70)	(2.73)	(2.55)	(3.64)
Total Fodder	**774736**	**704939**	**653973**	**582714**
	(100.00)	**(100.00)**	**(100.00)**	**(100.00)**

1990-94. Amritsar and Sangrur are the leading districts in terms of area under berseem cultivation in the state. During the period, 1990-91 to 2008-09 (period III), all the districts showed the decrease in area, except Hoshiarpur district. The area under maize fodder was found to decrease continuously from average of about 21 thousand hectares during the period 1990-94 to about as compared to 17 thousand hectares during the period 2000-04, but has shown the increase

TABLE 3—AVERAGE ANNUAL COMPOUND GROWTH RATES OF AREA AND THEIR COEFFICIENT OF VARIATION (CVs*) OF MAJOR FODDER CROPS, PUNJAB, 1990-91 TO 2008-09

(per cent per annum)

Crop	1990-91 to 1999—00 (Period-I)	2000-01 to 2008-09 (Period-II)	1990-91 to 2008-09 (Period-III)
Kharif			
Sorghum	-3.17	-5.44	-4.03**
	(11.05)	(21.03)	(22.36)
Bajra	0.98	-4.02*	-0.36
	(9.91)	(15.29)	(13.15)
Guara	-14.65**	3.55	1.55
	(33.22)	(21.64)	(29.19)
Maize	-6.79	-8.30	-11.74
	(31.62)	(30.90)	(65.94)
Others	-16.62*	5.56	-8.10
	(47.33)	(62.22)	(63.18)
Sub-total	-3.70	-4.10**	-3.17
	(12.46)	(12.80)	(17.86)
Rabi			
Berseem	-1.90	-2.90**	-2.0
	(8.27)	(8.72)	(11.54)
Oats	3.11**	-0.24	1.06
	(7.62)	(9.35)	(9.73)
Others	0.92	6.60	0.38
	(36.32)	(26.77)	(32.53)
Sub-total	-0.70	-1.52*	-1.19**
	(6.14)	(5.44)	(7.75)
Summer			
Maize	-1.14	4.19	-0.80
	(19.32)	(37.84)	(30.15)
Total Fodder	**-2.25**	**-2.59****	**-2.15****
	(8.77)	**(7.40)**	**(12.08)**

NOTE : figures in the parentheses are coefficient of variation.
*significant at 5 per cent level.
**significant at I per cent level.

during the recent years (2005-09) when the area has again reached to the average of about 21 thousand hectares. Faridkot and Amritsar are the leading districts in terms acreage of maize fodder in the state. During the period, 1990-91 to 2008-09 (period III), Hoshiarpur district showed the highest significant increase in area (21.3 per cent per annum), while Ferozpur district showed the highest significant decrease in area (-34.78 per cent per annum) during this period (Table 3).

Socio-economic characteristics of fodder growers

The average operational holding size of sample household was 5.88 hectares (Table 4). The average sample household was found to possess assets worth about 3 lakh and the asset value was found to increase with the increasing farm size. The average sample households were found to possess 0.79 tractors and 1.27 electric motors and the proportion was found to increase with the increasing farm size. Buffalo was found to be the most preferred livestock of the sample households as consumers of the

Punjab state prefer buffalo milk due to its high fat content. Paddy and wheat were the major kharif and rabi crops in the study area grown on about 70 and 83 per cent area respectively (Table 5). Fodder was grown in the kharif, rabi and summer seasons in the state. During kharif season, sorghum, bajra and maize were the important fodder crops and the net cropped area under these crops was about 7, 3 and one per cent respectively. During rabi season, berseem and oat are the important fodder crops and the net cropped area under these crops was about 8 and one per cent respectively. Maize was the summer fodder crop grown on about 6 per cent of the net cropped area. More number of farmers reported increased the area, production and productivity under sorghum, berseem and maize fodder during kharif, rabi and summer seasons During the last 10 years period, more number of dairy farmers observed increase in buffalo population and decrease in cattle population and about 45 per cent of the dairy farmers observed the increase in buffalo milk productivity, which was higher in case of productivity of cattle milk which was revealed by about 29 per cent of the dairy farmers. The practice of stall feeding as well as grazing was prevalent in the study area as the sample respondents were rearing only cattle and livestock on their farms.

During all the seasons, the in milk animals were found to feed more green fodder as compared to dry/male animals, which was true in case of all farm size categories (Table 6). Amongst in milk animals, the cross bred animals were found to fed higher doses of green fodder as compared to buffaloes, which may be due to higher fodder requirements for cross bred animals because of their higher productivity of milk. Amongst all the seasons, the animals

TABLE 4—AVERAGE LAND HOLDING OF SAMPLE HOUSEHOLDS, PUNJAB, 2008-09

(Hectares)

Particulars	Farm Size category					
	Marginal	Small	Semi-medium	Medium	Large	Overall
Owned land						
Irrigated	1.44	1.32	2.43	4.60	11.31	4.46
Unirrigated	-	0.03	-	0.06	-	0.02
Total	1.44	1.35	2.43	4.66	11.31	4.48
Leased-in land						
Irrigated	-	0.10	0.54	1.42	4.99	1.51
Unirrigated	-	-	-	-	-	-
Total	-	0.10	0.54	1.42	4.99	1.51
Leased-out land						
Irrigated	0.83	-	-	0.04	-	0.11
Unirrigated	-	-	-	-	-	-
Total	0.83	-	-	-	-	0.11
Total operational land						
Irrigated	0.61	1.44	2.97	5.98	16.30	5.86
Unirrigated	-	0.01	-	0.06	-	0.02
Total	0.61	1.45	2.97	6.04	16.30	5.88

TABLE 5—CROPPING PATTERN OF SAMPLE HOUSEHOLDS, PUNJAB, 2008-09

(% to net cropped area)

Season/Crop	Marginal	Small	Semi-medium	Medium	Large	Overall
A. Kharif Crops						
1. Paddy	43.33	48.86	56.55	65.39	77.97	70.04
2. Maize	13.83	17.59	17.89	13.30	2.57	8.43
3. Cotton	-	4.47	-	0.57	1.77	1.29
4. Sugarcane	-	1.12	0.85	2.92	1.24	1.72
5. Vegetable	-	1.12	7.03	2.64	4.48	3.97
6. Pulses	-	-	0.85	0.43	0.09	0.28
7. Any other	-	-	-	-	0.60	0.31
Fodder	-		-	-	-	-
1. Maize	-	-	0.64	2.00	0.09	0.76
2. Sorghum	25.81	15.36	7.03	7.83	4.84	6.52
3. Bajra	16.59	6.70	7.77	3.55	1.71	3.35
Net cropped area	100.00	100.00	100.00	100.00	100.00	100.00
B. Rabi Crops						
1. Wheat	69.61	88.79	81.04	86.90	80.55	82.90
2. Sunflower	-	-	0.96	0.86	1.77	1.30
3. Sarson	1.84	-	-	-	-	0.02
4. Sugarcane	-	1.12	0.85	2.92	1.24	1.72
5. Maize	-	-	-	0.43	0.89	0.60
6. Vegetable	-	3.63	5.54	11.91	11.09	10.32
7. Any other	-	-	-	-	0.89	0.46
Fodder						
1. Berseem	27.65	16.75	14.65	7.33	6.81	8.49
2. Oats	0.44	0.56	4.20	0.86	1.04	1.30
Net cropped area	100.00	100.00	100.00	100.00	100.00	100.00
C. Summer Crops						
Maize	0.10	0.18	0.22	0.48	0.62	0.32
Fodder	-	-	-	-	-	-
Maize	17.51	12.56	12.46-	7.10	2.68	5.75
Fruits	-	-	-	-	-	-
1. Kinnow	-	-	-	1.14	3.10	1.97
2. Safeda	-	3.07	1.28	0.29	-	0.36
3. Poplar	-	-	-	-	0.53	0.28
4. Fisheries	-	-	-	-	0.89	0.46
Net cropped area (ha.)	0.61	1.45	2.97	6.04	16.30	5.88

TABLE 6—SEASON-WISE FEEDING PRACTICES FOR LIVESTOCK POPULATION ADOPTED BY OVERALL FARMERS, SAMPLE HOUSEHOLDS, PUNJAB, 2008-09

Kg/animal/day

Season/Crop	In Milk Animals			Dry animals			Male		Young Stock
	Ind. cows	X-bred	Buffalo	Ind. cows	X-bred	Buffalo	Cattle	Buffalo	
A. Rainy Season									
1. Green Fodder									
i. Maize	-	4.7	2.4	-	3.9	4.2	2.9	0.7	1.2
ii. Sorghum	15.5	18.4	17.1	-	19.6	13.7	8.7	17.2	5.8
iii. Bajra	-	6.4	5.0	-	1.8	5.0	3.2	6.7	3.2
2. Dry fodder									
i. Wheat straw	-	4.0	5.5	-	2.5	3.9	2.9	6.5	0.3
ii. Paddy straw	-	0.03	0.02	-	-	-	-	-	-
3. Grains									
i. Wheat	-	0.7	0.7	-	-	-	-	-	0.03
ii. Maize	-	0.1	0.1	-	-	-	-	-	-
4. Concentrates									
i. Mixed feed	0.3	1.9	2.2	-	-	-	-	-	0.1
ii. Oil cakes	-	0.5	0.5	-	-	-	-	0.1	0.01
B Winter season									
I. Green Fodder									
i. Berseem	19.5	29.0	27.1	-	23.1	21.2	14.8	15.8	6.2
ii Oats	-	1.4	0.8	-	0.1	0.5	0.8	0.8	0.2
2. Dry fodder									
i. Wheat straw	2.5	6.5	7.4	-	7.1	7.3	6.3	7.2	0.9
ii. Paddy straw	-	0.1	-	-	0.1	0.1	-	0.7	-
iii. Maize straw	5.0	0.2	0.2	-	0.1	-	0.3	1.3	-
3. Grains									
i. Wheat	-	0.4	0.4	-	-	-	-	-	-
4. Concentrates									
i. Mixed feed	0.3	1.7	2.1	-	-	-	-	-	0.1
ii. Oil cakes	-	0.4	0.5	-	-	-	-	-	-
C. Summer season									
1. Green Fodder									
i. Maize	-	11.7	11.0	-	4.8	4.9	2.8	5.3	4.0
ii. Berseem	10.9	8.5	8.6	-	12.9	15.2	8.0	6.0	3.1
2. Dry fodder									
i. Wheat straw	3.5	5.4	5.7	-	4.5	4.7	7.6	6.7	0.8
ii. Paddy straw	-	0.2	0.2	-	1.5	2.4	0.7	0.2	-
iii. Maize	2.5	0.2	0.3	-	0.4	0.5	0.8	0.2	0.1
3. Grains									
i. Wheat	0.8	0.6	0.5	-	0.5	0.2	0.5	0.2	0.2
ii. Maize	0.8	0.2	0.1	-	0.3	0.3	0.7	0.2	0.1
iii. Paddy	-	0.1	0.1	-	0.3	0.3	0.1	-	-
4. Concentrates									
i. Mixed feed	1.0	1.4	1.6	-	-	-	-	-	-
ii. Oil cakes	-	0.3	0.4	-	0.6	-	-	0.5	-

were fed the least doses of green fodder on per day basis in the summer season. The young stock was found to feed green fodder. The animals were also fed the dry fodder in form of wheat and paddy straw during rainy season, which was fed more to male buffaloes as compared to other animals. The grains and concentrates were found to be fed mostly to the in milk animals and young stock.

Economics of production for fodder crops

The operational cost on per hectare basis for sorghum crop was found to vary between Rs. 9956 for small farms to Rs. 13823 for the medium farms. The variation is due to the level of cost of human labour incurred by these farms. On overall basis, the total operational cost on per hectare basis was found to be Rs. 11946. Amongst variable cost components, the share of human labour was more than 71 per cent. It shows that sorghum cultivation is highly labour intensive and the farmers have to incur highest expenses on it, which is particularly required during the harvesting of the fodder. Expenses on machine labour, FYM, fertilisers and seed were the other important components of the variable cost. The operational cost on per hectare basis for berseem crop was found to vary between Rs. 17561 for semi-medium farms to Rs. 19521 for the large farms which is due to the high level of cost of human labour incurred by large farms. On overall basis, the total operational cost on per hectare basis was found to be Rs 18231. Human labour was found to take larger proportion of the cost as its share was about 66 per cent. Most of the labour is required during the harvesting of the crop, which is done in 6-7 cuttings in about two months period. Expenses on machine labour, fertilisers and seed were the other important components of the operational cost and the expenses on these were about 11, 10 and 7 per cent of the total operational cost respectively. The operational cost on per hectare basis for maize fodder was found to vary between Rs. 8525 for small farms to Rs. 11851 for the medium farms which is due to the highest level of cost of human labour incurred by medium

TABLE 7—ECONOMICS OF FODDER CROPS VIS-A-VIS COMPETING CROPS, SAMPLE HOUSEHOLDS, 2008-09

Particulars	Marginal	Small	Semi-medium	Medium	Large	Overall
Kharif fodder: Sorghum						
Yield(qtls/ha)	358	427	494	420	482	448
Price(Rs/qtls)				57	55	56
Gross returns	19698	23929	26676	23934	26491	25082
Total Variable cost	10613	9956	10131	13823	12899	11946
Returns over variable cost	9085	13973	16545	10111	13592	13136
Competing crop during Kharif season : Paddy						
Yield(qtls/ha)	57	55	62	64	67	59
Price(Rs/qtls)	775	775	775	775	775	775
Gross returns	44175	42625	48050	49600	51925	45725
Total Variable cost	15276	15390	16368	16832	17554	15635
Returns over variable cost	28899	27235	31682	32768	34371	30090
Rabi fodder: Berseem						
Yield(qtls/ha)	825	865	773	823	914	855
Price(Rs/qtls)	47	48	52	49	48	49
Gross returns	38775	41520	40196	40327	43872	41895
Total Variable cost	18726	18887	17561	16856	19521	18231
Returns over variable cost	20049	22633	22635	23471	24351	23664
Competing crop during rabi season: Wheat						
Main Product(Qtls/hac)	44	49	52	47	49	47
Price(Rs/qtls)	1080	1080	1080	1080	1080	1080
By Product(qtls/hac)	44	49	52	47	49	47
Price(Rs/qtl)	125	130	120	125	136	125

TABLE 7—ECONOMICS OF FODDER CROPS VIS-A-VIS COMPETING CROPS, SAMPLE HOUSEHOLDS, 2008-09—*Contd.*

Particulars	Marginal	Small	Semi-medium	Medium	Large	Overall
Gross returns	53020	59290	62400	56635	59584	56635
Total Variable cost	15561	19266	19711	16895	17290	17129
Returns over variable cost	37459	40024	42689	39740	42294	39506
Summer fodder: Maize						
Yield (qtls/ha)	346	358	351	358	371	361
Price (Rs/qtls)	54	58	60	58	57	56
Gross returns	18673	20773	21044	20773	21119	20220
Total Variable cost	8525	9457	9434	11851	9614	8948
Returns over variable cost	10148	11316	11610	8922	11505	11272
Competing: crop during summer season : Maize Grain						
Yield (qtls/ha)	35	32	37	42	44	37
Price (Rs/qtls)	720	730	735	740	730	725
Gross returns	25200	23360	27195	31080	32120	26825
Total Variable cost	11200	9920	11655	12600	13640	11285
Returns over variable cost	14000	13440	15540	18480	18480	15540

farms. On overall basis, the total operational cost on per hectare basis was found to be Rs. 8948. About 60 per cent of the operational cost was incurred on human labour, most of which is required during the harvesting of the crop. The expenses on hired labour were found to increase with the increase in farm size. It shows that the marginal farms were more depedant upon the family labour for carrying out various agricultural operation, while the large farms incurred the huge expenses (Rs. 5907/ha) on the hired labour. Expenses on fertilisers, machine labour and seed were the other important components of the operational cost and the expenses on these were about 13, 12 and 12 per cent of the total operational cost respectively.

During the kharif season, paddy is the most important crop of the state. The results in Table 7 showed that the returns over variable cost fetched from paddy on per hectare basis were more than double on overall farms as well as all the farm categories except for the semi-medium farms. Berseem was found to be more remunerative as compared to sorghum but still the returns over variable cost were only 65 per cent as compared to the most important competing crop during the rabi season (wheat). Likewise, during the summer season, maize fodder was found to be less remunerative as compared to most important competing crop during the season i.e. maize grain. The returns over variable cost for maize fodder were only 70 per cent as compared to maize fodder during the season. Only a few farmers were growing fodder on commercial scale as these crops were found to be less remunerative than the competing paddy, wheat and maize crops. Those farmers who were either rearing the livestock or want to put the area under less time and input consuming crops were growing fodder on the commercial scale.

Processing and Marketing system for fodder crops

Only a few farmers were growing fodder on commercial scale as these crops were found to be less remunerative than the competing paddy and wheat crops. There were two marketing agencies operating in the study area which are handling the fodder sold by the growers. These are forwarding/commission agent and consumer. The most preferred source/agent was the forwarding/ commission agent. More than 51 per cent volume of the total produce was directly sold to the forwarding/ commission agent by More than 23 per cent of fodder growers. Remaining produce was directly sold to the consumers by the sorghum growers (Table 8).

The following three marketing channels were observed in sample fodder growers in the study area for disposal of their produce.

Channel-I: Producer-Forwarding agent/Commission agent-Dairy owner (Consumer).

Channel-II: Producer-Forwarding agent/Commission agent-Chaff cutter-Consumer.

Channel-III: Producer -Consumer.

In channel I, the produce was directly taken by the producer to the forwarding/commission agent, who were

forwarding the produce to the big dairy owners keeping in view the fodder demanded, through the chaff cutters. The forwarding/commission agent, charges their commission from the producer as well as from the dairy owner/buyer. The chaff cutters charges for the various services like, chaffing, weighing, packing, loading unloading, transportation etc. from the dairy owner, to whom the produce is ultimately supplied. In channel II, the chaff cutter purchases the produce from forwarding/commission agent, who charges their commission from the producer as well as buyer. The chaff cutters provide the various services like, chaffing, weighing, packing, loading unloading, transportation etc. from the consumer to whom the produce is ultimately supplied. In channel III, the produce is directly disposed of to the consumers in the village itself. In channel-I for the sale of sorghum, the producer's share in consumer's rupee was found to vary from 74 to 77 per cent for the different fodder crops. In channel-II the producer's share in consumer's rupee was about 65 to 70 per cent for different crops (Tables 9 and 10).

TABLE 8—DISPOSAL PATTERN OF FODDER CROPS, SAMPLE HOUSEHOLDS, 2008-09, PUNJAB

Particulars		Small	Semi-medium	Medium	Large
Sorghum					
l. Forwarding/commission agent					
Number		-	-	3	4
				(23.0)	(25.0)
Quantity (Qtls)		-	-	1871	976
				(960)	(880)
2. Consumer					
Number		-	-	10	12
				(77.0)	(75.0)
Quantity (Qtls)		-	-	87	132
				(40)	(120)
Total	Number	-	-	13	16
				(100.0)	(100.0)
	Quantity (Qtls)	-	-	1958	1104
				(100.0)	(100.0)
Berseem					
l. Forwarding/commission agent					
Number		2	3	-	3
		(33.0)	(30.0)		(27.0)
Quantity (Qtls)		257	2235	-	5615
		(51.0)	(82.0)	-	(89.0)
2. Consumer					
Number		4	7	-	8
		(67.0)	(70.0)	-	(73.0)
Quantity (Qtls)		250	500	-	700
		(49.0)	(18.0)	-	(11.0)
Total	Number	6	10	-	11
		(100.0	(100.0)	-	(100.0)
	Quantity (Qtls)	507	2735	-	6315
		(100.0)	(100.0)		(100.0)

TABLE 8—DISPOSAL PATTERN OF FODDER CROPS, SAMPLE HOUSEHOLDS, 2008-09, PUNJAB—*Contd.*

Particulars		Small	Semi-medium	Medium	Large
Maize					
1. Forwarding/commission agent					
Number		2	6	6	1
		(33.0)	(50.0)	(54.0)	(13.0)
Quantity (Qtls)		183	980	416	922
		(79.0)	(91.0)	(78.0)	(79.0)
2. Consumer					
Number		4	6	5	7
		(67.0)	(50.0)	(46.0)	(87.0)
Quantity (Qtls)		50	100	120	250
		(21.0)	(9.0)	(22.0)	(21.0)
Total	Number	6	12	11	8
		(100.0)	(100.0)	(100.0)	(100.0)
	Quantity(Qtls)	233	1080	536	1172
		(100.0)	(100.0)	(100.0)	(100.0)

NOTE: Number and quantity indicate number of growers selling the produce and quantity of total produce sold (in quintals) through a particular market functionary

Figures in parentheses show percentages to total number and total quantity

TABLE 9—MARKETING COSTS, MARGINS AND PRICE SPREAD ANALYSIS OF SORGHUM AND BERSEEM FODDER CROP DURING PEAK SEASON IN DIFFERENT CHANNELS PUNJAB, 2008-09

(Rs/qtl)

Particulars/channels	Small			Semi-medium			Medium			Large			Overall		
	Ch-1	Ch-2	Ch-3	Ch-1	Ch-2	Ch-3	Ch-1	Ch-2	Ch-3	Ch-1	Ch-2	Ch-3	Ch-1	Ch-2	Ch-3
Sorghum															
Net price received by the producer	-		-		-		48.0 (73.6)	48.0 (69.5)	46.0 (100.0)	46.6 (70.6)	46.6 (70.6)	43.0 (100.0)	47.4 (73.8)	47.4 (70.5)	44.0 (100.0)
Marketing costs of producer	-		-		-		9.0 (13.8)	9.0 (13.0)	-	8.4 (12.7)	8.4 (12.7)	-	8.6 (13.4)	8.6 (12.8)	-
Selling price of Prducer	.-		-		-		57.0 (87.4)	57.0 (82.5)	-	55.0 (87.0)	55.0 (83.3)	-	56.0 (87.2)	56.0 (83.3)	-
Purchase price of chaff cutter	-		-		-		-	57.0 (82.5)	-	-	55.0 (83.3)	-	-	56.0 (83.3)	-
Costs incurred by Chaff caterer	-		-		-		-	4.1 (5.9)	-	-	4.0 (6.1)	-	-	4.0 (5.9)	-
Net margins of chaff cutter	-		-		-		-	8.0 (11.6)	-	-	7.0 (10.6)	-	-	7.2 (10.7)	-
Costs incurred by Dairy owner/Consumer	-		-		-		-	8.2 (12.6)	-	-	8.2 (13.0)	-	-	8.2 (12.8)	-
Consumer's price	-		-		-	-	65.2 (100.0)	69.1 (100.0)	46.0 (100.0)	63.2 (100.0)	66.0 (100.0)	43.0 (100.0)	64.2 (100.0)	67.2 (100.0)	44.0 (100.0)
Berseem															
Net price received by the producer	39.0 (69.6)	39.0 (62.7)	38.0 (100.0)	44.5 (74.2)	44.5 (67.4)	42.5 (100.0)	-	-	-	41.2 (73.6)	41.2 (63.9)	39.5 (100.0)	41.9 (73.5)	41.9 (65.00)	40.5 (100.0)
Marketing costs of producer	9.0 (16.1)	9.0 (14.5)	-	7.5 (12.5)	7.5 (11.4)	-	-	-		6.8 (12.1)	6.8 (10.5)	-	7.1 (12.5)	7.1 (11. 00)	-
Selling price of Producer	48.0 (85.7)	48.0 (77.2)	-	52.0 (86.7)	52.0 (78.8)	-	-	-	-	48.0 (85.7)	48.0 (74.4)	-	49.0 (86.0)	49.0 (76.0)	-
Purchase price of chaff cutter	-	48.0 (77.2)	-	-	52.0 (78.8)	-	-	-	-	-	48.0 (74.40)	-	-	49.0 -	-
Costs incurred by Chaff caterer	-	4.0 (6.40)	-	-	4.0 (6.1)	-	-	-	-	-	4.0 (6.2)	-	-	4.0 (6.2)	-
Net margins of chaff cutter	-	10.2 (16.4)	-	-	10.0 (15.2)	-	-	-	-	-	12.5 (19.4)	-	-	11.5 (17.8)	-
Costs incurred by Dairy owner/Consumer	8.0 (14.3)	-	-	8.0 (13.3)	-	-	-	-	-	8.0	-	-	8.0 (14.0)	-	-
Consumer's price	56.0 (100.0)	62.2 (100.0)	38.0 (100.0)	60.0 (100.0)	66.0 (100.0)	42.5 (100.0)	-	-	-	56.0 (100.0)	64.5 (100:0)	39.5 (100.0)	57.0 (100.0)	64.5 (100.0)	40.5 (100.0)

*Includes Chaffing, Weighing, Packing, Loading/unloading, Transportation etc. charges.

Figures in parentheses show percentage of consumer 'price.

Channel-1 :Producer- Forwarding/commission agent-Dairy Owner(consumer).

Channel-2: Producer- Forwarding/commission agent -Chaff cutter- Consumer.

Channel-3: Producer-Consumer.

TABLE 10—MARKETING COSTS, MARGINS AND PRICE SPREAD ANALYSIS OF MAIZE FODDER CROP DURING PEAK SEASON IN DIFFERENT CHANNELS, PUNJAB, 2008-09

(Rs/qtl)

Particulars/channels	Small			Semi-medium			Medium			Large			Overall		
	Ch-1	Ch-2	Ch-3	Ch-1	Ch-2	Ch-3	Ch-1	Ch-2	Ch-3	Ch-1	Ch-2	Ch-3	Ch-1	Ch-2	Ch-3
Net price received by the producer	50.0 (75.3)	50.0 (69.2)	49.0 (100.0)	52.0 (76.0)	52.0 (69.3)	49.0 (100.0)	50.7 (76.4)	50.7 (68.7)	48.0 (100.0)	50.0 (76.5)	50.0 (69.3)	48.5 (100.0)	50.9 (76.7)	50.9 (70.7)	48.5 (100.0)
Marketing costs of producer	8.0 (l2.0)	8.0 (11.1)	-	8.0 (11. 7)	8.0 (10.7)	-	7.3 (11.0)	7.3 (9.9)	-	7.0 (l0.7)	7.0 (9.7)	-	7.1 (10.7)	7.1 (10.0)	-
Selling price of Producer	58.0 (87.3)	58.0 (80.2)	-	60.0, (87.7)	60.0 (80.0)	-	58.0 (87.3)	58.0 (78.6)	-	57.0 (87.2)	57.0 (78.9)	-	58.0 (87.3)	58.0 (80.6)	-
Purchase price of chaff cutter	--	58.0 (80.2)	-	-	60.0 (80.0)	-	-	58.0 (78.6)	-	-	57.0 (78.9)	-	-	58.0	- (80.6)
Costs incurred by Chaff caterer	-	4.8 (6.6)	-	-	4.8 (6.4)	-	-	4.8 (6.5)	-	-	4.7 (6.5)	-	-	4.7 (6.5)	-
Net margins of chaff cutter	-	9.5 (13.1)	-	-	10.2 (13.6)	-	-	11.0 (14.9)	-	-	10.5 (14.5)	-	-	10.1 (14.0)	-
Costs incurred by Dairy owner/Consumer	8.4 (12.7)	-	-	8.4 (12.3)	-	-	8.4 (12.7)	-	-	8.4 (12.8)	-	-	8.4 (12.7)	-	-
Consumer's price	66.4 (100.0)	72.3 ,(100.0	49.0 (100.0)	68.4 (100.0)	75.0 (100.0)	49.0 (100.0)	66.4 (100.0)	73.8 (100.0)	48.0 (100.0)	65.4 (100.0)	72.2 (100.0)	48.5 (100.0)	66.4 (100.0)	72.0 (100.0)	48.5 (100.0)

*lncludes Chaffing, Weighing, Packing, Loading/unloading, Transportation etc charges.

Figures in parentheses show percentage of consumer ‘price.

Channel-1:Producer- Forwarding/commission agent-Dairy Owner (consumer.)

Channel-2: Producer- Forwarding/commission agent -Chaff cutter- Consumer.

Channel-3: Producer-Consumer.

The practice of fodder processing is not popular in Punjab. Only less than 5 per cent of the fodder growers were found to practice it. The green fodder in the state are available throughout the year as multi cut varieties of fodder have prolonged the harvesting time of the fodder crops in the state. Besides, the dry fodder (mostly wheat straw) is easily and cheaply available in the state due to the predominance of wheat crop during the rabi season. Therefore, when the green fodder is in short supply, the dry fodder is available in the state. Even the farmers who are processing the fodder were of the view that the processed fodder is not preferably fed to the milch animals as it induces smell in the milk. Through processing, the fodder can be fed to animals as green feed; as hay, i.e. crops harvested dry or left to dry if harvested green; or as silage products. Silage or ensilage is a method of preservation of green fodder through fermentation to retard spoiling and this method of processing is more popular in Punjab as compared to hay making. This is practised during the kharif season when sorghum, bajra and chary are mixed, chaffed and put in the underground pit. The average storage capacity of the pit was found to vary between 1500 quintals for medium size farms to 3000 quintals for large size farms. The medium size farms were found to utilise about 80 per cent of the capacity, while it was cent per cent in case of large farms. The storage period was up to one year from the time of storage (July to August). Less than one per cent of the produce was found to be spoiled as the rain water enters from the corners through the sheets used. Regarding the post harvest operational cost involved in for silage making, Table 11 shows that it was about Rs. 11/q. About 74 per cent of the operational cost has to be incurred during chaffing followed by transportation (18 per cent) and pit making (about 6 per cent).

TABLE 11—POST HARVEST OPERATIONAL COSTS FOR SILAGE MAKING, SAMPLE HOUSEHOLDS, 2008-09, PUNJAB

(Rs./Q)

Particulars	Marginal	Small	Semi-medium	Medium	Large	Overall
Transportation	-	-	-	1.9 (16.5)	2.1 (19.1)	2.0 (17.7)
Chaffing	-	-	-	8.5 (73.9)	8.0 (72.7)	8.3 (73.5)
Pit making	-	-	-	0.7 (6.1)	0.7 (6.4)	0.7 (6.2)
Chemical used	-	-		0.2 (1. 7)	-	0.1 (0.9)
Sheet used	-	-	-	0.2 (1. 7)	0.2 (1.8)	0.2 (1.8)
Total	-	-	-	11.5 (100.0)	11.0 (100.0)	11.3 (100.0)

Problems faced by fodder growers

Supply of poor quality and un-recommended varieties of seed, shortage of labour especially during harvesting of the crop, lack the technical knowledge, acquisition of credit were the major problems faced by the fodder growers during production of these crops in the study area (Table 12). Low price in the market, lack of market information and delayed payment for the produce by the commission agents in the market were reported as the major marketing problem confronted by fodder growers of the study area (Table 13).

TABLE 12—PROBLEMS RELATED TO THE PRODUCTION OF FODDER CROPS, SAMPLE HOUSEHOLDS, 2008-09, PUNJAB

(% multiple response)

Particulars	Marginal	Small	Semi-medium	Medium	Large
Sorghum					
1. Seed Quality	37	24	29	36	27
2. Input delivery	-	-	-	-	-
3. Expenditure on production	-	-	-	-	-

TABLE 12—PROBLEMS RELATED TO THE PRODUCTION OF FODDER CROPS, SAMPLE HOUSEHOLDS, 2008-09, PUNJAB—*Contd.*

(% multiple response)

Particulars	Marginal	Small	Semi-medium	Medium	Large
4. Insect-pests and diseases	-	-	-	-	-
5. Technical knowledge	24	15	26	27	18
6. Access to credit	24	34	25	31	18
7. Availability and cost of labour	-	-	9	19	36
8. Any other					
Berseem					
1. Seed Quality	34	25	45	38	48
2. Input delivery	-	-	-	-	-
3. Expenditure on production	-	-	-	-	-
4. Insect-pests and diseases	-	-	-	-	-
5. Technical knowledge	31	18	25	29	31
6. Access to credit	25	29	21	34	32
7. Availability and cost of labour	-	-	9	34	36
8. Any other					
Maize					
1. Seed Quality	31	42	31	22	27
2. Input delivery	-	-	-	-	-
3. Expenditure on production	-	-	-	-	-
4. Insect-pests and diseases	-	-	-	-	-
5. Technical knowledge	31	25	24	32	24
6. Access to credit	19	24	31	21	28
7. Availability and cost of labour	-	-	21	28	39
8. Any other	22	20	23	16	7

TABLE 13—PROBLEMS RELATED TO THE MARKETING OF FODDER CROPS, SAMPLE HOUSEHOLDS, 2008-09, PUNJAB

(% multiple response)

Problem	Farm size category					
	Marginal	Small	Semi-medium	Medium	Large	Overall
Sorghum						
1. Market information	-	-	-	33	25	29
2. Output price related problems	-	-	-	33	50	43
3. Packing material	-	-	-	-	-	-
4. Packaging	-	-	-	-	-	-
5. Transportation	-	-	-	-	-	-
6. Delay in the payments	-	-	-	-	-	-
7. Marketing costs	-	-	-	-	-	-
8. Other storage facilities	-	-	-	-	-	-
9. Role of intermediaries	-	-	-	33	33	33
10. Any other	-	-	-	-	-	-

TABLE 13—PROBLEMS RELATED TO THE MARKETING OF FODDER CROPS, SAMPLE HOUSEHOLDS, 2008-09, PUNJAB—*Contd.*

(% multiple response)

Problem	Farm size category					
	Marginal	Small	Semi-medium	Medium	Large	Overall
Berseem						
1 . Market information	-	50	33	-	33	38
2. Output price related problems	-	50	33	-	-	25
3. Packing material	-	-	-	-	-	-
4. Packaging	-	-	-	-	-	-
5. Transportation	-	50	-	-	-	13
6. Delay in the payments	-	-	-	-	-	-
7. Marketing costs	-	-	-	-	-	-
8. Other storage facilities	-	-	-	-	-	-
9. Role of intermediaries	-	-	-	-	-	-
10. Any other	-	-	-	-	-	-
Maize fodder						
1. Market information	50	17	33	-	27	50
2. Output price related problems	50	33	33	-	33	50
3. Packing material	-	-	-	-	-	-
4. Packaging	-	-	-	-	.-	-
5: Transportation	50	-	-	-	6	50
6. Delay in the payments	-	-	33	-	13	-
7. Marketing costs	-	-	-	-	-	-
8. Other storage facilities	10	-	-	-	5	10
9. Role of intermediaries	-	-	-	-	-	-
10. Any other	-	-	-	-	-	-

Policy implications

To achieve the envisaged growth of 4 per cent per annum in agriculture, the dairy sector has to grow by much faster rate. To meet the ever increasing demand of milk and milk products in India, the number as well as the productivity of the animals should be increased. But as the animals are facing malnutrition, under-nutrition or both, which is due to inadequate supply of feed and fodder in the country. Due to heavy pressure of growing wheat and paddy, the area under fodder has been decreasing, and so as the composition of the live-stock population. As a viable means of diversification, cultivation of fodder should be increased along with increase in livestock population, in order to make it more productive. The higher profitability of a crossbred cow-herd unit is because of a higher milk yield. There is a tremendous possibility for increasing cow's milk production if scientific methods are used. Such an increase in buffalo's milk production is difficult, as high milk-yielding genetic stock is not available.

Farmers were suggesting to improve the quality of seedlings and frequent checks by the Department officials can help in this direction. More emphasis is needed to evolve the high yielding varieties for various fodder crops as presently these are regarded as lesser important crops. The centre government grant of Rs. 6 crore to the State Government during 2009-10 and 2010-11 for providing subsidies to purchase quality berseem seed to cattle farmers, need to be increased keeping in view the serious problem of non-availability of quality seed for various fodder crops in the state. Further, the state government

needs to use such subsidies more effectively for right cause and concern. The primary agricultural credit cooperative societies and other funding agencies should be persuaded to provide adequate short-term credit facilities to cover the operational cost. There is need to make more efforts for effective extension for these hitherto neglected crops so that the farmers may be able to know the latest know how regarding these crops. On the marketing front, most of the fodder growers were in favour of establishment of regulated markets in the region. To stabilize the prices, the farmers were in favour of establishment of better market infrastructure by the government so that the prices may not go down by the certain minimum level and they may come out of the clutches of the commission agents. The state has abundant roughage (wheat and rice crop), which can be used in making silage through processes developed and recommended by Punjab Agricultural University, Ludhiana. The centre provides a subsidy of 80 per cent for making silo pits with automatic loader. To promote the processing of fodder, these facilities are needed to be spread to more number of farmers.

RESEARCH INVENTY: International Journal of Engineering and Science
ISBN: 2319-6483, ISSN: 2278-4721, Vol. 2, Issue 1
(January 2013), PP 40-47
www.researchinventy.com

Cntfet Technology Based Precision Full-Wave Rectifier Using Ddcc

[1]Gavendra Singh, [2]Umesh Kumar, [3]Rajeev Ranjan
[1, 2, 3](Student, Delhi Technological University, Delhi)

Abstract -*This paper is the HSPICE implementation of 32nm CNTFET technology based rectifier using DDCC (differential difference current conveyor). The circuit proposes low design complexity, high temperature stability, larger bandwidth of operation and higher packaging density. The circuit also offers high input impedance and lower output impedance. Simulation result shows the performance of the circuit design validity.*

Keywords – *CMOS, CNTFET, DDCC, HSPICE, rectifier,*

I. INTRODUCTION

Full-wave rectifier is used in RF demodulator, piecewise linear function generator, AC voltmeter, watt meter, and various nonlinear analog signal processing circuits[9]. A typical rectifier realized by using diodes, cannot rectify signals whose amplitudes are less than the threshold voltage(approximately 0.7V for silicon diode and approximately 0.3 for germanium diode).As a result diode-only rectifiers are used in only those applications in which the precision in the range of threshold voltage is insignificant, such as RF demodulators and DC voltage supply rectifiers, but for applications requiring accuracy the range of threshold voltage the diode-only rectifier cannot be used be used. This can be overcome by using integrated circuit rectifiers instead. The precision rectifiers based on operational amplifier (op-amp), diodes and resistors are presented. However, the classical problem with conventional precision rectifiers based on op-amps and diodes is that during the no conduction / conduction transition of the diodes, the op-amps must recover with a finite small-signal[9][10], dv/dt, (slew-rate) resulting in significant distortion during the zero crossing of the input signal. The use of the high slew-rate op-amps does not solve this problem because it is a small signal transient problem. The gain-band width is a parameter of op-amp that limits the high frequency performance of this scheme. Moreover, since these structures use the op-amp and the resistors, it is not suitable for IC fabrication. The proposed full-wave rectifier circuit shows better precision.

In the previous works on DDCC[7] with CMOS (350nm), the circuits suffer from the problem of leakage current. Also, the design was having lower packaging density. Current-mode circuits have always been a better choice for accuracy and high frequency performances. Differential difference current conveyor (DDCC) can be counted as the combination of CCII and DDA (differential difference amplifier) with their advantages[7][9]. The DDCC implementation with carbon nanotube field effect transistor shows better high frequency performance.

Fig.1- symbol for nCNTFET (a) and pCNTFET (b)

The proposed CNTFET[2][3] features large and small signal application, a compact model of intrinsic channel[2] region of MOSFET-like single-walled carbon nanotube[1] FET. We project a 13 times CV/I improvement of the intrinsic CNTFET with (19, 0) CNT over the bulk n-type MOSFET at the 32-nm node. The electrical symbols of nCNTFET and pCNTFET are shown in fig-1.

The rest of the paper is orgnanized as followes. The section-II will be consisting of the carbon nanotube field effect transistor basic introduction with design parameters[1] and device response implementation in HSPICE. In the section-III we shalll go for the basics of differential difference current convayor(DDCC) and it performance comparision when CMOS and CNTFET technologies are used to design it(DDCC). In the section-IV, we shall go for the design of precision full-wave rectifier usign CNTFET based DDCC.

II. CNTFET TECHNOLOGY

The six-capacitor model[2][3] is shown fig.-2, assuming that all the carriers from +k branches[2] are assigned to the source and that all the carriers from −k branches[2] are assigned to the drain. The I–V characteristics of the CNTFET are shown in Fig. 3, and they are similar to those of MOSFET. The CNTFET device current is saturated at higher V_{ds} (drain-to-source voltage) as shown in Fig. 2, and the ON-current decreases due to energy quantization in the axial direction at 32 nm (or less) gate length . The threshold voltage is defined as the voltage required to turn on the transistor, and the threshold voltage of the intrinsic CNT channel can be approximated to the first order as the half bandgap, which is an inverse function of the diameter mentioned in equ.1.

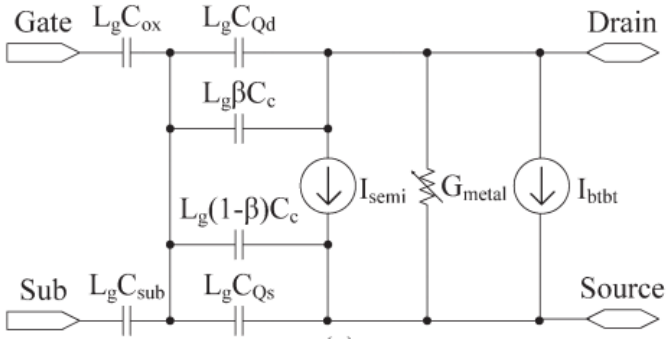

Fig 2- Six-capacitor equivalent model of CNTFET

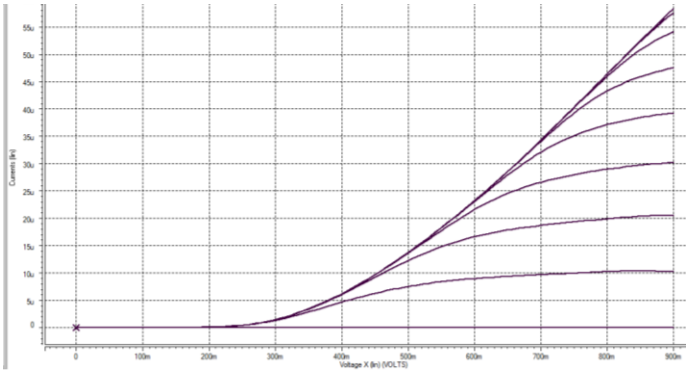

Fig3- Transfer characteristics of nCNTFET transistor

$$V_{th} \approx \frac{E_g}{2e} = \frac{\sqrt{3}}{3}\frac{aV_\pi}{eD_{CNT}} \qquad (1)$$

where a =2.49 ˚ A is the carbon-to-carbon atom distance, Vπ =3.033 eV is the carbon π–π bond energy in the tight bonding model, *e* is the unit electron charge, and DCNT is the CNT diameter. Then, the threshold voltage of the CNTFETs using (19, 0) CNTs[1] as channels is 0.289 V because DCNT of a (19, 0) CNT is 1.49 nm. Simulation results have confirmed the correctness of this threshold voltage. Parameters for design are specified as follows:

```
q=1.60e-19          $ Electronic charge
Vpi=3.033           $ The carbon PI-PI bond energy
d=0.144e-9          $ The carbon PI-PI bond distance
a=0.2495e-9         $ The carbon atom distance
pi=3.1416           $ PI, constant
h=6.63e-14          $ Planck constant,X1e20
h_ba=1.0552e-14     $ h_bar, X1e20
k=8.617e-5          $ Boltzmann constant
epso=8.85e-12       $ Dielectric constant in vacuum
Cgsub=30e-12        $ Metal gate (W) to Substrate fringe capacitance per unit length, approximated as
                      30af/um, with 10um thick SiO2 default 30e-12
Cgabove=27e-12      $ W local interconnect to M1 coupling capacitance, 500nm apart, infinite large plane
                      default 27e-12
Cc_cnt=26e-12       $ The coupling capacitance between CNTs with 2Fs=6.4nm, about 26pF/m
Ccabove=15e-12      $ Coupling capacitance between CNT and the above M1 layer, 500nm apart, default
                      15e-12
Cc_gate=78e-12      $ The coupling capacitance between gates with 2F=64nm, about 78pF/m, W=32nm,
                      H=64nm, contact spacing 32nm default 78e-12
Ctot='Cgsub+Cgabove+Cc_gate+Cc_gate'   $ total coupling capacitance for gate region
Lceff=200e-9        $ The mean free path in intrinsic CNT, estimated as 200nm
phi_M=4.5           $ Metal work function default=4.6
phi_S=4.5           $ CNT work function
```

III. THE DDCC DEVICE

The electrical symbol of DDCC[8] is shown in Fig-3(a). It has three voltage input terminals: Y1, Y2and Y3, which have high input impedance. Terminal X is a low impedance current input terminal. There is a high impedance current output terminal Z. . The input-output characteristics of ideal DDCC are described in fig-3(b).

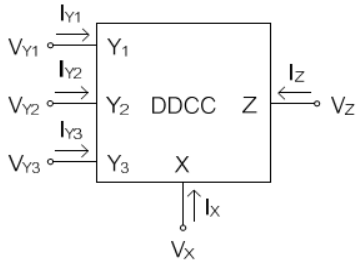

(a)

(b)

$$\begin{pmatrix} V_X \\ I_{Y1} \\ I_{Y2} \\ I_{Y3} \\ I_Z \end{pmatrix} = \begin{pmatrix} 1 & -1 & 1 & 0 \\ 0 & 0 & 0 & 0 \\ 0 & 0 & 0 & 0 \\ 0 & 0 & 0 & 0 \\ 0 & 0 & 0 & 1 \end{pmatrix} \begin{pmatrix} V_{Y1} \\ V_{Y2} \\ V_{Y3} \\ I_X \end{pmatrix}$$

Fig 3. DDCC ciruit symbol(a) and characteristics(b)

the circuit diagram for the DDCC device(CNTFET Technology based) is shown in fig-4 where pCNTFET and nCNTFET can be replace by pMOS and nMOS respectivily for MOS based device implentation.

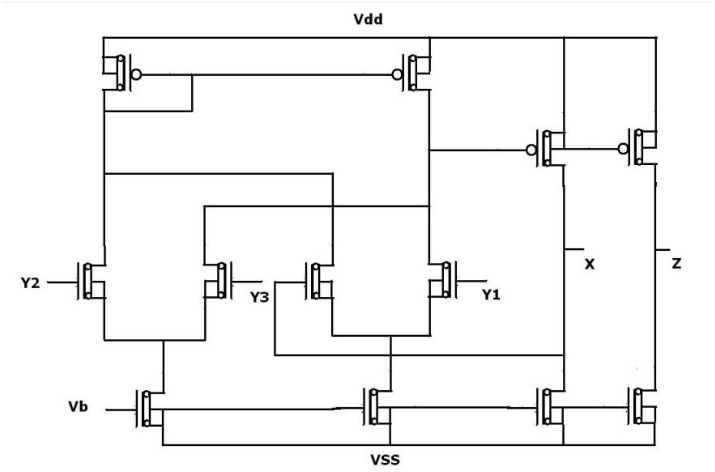

Fig4- circuit diagram of DDCC

The characteristics of the DDCC device can be view in fig.-5 where V_x vs. $V_y1$has been indicated with parametric analysis with respect to V_{y2}.

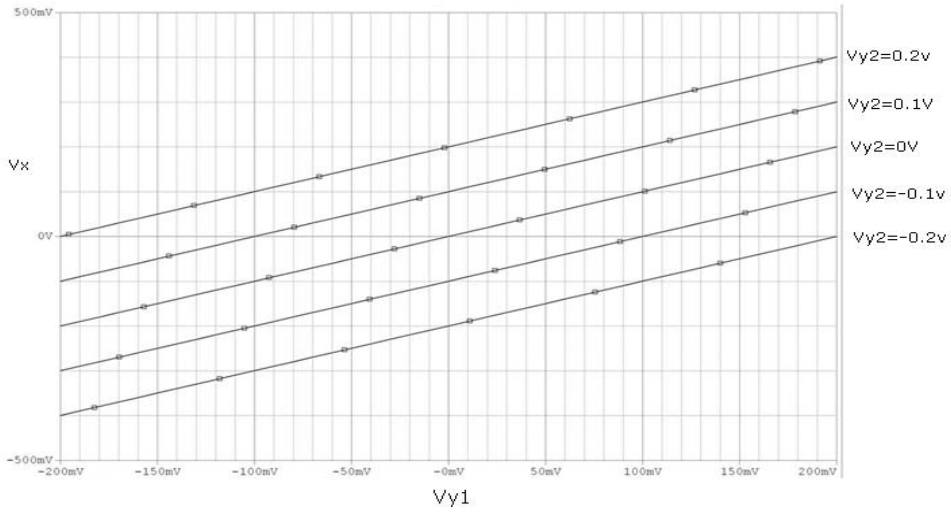

Fig. 5- Input-output characteristics of DDCC

The ciruit realization in HSPICE[2][3] can be done with following program:

```
.TITLE 'ddcc_CNFET'
*****************************************************
*For optimal accuracy, convergence, and runtime
*****************************************************
.options POST
.options AUTOSTOP
.options INGOLD=2     DCON=1
.options GSHUNT=1e-12 RMIN=1e-15
.options ABSTOL=1e-5  ABSVDC=1e-4
.options RELTOL=1e-2  RELVDC=1e-2
.options NUMDGT=4     PIVOT=13

.param   TEMP=27
*****************************************************
*Include relevant model files
*****************************************************
```

```
.lib 'CNFET.lib' CNFET
**************************************************
*Beginning of circuit and device definitions
**************************************************

*Some CNFET parameters:
.param Ccsd=0      CoupleRatio=0
.param m_cnt=1     Efo=0.6
.param Wg=0        Cb=40e-12
.param Lg=32e-9    Lgef=100e-9
.param Vfn=0       Vfp=0
.param m=19        n=0
.param Hox=4e-9    Kox=16

********************************************************************************
* Define power supply
********************************************************************************
* DUMMY VOLTAGE SOURCE
*V1 11 0 DC 0.3V
v2 5 0 dc 0V
v3 8 0  dc 0v
vb 6 0 dc -0.7v

*sin voltage sources for transient analysis
V1 11 0 sin 0 0.2V 1khz
*V2 5 0 sin 0 0.3V 1khz
*V3 6 0 sin 0 0.3V 1khz

*ac source for ac sweep analysis
*V1 11 0 ac  0.2V

* APPLIED VOLTAGE
VDD 1 0 DC 0.9V
VSS 0 2 DC 0.9V

********************************************************************************
* Main Circuits
********************************************************************************

M1 4 5 7 7 NCNFET Lch=Lg  Lgeff='Lgef' Lss=32e-9  Ldd=32e-9
+ Kgate='Kox' Tox='Hox' Csub='Cb' Vfbn='Vfn' Dout=0  Sout=0  Pitch=20e-9  n1=m  n2=n  tubes=3

M2 9 8 7 7 NCNFET Lch=Lg  Lgeff='Lgef' Lss=32e-9  Ldd=32e-9
+ Kgate='Kox' Tox='Hox' Csub='Cb' Vfbn='Vfn' Dout=0  Sout=0  Pitch=20e-9  n1=m  n2=n  tubes=3

M3 4 12 10 10 NCNFET Lch=Lg  Lgeff='Lgef' Lss=32e-9  Ldd=32e-9
+ Kgate='Kox' Tox='Hox' Csub='Cb' Vfbn='Vfn' Dout=0  Sout=0  Pitch=20e-9  n1=m  n2=n  tubes=3

M4 9 11 10 10 NCNFET Lch=Lg  Lgeff='Lgef' Lss=32e-9  Ldd=32e-9
+ Kgate='Kox' Tox='Hox' Csub='Cb' Vfbn='Vfn' Dout=0  Sout=0  Pitch=20e-9  n1=m  n2=n  tubes=3

M5 4 4 1 1 PCNFET Lch=Lg  Lgeff='Lgef' Lss=32e-9  Ldd=32e-9
+ Kgate='Kox' Tox='Hox' Csub='Cb' Vfbp='Vfp' Dout=0  Sout=0  Pitch=20e-9  n1=m  n2=n  tubes=3

M6 9 4 1 1 PCNFET Lch=Lg  Lgeff='Lgef' Lss=32e-9  Ldd=32e-9
+ Kgate='Kox' Tox='Hox' Csub='Cb' Vfbp='Vfp' Dout=0  Sout=0  Pitch=20e-9  n1=m  n2=n  tubes=3

M7 12 9 1 1 PCNFET Lch=Lg  Lgeff='Lgef' Lss=32e-9  Ldd=32e-9
```

```
+ Kgate='Kox' Tox='Hox' Csub='Cb' Vfbp='Vfp' Dout=0  Sout=0  Pitch=20e-9  n1=m  n2=n  tubes=3

M8 13 9 1 1 PCNFET Lch=Lg  Lgeff='Lgef' Lss=32e-9  Ldd=32e-9
+ Kgate='Kox' Tox='Hox' Csub='Cb' Vfbp='Vfp' Dout=0  Sout=0  Pitch=20e-9  n1=m  n2=n  tubes=3

M9 7 6 2 2 NCNFET Lch=Lg  Lgeff='Lgef' Lss=32e-9  Ldd=32e-9
+ Kgate='Kox' Tox='Hox' Csub='Cb' Vfbn='Vfn' Dout=0  Sout=0  Pitch=20e-9  n1=m  n2=n  tubes=3

M10 10 6 2 2 NCNFET Lch=Lg  Lgeff='Lgef' Lss=32e-9  Ldd=32e-9
+ Kgate='Kox' Tox='Hox' Csub='Cb' Vfbn='Vfn' Dout=0  Sout=0  Pitch=20e-9  n1=m  n2=n  tubes=3

M11 12 6 2 2 NCNFET Lch=Lg  Lgeff='Lgef' Lss=32e-9  Ldd=32e-9
+ Kgate='Kox' Tox='Hox' Csub='Cb' Vfbn='Vfn' Dout=0  Sout=0  Pitch=20e-9  n1=m  n2=n  tubes=3

M12 13 6 2 2 NCNFET Lch=Lg  Lgeff='Lgef' Lss=32e-9  Ldd=32e-9
+ Kgate='Kox' Tox='Hox' Csub='Cb' Vfbn='Vfn' Dout=0  Sout=0  Pitch=20e-9  n1=m  n2=n  tubes=3

*.DC V2 -0.3 0.3 0.001
*+LIN V1 -0.3 0.3 0.1

.tran 0 10ms 1u

*.ac dec 10 1 100G
.probe
.end
```

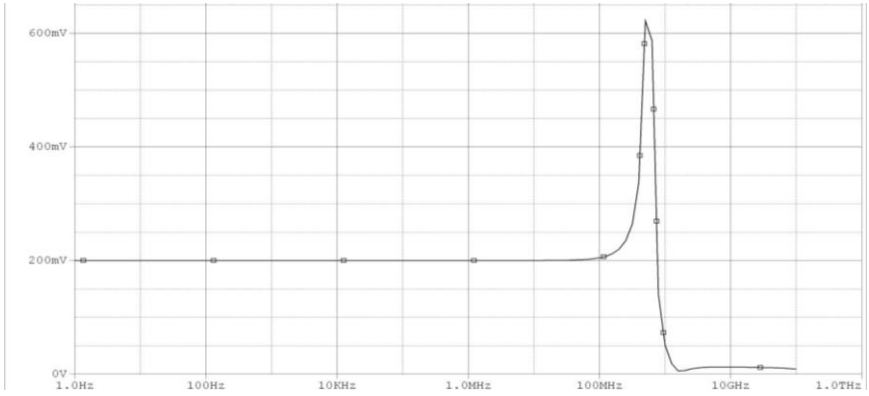

(a)

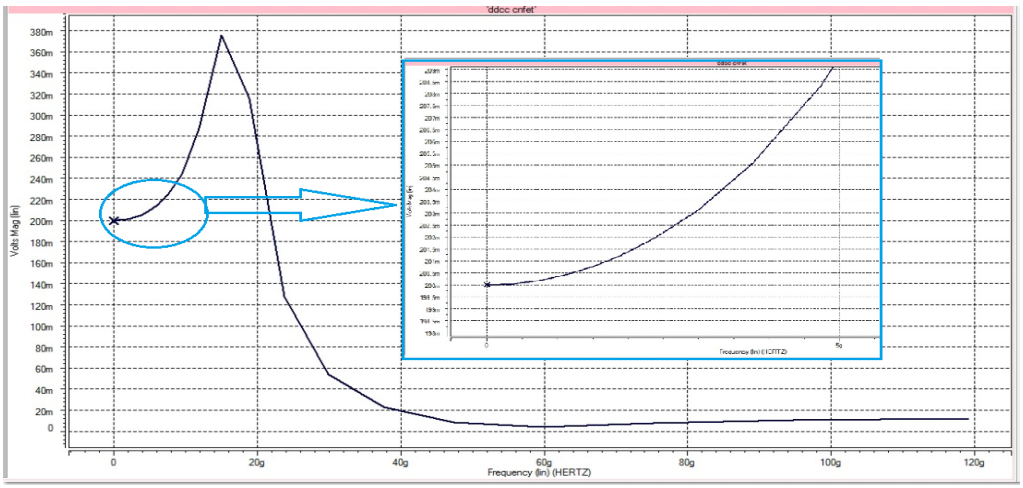

(b)

Fig 6– AC characteristics of the DDCC (a) using MOS (350nm) technology having voltage consistencyof 4.5% for 200mV, upto 100MHz and (b)using CNTFET having voltage consistencyof 4.5% for 200mV, upto 5GHz.

In the fig-6 even though the response of the CNTFET based DDCC device doesn't have good high frequency response but upto 5 GHz it has a good voltage consistency comparitively the CMOS (350nm) technology.

IV. CIRCUIT REALIZATION OF PRECISION FULL-WAVE RECTIFIER

The full-wave rectifier circuit is shown fig- 7. This circuit uses only two DDCCs[4].The positive output voltage of the DDCC1 is connected to the negative output voltage of the DDCC2.

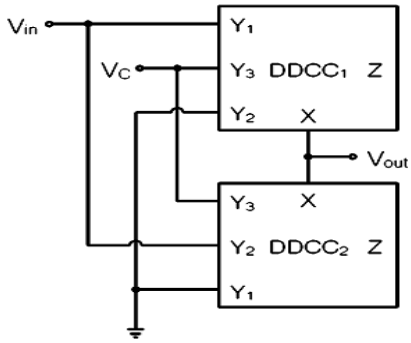

Fig.7. Full wave Rectifier circuit

The full-wave operation is as follows:

When Vin>0, the voltage Vin is followed by the DDCC1 to the voltage Vout at X terminal while the DDCC2 is tum-off. In addition, whenVin<0, the voltage Vin is followed by the DDCC2 to the voltage Vout at X terminal while the DDCC1 is cut-off .From the operation of the given full-wave rectifier explained.,the relations between the input voltageVin, and the output voltageVout, can be expressed as

$V_{in} > 0$; $V_{out}=V_{in}$: $DDCC_1$= on

$V_{in} < 0$; $V_{out}= -V_{in}$: $DDCC_2$=on

The complete output voltage of Fig.4 can be expressed as

$V_{out}= | V_{in}|$

Therefore, the given circuit provides the full-wave rectification[9]. Vc is auxiliary voltage. The circuit performance is shown in fig-8.

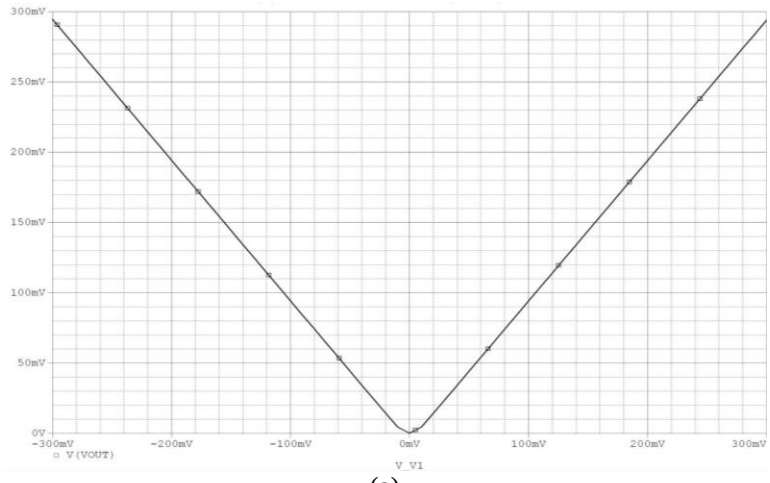

(a)

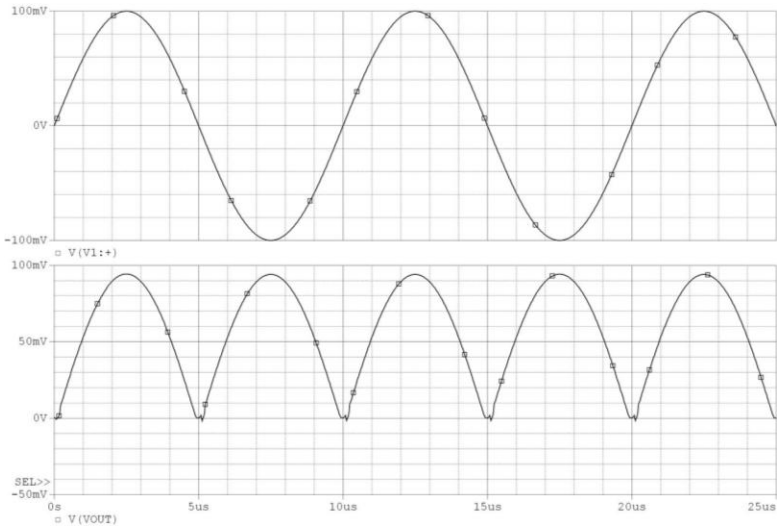

(b)

Fig. 8-precision full-wave rectifier response (a) and (b)

From above it is obvious that this rectifier can rectify any signal as low as 5 mv whereas for conventional rectifiers like full-wave rectifier[10][11] the minimum applied voltage should be above the Knee voltage of the semiconductor material being used (which is 0.7 V for silicon and 0.3v for germanium). This is a significant advantage of this circuit.

V. CONCLUSION

Realization of DDCC block is done with 50 times improved frequency response using carbon nanotube field effect transistor (single-walled-MOSFET like CNTFET). This DDCC has higher temperature stability, very high device density, high input impedance and low output impedance hence it easy to drive loads without using a buffering device. The implementation of precision full-wave amplifier has been successfully achieved. It can be applied in various non- linear analog signal processing circuits. The performance of the proposed circuit is confirmed from HSPICE simulation results. Since the CNTFET technology works on 0.9 Vdc drive voltage, the circuit is very power efficient.

REFERENCES

[1] M. S. Dresselhaus, G. Dresselhaus, R. Saito "PHYSICS OF CARBON NANOTUBE"1995 *Elsevier Science Ltd.*

[2] J. Deng and H.-S. P. Wong, "A compact SPICE model for carbon nanotube field effect transistors including non-idealities and its application—Part I: Model of the intrinsic channel region," *IEEE Trans. Electron Devices, vol. 54, no. 12, pp. 3186–3194, Dec. 2007.*

[3] J. Deng and H.-S. P. Wong, "A compact SPICE model for carbon nanotubefield effect transistors including non-idealities and its application—Part II: Full device model and circuit performance benchmarking," *IEEE Trans. Electron Devices, vol. 54, no. 12, pp. 3195–3205, Dec. 2007.*

[4] Kumngern, M.; Saengthong, P.; Junnapiya, S. "DDCC-based full-wave rectifier" *5th International Colloquium on Signal Processing & Its Applications, 2009. CSPA 2009.*

[5] B. Gilbert, "Translinear circuit: a proposed classification," *Electronics Letters, vol. 11, pp. 14-16, 1975.*

[6] E. W. Greeneich, "Analog integrated circuit," *Chapman & Hall, New York, 1997.*

[7] M. Kumngern and K. Dejhan, "DDCC-based quadrature oscillator with grounded capacitors and resistors," *Active and Passive Electronic Components, vol. 2009, pp. 1-5, 2009, doi:10.1155/2009/987304.*

[8] Usa Torteanchai, Montree Kumngern, Kobchai Dejhan "A CMOS Log-Antilog Current Multiplier/ Divider Circuit Using DDCC" *TENCON 2011 - 2011 IEEE Region 10 Conference.*

[9] S. J. G. Gift, "A high-performance full-wave rectifier circuit" *International Journal of Electronics,vol.89,pp.467-476,2000.*

[10] C.Toumazou, F. J. Lidgey,and S. Chattong, "High frequency current conveyor precision full-wave rectifier"*ElectronicsLetters,vol.30,pp. 745-746,1994.*

[11] Z. Wang, "Full-wave precision rectification that is performed in current domain and very suitable for CMOS implementation" *IEEE Transactions on Circuits and systems-I,vol.39, pp.456-462,1992.*

ARTICLE IN PRESS

Optics Communications ▮ (▮▮▮▮) ▮▮▮–▮▮▮

Contents lists available at SciVerse ScienceDirect

Optics Communications

journal homepage: www.elsevier.com/locate/optcom

Design of large-mode-area three layered fiber structure for femtosecond laser pulse delivery

Babita [a,*], Vipul Rastogi [a], Ajeet Kumar [b]

[a] Department of Physics, Indian Institute of Technology Roorkee, Roorkee 247 667, India
[b] Department of Applied Physics, Delhi Technological University, New Delhi 110 042, India

ARTICLE INFO

Article history:
Received 29 September 2012
Received in revised form
26 November 2012
Accepted 27 November 2012

Keywords:
Optical fiber
Ultra-short pulse
Large-mode-area
Femtosecond laser pulse delivery
Pulse propagation
High peak power

ABSTRACT

This paper presents three layered fiber that has been designed for delivering pulses of 100-fs through the fundamental mode. Design of the fiber ensures no intermodal coupling, low bending loss, and high fabrication tolerances while maintaining large-mode-area. We numerically demonstrate propagation of 55.5-kW peak power, 1550-nm wavelength, 100-fs duration laser pulse through fundamental mode of 4-m long fiber having mode area of 1900 μm^2. Mode stability while propagation through the fiber has been ascertained by keeping enough spacing between the effective indices of LP_{01} and LP_{11} modes. Distortion-free propagation of the pulse has been achieved by keeping ratio of dispersion to nonlinear length close to 1.

1. Introduction

We propose a design of three layer fiber structure for distortion-free delivery of high peak power ultra-short laser pulses over a distance of few meters. In several applications it is advantageous to deliver ultra-short pulses (USPs) through an optical fiber over a distance of few meters to some specific location. One such example is biological basic research and clinical applications, which require miniaturized microscopes and multi-photon endoscopes to image living cells and intact tissues [1,2]. Multi-photon imaging systems that use free space optics are cumbersome in design, non-compact and difficult to maintain. This limits the use of free space optics multi-photon systems in the medical field. An aforementioned optical fiber which can deliver high peak power ultra-short pulses is attractive for aforementioned applications to develop flexible and miniaturized instruments. However, nonlinear effects, optical damage threshold and dispersion in a conventional optical fiber make distortion-free transport of high-peak-power ultra-short pulses difficult. Femtosecond pulses, which are usually used in these applications, have peak power in kW regime even with moderate energy. When these pulses pass through the small core of a conventional fiber, optical power density reaches up to GW/cm^2. At these high power densities optical damage can occur and nonlinearity can distort the pulse by self phase modulation (SPM). One way to avoid SPM is to reduce optical power density by using large-core fibers. In conventional large-core fibers intermodal dispersion significantly distorts ultra-short pulses. Moreover, the beam quality in a multi-mode fiber is not good due to the presence of several modes. To preserve the pulse during propagation through the fiber, one needs to compensate for or minimize dispersive and nonlinear effects. Dispersion can be compensated by suitable frequency chirp on input pulses. One approach to reduce nonlinearity is to increase mode area by increasing the core size and correspondingly decreasing the numerical aperture (NA) while maintaining single-mode operation. While decrease in NA yields extremely high bending loss because of weak mode confinement, increase in core radius leads to multi-mode cross-coupling and conflicts with single-mode operation, which is necessary for high resolution microscopy. To circumvent this problem specialty optical fibers are used for the transport of such high-peak-power ultra-short pulses. Some of these fibers are photonic crystal fibers (PCFs) [3,4], rod-type fibers [5], and few-mode fibers [6,7,8]. PCF can show efficient single-mode operation and can maintain good beam quality in the output pulses. However, in PCFs because of large core, intermodal spacing is not large enough and mode coupling remains an issue. Rod type fiber has also been introduced for delivery of high-peak-power USPs [5]. These fibers maintain single mode operation with large mode area. However, inflexibility of the fiber remains an issue in

* Corresponding author.
E-mail address: babitaphy@gmail.com (Babita).

0030-4018/$ - see front matter © 2012 Elsevier B.V. All rights reserved.
http://dx.doi.org/10.1016/j.optcom.2012.11.092

compact packaging and in miniaturization. Recently, Ramachandran et al. have demonstrated delivery of high-peak-power ultrashort pulses using higher order mode fibers [6]. These fibers show very large-mode-area up to 3200 μm^2 by selective excitation of higher-order-mode. Enough intermodal spacing reduces the possibility of modal cross coupling [7]. But this technique uses long period grating for mode conversion which increases the complexity of the system.

In this paper we propose a design of three layered fiber structure for delivery of high energy fs-pulses through the fundamental mode of the fiber. The design is not susceptible to mode coupling and has sufficiently low bending loss. The modal purity at the output is maintained by leaking out higher order modes. In the proposed structure LP_{01} and LP_{11} modes are guided whereas all the other modes are leaked out owing to their high leakage loss. A sufficiently large index difference between the LP_{01} and LP_{11} modes ensured in the design prevents coupling between them. We numerically demonstrate distortion-free propagation of 100-fs, 55.5-kW peak power laser pulses over 4-m length of the fiber with mode area of about 1900 μm^2.

2. Fiber design

Laser pulses when propagate through the fiber are affected by material dispersion and nonlinearities induced by their confinement to small core of the waveguide. Even a moderate peak power pulse gets distorted during propagation through the fiber because of nonlinearities and dispersion. Distortion-free propagation of USPs in a fiber requires a balance between pulse broadening due to dispersion and pulse distortion due to SPM. These effects are usually characterized by the two parameters called dispersion length L_D and nonlinear length L_{NL} and are given by the following equations [10]:

$$L_D = -\frac{2\pi c}{\lambda_0^2}\frac{\tau^2}{D} \text{ and } L_{NL} = \frac{A_{eff}\lambda}{2\pi nP} \tag{1}$$

where c is the speed of light in vacuum, τ is the pulse duration, λ_0 is the center wavelength, A_{eff} is the effective mode area, n is the nonlinear refractive index of the fiber material, and P is the peak power. D is the fiber dispersion and is defined as

$$D = -\frac{\lambda_0}{c}\frac{d^2 n_{eff}}{d\lambda_0^2} \tag{2}$$

where n_{eff} is the propagation constant of the mode of the fiber. In order to avoid nonlinear effects during propagation of high energy ultra-short pulses, one requires very high values of A_{eff}. Scaling up the core dimensions of the fiber for high energy USP propagation requires lowering the numerical aperture (NA) of the fiber. This makes the fiber susceptible to mode instability due to mode-coupling and high bend loss. The mode coupling effects limit the mode area in a low NA fiber to 800 μm^2 [6]. It is preferred to have spacing between the adjacent modes, $\delta_{neff} = n_{eff}(LP_{0\,m}) - n_{eff}(LP_{1\,m})$, greater than 1.5×10^{-4} to avoid mode-coupling [8]. In PCF this spacing is 1×10^{-4} while in higher order mode (HOM) fibers this can go up to 5×10^{-4} [7]. In the aforementioned applications typical length of the fiber used is couple of meters and sensitivity to bends should not be large for bending radii larger than 20 cm [9]. Therefore, it is critical to design a fiber having single-mode operation with large A_{eff}, low bend loss and sufficient mode spacing to avoid intermodal coupling.

To address the issues stated above we have designed a three layered fiber structure with core refractive index n_1, depressed cladding index n_2, and outer cladding index n_s. The refractive index profile along with the mode intensity profile of the fiber is shown in Fig. 1. The outer clad of the fiber can be realized by pure silica, the core can be realized by Ge up doping and the depressed cladding can be made by F down doping. Relative index difference of the core and the depressed cladding regions relative to pure silica (n_s), are defined as $\Delta_1 = (n_1^2 - n_s^2)/(2n_1^2)$ and $\Delta_2 = (n_s^2 - n_2^2)/(2n_s^2)$. The various parameters of the designed fiber are given as

$$a = 30\ \mu m;\ b = 15\ \mu m;\ c = 17.5\ \mu m;\ D_1 = 0.03\% \text{ and } D_2 = 0.08\%,\ \lambda = 1550\ nm \tag{3}$$

where a is core radius of the fiber, b is width of the depressed cladding and c is the width of the outermost layer. The fiber supports several modes owing to large value of the core radius. The values of Δ_1 and Δ_2 are so chosen as to make all the modes leaky except LP_{01} and LP_{11} modes. Such values of index difference can be realized by standard fabrication technique [11]. We have used transfer matrix method (TMM) to analyze the modal properties of the fiber [12]. For the above mentioned designed parameters the fiber introduces 8.2 dB/m leakage loss to LP_{02} which is large enough to strip off the mode within 2.5 m length of the fiber by introducing 20 dB loss. The depressed cladding index and width are so chosen as to have sufficiently large A_{eff} while maintaining the mode stability. A_{eff} of the fundamental mode has been calculated using Gaussian approximation [13]. Variation in A_{eff} and mode stability with Δ_1 is shown in Fig. 2. An increase in Δ_1 confines more power inside the core and also increases intermodal spacing that causes decrease in the A_{eff} and the increase in δ_{neff} of the designed fiber. Here δ_{neff} is mode spacing between LP_{01} and LP_{11} mode of the designed fiber. The value of Δ_1 is so chosen as to have value of A_{eff} as large as 1900 μm^2. We have also studied the effect of variation in Δ_2 on A_{eff} and δ_{neff} as shown in Fig. 3. When we increase Δ_2, the depressed cladding index goes down and confinement of the power in the core increases. This results in a decrease in A_{eff} whereas an increase in δ_{neff}. We see from Figs. 2 and 3 that by decreasing the values of Δ_1 and Δ_2 we could have achieved even larger A_{eff} than 1900 μm^2 with sufficient mode spacing. However we have chosen values of Δ_1 and

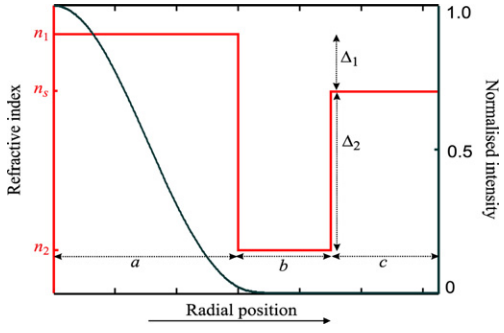

Fig. 1. Refractive index profile of the fiber along with normalized intensity profile of fundamental mode.

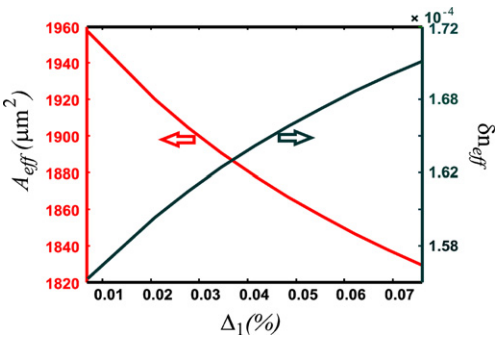

Fig. 2. Variation in A_{eff} and mode stability with Δ_1.

Please cite this article as: Babita, et al., Optics Communications (2012), http://dx.doi.org/10.1016/j.optcom.2012.11.092

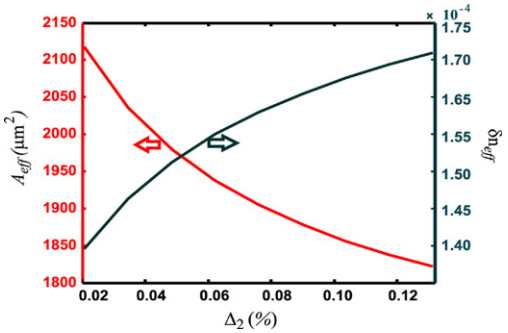

Fig. 3. Variation in A_{eff} and mode stability with Δ_2.

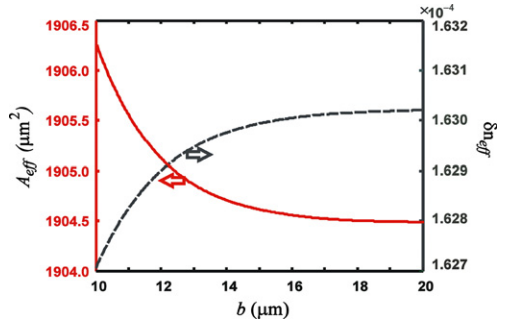

Fig. 4. Variation in A_{eff} and mode stability with b.

Δ_2 in such a way that except LP_{01} and LP_{11} all the modes are leaky and index contrast can be achieved with standard fabrication technique. To achieve maximum A_{eff} with sufficiently large δ_{neff} we have also studied the effect of variations in b on A_{eff} and δ_{neff} as shown in Fig. 4. One can see that variations in b do not cause significant change in A_{eff} and δ_{neff} and the fiber shows good tolerance towards variations in b. The effective area of the fundamental mode of the fiber, thus, designed and represented by parameter given in Eq. (3) is 1900 μm² and δ_{neff} is 1.63×10^{-4}, which is higher than those shown by PCF [8] and ensures mode stability. Dispersion is also an important property of the fiber design as higher order dispersive effects can distort ultra-short optical pulses in both the linear and nonlinear regime. Nonlinear effects in fiber show different behavior depending on the sign of the dispersion coefficient. Dispersion (D) of the fundamental mode of the fiber has been calculated by Eq. (2). Variation of D with wavelength is shown in Fig. 5. In view of ultra-short duration of the pulses, we have also calculated the third order dispersion coefficient β_3. The value of D at 1550-nm center wavelength is +21.7 ps/(nm km) which helps in balancing the nonlinear effects. β_3 is of the order of 10^{-4} and has insignificant effect for propagation over a few meters length of the fiber considered here. The macrobending loss of the fiber has been calculated by using the following formula [14,15]:

$$\alpha_{macro} = \frac{10}{\log_e 10}\left(\frac{\pi V^8}{16aR_bW^3}\right)^{1/2}\exp\left(-\frac{4R_bW^3\Delta_1}{3aV^2}\right)\frac{\left[\int_0^\infty (1-g)Er\,dr\right]^2}{\int_0^\infty E^2 r\,dr} \tag{4}$$

where E is the radial part of the field of the fundamental mode, R_b is the bending radius, a is core radius of the fiber. Other parameters of Eq. (4) are given as

$$g = \begin{cases} 0, & 0<r<a \\ \frac{n_1-n_2}{n_1-n_s}, & a<r<b \\ 1, & r>b \end{cases} \tag{5}$$

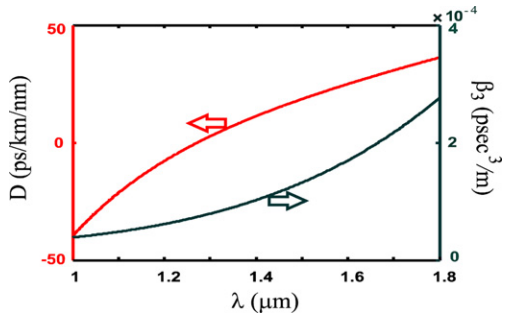

Fig. 5. Variation in dispersion and β_3 with wavelength.

and

$$V = k_0 a\sqrt{n_1^2-n_2^2};\ W = a\sqrt{\left(\beta^2-(k_0n_2)^2\right.} \tag{6}$$

The fiber shows bend loss of 0.008 dB/m at 5-cm bend radius. The fiber has negligible loss for bending radii occurring in applications like multi-photon microscopy.

3. Discussion and analysis

Pulse propagation through the fiber can be characterized by parameter L_D/L_{NL}, where L_D and L_{NL} are defined by Eq. (1). When $L_D/L_{NL}<1$, pulse evolution along the fiber is dominated by dispersion and pulse will get broaden in absence of any chirp otherwise it stretches or compresses in time, depending on the sign of initial chirp. However, if $L_D/L_{NL}>1$ then nonlinearity dominates during the evolution of the pulse and pulses suffer spectral narrowing or broadening and do not retain the original shape. In order to avoid nonlinearities, one needs to limit peak power to make L_{NL} larger than L_D. It makes sure that linear stretching happens in shorter time so that the nonlinear interactions do not build up. However, if $L_D/L_{NL}\sim1$ dispersion D is balanced by the nonlinear effect of SPM, and fundamental soliton propagation can occur. If a hyperbolic secant pulse is launched inside an ideal lossless fiber, then the pulse having width τ and peak power P_0 propagates undistorted without change in shape for long distances. Quantitatively the peak power required for fundamental soliton propagation is given by [10]

$$P_0 = \frac{\lambda_0^3 DA_{eff}}{4\pi^2 cn\tau^2} \tag{7}$$

In the proposed fiber design, the dispersion at 1550-nm center wavelength is 21.7 ps/(nm km), the peak power for soliton propagation of 100-fs pulse is 55.5 kW, where we have used $n=2.4\times10^{-20}$ m²/W [16]. To study pulse dynamics through the fiber we have launched a secant-hyperbolic un-chirped pulse into the fiber and studied its propagation dynamics by solving the nonlinear Schrödinger equation by split step Fourier method [10]. In the simulation of pulse propagation through the fiber, we have considered second order group velocity dispersion (GVD), third order dispersion, SPM and transmission loss of 0.2 dB/km. Since the pulses are of the order of 100-fs duration, we have also taken into account self-steepening and Raman scattering. We have estimated Raman scattering by parameter τ_R which has value T_R/τ, T_R being Raman time constant. We have considered value of T_R as 3 fs at 1550-nm wavelength [10]. Self-steepening has been taken into account by parameter $s=1/(\omega_0\tau)$, where ω_0 is central frequency of the pulse. Evolution of the sech pulse through 4-m length of the fiber is shown in Fig. 6(a) and the corresponding contour plot is shown in Fig. 6(b). Chirping due to nonlinearity and chirping due to dispersion cancel each other which results in a near distortion free propagation of the pulse through 4-m length of the fiber and can

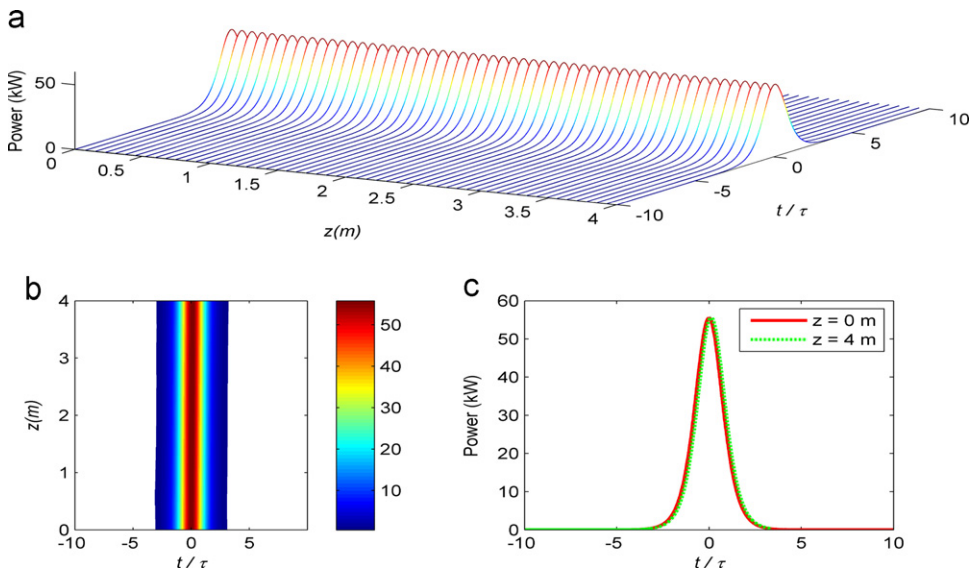

Fig. 6. (a) Propagation of a sech pulse in the fiber, (b) corresponding contour plot, (c) input and output temporal profiles of sech pulse.

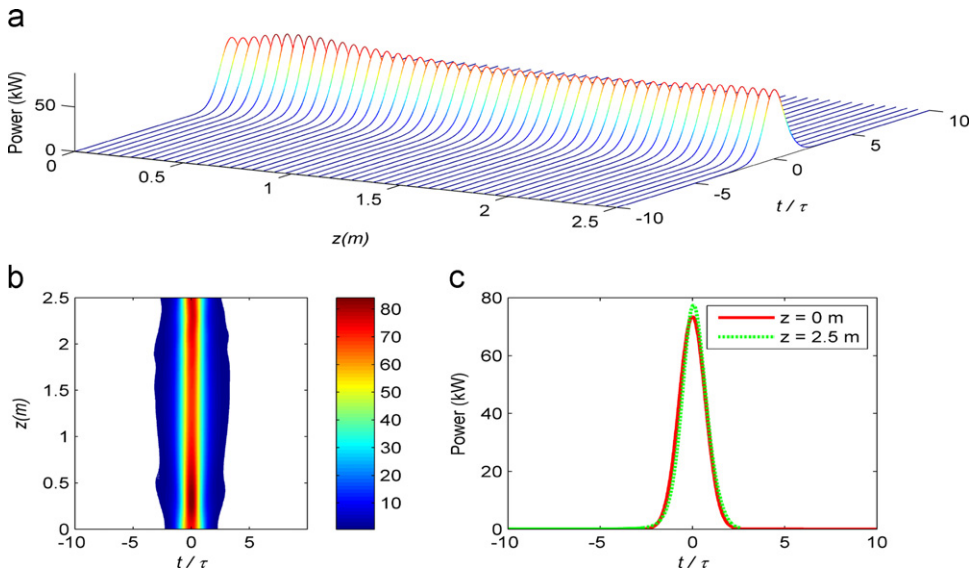

Fig. 7. (a) Propagation of a Gaussian pulse in the fiber, (b) corresponding contour plot, (c) input and output temporal profiles of the Gaussian pulse.

also be seen in Fig. 6(c). Apart from the sech soliton solution, we have also studied the propagation of a Gaussian pulse through the fiber. A 100-fs Gaussian pulse has been propagated through the fiber and its peak power has been adjusted to 73.5 kW so as to obtain near distortion free propagation. The pulse evolution along with the contour plot is shown in Fig. 7(a) and (b), respectively. We can see that the pulse tries to attain balance between the nonlinearity and dispersion and fluctuates between the broadened state and the compressed state. The fluctuations, however, are not pronounced and the propagation is near distortion free over 2.5-m length of the fiber. The temporal profiles of the Gaussian-shaped pulses at the input and output end of the fiber are shown in Fig. 7(c) which shows that pulse of the shape is retained with slight compression.

4. Conclusion

A three layered fiber design having mode area 1900 μm^2 has been proposed for the delivery of high power femtosecond laser pulses. The modal purity at the output has been maintained by leaking out HOM except LP_{11}. Mode stability has been ensured sufficient mode spacing between LP_{01} and LP_{11} modes ensures mode stability. We have numerically demonstrated the near distortion-free propagation of 100-fs, 55.5-kW peak power sech pulses and 73.5-kW peak power Gaussian pulses over 4.0-m and 2.5-m lengths of the fiber respectively. The fiber should be a good candidate for ultra-short high peak delivery.

References

[1] W. Denk, J.H. Strickler, W.W. Webb, Science 248 (1990) 73.
[2] W.R. Zipfel, R.M. Williams, W.W. Webb, Nature Biotechnology 21 (2003) 1369.
[3] S.P. Tai, M.C. Chan, T.H. Tsai, S.H. Guol, L.J. Chen, C.K. Sun, Optics Express 12 (2005) 6122.
[4] X. Peng, M. Mielke, T. Booth, Optics Express 19 (2011) 923.
[5] Y. Zaouter, D.N. Papadopoulos, M. Hanna, J. Boullet, L. Huang, C. Aguergaray, F. Druon, E. Mottay, P. Georges, E. Cormier, Optics Letters 33 (2008) 107.
[6] J.W. Nicholson, S. Ramachandran, S. Ghalmi, M.F. Yan, P. Wisk, E. Monberg, F.V. Dimarcello, Optics Letters 31 (2006) 3191.

Please cite this article as: Babita, et al., Optics Communications (2012), http://dx.doi.org/10.1016/j.optcom.2012.11.092

[7] S. Ramachandran, J.W. Nicholson, S. Ghalmi, M.F. Yan, P. Wisk, E. Monberg, F.V. Dimarcello, Optics Letters 31 (2006) 1797.
[8] S. Ramachandran, S. Ghalmi, M. F. Yan, P. Wisk, E. Monberg, F. V. Dimarcello, Scaling to ultra-large-Aeff using higher-order-mode fibers, in: Proceedings of Conference on Lasers and Electro-Optics,2006, CThAA2.
[9] T. Le, G. Tempea, Z. Cheng, M. Hofer, A. Stingl, Optics Express 17 (2009) 1240.
[10] G.P. Agrawal, Nonlinear Fiber Optics, Chaps, Academic, San Diego, 2001, pp.2
[11] T.P. Tanaka, S. Onoda, M. Sumi, Applied Optics 15 (1976) 1121.
[12] K. Thyagarajan, S. Diggavi, A. Taneja, A.K. Ghatak, Applied Optics 30 (1991) 3877.
[13] A.D. Yablon, Optical Fiber Fusion Splicing, Springer, Berlin Heidelberg, 2010.
[14] A.W. Snyder, J.D. Love, in: Optical Waveguide Theory, Chapman and Hall, 1983.
[15] D. Marcuse, Journal of Optical Society of America 66 (1976) 216.
[16] H. Garcia, A.M. Johnson, F.A. Oguama, S. Trivedi, Optics Letters 28 (2003) 1796.

Please cite this article as: Babita, et al., Optics Communications (2012), http://dx.doi.org/10.1016/j.optcom.2012.11.092

Electrical Power and Energy Systems 47 (2013) 394–401

Contents lists available at SciVerse ScienceDirect

Electrical Power and Energy Systems

journal homepage: www.elsevier.com/locate/ijepes

Detection and tracking of short duration variations of power system disturbances using modified potential function

Rajiv Kapoor [a,*], Manish Kumar Saini [b]

[a] Electronics & Comm. Engg. Deptt., Delhi Technological University, New Delhi 110 045, India
[b] Electrical Engg. Deptt., D.C.R. University of Science and Technology, Murthal, Sonepat 131 039, India

ARTICLE INFO

Article history:
Received 8 May 2010
Received in revised form 3 October 2012
Accepted 25 October 2012
Available online 23 December 2012

Keywords:
Power system disturbances
Potential function
Sample Tracking
Real Time Analysis

ABSTRACT

This study introduces a modified potential function based modeling approach for real-time disturbance tracking. Real-time tracking requires the least complex techniques for processing and classification and still provide accurate results. Time required to detection of the power quality disturbance should be small enough so that the further mitigation action may be taken. The proposed FRTD algorithm is able to detect the disturbances in 3–5 samples. The proposed FRTD algorithm is principally based upon potential function, which has been modified so as to give the one-dimensional position vector corresponding to the voltage sag and swell, with complexity $O(1)$ with no pre-process complexity. The method detects the transient in 3–5 samples at sampling frequency of 12.8 kHz. Potential function uses the current nonlinear drift velocity vector along with a prior knowledge of the power system disturbance to compute the unknown parameter in the form of diffusion matrix, D_t. The parameter D_t has been used to detect the events in the signal. Magnitude of D_t play vital role to detect the events. FRTD algorithm has been tested to track and detect the power system disturbances such as voltage sag, swell, and transient. The algorithm has been tested on hardware interfaced with MATLAB. 1000 samples of different types of power system disturbances such as voltage swell, voltage sag, oscillatory-transient and impulsive-transient have been tested. FRTD algorithm is having the efficiency of 99.83%.

1. Introduction

The importance of power system disturbances detection is ever increasing due to the wide use of delicate electronic devices. Voltage swell and sag can occur due to lightning, capacitor switching, motor starting, nearby circuit faults, or accidents and can lead to power interruptions. Harmonic current due to nonlinear loads throughout the network also degrade the quality of services to the sensitive high-tech customers, such as India's IT parks in Bangalore, Hyderabad and many other places. The massive rapid transit system (MRT), Metro Railways in Delhi and few other places in India have facilitated the massive use of semiconductor technologies in the auto-traction systems, resulting in the increased level of harmonic distortion. The solution of the power system disturbance related problems requires continuous monitoring and the acquisition of large amount of data from the distribution system. In [4], author emphasizes the need of an automated power system disturbances detection and classification system to determine the cause of power system disturbances.

Several signal processing and statistical analysis tools have been discussed for the detection and classification of power system disturbances. Intelligent techniques and optimization techniques used the said field have been discussed in detail [15]. The applications of wavelets for the detection and classification of different voltage events have been provided. Wavelet transform is the major signal processing technique in the field of power quality. Comprehensive analysis of reported work on wavelet transform has been presented in [3].

In [6], authors proposed the framework in four parts; voltage anomaly detection algorithm, wavelet transform, normalization and codification, and Fuzzy-ARTMAP-neural network for the recognition of events. To detect voltage anomaly, the magnitude of the voltage waveform is estimated which based on the representation of sine waves. Wavelet transform has been used for the extraction of the features from the disturbed sine wave. Normalization and codification has been done for the classification from Fuzzy-ARTMAP neural network.

In [8], authors suggested the classification strategy of different type of transients on the basis of wavelet transform. Wavelet energy entropy and wavelet energy weight have been selected as feature set for detection purpose. Back-propagation neural network has been trained using the proposed feature set and afterward the same has been used for the classification of transients. The study is based on the transients occurred in 512 kV transmission line.

* Corresponding author. Tel.: +91 130 2484124.
E-mail address: rajivkapoor@dce.ac.in (R. Kapoor).

0142-0615/$ - see front matter © 2012 Elsevier Ltd. All rights reserved.
http://dx.doi.org/10.1016/j.ijepes.2012.10.053

In [12], authors have been suggested wavelet packet transform for the feature extraction. From extracted features set, the optimum selection of features have been carried out using genetic algorithm and simulated annealing. The selected features have been used for the automatic classification of power quality events using support vector machine. Kernel parameters of support vector machine are estimated in a fully automatic way.

Authors focuses on the use of easy to compute statistical estimator to detect anomalies which preserve the frequency of the power line. Estimators used are variance, skewness and kurtosis. Authors shows the variation in estimators according to symmetric and asymmetric nature of disturbances. Therefore, the characterization of the disturbances has been done with the help of higher-order statistics in [2].

In [13], authors considered the different type of voltage dip depends upon different applications. The study is useful to avoid false alarms due to different kind of voltage dip. Authors have been compared the performance of approaches based on root mean square, Wavelet transform, Kalman filtering, peak voltage, missing voltage and generalized likelihood ratio test on different kinds of voltage dips.

In [1], authors used the discrete wavelet transform to remove noise from captured data and to enhance the performance of Kalman filter which used to extract the two parameters (amplitude and slope of amplitude) from captured voltage waveform. The two parameters have been utilized to frame the rule-base of fuzzy expert system. Fuzzy expert system is applied with 10 rules on two parameters to classify the distorted waveform.

Power system disturbances are characterize in terms of sample matrix, correlation matrix, variance, eigen values, eigenvector and normalized total error signals. Neuro-fuzzy classifier based on principle component analysis (PCA) approach, is used for classification purpose in [14]. But PCA approach is scale invariant and it is linear combinations of all the original variables. Thus, it is often difficult to interpret the results.

In [11], authors proposed a method to isolate the multiple disturbances by using independent component analysis. The performance of independent component analysis have been compared with Wavelet transform for decomposition of multiple power quality disturbances by applying on synthetic data, simulated data, as well as actual power system signals.

In [9], authors suggested a framework for classification of single/multiple power quality events. The multiple power quality events have been separated using correlation function and afterward the concept of hybrid demodulation and MUSIC algorithm have been utilized with fuzzy classifiers to classify the single/multiple power quality events.

In [10], authors proposed the identification and classification of power quality disturbances. S-transform and time–time transform have been utilized for the analysis of signals. Probabilistic neural network based feature selection has been utilized where probabilistic neural network based feature selection is constructed by combining a fully informed particle swarm with an adaptive probabilistic neural network. Probabilistic neural network based feature selection approach is capable of efficiently eliminating the nonessential features to improve the overall reliability.

In [16], authors proposed a method for the classification of the short duration disturbances by using the S-transform module time frequency matrix similarity scheme. This scheme is based on first establishing the standard module time–frequency matrix for various short duration disturbances and then calculating the similarity grade between the module time–frequency matrix of tested and the standard disturbances and finally these tested short duration disturbances are classified according to this similarity scheme.

All these techniques can detect the power system disturbances but the number of samples required are large and hence the complexity of the algorithm is high enough so as not to allow to work in the real-time. The proposed FRTD algorithm uses the potential function for determining the drift velocity vector (represent the change in power signal). FRTD algorithm has been modified so as to give the one-dimensional position vector corresponding to the voltage sag and swell, with complexity $O(1)$ with no pre-process complexity. Only two samples are sufficient to find out the drift velocity vector. With the help of drift velocity vector along with a prior knowledge of the power system disturbance, to compute the unknown parameter in the form of diffusion matrix, D_t . The parameter D_t has been used to detect the events in the signal. Magnitude of D_t play vital role to detect the events. FRTD algorithm has been tested to track and detect the power system disturbances such as voltage swell, voltage sag, oscillatory-transient and impulsive-transient. The algorithm has been tested on hardware interfaced with MATLAB. Therefore, performance of proposed FTRD algorithm is also analyzed in real-time environment. The proposed FRTD algorithm has been implemented and tested in Power System Laboratory, Delhi Technological University, New Delhi. FRTD algorithm is having the efficiency of 99.83%.

Section 2 gives knowledge about generation of power system disturbances. Section 3 describes briefly about potential function. Section 4 explains proposed FRTD algorithm. Section 5 gives the detailed discussion on results obtained. Conclusion has been given in Section 6.

2. Event generation and simulation

It is always necessary to test the proposed algorithm in real time environment. Therefore, real-time power system disturbance generation and detection using proposed algorithm has been done in the Power System Laboratory, Delhi Technological University, New Delhi. Voltage sag, swell, transient have been generated and analyzed. These events are used to test the efficiency of proposed algorithm. Voltage sag refers to a fall in the voltage waveform at the receiver's end for a small interval of time. Voltage sags are caused due to the sudden switching-on of a large load. A large load means that the device under consideration draws a large input current, which causes a large voltage drop due to the impedance of the line, thus resulting in net reduction in the voltage at the receiving end. Fig. 1a represents a circuit which causes the occurrence of voltage sag due to the sudden switching-on of an large load. The switch S represents the sudden switching operation. If the load is connected to the line suddenly at 0.16 s, the output thus obtained is shown in Fig. 1b.

A voltage swell is a short duration increase in voltage waveform. A voltage swell is a short duration increase in voltage. Transfer of load from the utility source to the standby generator source during loss of utility power. Most facilities contain emergency generators to maintain power to critical loads in case of an emergency. Sudden rejection of loads to a generator has been used to create significant voltage swells. Sudden application of loads ($3-\phi$ induction motor 20 kV A, 460 V, 50 Hz, 1440 RPM) to a generator has also been used to create significant voltage sags. Both have been demonstrated in Laboratory to get voltage swell and voltage sag shown in Fig. 2a and b. Switching of a large load has been used to generate transient power system disturbance shown in Fig. 3, output of potential function for this transient power system disturbance is shown in Fig. 6. Voltage amplitude has been normalized to per unit system for further processing. As elaborated in the next section, drift parameter (μ), diffusion matrix (D), and random process (Ψ) have been used to represent the change in standard sine signal i.e. for a particular perturbation, the diffusion matrix turns out to be specific. Thus, the diffusion matrix provides a noble approximation for detection of power system disturbances. The

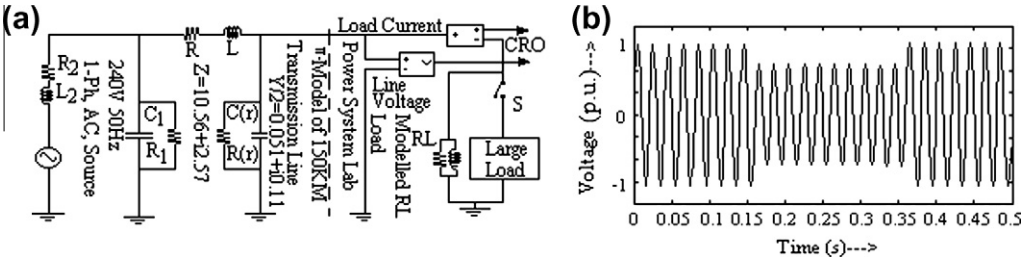

Fig. 1. (a) Voltage sag due to sudden switching-on of a large load (b) Output waveform of (a).

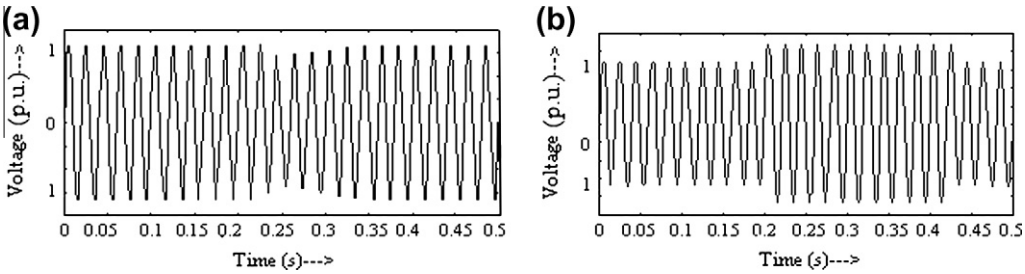

Fig. 2. (a) Generated voltage sag and (b) generated voltage swell.

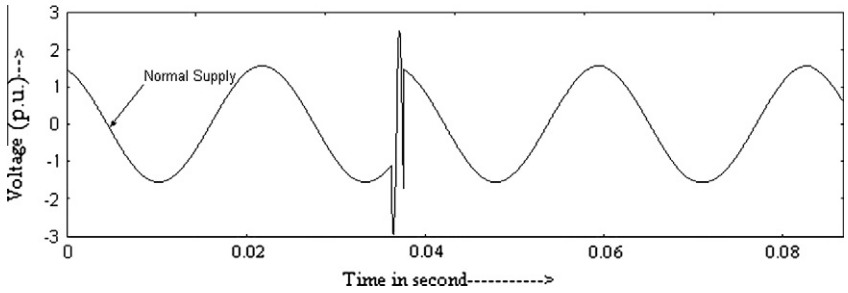

Fig. 3. Generated transient power system disturbance.

proposed algorithm has been used to accomplish. The task of detection of power system disturbance is described in detail in the coming section.

3. Potential function

Let x denotes a point in R^p for one-dimensional case p is one. A potential function $V(x)$ is a real-valued function of location and provides simpler representation of change of location with time than those based on modeling velocities directly. The equation for change of location with time in potential field $V(x)$ is

$$dx(t) = -\nabla(V(x))dt \tag{1}$$

assuming $V(x)$ is differentiable and with ∇ denotes the gradient. The entity dx/dt is known as a vector field. The estimation method has been motivated by stochastic gradient systems and can be written in the time invariant case as:

$$dx(t) = \mu(x(t))dt + \sigma(x(t))dB(t) \tag{2}$$

Here expression (2) describes a particular stochastic differential equation (SDE) with $B(t)$ a one-dimensional Brownian motion and σ a singular value. The drift term μ here has the special form $-\nabla V$ for some real-valued function V. The basic problem assumes the model (2) and seek to learn $V(x)$ from the given data $(t_i, x(t_i)$, $i = 1, 2, \ldots, n)$. These particles will be viewed as locations at successive times, t_i of a particle moving along a trajectory of the process (2). Supposing that $\nabla V(x)$ is a smooth function of x and that the observation times are close together, one can set down the following approximation to (2):

$$x(t_{i+1}) - x(t_i) = -\nabla V(x(t_i))(t_{i+1} - t_t) + (t_{i+1} - t_i)^{1/2}\sigma Z_{i+1} \tag{3}$$

For $i = 1, 2, \ldots, n$ with σ a singular value and with the Z_i independent one-dimensional variants having mean 0 and covariance 1. The reason for the multiplier $(t_{i+1} - t_i)^{1/2}$ is that for real valued Brownian $Var(dB(t)) = dt$. The approximation

$$x(t_{i+1}) - x(t_i)/(t_{i+1} - t_i) = \mu(x(t_i)) + (t_{i+1} - t_i)^{-1/2}\sigma Z_{i+1} \tag{4}$$

for the SDE was employed [7]. Suppose V is linear in a vector-valued parameter β and $V(x) = \phi(x)^T\beta$ with ϕ being an L by 1 vector of functions of known parameter and β being an L by 1 unknown parameter. The gradient of V is $\nabla\phi(x)^T\beta$. One of the following methods can be employed for the estimation of V. Methods can be employed for the estimation of V:

(i) Consider $V(x) = \sum \beta_m x^m$, where $m = (m_1, m_2, \ldots, m_p)$ and $x^m = x_1^{m_1}, \ldots, x_p^{m_p}$, with $\sum$ over$m_1, m_2, \ldots, m_p \geqslant 0$ and $1 \leqslant m_1 + m_2 + \cdots + m_p \leqslant M$. One could employ a trigonometric polynomial, a spline function, or a wavelet expansion here. Many functions, V, can be well approximated by taking M large. In practice, one might employ M_n with M_n increasing with n.

(ii) Consider nodal points $u_l, l = 1, \ldots, L$ in R^p and set $V(r) = \sum \beta_l K(x - u_l)$ for some real-valued differentiable kernel K. As a specific example of K, one has the radial basis thin plate splines [5].

$$K(x) = |x|^{2q-p} log|x| \text{ for } p \text{ even}, K(x) = |x|^{2q-p} \text{ for } p \text{ odd} \quad (5)$$

Here q denotes the order of differentiability of K, $2q - p > 0$, and $|x| = (x^T x)^{1/2}$. An expression like (5) leads to a smooth representation for V.

(iii) The term attractor signifies the targeted direction of change in location of particle and repellor is the position of particle. Consider a region A and a point x outside A. A potential function can be set down leading to attraction or repulsion from A. Specifically, if one lets $d_A(x)$ denote the minimum distance from the point x outside A to A and sets $V(x) = \beta d_A(x)^\alpha$, then for $\alpha > 0$, one has attraction to A and repulsion to A if $\alpha < 0$. One can reverse attraction and repulsion by changing the sign of d_A. it can be convenient to use $V(x) = \beta_1\ log d_A(x) + \beta_2 d_A(x)$ for similar purpose. the functional forms of methods 1–3 may be added together to provide other forms.

The $\{Z_i\}$in expression (4) could be non-Gaussian and maximum likelihood estimation employed. The representation (3) with x in R^p and $\nabla V(x) = \nabla\phi(x_i)^T\beta$ will be employed. The value $x(t_i)$ will be written x_i. Consider the p by 1 vector $(x_{i+1} - x_i)/(t_{i+1} - t_i)^{1/2}$. Following expression (4), the model has the form

$$(x_{i+1} - x_i)/(t_{i+1} - t_i)^{1/2} = -\nabla\phi(x_i)^T\beta(t_{i+1} - t_i)^{1/2} + \sigma Z_{i+1} \quad (6)$$

$i = 1, \ldots, n - 1$. Involving the L by 1 vector β, the L by p matrix $\nabla\phi(x_i)$, the p by p matrix σ, and the p by 1 vector Z_{i+1}. Suppose $\sigma = \sigma I$ with σ positive and I the p by p identity matrix. Stack the $n - 1$ values $(x_{i+1} - x_i)/(t_{i+1} - t_i)^{1/2}$, $i = 1, \ldots, n - 1$ vertically to form the $(n - 1)p$ by 1 array Y_n. Stack the $(n - 1)$ matrices $-\nabla\phi(x_i)^T(t_{i+1} - t_i)^{1/2}$ to form the $(n - 1)p$ by L matrix X_n. Stack the $(n - 1)$ values σZ_{i+1} to form ε_n. Then one has the regression model

$$Y_n = X_n\beta + \varepsilon_n \quad (7)$$

with the difference from ordinary regression that Y_n and X_n are statistically dependent.

4. Fast real-time tracking and detection (FRTD) algorithm for power system disturbance

This paper presents a algorithm for real-time tracking and detection of power system disturbances using the model of stochastic gradient systems and Brownian motion. The power system disturbance patterns have been modeled by stochastic differential equations. Firstly, Eq. (2) includes a known parameter (which is a nonlinear function of the drift velocity); secondly, an unknown parameter which appropriately model the change in location of the particle as a random process. The proposed solution calculates a 'diffusion matrix', specific to the power system disturbance patterns. Stochastic differential equation used to describe the movement of a signal sample at time t and location $x(t) = \{X(t)\}'$ can be described as:

$$[dX(t)] = [\mu_x\{x(t), t\}]dt + D_t\{x(t), t\}[d\Psi_x(t)] \quad (8)$$

In Eq. (8), $dX(t)$ is the incremental step change in x-direction. $\mu_t = (\mu_x)'$ is the translation drift parameter and represents the instantaneous velocity of the signal sample at time t and position $x(t)$; D_t is the diffusion matrix which describes the correlation between the steps in x-direction over the time. Ψ_x is a random process with mean values equal to 0. The real-time tracking has been done by calculating the drift velocity (μ_i) of the power signal samples from two consecutive instant values. If (x_i) and (x_{i+1}) are the successive instant values at time instance t_i and t_{i+1}, the drift velocity is given by

$$v_i = \frac{\sqrt{(x_i - x_{i+1})^2}}{(t_i - t_{i+1})} \quad (9)$$

This gives an indication of the drift velocity vector of the pattern in two consecutive samples, μ_t (drift parameter). $t_s = t_i - t_{i+1}$ signifies sampling time of the power system disturbances. FRTD algorithm for detection of power system disturbance:

1. Modeling the waveform as per the Stochastic Differential Equation (SDE) as in Eq. (2), then the drift velocity vector has been found.
2. The drift vector μ_t has been used to find the D_t which gives the fair approximation about the perturbation occurred in the power system disturbances.
3. Approximation of Ψ_x plays an important role in approximating the patterns, increasing the value of Ψ gives a smaller envelope and vice versa, in this work the value of $d\Psi$ assumed is 1 so as to reduce the complexity involved.
4. Finally, correlate of diffusion matrix for every two samples, with D_t of standard sine wave for the detection of event has been carried out.
   (i) If there is no change detected in gradient of D_t, it means there is no event present in the power signal.
   (ii) If there is change detected in gradient of D_t, it means there is event present in the power signal.
5. After sign check, the next check is for threshold value (λ) of D_t.
   (i) If it excceds the λ, then input classified as transient power system disturbance.
   (ii) If the gradient of D_t changes from positive to negative and if the value of D_t is less than λ_1; it means sag is present otherwise sag is not present.
   (iii) If the gradient of D_t changes from negative to positive and if the value of D_t is excced than λ_2; it means swell is present otherwise swell is not present.

Diffusion matrix has been estimated after modeling of SDE and determining the drift velocity. To detect the changes present in the diffusion matrix, correlation has been performed between diffusion matrix for every two samples, and with D_t of standard sine wave. The threshold values of magnitude of diffusion matrix have been decided to detect the sag, swell and transient present in the power signal. The detection of power system disturbances has been carried out at the beginning of disturbances but the end of the disturbances is the matter of interest of FRTD algorithm. At the end of the event, the response of FRTD algorithm represent the reverse results than conventional results i.e. in the case of end of voltage sag, the amplitude changes to lower value to higher value. The gradient of the diffusion matrix is positive, then it is detected as swell. After every sag there is a swell which is considered as the end of sag. Therefore, the events are detected at the beginning in few sample and further result section elaborate the performance of FRTD algorithm.

5. Results and discussion

Modeling of drift vector has been carried out according to the Eq. (2). Drift velocity has been calculated from Eq. (9) between two consecutive samples. Diffusion matrix has been calculated for two samples. If input power signal is standard sine wave, then D_t has been represented by a straight line at zero level on x-axis. Now, for every two samples, another diffusion matrix, D_t has been determined. Correlation between diffusion matrix, D_t of two consecutive samples and standard sine wave has been represented

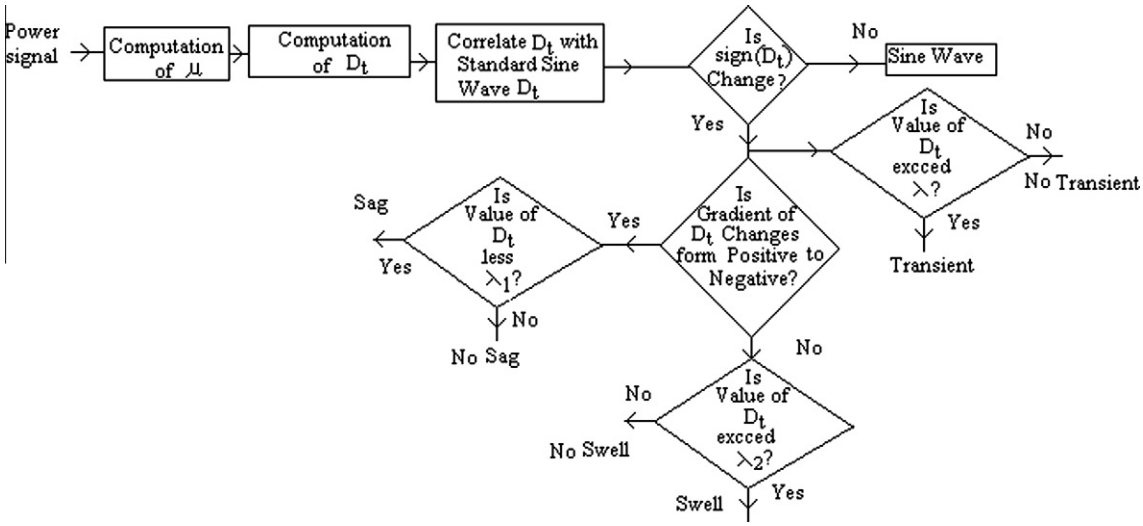

Fig. 4. FRTD algorithm.

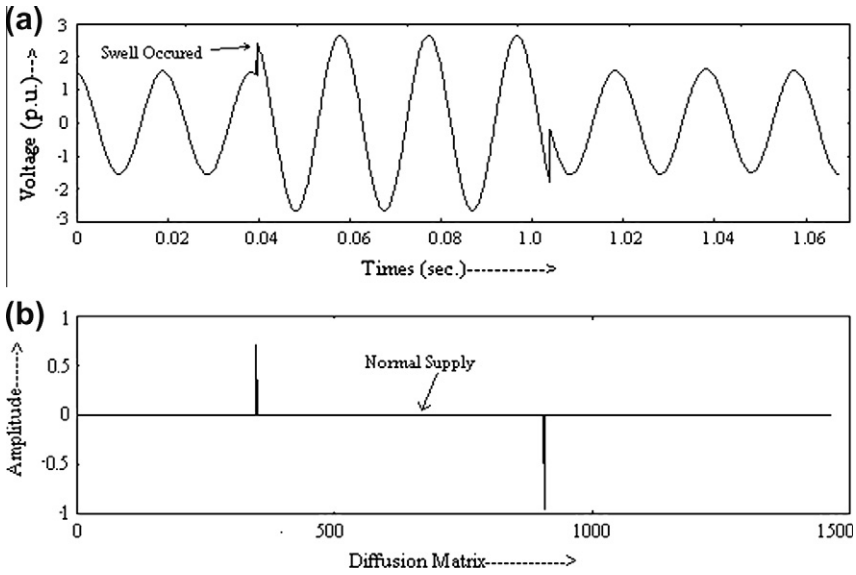

Fig. 5. Detection of swell power system disturbance.

at zero level x-axis component when no change in gradient of D_t as plotted in Figs. 5 and 6. If any change is present into the input power signal, then a change has been occured in the value of correlation matrix as shown in Figs. 5 and 6. If diffusion matrix have a change of gradient from positive to negative and if the value of D_t is less than λ_1, then it means sag is present otherwise sag is not present. If diffusion matrix have a change of gradient from positive to negative and if the value of D_t is e excced than λ_2, then it means swell is present otherwise swell is not present. Another check has been introduced, in the FRTD algorithm as in Fig. 4. If the value of D_t exceeds from the threshold value, λ, then transient is present in the input power signal.

Fig. 5a shows the input voltage swell signal available for proposed FRTD algorithm. In Fig. 5b, correlated diffusion matrix has been shown. Before $t = 0.04$ s, the D_t of standard sine wave is represented by a straight line at zero level on x-axis. At $t = 0.04$ s, a change in input signal is observed which is rise in voltage. Correspondingly, drift velocity is calculated to determine the diffusion matrix D_t. Now, the correlated D_t alters from the zero level and rises in the positive direction such that its amplitude excced the threshold value λ_2. Hence, it signifies as voltage swell. At $t = 1.0033$ s, a decrease in amplitude of input signal is observed and its correlated D_t alters and it goes in the negative direction which shows end of the swell. Correlated D_t of post event wave is represented by a straight line at zero level on x-axis.

Fig. 6a shows the input voltage oscillatory-transient signal available for proposed FRTD algorithm. In Fig. 6b, the plot of correlated diffusion matrix has been shown. Before $t = 0.0366$ s, a change is observed in input signal which is decrease in voltage. Corresponding value of correlated D_t also decreases in negative direction. Till $t = 0.03733$ s, the signal oscillates and its correlated D_t also varies according to variation present into the signal between $t = 0.0366$ s to $t = 0.03733$ s. At $t = 0.03733$ s rise in voltage is observed in input signal and correspondingly value of its correlated D_t also changes and rises in positive direction such that its amplitude exceeds the threshold value λ which classifies it as an

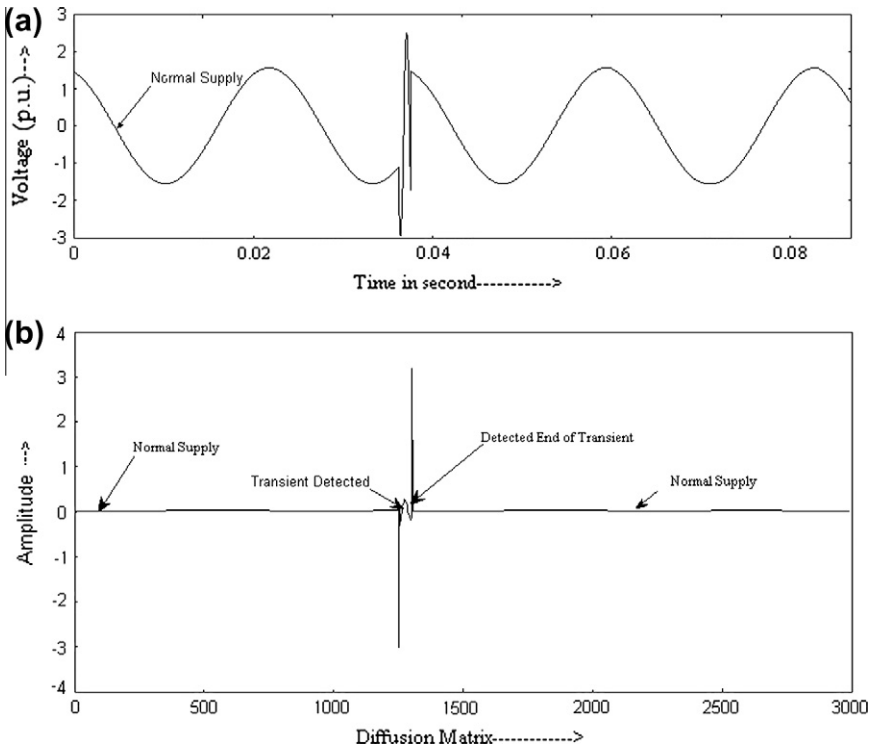

Fig. 6. Detection of transient power system disturbance.

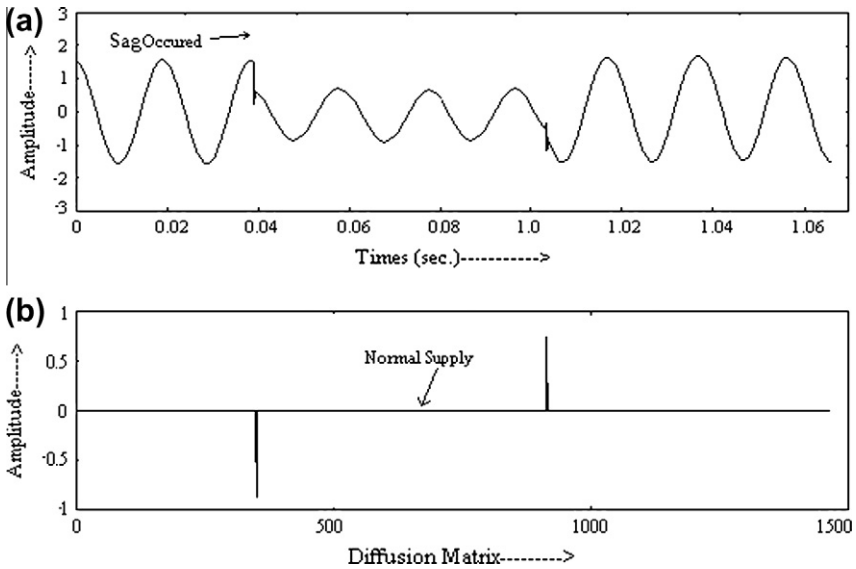

Fig. 7. Detection of sag power system disturbance.

oscillatory-transient. Correlated D_t of post event wave is represented by a straight line at zero level on x-axis.

Fig. 7a shows the input voltage sag signal available for proposed FRTD algorithm. In Fig. 7b, the plot of correlated diffusion matrix has been shown. Before $t = 0.04$ s, the D_t of standard sine wave is represented by a straight line at zero level on x-axis. At $t = 0.04$ s, a change in input signal is observed which is dip in the voltage. Correspondingly, drift velocity is calculated to determine the diffusion matrix D_t. Now, the correlated D_t alters from the zero-level and decreases in the negative direction such that its amplitude is less the threshold value λ_1. Hence, it signifies as voltage sag. At $t = 1.0033$ s, a increase in amplitude of input signal is observed and its correlated D_t alters and it goes in the positive direction which shows end of the swell. Correlated D_t of post event wave is represented by a straight line at zero-level on x-axis.

Fig. 8a shows the input voltage impulsive-transient signal available for proposed FRTD algorithm. In Fig. 8b, plot of correlated diffusion matrix has been shown. Before $t = 0.08$ s, the D_t of standard sine wave is represented by a straight line at zero-level on x-axis. At $t = 0.08$ s, a change in input signal is observed which is steep rise in voltage and its correlated D_t changes from zero-level to upward in the positive direction such that its amplitude exceeds the threshold value λ which signifies it an transient. Correlated D_t of post event wave is represented by a straight line at zero-level on x-axis.

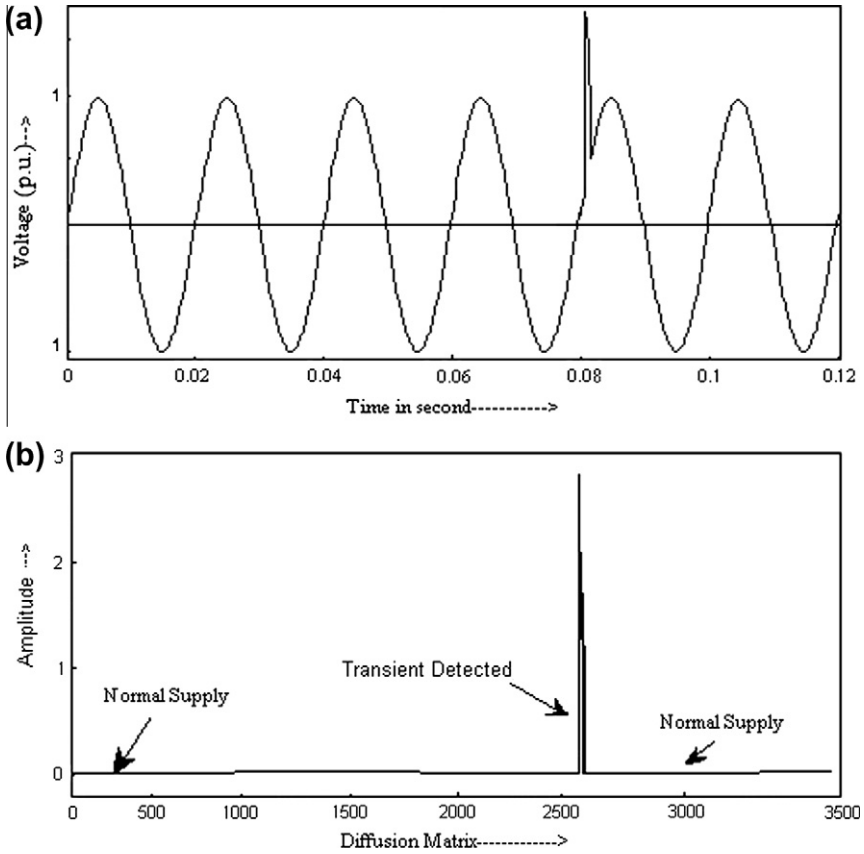

Fig. 8. Detection of transient power system disturbance.

Fig. 9. Real-time hardware implementation of FRTD algorithm.

Block diagram of hardware implementation of proposed FRTD algorithm is shown in Fig. 9. Input voltage of power signal has been reduced using step-down transformer. Further, ADC has been utilized to convert the analog signal to digital signal and then data acquisition unit has been used to acquire the data. Then, MATLAB 7.0 has been used to scale up the voltage level as that of input voltage then FRTD algorithm has been used to detect the power system disturbance. The FRTD algorithm has been tested in real-time environment as shown in Fig. 9 on 1000 sample each of all three types of power system disturbance. FRTD algorithm has been compared with the other techniques which is shown in Table 1. Proposed FRTD algorithm is having the classification rate 99.8%, 99.7% and 100% for voltage sag, voltage swell and transient respectively. FRTD algorithm is having the efficiency of 99.83%.

Table 1
Performance comparison of FRTD algorithm.

S.no.	Event	[6]	[12]	FRTD algorithm
1.	Voltage sag	98.46	90	99.8
2.	Voltage swell	100	93	99.7
3.	Transient	100	86	100
4.	Average	99.48	89.66	99.83

6. Conclusion

FRTD algorithm has been used to detect real-time power system disturbances present in the input power signal. It is observed that FRTD algorithm tracks transient in just three samples and sag/swell in two samples, which makes possible for real-time detection. If input power signal is standard sine wave, then diffusion matrix has been represented by a straight line at zero-level on *x*-axis. Limitation of proposed method has been also observed. If input voltage swell (power signal) has high magnitude, then the diffusion matrix value exceeds to the threshold value. In that case, proposed algorithm miss-classify it as transient. Potential function can further be exploit for detection of other power system disturbances.

References

[1] Abdelsalam AA, Eldesouky AA, Sallam AA. Classification of power system disturbances using linear Kalman filter and fuzzy-expert system. Int J Electr Power Energy Syst 2012;43:688–95.
[2] Aguera-Perez A, Palomares-Salas JC, Rosa JJGdl, Sierra-Fernandez JM, Ayora-Sedeno d, Moreno-Munoz A. Characterization of electrical sags and swells using higher-order statistical estimators. Measurement 2011;44:1453–60.
[3] Barros J, Diego RI, Apraiz MD. Applications of wavelets in electric power quality: voltage events. Int J Electr Power Syst Res 2012;88:130–6.

[4] Bollen MHJ, Gu IYH. Signal processing of power quality disturbances. John Wiley and Sons; 2006.
[5] Brillinger D. A potential function approach to the flow of play in soccer, J. Quant Anal Sports 2007;3(1).
[6] Decanini JGMS, Tonelli-Neto MS, Malange FCV, Minussi CR. Detection and classification of voltage disturbances using a fuzzy-artmap-wavelet network. Int J Electr Power Syst Res 2011;81:2057–65.
[7] Brillinger DR, Preisler HK, Ager AA and Kie JG. The use of potential functions in modeling animal movement. Data Analysis from Statistical Foundations, A.K.M.E. Saleh, In: Huntington, NY, Nova, editor. 2001. p. 1-25. http://www.stat.berkeley.edu/~brill/Papers/fraser8.pdf
[8] He Z, Gao S, Chen X, Zhang J, Bo Z, Qian Q. Study of a new method for power system transients classification based on wavelet entropy and neural network. Int J Electr Power Energy Syst 2011;33:402–10.
[9] Kapoor R, Saini MK. Hybrid demodulation concept and harmonic analysis for single/multiple power quality events detection and classification. Int J Electr Power Energy Syst 2011;33:1608–22.
[10] Lee C-Y, Shen Y-X. Optimal feature selection for power quality disturbances classification. IEEE Trans Power Deliv 2011;26(4):2342–51.
[11] Lima MAA, Cerqueira AS, Coury DV, Duque CA. A novel method for power quality multiple disturbance decomposition based on independent component analysis. Int J Electr Power Energy Syst 2012;42:593–604.
[12] Manimala K, Selvi K, Ahila R. Optimization techniques for improving power quality data mining using wavelet packet based support vector machine. Neurocomputing 2012;77:36–47.
[13] Moschitta A, Carbone P, Muscas C. Performance comparison of advanced techniques for voltage dip detection. IEEE Trans Instrum Meas 2012;61(5): 1494–502.
[14] Pires VF, Amaral TG, Martins JF. Power quality disturbances classification using 3-d representation and PCA based neuro-fuzzy approach. Int J Expert Syst Appl 2011;38:11911–7.
[15] Saini MK, Kapoor R. Classification of power quality events – a review. Int J Electr Power Energy Syst 2012;43:11–9.
[16] Xiao X, Xu F, Yang H. Short duration disturbance classifying based on s-transform maximum similarity. Int J Electr Power Energy Syst 2009;31: 374–8.

Hindawi Publishing Corporation
Journal of Engineering
Volume 2013, Article ID 648540, 5 pages
http://dx.doi.org/10.1155/2013/648540

Research Article

Electronically Tunable Transimpedance Instrumentation Amplifier Based on OTRA

Rajeshwari Pandey,[1] Neeta Pandey,[1] and Sajal K. Paul[2]

[1] *Department of Electronics and Communication Engineering, Delhi Technological University, Delhi, India*
[2] *Department of Electronics Engineering, Indian School of Mines, Dhanbad, India*

Correspondence should be addressed to Neeta Pandey; n66pandey@rediffmail.com

Received 31 August 2012; Revised 6 November 2012; Accepted 7 November 2012

Academic Editor: Jiun-Wei Horng

Operational transresistance amplifier (OTRA) is the most suitable analog building block (ABB) for transimpedance type signal processing due to its very nature of current input and voltage output. In this paper, OTRA-based transimpedance instrumentation amplifier (TIA) is presented. It provides high differential gain and bandwidth, which is independent of gain. It also offers high common-mode rejection ratio (CMRR). The amplifier gain can be controlled electronically by implementing resistors using MOS transistors operating in linear region. The circuit can be made fully integrated. The proposed circuit is insensitive to parasitic input capacitances and input resistances due to the internally grounded input terminals of OTRA. Theoretical analysis is verified through PSPICE simulations and experimentation.

1. Introduction

An instrumentation amplifier (IA) faithfully amplifies low level differential signals in the presence of high com-mon-mode noise which makes it especially suitable as input stage of a signal processing system. The conventional voltage-mode instrumentation amplifiers based on operational amplifier are not capable of operating at higher frequencies because of slew rate and fixed gain-bandwidth product limitations [1]. The current mode approach has gained a lot of importance in the recent past due to its inherent wide bandwidth which is virtually independent of closed loop gain, greater linearity, and large dynamic range [1]. Thus the current-mode instrumentation amplifiers [2–4] are superior, in performance, to their voltage mode counterpart in terms of CMRR and frequency range of operation. The literature survey reveals that, currently, most of the current mode instrumentation amplifiers (CMIAs) use the second-generation current conveyor (CCII) [2–4]. These configurations are suitable for amplification of signals from voltage-source transducers. For amplification of signals from current-source transducers, TIA would be a better choice wherein the current input can be directly processed without conversion to voltage signal. An op-amp-based TIA is presented in [5], however, it uses two current to voltage converters followed by an amplifier. OTRA being a current input voltage output ABB is inherently suitable for TIA implementation [6]. Therefore, in this paper an OTRA-based TIA has been proposed. It offers a high differential gain and a bandwidth which is independent of gain, unlike a traditional voltage-mode IA. It also provides high common-mode rejection ratio (CMRR).

2. The Proposed Circuit

OTRA is a three terminal device, shown symbolically in Figure 1, and its port relations are characterized by (1), where R_m is the transresistance gain of OTRA. For ideal operations, R_m approaches infinity and forces the input currents to be equal. Thus, OTRA must be used in a negative feedback configuration [7, 8]. It is also free from parasitic input capacitances, and

$$\begin{bmatrix} V_p \\ V_n \\ V_O \end{bmatrix} = \begin{bmatrix} 0 & 0 & 0 \\ 0 & 0 & 0 \\ R_m & -R_m & 0 \end{bmatrix} \begin{bmatrix} I_p \\ I_n \\ I_O \end{bmatrix} \quad (1)$$

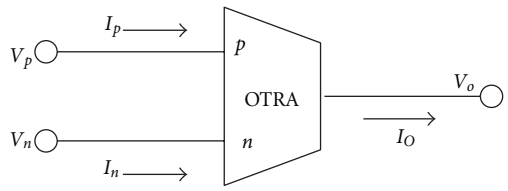

Figure 1: OTRA Circuit symbol.

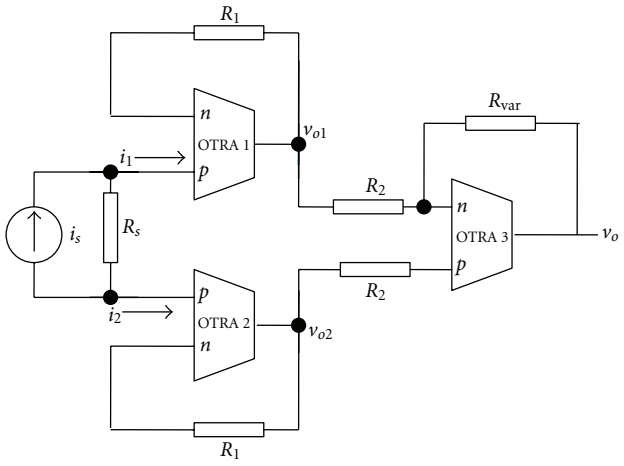

Figure 2: The proposed TIA.

resistances as its input terminals are virtually grounded, and, hence, nonideality problem is less in circuits implemented with OTRA. Figure 2 shows the proposed circuit. It consists of three OTRAs and five resistors. The differential transimpedance gain (A_d) for the amplifier can be computed as follows:

$$v_{o1} = i_1 R_1, \tag{2}$$

$$v_{o2} = i_2 R_1, \tag{3}$$

$$A_d = \frac{v_0}{i_2 - i_1} = \frac{R_{\text{var}} R_1}{R_2}. \tag{4}$$

It can be seen from (4) that A_d can be varied by varying the resistance R_{var}.

Ideally the transresistance gain R_m is assumed to approach infinity. However, practically R_m is a frequency dependent finite value [8]. Considering a single pole model for the transresistance gain, R_m can be expressed as

$$R_m(s) = \left(\frac{R_0}{1 + s/\omega_0}\right), \tag{5}$$

where R_0 is low frequency transresistance gain, and ω_0 is the pole angular frequency of the OTRA.

For high frequency applications, the transresistance gain $R_m(s)$ reduces to

$$R_m(s) \approx \left(\frac{1}{sC_p}\right), \tag{6}$$

where $C_p = 1/R_0\omega_0$ and is the parasitic capacitance of OTRA.

Taking this effect into account, output voltages at different nodes are given as

$$v_{o1} = \frac{i_1 R_1}{1 + sC_{P1}R_1}, \tag{7}$$

$$v_{o2} = \frac{i_2 R_1}{1 + sC_{P2}R_1}, \tag{8}$$

$$v_0 = \frac{R_1 R_{\text{var}}}{R_2\left(1 + sC_{P3}R_{\text{var}}\right)}\left(\frac{i_2}{\left(1 + sC_{P1}R_1\right)} - \frac{i_1}{\left(1 + sC_{P2}R_1\right)}\right), \tag{9}$$

where C_{p1}, C_{p2}, and C_{p3} are the parasitic capacitances of OTRA1, OTRA2, and OTRA3, respectively.

Considering $C_{p1} = C_{p2}$ in (9), the A_d of the circuit given by (4) modifies to

$$A_d = \frac{v_0}{i_2 - i_1} = \frac{R_{\text{var}} R_1}{R_2}\varepsilon_{\text{uc}}(s), \tag{10}$$

where

$$\varepsilon_{\text{uc}}(s) = \frac{1}{\left(1 + sC_{P1}R_1\right)\left(1 + sC_{P3}R_{\text{var}}\right)} \tag{11}$$

is the uncompensated error function.

From (9), it is to be noticed that the gain A_d can be adjusted by $R_{\text{var}}R_1/R_2$, and the bandwidth is controlled by $\varepsilon_{\text{uc}}(s)$. Thus, the gain of the amplifier can be adjusted by varying R_{var} without affecting the bandwidth (BW).

From (9), by using $i_1 = i_2 = i_c$, the transimpedance common-mode gain (A_c) can be computed as

$$A_c = \frac{v_0}{i_c} = \frac{R_1 R_{\text{var}}}{R_2\left(1 + sC_{P3}R_{\text{var}}\right)} \times \left(\frac{1}{\left(1 + sC_{P2}R_1\right)} - \frac{1}{\left(1 + sC_{P1}R_1\right)}\right). \tag{12}$$

The performance parameter CMRR which defined as the ratio of differential gain to common-mode gain can be computed as

$$\text{CMRR} = \frac{A_d}{A_c} = \frac{2 + s\left(C_{p1} + C_{p2}\right)R_1}{s\left(C_{P1} - C_{p2}\right)R_1}. \tag{13}$$

For high frequency applications, compensation methods must be employed to account for the error $\varepsilon_{\text{uc}}(s)$ introduced in (4) and given by (11). High frequency passive compensated topology of the TIA is shown in Figure 3. Routine analysis of Figure 3 results in

$$A_d = \frac{v_0}{i_2 - i_1} = \frac{R_{\text{var}} R_1}{R_2}\varepsilon_c(s), \tag{14}$$

where

$$\varepsilon_c(s) = \frac{1}{\left(1 + R_1 s\left(C_{P1} - C_1\right)\right)\left(1 + R_{\text{var}} s\left(C_{P3} - C_3\right)\right)} \tag{15}$$

is the compensated error function.

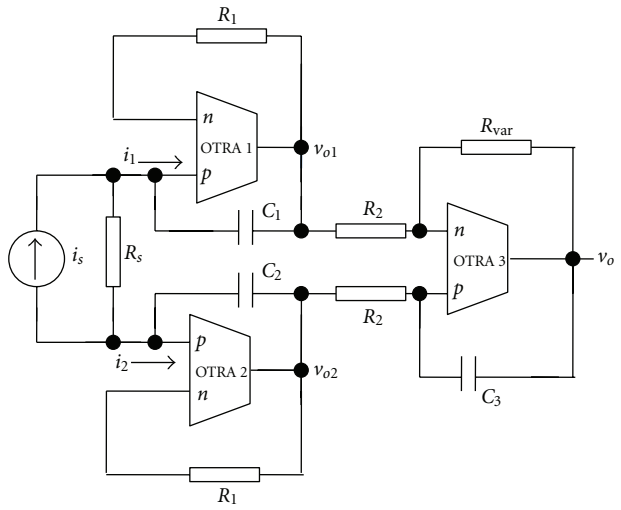

Figure 3: TIA with high frequency compensation.

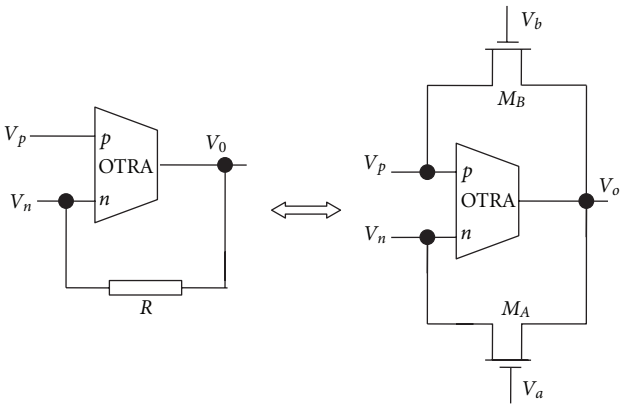

Figure 4: MOS implementation of a linear resistance connected between negative input and output terminals of OTRA.

By taking $C_1 = C_2 = C_{p1}$ and $C_3 = C_{p3}$, $\varepsilon_c(s)$ reduces to 1, which makes (14) the same as (4). The effect of single pole model of R_m can thus be eliminated.

It is well know that the linear passive resistor consumes a large chip area as compared to the linear resistor implementation using transistors operating in nonsaturation region. The differential input of OTRA allows the resistors connected to the input terminals of OTRA to be implemented using MOS transistors with complete nonlinearity cancellation [8]. Figure 4 shows a typical MOS implementation of resistance connected between negative input and output terminals of OTRA. The resistance value may be adjusted by appropriate choice of gate voltages of these transistors thereby making gain of TIA electronically tunable. The value of resistance so obtained is expressed as

$$R = \frac{1}{\mu_n C_{ox} (W/L)(V_a - V_b)}, \tag{16}$$

where μ_n, C_{ox}, W, and L are electron mobility, oxide capacitance per unit gate area, effective channel width, and effective channel length of MOS, respectively. V_a and V_b are the gate voltages. Thus, MOS transistor implementation of R_1, R_2, and R_{var} not only makes the TIA gain electronically tunable but also makes the circuit suitable for integration. Figure 5 shows the MOS-based implementation of the proposed TIA.

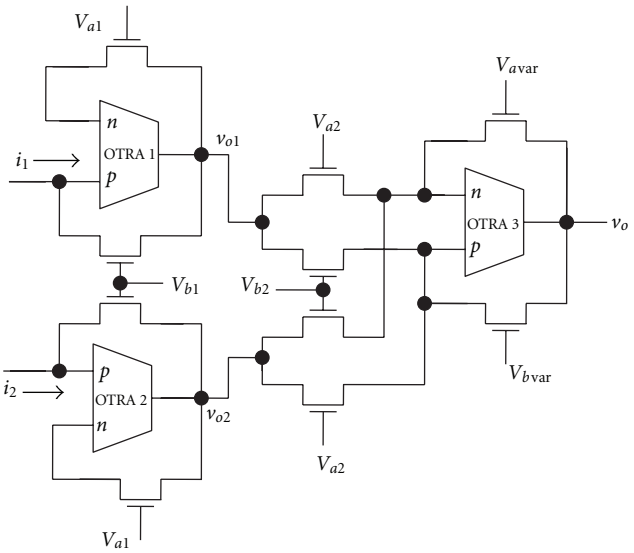

Figure 5: MOS-based implementation of the proposed TIA.

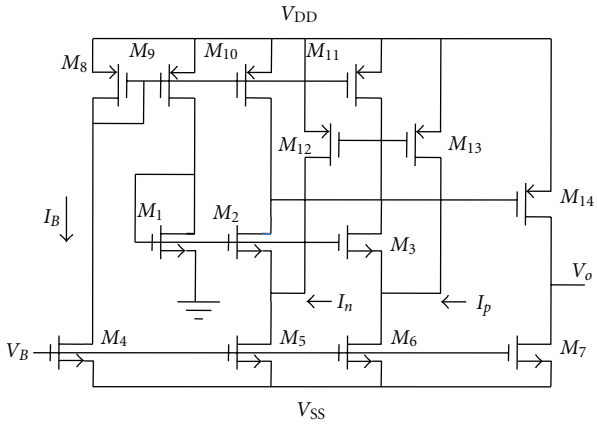

Figure 6: CMOS implementation of OTRA [9].

3. Simulation and Experimental Results

The performance of the proposed TIA is verified through SPICE simulation using 0.5 μm CMOS process parameters provided by MOSIS (AGILENT). CMOS implementation of the OTRA [9] shown in Figure 6 is used for simulation. Aspect ratios used for different transistors are the same as in [9] and are given in Table 1. The taken supply voltages are ±1.5 V.

Figure 7(a) shows the frequency response of the proposed amplifier. The input differential current was chosen as 5 mA. The component values are taken as R_1 = 5 KΩ and R_2 = 1 KΩ. R_{VAR} is assigned values as 10 KΩ, 5 KΩ, and 0.8 KΩ,

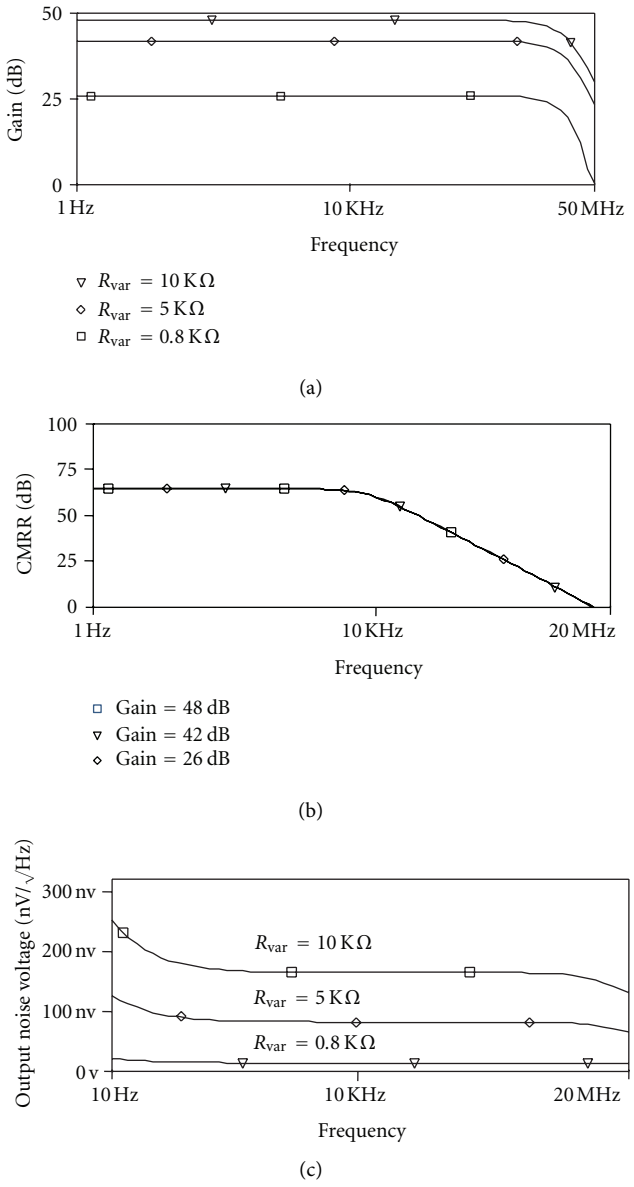

Figure 7: (a) Frequency response of the proposed TIA, (b) CMRR response of the proposed TIA, and (c) output noise spectral density of the proposed TIA.

Table 1: Aspect ratio of the transistors in OTRA circuit.

Transistor	W (μm)/L (μm)
M1–M3	100/2.5
M4	10/2.5
M5, M6	30/2.5
M7	10/2.5
M8–M11	50/2.5
M12, M13	100/2.5
M14	50/0.5

the differential gains obtained were 48 dB, 42 dB, and 26 dB, respectively. The 3 dB frequency of the amplifier is 10 MHz

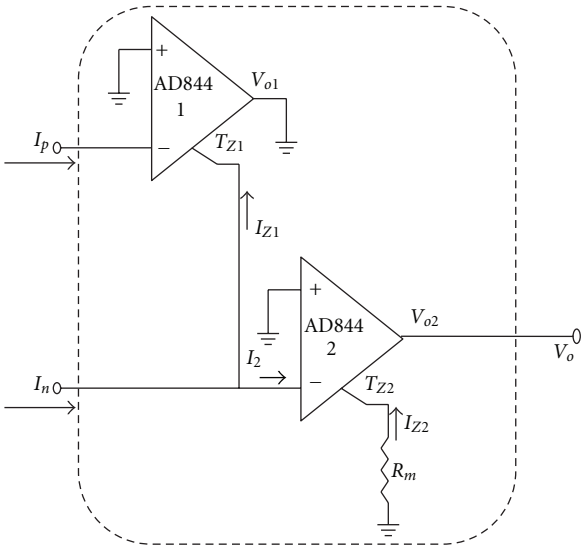

Figure 8: OTRA realization using commercial IC AD 844AN [10].

for all the three cases confirming that the bandwidth of the amplifier is independent of gain. Total power consumption of the proposed TIA is simulated to be 4.93 mW.

Figure 7(b) shows the CMRR response of the circuit for differential gains of 26, 42, and 48 dB. It is observed that the proposed TIA exhibits a CMRR magnitude of 64.5 dB and bandwidth of 10 KHz, which is independent of gain.

The simulation results of the noise performance analysis of the proposed TIA are depicted in Figure 7(c). The component values are chosen to be the same as for differential gain. It may be noticed from the Figure 7(c) that the noise level being low would result in high signal-to-noise ratio of the TIA.

A hardware prototype of the proposed TIA is also designed to test its functionality experimentally. The OTRA is realized using commercial IC AD 844AN [10] as shown in Figure 8. Supply voltages used are ±5 V. The experimental and simulated frequency response for the TIA, for R_1 = 5 KΩ, R_2 = 1 KΩ, and R_{VAR} = 10 KΩ, are shown in Figure 9(a), and CMRR response is shown in Figure 9(b). The slight variations in experimental and simulated results may be due to tolerance of the component values. Observed outputs showing the performance of the proposed TIA at 70 KHz and 2 MHz for R_1 = 5 KΩ, R_2 = 1 KΩ, and R_{VAR} = 10 KΩ are given in Figure 9(c).

4. Conclusion

An OTRA-based TIA is presented which is suitable for amplification of signals from current-source transducers. The circuit provides high gain for a wide range of frequencies, and the bandwidth of the amplifier is independent of its gain. The proposed circuit, to the best knowledge of authors, is the only current mode TIA. A voltage mode op-amp-based transresistance instrumentation amplifier is proposed in [5] which uses three op-amps and nine resistors, a quite large number as compared to the proposed TIA. Also, the amplifier of [5]

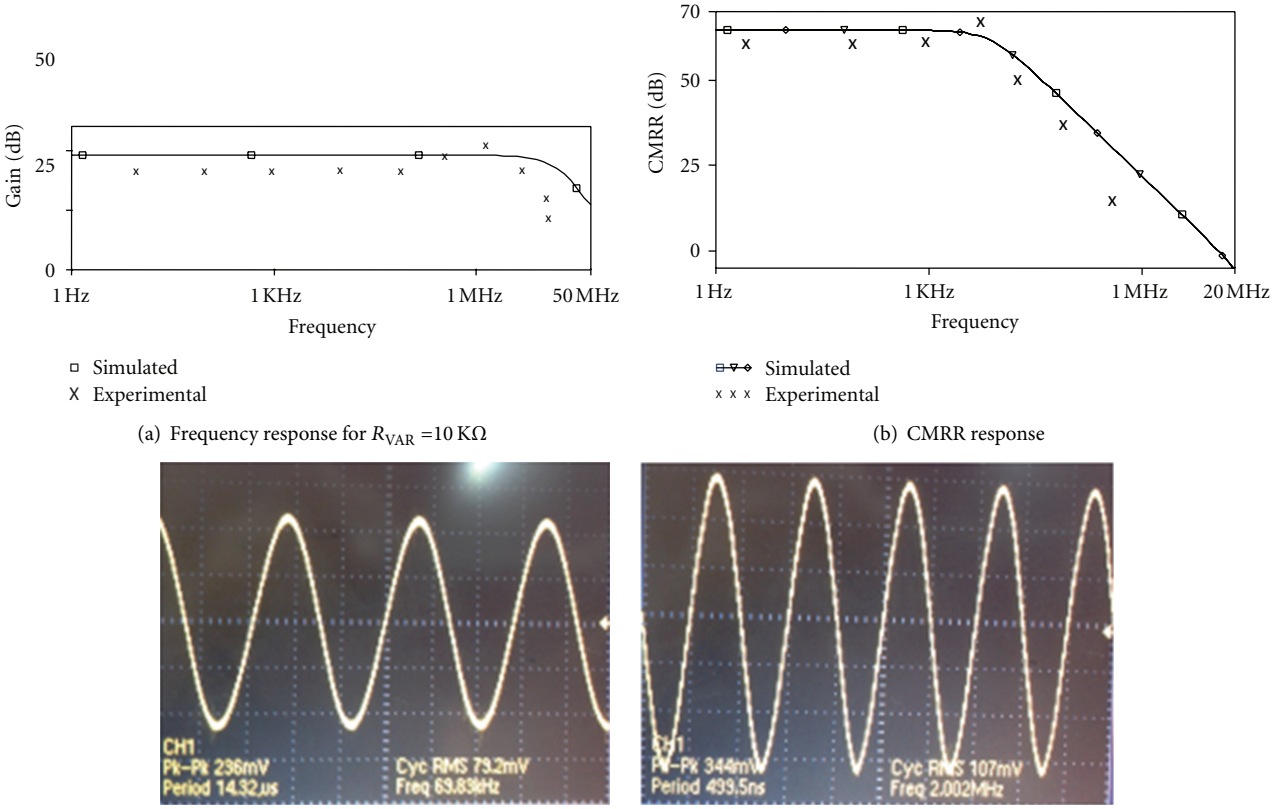

(a) Frequency response for R_{VAR} =10 KΩ

(b) CMRR response

(c) Observed output for 70 KHz input and observed output for 2 MHz input

Figure 9: Experimental results of the proposed TIA.

was designed, for a specific low frequency application in a gamma-ray dosimeter, and its other performance parameters are not available for comparison.

The gain of the proposed amplifier can be electronically tuned by implementing the passive resistor using MOS transistor. This also makes the circuit fully integrated. The proposed circuit can easily be compensated for parasitics. It provides advantages of current mode design techniques and at the same time provides voltage output suitable for driving existing voltage mode circuits. Theoretical propositions are verified through PSPICE simulations and experimental results.

References

[1] C. Toumazou, F. J. Lidgey, and D. G. Haigh, *Analogue IC Design: The Current Mode Approach*, chapter 1, Peregrinus, Stevenage, UK, 1990.

[2] Q. S. Zhu, F. J. Lidgey, and W. J. Su, "High CMRR, second generation current-mode instrumentation amplifiers," in *Proceedings of the IEEE International Symposium on Circuits and Systems*, vol. 2, pp. 1326–1328, May 1993.

[3] K. Koli and K. A. I. Halonen, "CMRR enhancement techniques for current-mode instrumentation amplifiers," *IEEE Transactions on Circuits and Systems I*, vol. 47, no. 5, pp. 622–632, 2000.

[4] Y. H. Ghallab, W. Badawy, K. V. I. S. Kaler, and B. J. Maundy, "A novel current-mode instrumentation amplifier based on operational floating current conveyor," *IEEE Transactions on Instrumentation and Measurement*, vol. 54, no. 5, pp. 1941–1949, 2005.

[5] D. C. Agouridis and R. J. Fox, "Transresistance instrumentation amplifier," *Proceedings of the IEEE*, vol. 66, no. 10, pp. 1286–1287, 1978.

[6] S. Kilinç and U. Çam, "Transimpedance type fully integrated biquadratic filters using operational transresistance amplifiers," *Analog Integrated Circuits and Signal Processing*, vol. 47, no. 2, pp. 193–198, 2006.

[7] J. J. Chen, H. W. Tsao, and C. C. Chen, "Operational transresistance amplifier using CMOS technology," *Electronics Letters*, vol. 28, no. 22, pp. 2087–2088, 1992.

[8] K. N. Salama and A. M. Soliman, "CMOS operational transresistance amplifier for analog signal processing," *Microelectronics Journal*, vol. 30, no. 3, pp. 235–245, 1999.

[9] H. Mostafa and A. M. Soliman, "A modified CMOS realization of the operational transresistance amplifier (OTRA)," *Frequenz*, vol. 60, no. 3-4, pp. 70–76, 2006.

[10] Y. K. Lo and H. C. Chien, "Current-mode monostable multivibrators using OTRAs," *IEEE Transactions on Circuits and Systems II*, vol. 53, no. 11, pp. 1274–1278, 2006.

Frequency Dependence of Noise Performance Metrices for Gate Electrode Work Function Engineered Recessed Channel MOSFET

Ajita Agarwala and Rishu Chaujar

***Abstract*—This paper discusses the noise assessment, using ATLAS device simulation software, of a gate electrode work function engineered recessed channel (GEWE-RC) MOSFET involving an RC and GEWE design integrated onto a conventional MOSFET. Furthermore, the behavior of GEWE-RC MOSFET is compared with that of a Recessed Channel(RC) MOSFET having the same device parameters. This paper thus optimizes and predicts the feasibility of a novel design, i.e., GEWE-RC MOSFET for high-performance applications where device scaling and noise reduction are a major concern. The noise metrics taken into consideration are: minimum noise figure, optimum source impedance and noise conductance. The statistical tools auto correlation and cross correlation are also analysed owing to the random nature of noise.**

***Index Terms*—ATLAS device simulator, correlation, GEWE-RC MOSFET, minimum noise figure, noise conductance, optimum source impedance.**

I. Introduction

To achieve higher speeds and packing densities, the world has witnessed the miniaturization of the basic MOS device structure. Today, CMOS technology has an established place in the design of multi-gigahertz communication circuits. This is due to the continuing down-scaling of MOS devices, which improves their RF performance characteristics. As the MOSFET is shrunk, some unwanted effects are observed such as punchthrough, hot carrier injection, noise in RF range, and dependence of threshold voltage on channel dimensions, DIBL and other short channel effect (SCEs) which affect the performance of the device in a negative manner. As MOSFET device sizes and signal levels are aggressively scaled down, the low-frequency noise (LFN) properties become increasingly important. This is because the signals are no longer significantly higher than the LFN, especially since the LFN level increases significantly as the device's size is scaled down. As the issue of noise becomes increasingly important in deep-submicron MOSFETs, it is necessary to be able to accurately measure and model the noise parameters of MOSFET to fully characterize its noise performance.

Manuscript received October 14, 2012; revised December 24, 2012. Frequency Dependence of Noise Performance Metrices for Gate Electrode Work function Engineered Recessed Channel MOSFET.

A. Agarwala and R. Chaujar are with the Delhi Technological University, Delhi, India (e-mail: ajitaagarwala90@gmail.com; rishuchaujar@rediffmail.com).

II. Analyzing GEWE-RC MOSFET

Recessed MOSFETs are known to alleviate many of the SCEs [1], [2]. This has been achieved by separating the source and drain(S/D) regions by a groove. Several studies have reported that the potential barrier formed at each recess corner is responsible for suppressing the SCEs, hot-carrier effects and punch-through. It is also responsible for the degradation of current driving capability and threshold voltage. The recessed MOSFET, however, in conjunction with dual material gate (DMG) architecture [3], [4], named as Gate electrode work function engineered recessed channel (GEWE-RC) MOSFET, as shown in fig 1, enhances drain current characteristics, average carrier velocity and suppresses SCEs, thereby proving superior to the recessed channel(RC) MOSFET. GEWE-RC MOSFET has the work function of metal gate1 towards the source i.e. controlling gate (M1) greater than that of metal gate 2 towards the drain i.e. screening gate (M2) i. e.$\varphi M1 > \varphi M2$. With this DMG architecture, the step potential profile, due to different work functions of two metal gates, ensures reduction of SCEs and screening of the channel region under the controlling gate from the drain potential variations. Thus, the average electric field in the channel is enhanced, improving the electron velocity near the source and, hence, the carrier transport efficiency. Some past works on this device such as RF analysis [5] and linearity analysis [6] have been done before and they suggest the feasibility [7] of this model. The work has been complied in Chaujar et al. The GEWE-RC MOSFET [8] (Fig. 1) considered in this study which integrates the potential benefits of Recessed MOSFETs with DMG architecture also enhances the noise performance of scaled devices in comparison to the RC MOSFET.

For the purpose of the above mentioned noise analysis, structural design parameters, such as gate length, junction depth, substrate doping, gate metal work function and thickness of the oxide layer are tuned in GEWE-RC MOSFET to attain the best performance. The noise metrics examined are the minimum noise figure, NFmin, and optimum source admittance, Yopt, or impedance, Zopt, as they are important in the design of low noise RF circuits such as low noise amplifiers (LNA) and mixers. But as noise is a random phenomenon, the statistical tools auto correlation and cross correlation are also analysed to support the simulation results obtained.

All simulations have been performed using ATLAS device simulation software. The models activated in simulation comprise the inversion layer Lombardi CVT mobility model along with the Shockley– Read–Hall (SRH) and Auger

DOI: 10.7763/IJIEE.2013.V3.351

recombination models for minority carrier recombination. Furthermore, we adopt the hydrodynamic energy transport model which includes the continuity equations, momentum transport equations, energy balance equations of the carriers and Poisson's equation [9]. It can model the non-local transport phenomenon, and hence presents a higher accuracy than the drift–diffusion method. The quantum corrections have not been taken into account because the quantum mechanical effects become significant when the gate oxide thickness is below 30 ℃A or 3 nm. In our study, since the gate oxide thickness is 3 nm, the quantum corrections are ignored [10].

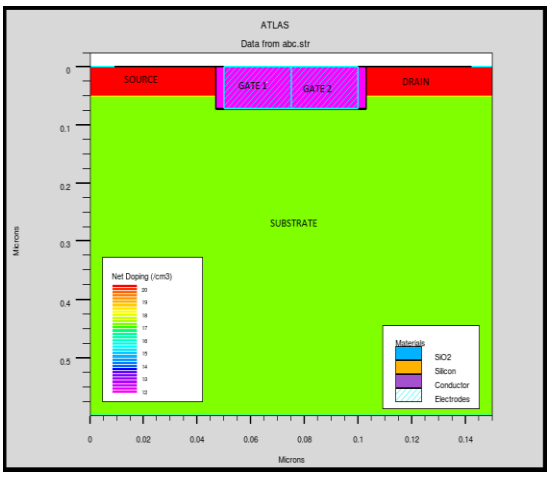

Fig. 1. The architecture of GEWE-RC MOSFET made using ATLAS device simulator. Device width (W)= 1 μm, Groove depth (d)= 70 nm, NA = 1X1017 cm-3, Source/Drain doping, ND = 1x1020 cm-3, tox = 3 nm, εox = 3.9. Work function (φ M2) = 4.1eV for GEWE-RC and for RC, (φ M2) = 4.77eV and (φ M1) = 4.77eV for both. Effective channel length for both is 96nm. Source/Drain junction depth is 50nm.

III. Noise Analysis

Noise performance of a modern small-area MOS devices is dominated by random telegraph signal (RTS) fluctuations [11], [12]. Their origin is the capture and subsequent emission of charge carriers at discrete trap levels near the Si−SiO_2 interface [13], [14]. For deep-submicrometer devices, the number of traps with energy within a few kT close to the surface Fermi level is small [12]. Both, the number of traps and their position over the channel are random variables [13], [14]. Traps located in the gate oxide near the interface to the silicon capture and reemit some of the carriers responsible for the current flowing between the source and the drain of the device [14]. Hence, the carrier transport efficiency is hampered. Now let us see the indivisual parameters taken into consideration.

A. Minimum Noise Figure

The Fig. 2 explains the effect of frequency on the noise behavior of GEWE-RC MOSFET and the RC MOSFET designs (with the same specifications), in terms of minimum noise figure. Results clearly reveal that noise figure for the both of these MOSFETs increases with the increasing frequency. Although, it is noteworthy that the noise figure for the RC MOSFET and GEWE-RC MOSFET at 1000Hz is 0.275065dB and 0.000212794dB respectively. Although, at higher frequencies the value of NF_{min} for both the devices is almost the same. This observation can be mainly attributed to the work function difference of the gates in the GEWE-RC architecture, due to which a step-potential is introduced in the channel [15]. There exists a screening of the channel region from the drain induced variations due to which the number of carriers entering the channel remains comparatively less varied [15]. Also, the vertical electric field is reduced due to which the trapping of the carriers near the Si-SiO_2 reduces, which results in the improved carrier transport efficiency [16].

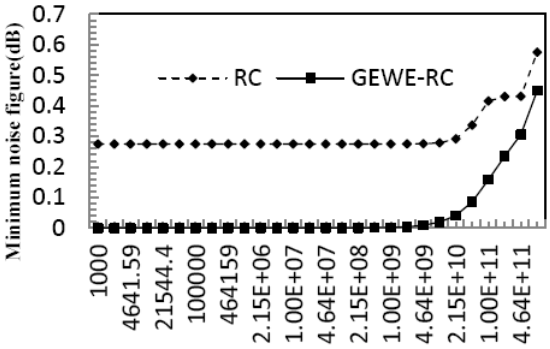

Fig. 2. Minimum noise figure (nf_{min})

B. Optimum Source Impedance

The Fig. 3 gives the behavior of optimum source impedance ($Z_{OPT}=R_{OPT}+jX_{OPT}$) with respect to frequency. Because the oxide layer acts as a dielectric, there is essentially never any current between the gate and the channel during any part of the signal cycle [17]. As the oxide thickness is being continuously shrunk due to the scaling of the MOSFET, the MOSFET should have a large source impedance to avoid destruction by electrostatic charges. In the Fig. 3 it can be vividly seen that optimum impedance for GEWE-RC MOSFET is much higher than that of the RC MOSFET.

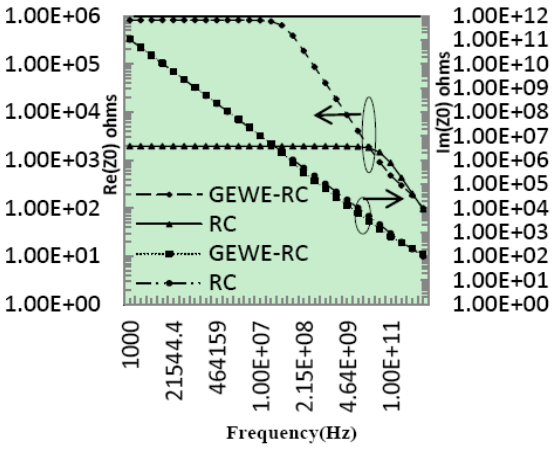

Fig. 3. Optimum source impedance (Z0)

C. Noise Conductance

Spectral density of a noise current generator is measured in conductance units at a specified frequency. It can be seen from Fig. 4 that the noise conductance for GEWE-RC is less than that of RC MOSFET. This can be mainly attributed to the lower DIBL in the DMG structure incorporated along with RC in GEWE-RC MOSFET.

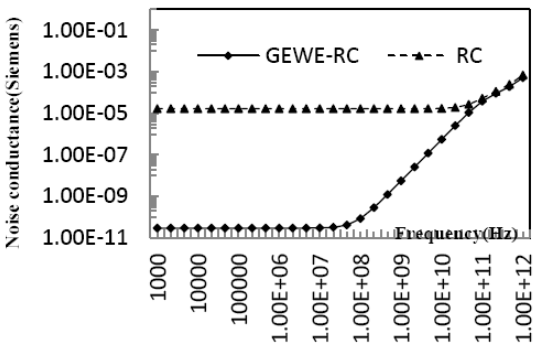

Fig. 4. Noise conductance

D. Autocorrelation and Cross Correlation

The MOSFET is considered as a two port device(Fig. 5) i.e. the noise induced at the gate is separated from the MOSFET and is depicted by V1 and the noise received at the output is replaced by a voltage V2 [18]. Since noise is a random phenomenon, some statistical analysis is indispensible for this research. Thus, the autocorrelation and cross correlation of the voltages at the two ports of the devices are compared. From the above analysis it can be inferred that surface scattering with the Si-SiO_2 gate interface is noticeably reduced in the GEWE-RC MOSFET because of a lower vertical electric field. Therefore, isotropic scatterings present a reduced prevalence in this device [19]. Thus it can be concluded that the mean free path (λ) of carriers crossing the channel as a function of the frequency is much larger than in the recessed channel transistor [15]. This reduced influence of isotropic scatterings implies that the scattering mechanisms are not so effective in breaking the correlation between gate and drain current, which leads to higher cross correlation(i.e. V1.V2*) between them[20]. Fig. 6 depicts such behaviour. Auto correlation is the cross correlation of a signal with itself. As can be seen by Fig. 7, there is higher auto correlation between the input(i.e. V1.V1*) and output voltages(i.e. V2.V2*) in GEWE-RC MOSFET than the RC MOSFET depicting lesser intrinsic noise in the former than the latter.

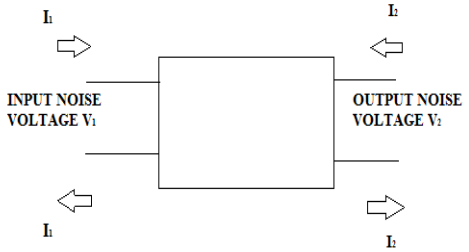

Fig. 5. MOSFET as a two port device where the input noise is replace by a voltage V1 and the noise received at the output is replaced by V2

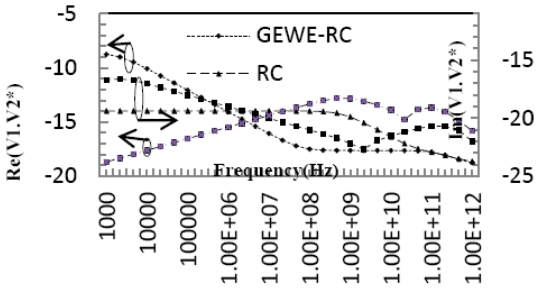

Fig. 6. Cross correlation

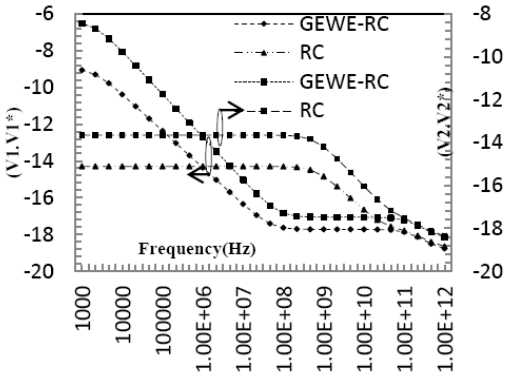

Fig. 7. Auto correlation

IV. Conclusion

As shown in this work, from the analysis of the microscopic noise sources and dynamic performance of the devices; GEWE-RC MOSFET exhibits superior noise performance in comparison to its RC counterpart. It can be concluded that the reduced induced gate noise and stronger cross correlation are responsible for the noticeable improvements observed in the intrinsic minimum noise figure. Hence, proving its potency for low power, low noise and low supply voltage applications. Lower noise figure and higher optimum source impedance pertained by the GEWE-RC architecture strengthens the idea of using it for such applications, thereby giving a new opening for usage in RF applications.

References

[1] E. Takeda, H. Kume, and S. Asai, "New grooved-gate MOSFET with drain separated from channel implanted region (DSC)," *IEEE Trans. Electron Devices* vol. 30, pp. 448–56, 1983.

[2] S. Sreelal, C. K. Lau, and G. S. Samudra, "Parasitic capacitance characteristics of deep sub micrometer grooved gate MOSFETs," *Semicond. Sci. Technol*. vol. 17, pp. 179–88, 2002.

[3] W. Long and K. K. Chin, "Dual material gate field effect transistor (DMGFET)," *IEDM Tech*. Dig. pp. 549–552, 1997.

[4] X. Zhou, "Exploring the novel characteristics of hetero-material gate field-effect transistors (HMGFET's) with gate-material engineering," *IEEE Trans. Electron Devices*, vol. 47, pp. 113–20, 2000.

[5] R. Chaujar, R. Kaur, M. Saxena, M. Gupta, and R. S. Gupta, "GEWE-RC MOSFET: A solution to CMOS technology for RFIC design based on the concept of intercept point," *International Conference on Recent Advances in Microwave Theory and Applications*, pp. 661 –664, 2008.

[6] R. Chaujar, R. Kaur, M. Saxena, M. Gupta, and R. S. Gupta, "Intermodulation distortion and linearity performance assessment of 50-nm gate length l-dumgac mosfet for rfic design," *Superlattices and Microstructures*, vol. 44, pp. 143-152, 2008.

[7] R. Chaujar, R. Kaur, M. Saxena, M. Gupta, and R. S. Gupta, "2007 On-state and switching performance investigation of sub-50nm L-DUMGAC MOSFET design for high-speed logic applications," *Semiconductor Device Research Symposium, International*, pp 1-2, 2007.

[8] R. Chaujar, R. Kaur, M. Saxena, M. Gupta and R. S. Gupta, "2008 Laterally amalgamated dual material gate concave (l-dumgac) mosfet," *ULSI Microelectron*. Eng. vol. 85, pp. 566–576, 2008.

[9] ATLAS Device Simulator, *SILVACO International*, 2011.

[10] S. H. Lo, D. A. Buchanan, Y. Taur, and W. Wang, "1997 Quantum-mechanical modeling of electron tunnelling current from the inversion layer of ultra-thin-oxide nMOSFET's," *IEEE Electron Device Lett*, vol. 18, pp. 209–211, 1997.

[11] R. Brederlow, W. Weber, D. Schmitt-Landsidel, and R. Thewes, "1999 Fluctuations of the low frequency noise of MOS transistors and their modeling in analog and RF-circuit," *IEDM Tech*. Dig. pp. 159–162, 1999.

[12] M. Sáden, O. Marinov, M. J. Deen, and M. Ostling, "2002 A new model for the low-frequency noise and the noise level variation in

polysilicon emitter BJTs," *IEEE Trans. Electron Devices*, vol. 49, pp. 514–519, 2002.
[13] T. Boutchacha and G. Ghibaudo, "1998 Low frequency noise characterization of 0.18 μm Si CMOS transistors," *Phys. Status Solidi, A*, vol. 167, no. 1, pp. 261–270, 1998.
[14] E. Simoen, B. Dierickx, C. L. Clayes, and G. J. Declerck, "1992 Explaining the amplitude of RTS noise in submicrometer MOSFETs," *IEEE Trans. Electron Devices*, vol. 39, no. 2, pp. 41, 1992.
[15] R. Chaujar, R. Kaur, M. Saxena, M. Gupta, and R. S. Gupta, "2008 TCAD Assessment of Gate Electrode Workfunction Engineered Recessed Channel (GEWE-RC) MOSFETand Its Multilayered Gate Architecture—Part I: Hot-Carrier-Reliability Evaluation*," IEEE Trans on Electron Devices* 2008, vol. 55, issue 10, pp. 2602-2613.
[16] F. C. Hou, G. Bosman, and M. E. Law, "2003 Simulation of oxide trapping noise in submicron n-channelMOSFETs," *IEEE Trans. Electron Devices*, vol. 50, no. 3, pp. 846–852, 2003.
[17] G. Ribes, J. Mitard, M. Denais, S. Bruyere, F. Monsieur, C. Parthasarathy, E. Vincent, and G. Ghibaudo, "2005 Review on high-k dielectrics reliability issues," *IEEE Trans. Device Mater*. Rel., vol. 5, no. 1, pp. 5–19, 2005.
[18] L. Belostotski and J. W. Haslett, "2008 Two-port noise figure optimization of source-degenerated cascode CMOS LNAs," *Analog Integr. Circuits Signal Process*, vol. 55, no. 2, pp. 125–137.
[19] R. Rengel and M. J. Martń, "2010 Electronic transport in laterally asymmetric channel MOSFET for RF analog applications," *IEEE Trans. Electron Devices*, vol. 57, no. 10, pp. 2, 2010.
[20] R. Rengel and M. J. Martń, "2010 Electronic transport in laterally asymmetric channel MOSFET for RF analog," *Applications IEEE Trans. Electron Devices*, vol. 57, no. 10, pp. 2, 2010.

R. Chaujar (M'09) received her B.Sc. (H), M.Sc. and Ph.D degrees in Electronics from the University of Delhi, India, in 2003, 2005, and 2009 respectively. She is presently working as an Assistant Professor in Department of Engineering Physics, Delhi Technological University (Formerly Delhi College of Engineering), New Delhi, India and is involved in teaching the B. Tech and M. Tech courses.

A. Agarwala was born in Bareilly, India on 4 December, 1990. She is currently pursuing her final year in Bachelors of Technology in Engineering Physics with Majors in Electronics from Delhi Technological University, India. Her area of interest includes simulation of Sub-100nm gate engineered Grooved Gate/Concave MOSFET. She has authored 3 papers in international conferences and journals. She has visited U.K. in January 2012 and USA in June 2012 to present her papers in international conferences.

Delhi Business Review ✠ Vol. 13, No. 2 (July - December 2012)

Keynote Address

GLOBALISATION AND HIGHER EDUCATION IN INDIA
CHALLENGES AND STRATEGIES

P.B. Sharma*

PURPOSE
TO understand and evaluate current status of higher education in India, underline lacunae, and recommend proper strategies to bridge the gaps in terms of quantity and quality of higher education as obtaining in developed countries of the world and in India matching with global standards by bringing synergy through research and innovations compatable with the sustainbility.

Design/Methodology/Approach*: Descriptive, based on authentic secondary data.*

Findings*: Indian Technological Universities and institutions both at UG and PG level need serious relook at processes employed for creation of knowledge and dissemination of knowledge to prepare both teachers and students resulting into wholistic personality development.*

Research Limitations/Implications*: Limitations of keynote address.*

Practical Implications: *If properly implemented, it would go a long way in value addition in terms of knowledge, skill and applicability.*

Originality/Value: *Provides a window of a fresh look at the existing scenario of higher education both in India and globally.*

Key Words: Higher Education, Knowledge Management, Educational Reforms, Industry Institute Interaction, Integrating Capabilities with Values, Global Outreach.

Introduction

India's emergence as third largest economy of the world in terms of purchasing power parity is largely attributable to the impressive growth of science & technology, management education and their impact on nation's economy. Be it the Green Revolution of late 60's or the IT Revolution of the late 90's, or the Space Revolution of the recent times, India's Science and Technology manpower has stood test of time and demonstrated exemplary capabilities of meeting requirement of quality manpower in tune with the requirements of technology and innovative support providing to India's industrial R&D. Sustainability in terms of ever growing number of engineers and technologists, who hold the key for future hope to turn the potentials of Indian economy into a World economy surpassing even China in about 10-12 years times, and US in 15-20 years time.

The sound foundation of science and technology education provided by the Indian Universities and institutions of engineering and technology has given the necessary platform to Indian Scientists, Engineers and Technocrats to tackle the challenge of globally competitive industry and work environment.

* *Professor and Founder Vice Chancellor, Delhi Technological University, Delhi, India.*

The impressive track record of growth with quality of India's leading R&D organizations such as ISRO, DRDO, BARC, IARI, Institute of Genomics, Institute of Immunology and the pre-eminence position attained by India's leading science and technological universities such as IISc, TIFR, AIIMS, IITs, DTU (formerly DCE). BITS Pilani, Thapar Institute, Jadhavpur University, Anna University speaks volume for India's impressive growth of science and technology prowess. This has been further strengthened by high quality management education provided by the IIMs and a host of other leading management institutions in India to provide the necessary managerial talent for India's rapidly growing industry and technology base. Indian engineers, technologists and techno-managers have received worldwide recognition for their innovativeness as well as their creative abilities. This is our core strength and we need to further revitalize it to meet the challenges of globalised higher education in India. The focus has necessarily to be on worldclassness, techsavvyness and for creating capable human resource to meet the requirements of the industries of today as well as to create the industries of tomorrow.

This however should not overshadow the concern raised by the industries and industry associations at home about low employability of engineering and technology graduates nor should it negate the serious concern raised by very many about erosion of science and science education in India. These concerns are primarily based on India's highly impressive yet largely uncontrolled expansion of technical education during the last one decade and science education taking a backseat in the rush for admissions to engineering and technology courses.

The present paper addresses the issue of meeting the challenge of the Knowledge Age in India's Higher Education as also to create an upsurge for synergy between science and engineering and the necessary thrust on the troika of education, research and innovation in Indian Universities and institutions of higher learning.

India's Higher Education System

India's Higher Education today comprises of over 500+ Universities including over 150 deemed universities and State Technological Universities in addition to a highly impressive management and technology education system which has received worldwide recognition for the quality of its graduates from IITs, IIMs and a good number of other premier institutions including Delhi College of Engineering now Delhi Technological University, BITS Pilani, Thapar Institute of Technology now Thapar University, Jadhavpur University, Anna University and good number of NITs and other premier management institutions such as FMS of Delhi University, XLRI Jamshedpur, S.P. Jain Institute of Management and Research Mumbai, MDI Gurgaon and many others established under self-financing arrangement which include the Delhi School of Professional Studies and Research established by Prof. B.P. Singh himself an eminent Management Professor of Delhi University.

The vast technical education of India comprises of 11 IIMs, 12 IITs, 30 NITs, State Technological Universities in major states of Indian Republic and a large number of self-financing institutions spread across the country, admitting today **over 10 lakhs at UG and over 50000 at PG levels**. The impressive growth of technical education in India is given by Chopra and Sharma (2009) in their RETA Report to NAM Centre in Delhi (2009). The growth of engineering institutions amounts to 257 % over a period from 2000 to 2010 while the intake at UG level in these institutions has grown by 540% over the same period. While the growth is highly impressive so is the concern being voiced by the industry quarters and industry associations in respect of employability of engineering graduates. This becomes all the more important as the employability is being rated as low as 30% by the industry sectors. We need to seriously ponder over the areas of improvement both in respect of admissions as well as the teaching-learning processes employed to produce for the industry, ready to run professionals who would besides working in a knowledge intensive tech-savvy work environment will have the capability to excel in the knowledge age. While the communication skills are a major area of concern, it cannot be denied that the curriculum, teaching learning processes and quality of teachers form an important area which could have been addressed while planning for such an impressive growth.

Table 1: Growth of Degree Level Engineering Institutions (1947 to 1990)

Year	No. of Institutions	Students Intake	Intake per Institution (Average)
1950	50	3700	74
1960	110	16000	145
1970	145	18200	125
1980	158	28500	180
1990	337	66600	198

Source: AICTE Annual Reports and Technical Education in Independent India, 1947-1997.

Table 2: Growth of Degree Level Engineering Institutions (post-liberalization era 1991 onwards), updated from Chopra & Sharma 2009

Year	No. of Institutions	Students Intake	Intake per Institution (Average)
1990	337	66600	198
2000	776	185758	240
2003	1208	359721	298
2004	1265	404800	320
2005	1346	452260	336
2006	1511	550986	364
2007	1668	65290	392
2010	>2000	1000000 approx	500

Imperatives of the Knowledge Era

The knowledge has descended on the strength of the power of mind, power of connectivity and the power of networking unleashed by the IT revolution sweeping across the globe for the last two decade. In this new knowledge era it is imperative for the higher education sector to innovate its curriculum and teaching learning processes on one hand and adopt good practices which have enabled the rise of world-class universities in the developed countries. The important point to realize that it is the flexibility and the freedom of choice that has been the hallmark of the growth of the world class universities in the advanced countries. Compared to this we in India have worked with rigidity as being the hallmark of our university system.

It is ironical that we rigidly control our admission process based on the merit ranks in the entrance examinations for engineering and leave no space for consideration of the interest and aptitude of the candidate in a particular area of engineering activity. Once the discipline or branch of engineering is allotted that becomes the pathway for the growth in higher education, be it admissions to post graduate programs or even the job market. What we do not acknowledge is the fact that excellence emerges only when one is engaged in an activity in which he is interested and is capable of. The lack of engineering excellence in India is largely because of our efforts in the universities to push our students pursue studies in areas in which they may not be genuinely interested. This leads to cross over from engineering

to other non-engineering pursuit once a candidate graduates from a university. This is as far as the rigidity in admissions is concerned.

Likewise, our examination system and our teaching-learning processes also lack flexibility. Being too much tight-jacketed they tend to undertone the interest in engineering sciences and engineering technologies. This has a direct bearing on the lack of growth of innovations and new technology development in our higher education system. This is an area we need to address seriously to rejuvenate our technical education system to meet the challenge of the New Knowledge Era.

The other important imperative of the New Knowledge Era is that we must acknowledge that in the New Knowledge Age it is not just enough to know what is more important but how we keep our knowledge updated, share our knowledge with other like minded individuals and network with people and organizations to create a larger collective good by pooling of mind and pooling of brain-ware for the growth of New Knowledge and New Technologies. Creation of knowledge, sharing of knowledge and management of knowledge requires a tech-savvy education and research environment in our universities. A deeper penetration of knowledge systems for curriculum design, ICT enabled systems for curriculum delivery and e-Governance processes is required to empower all the stakeholders including the students and the faculty to meet the challenge of knowledge revolution in the New Knowledge Age. Further, the new knowledge age requires synergy between the world of learning and the world of engineering profession in the campuses of our universities more so in technological universities and institutes of technology. This would call for a renewed effort on enhancing institute - industry partnership both for improving the quality of curriculum as well as quality of education and research.

We need to seriously examine the issue of networking between Universities and Universities (U&Us), Universities and Institutions, Universities and Industries (U&Is) and Institutions with Industries (I&Is). In the new knowledge age neither the universities nor the industries can excel without the power of networking and collaborative working. Lastly, it is important to realize that in the new knowledge age the academic integrity, research integrity, and conformity to ethical and moral dimensions of the professionals has to be given a renewed focus to build tomorrow's society excelling on fair prosperity on one hand and joy, excitement, thrill and happiness of science and technology led development on the other.

This calls for emphasis on quality assurance through output/outcome based criteria and through developing attributes which would enable graduates to work in a global environment, would permeate to all countries and will help restructuring engineering curricula towards increased innovation and creativity and equipping all graduates with skills of cooperative and harmonious working in multidisciplinary and multicultural teams, Jha (2010). Indian institutions have been very slow in the use of applying management quality standards for their education processes and systems nor have many aspired for global accreditation, Chopra (2010). This has resulted into building of island of higher education in India and not a globally accredited higher technical education system as would be required for India of tomorrow, specially that tomorrow's India is being conceived as the Knowledge and Innovation Hub of the world. It is also important for us to understand that multiplicity of controls and over dozes of regulations are impediments to growth, progress and advancement of what is regulated, Singh (2010).

These imperatives of the New Knowledge Age have to find a place in the agenda for reform in the Universities in India if we have to prepare ourselves to greet the challenges of the New Knowledge Age.

Best Practices in Tech Education

Leading technological institutions and universities, in India have demonstrated some of the best practices in technical education. A brief of these practices is given below:

i) Teachers Evaluation by Students: This practice is prevalent in all IITs and in a number of reputed institutions wherein every teacher is evaluated by the students for the subjects he/she teaches. The evaluation is specific and is aimed to assess the academic performance of the faculty, his command

on the subject, his communication skills and the way he greets the teaching learning environment. This is done both for theory as well as practical subjects. The evaluation is on a 5 point scale ranging from excellent to not satisfactory. Because of this practice, the teachers in IITs and other reputed institutions in India have always been exhibiting high levels of teaching effectiveness and have been keeping themselves abreast with the latest developments in their respective fields. The quality of teaching will be significantly improved if this practice is introduced in technological universities and engineering institutions across the country too.

ii) Regular Review of Course Contents & Course Curricula: This practice is prevalent in all IITs and other reputed institutions wherein at the end of the semester all members of the faculty are required to submit any change/revision in the course content, deletion of the course/introduction of a new course in their subject schemes. The department academic committee examines these recommendations, which are further evaluated and approved by the course curriculum committee of the academic councils. This way each year the course contents and curriculum are reviewed and updated. What we need of course is to establish system of curriculum watch at the institution/university level and use the capabilities of the knowledge management systems for curriculum updation and curriculum innovation, Agarwal, Sharma and Kumar (2008).

iii) Introduction of Courses in the Emerging Areas: This practice is prevalent in all the leading institutions in the country including the IITs, BITS Pilani, Delhi Technological University etc. wherein courses in the emerging areas of high relevance to science and technology developments and relevant to the country's industrial and economic development are identified, developed and introduced in the course curriculum, both at undergraduate and postgraduate levels. This is a good practice to take care of the advancing frontiers of knowledge and introduction of new technologies in the technical education. It would further be beneficial to promote new programs at UG and PG levels in engineering and technology carefully developed along the concept of synergy between science and engineering. Programs in mathematics and computing, engineering physics, bio-engineering, medical engineering, infrastructure engineering could be well suited at UG and PG levels. While nano-science and engineering, material science and technology, space science and technology, medical engineering, autonomous systems design and such like courses which could be designed for joint deliveries by the science and engineering department should be promoted at the PG levels. This will promote trans-departmental culture so vital for the growth of excellence in science and engineering. This will also help in creating strong ties between science and engineering and will foster scientism, Sharma (2010).

iv) Promotion of Research Culture in the Technical Institutions: Promotion of postgraduate programmes, Ph.D. programmes and a culture of sponsored R&D projects has been the main strength of the IITs and other leading engineering and technology institutions in the country. IITs have been able to develop their own laboratories and excel in advanced areas of science and technology primarily because of the existence of a research culture in all departments of engineering and applied sciences. In the knowledge age it is important to realize that research culture can be percolated to the UG levels in engineering and technology institutions. Undergraduates are talented and possess high creative and innovative potential. Research culture at UG levels shall unleash and ignite the power of innovation and creative research. At Delhi Technological University, formerly Delhi College of Engineering, we have succeeded in percolating research culture to UG levels and a number of innovatively designed products such as Hybrid Car, Super Mileage Vehicle, Unmanned Anal Vehicle, Autonomous Underwater Vehicle and Autonomous Aircraft Systems have been rolled out on the strength of highly innovative genius of UG students from Delhi College of Engineering, now Delhi Technological University. It is a healthy sign that a number of other engineering institutions in India have now taken up the task of research and innovation at UG levels.

v) Industry Relevant Research and Consultancy by the Teachers: Teachers of institutions of engineering and technological universities, besides teaching are supposed to practice their knowledge and expertise for the benefit of the industry and society. This is best done by promoting a culture of

industrially relevant R&D and industrial consultancy projects to be undertaken by the institute's faculty. This practice is highly prevalent in IITs and a number of other premier institutions in the country. In an industrially driven R&D environment, teachers and students engage in industrially relevant knowledge creation and new product development. This way the gap between the laboratory level research and institutional innovations and the new product development in the industry is greatly bridged besides creating a healthy environment for transformation of knowledge into prosperity. The world class universities generate a significant proportion of their R&D budget from industry sponsored R&D projects and from the IPR generated by the teachers of the university. This practice ensures that the process of knowledge creation and industrial R&D go hand in hand in the academic circles of the University. Industry sponsored R&D is also the best way to promote inter-disciplinary research and innovative new product development. The faculty and the research scholars are also adequately rewarded for the intellectual property they generate alongside with their educational activities. This also ensures more effective utilization of the in-house resources and equipments in the laboratories. We in India need to significantly enhance our share of intellectual property and industry relevant research to transform India of today which is largely today a manpower development country to the research and innovation hub of tomorrow. This is all the more important as India is rapidly emerging as the chosen destination for the establishment of research and innovation center by great many multinational industries.

vi) Endowment Professorial Chairs: Industrial organization in the country sponsor creation of professorial chairs in engineering institutions specifically for the purpose of promotion of R&D and HRD in specified science and technology areas. This practice is highly prevalent in all IITs where almost all departments have more than one endowment chairs funded by the sponsoring organizations/ industries. The endowment Chair Professorships also bring in industry relevance in education and research in the institution. The Government may offer attractive incentives to the industries funding sponsored R&D and endowment Professorial Chairs in technological Universities and institutions of engineering in the country.

vii) Student Chapters of Professional Societies in the engineering colleges: Establishment of Student Chapters of National and International Professional Societies such as IEEE (USA), IEE (UK), ASME(USA), SAE(USA) etc. and Institution of Engineers (India), ISTE (India) goes a long way in improving the professional orientation of the students. This practice is prevalent in leading institutions in the country like the IITs, DCE, BITS Pilani and other leading institutions in the country.

viii) Industry sponsored Laboratories in Institutions: In certain areas of technology, industry sponsors establishment of specialized laboratories in the engineering colleges. This practice is prevalent in universities abroad. IIMs and other leading institutions in this country are also paying a greater attention to this aspect. Indian Technical education has opportunities of BHEL, NTPC, Wipro, Infosys, Tata lnfotech and even NIIT, GAIL, Siemens, Hewlett Packard, HCL setting up sponsored laboratories in the colleges of engineering. At least 1 laboratory in each department should be established under sponsorship of the industry. This will promote frontline technologies and bring industries close to the institutions.

ix) Technology incubation and techno-preneurship promotion: Technical education in the knowledge era has empowered both the teachers and the students with the power of connectivity and power of networking. This has created enormous potential for pursuit of innovation and new product development while at studies in an engineering institution. What is needed is to provide in house facilities for ideation, technology incubation and for promotion of student led start up campaign. Establishment of Technology and Business Incubation Unit. TBIP is one such good practice currently in Vogue in institutions like IITs and in other leading institutions in India. Initiatives like TBIP create the enabling environment and provide a systematic support for the growth of techno-preneurship.

x) Technology Enabled Education: In the new knowledge age it is an acknowledged fact that the

science and technology horizons are rapidly expanding. The half life of knowledge as well as of technology and skills is also rapidly reducing. In some areas such as IT and computing, the half life of knowledge and associated skills has been reduced to less than a year. The same is the case with even core disciplines like Mechanical, Electrical, Civil and Electronics. Here also, the change from macro to micro and even nano is impacting the capabilities of all of us to cope up with rapidly changing technology and knowledge base in these core disciplines. Further, engineering is no longer confined to a single discipline as engineering today is and shall surely be tomorrow a highly interdisciplinary pursuit in which human mind shall engage itself to create new designs, new forms, new products, new services, new business and even new strategic framework to work in the connected and networked economy. It is important, therefore, for us to acknowledge that the time has come when we have to declare, and declare boldly that each one of us knows something and no one knows everything. Students have to learn from teachers, the teachers have to learn from students, teachers and students together have to learn from their peers. What more that the students, teachers and peers together have to learn a lot from the vast knowledge reservoir which is being enriched regularly and rapidly by pooling the brainwaves of intelligent people around the world. In this changed paradigm we have to look for solutions to the pressing problems like shortage of quality faculty, design of innovated curriculum, designing and developing new delivery systems for knowledge dissemination and newer ways of developing prototypes, innovated products and services in a highly compressed time frame. It is in this context we have to perceive the role of technology in education specially, the role of ICT in education, more so, in higher technical education if we have to succeed in pooling together the vast body of knowledge and for enhancing the learnability as well as employability of the students.

Conclusion

India's higher education system requires a serious relook at the processes employed for creation and dissemination of knowledge in the institutions of higher learning and technological universities. The imperatives of new knowledge era are to be acknowledged and the challenge of the globalised higher education should be addressed by creating a tech-savvy education and research system. The synergy between science and engineering and creation of the troika of education, research and innovation in the university and institutional campuses holds the promise for preparing India to meet and greet the challenges of globalised higher education both in respect of creating the power of science and the might of technology together in technological institutions as also to create globally employable manpower and technology base to fuel today's as well as tomorrow's industries worldwide.

The opportunity to do so is already knocking at the doors of India's universities and institutions of higher learning. It is important that at this juncture to innovate and adopt best practices to revitalize the universities in India and shape them as world class universities of tomorrow.

References

Chopra, K.L. and Sharma, P.B. (2009) "RETA Report on Higher Technical Education in India — Profile of Growth and Future Perspectives", submitted to NAM Centre for Science and Technology, New Delhi, April.

Jha, C.S. (2010), "Engineering Education with International Perspective", Profile of Engineering Education in India, Indian National Academy of Engineering, pp.22-40.

Chopra, K.L. (2010), "Challenges Faced by Indian Engineering Education", Profile of Engineering Education in India, Indian National Academy of Engineering, pp.41-60.

Agarwal, Sanjay, Sharma, P.B., and Kumar, M. (2008), "Knowledge Management Framework for Improving Curriculum Development Processes in Technical Education", Third International Conference on Convergence and Hybrid Information Technology, ICCIT, Vol. 2, pp.885-890.

Singh, D.V. (2010), "Technical Education-Policies, Acts, Regulations and Verdicts", Profile of Engineering Education in India, Indian National Academy of Engineering, pp.193-227.

Sharma P.B. (2010), "Scientism: Combining Science with Technology for New Knowledge Society in India", STAND Special Issue 2010 - India a Knowledge Society, July, pp.34-36.

Machine Learning assisted Sentiment Analysis

Akshi Kumar
Department of Computer Engineering
Delhi Technological University
Delhi, India
akshi.kumar@gmail.com

Teeja Mary Sebastian
Department of Computer Engineering
Delhi Technological University
Delhi, India
teeja.sebastian@gmail.com

Abstract—***Enormous importance has been attributed to public opinion and sentiment as what people think has always influenced new business decisions, political mood, governance policies and personal choices. Also, the availability of opinionated user generated data has increased as people have started freely expressing their views on various cyber platforms like blogs, forums, review sites and social networks. This has spurred the unabated growth of opinion mining and sentiment analysis as important research areas. Opinion mining and sentiment analysis are computational techniques that seek to understand opinion and sentiment, subjectivity by analyzing unstructured opinion text. This paper illustrates the convergence of two prominent research areas, namely, Sentiment Analysis and Machine Learning where the latter has proven its merit as a technique for automated Sentiment Analysis.***

Keywords-***Sentiment Analysis; Opinion Mining; Machine learning***

I. INTRODUCTION

Recent years manifest the beginning and growth of the social web, in which individuals freely express, articulate and respond to opinion on a whole variety of topics. Simultaneously, today's information society challenges companies and individuals to create and employ mechanisms to search and retrieve relevant data from the huge quantity of information available and mining for opinions thereafter. Consequently, Sentiment Analysis [1] which automatically extracts and analyses the subjectivities and sentiments (or polarities) in written text has emerged as an active area of research. The enthusiasm shown by researchers in this field has been because they realize the importance attributed to public opinion and sentiment in businesses, governance and decision making processes. The goal of sentiment analysis is to create market/business/governance intelligence, to detect opportunities and issues, understand the public sentiment conveyed in different forms of textual communications. Sentiment analysis has found applications in gauging the success of particular campaigns, understanding potential consumers who are not favorably responding to products, understanding the competitions standing and in picking up on promising trends. It can also be used as an augmentation to present recommendation systems.

Most researchers have defined the Sentiment Analysis problem as essentially a text classification problem and machine learning techniques have proved their dexterity in resolving the sentiment analysis tasks. Although we can generalize Sentiment Analysis as a text classification problem, it comes with its own set unique challenges and issues which have to be addressed by the machine learning techniques.

To find the opinion bearing portions in a document we have to first understand that sentences in a document maybe objective or subjective. It is generally considered that subjective sentences are the opinion carriers in a document as subjective sentences express some personal belief or view and objective sentence expresses some factual information. But an objective sentence may state a fact but they might also be conveying some sentiment, for e.g. "Women are getting more opportunities in offices". Models cannot infer opinions from facts as they are trained on opinion words.

One may further think that sentiment orientation can be easily identified by a set of keywords. But coming up with the right set of keywords is not a trivial task as shown by Pang et al.[2]. This is because sentiment can also be expressed in subtle ways or sarcastically which makes its identification problematic when considered separately at the sentence level. Another problem is that some words have both strong positive and negative sentiment. Classifying them without knowing the context is a difficult task. Order dependence also manifests itself at more fine-grained levels of analysis: "A is better than B" conveys the exact opposite opinion from "B is better than A" [3]. Also, the increased use of informal English, abbreviations and bad spellings on Web platforms makes the sentiment conveyed difficult to comprehend and classify.

Addressing the issues mentioned above that range from tackling the vague definition of sentiment and the complexity of its manifestation in text, brings up new questions providing ample opportunities for both quantitative and qualitative work. To automate sentiment analysis, different approaches have been applied to predict the sentiments of words, expressions or documents. These include Natural Language Processing (NLP) and Machine

Learning algorithms like supervised learning[2,4,5,6,7], unsupervised learning [8,9,10,11] and semi-supervised learning[12,13,14].

This paper aims to probe the role machine learning as a prominent assisting technology that has ascertained substantial gains in automated sentiment analysis research and practice by developing standards and improving effectiveness.

II. TERMS AND DEFINITIONS

Formally stating, Sentiment Analysis is the computational study of opinions, sentiments and emotions expressed in text[1]. That is, sentiment analysis aims at detecting subjective information in a document and then determining the orientation of the sentiment expressed in the document. Researchers use the terms sentiment analysis, opinion mining, subjectivity analysis, review mining and appraisal extraction interchangeably.

The terms frequently used to define the Sentiment Analysis problem has been given below:

- Opinionated Document: A review, forum post, blog or tweet that contain sentences which expresses any kind of opinion, sentiment or emotion.
- Target Entity or Object: An individual, organization, product, service, issue or event that is being discussed in the opinionated document.
- Object Feature: The target entity can have features or components associated with it. For e.g. When the target entity is a camera, the shutter speed is a feature. Opinions can be expressed specifically about a feature instead of generally about the object e.g., the *battery life* of the phone is good.
- Opinion Holder: A person or an organization which expresses an opinion is called an opinion holder or opinion source. Authors of the blog post or a review are the opinion holders. In case of news articles the opinion holder is explicitly mentioned.
- Sentiment Orientation or Polarity: The orientation or polarity of the opinion is whether the opinion on a feature is positive, negative or neutral. Opinions vary in intensity from very strong to weak. For example a positive sentiment can range from content to happy to ecstatic. Thus, strength of opinion can be scaled and depending on the application the number of levels can be decided.

The following example in Figure 1 illustrates the basic terminology of sentiment analysis:

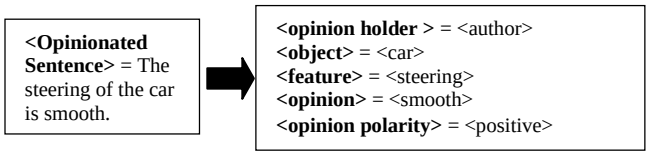

Figure 1: Example corresponding to Terminology of Sentiment Analysis

The objective in a sentiment analysis task is to find four parameters (the opinion, the opinion holder, the object, the feature) corresponding to each other. This is a challenging problem, as finding each parameter in itself is difficult enough.

Since 1940's, many knowledge-based systems have been built that acquire knowledge manually from human experts, which is very time-consuming and labor-intensive. To address this problem, Machine Learning algorithms have been developed to acquire knowledge automatically from examples or source data [15]. It is defined as "any process by which a system improves its performance" [16].

Machine Learning is programming computers to optimize a performance criterion using example data or past experience[17]. A learner (a computer program) processes data D representing past experiences and tries to either develop an appropriate response to future data, or describe in some meaningful way the data seen [18].

Machine Learning Algorithms can be broadly divided into Supervised, Unsupervised and Semi-Supervised learning algorithms. In supervised learning, the aim is to learn a mapping from the input to an output whose correct values are provided by a supervisor[17] Supervised Algorithms use labeled training data to create a function which would predict the correct output. In unsupervised learning, there is no supervisor and there is only input data. The aim is to find the regularities in the input. There is a structure to the input space such that certain patterns occur more often than others and these patterns help in prediction [17]. Semi-Supervised Algorithms use both labeled and unlabelled data for training purposes.

The following sections introduce and discuss the sentiment analysis as a text-classification problem and the multiplicity of machine learning techniques that have been employed by various researchers over the years for sentiment analysis problem.

III. SENTIMENT ANALYSIS AS A CLASSIFICATION TASK

Sentiment analysis is a challenging interdisciplinary task which includes natural language processing, web mining and machine learning. It is a complex task and encompasses several separate tasks, viz:

- Subjectivity Classification
- Sentiment Classification
- Object Feature Identification
- Opinion Holder Identification

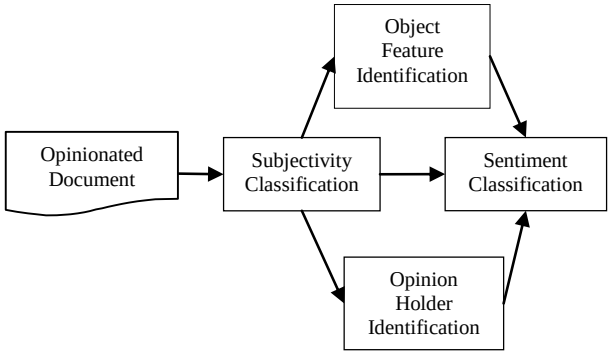

Figure 2: Tasks in Sentiment Analysis

A. Subjectivity Classification

As mentioned earlier, a document may contain both subjective and objective sentences. For sentiment analysis, it is beneficial to be able to differentiate between opinionated and non-opinionated sentences. Subjectivity classification is thus the task involving the classification of sentences/ phrases/ words as opinionated or not.

B. Sentiment Classification

After establishing that a sentence is opinionated, it is required to know the orientation of the opinion too. Sentiment classification can be a binary classification (positive or negative) [2], multi-class classification (extremely negative, negative, neutral, positive or extremely positive), regression or ranking[4].

C. Object and Feature Identification

Blogs and social media sites do not have a set target or predefined topic and tend to discuss diverse topics. Therefore in these scenarios it becomes essential to know the target entity [11, 19]. Also in case of review sites, the reviewer could talk about certain features of the target object and may like a few and dislike others. It thus, becomes necessary to differentiate between the different features of the object. Feature based opinion sentiment analysis which involves feature extraction and the corresponding opinion is also a goal pursued by researchers

D. Opinion Holder Identification

Detection of opinion holder [20] is to identify direct or indirect sources of opinion or emotion. They are important in genres like news articles and other formal documents. In such documents, the holder of the opinion maybe explicitly mentioned. In blogs and review sites the opinion holder is usually the author who can be identified by the login id.

All text processing approaches require converting text into a feature vector or engineer a suitable set of features. These representations may make the significant features available for machine learning approaches. Few of the features used in practice are given below [3]:

- Words and their frequencies
  Unigrams, bigrams and n-grams along with their frequency counts are considered as features. There has been contention on using word presence rather than frequencies to better describe this feature. Pang et al.[2] so showed better results by using presence instead of frequencies.
- Parts of Speech Tags
  Parts of speech like adjectives, adverbs and some groups of verbs and nouns are good indicators of subjectivity and sentiment.
- Syntax
  Syntactic patterns like collocations, are used as features to learn subjectivity patterns by researchers. The syntactic dependency patterns can be generated by parsing or dependency trees.
- Opinion Words and Phrases
  Apart from specific words, some phrases and idioms which convey sentiments can be used as features, e.g. ”cost someone an arm and leg”[1].
- Position of Terms
  The position of a term within a text can effect on how much the term affects overall sentiment of the text
- Negation
  Negation is an important but tricky feature to incorporate. The presence of a negation usually changes the polarity of the opinion but all appearances do it. For e.g., “no doubt it is the best in the market” .

Sentiment Analysis is formulated as a text-classification problem [3] and therefore traditional machine learning techniques are used for the subjectivity/sentiment classification task. High accuracy classification has been achieved by using a variety of techniques, most of which are heavily reliant on machine learning. Like most machine learning applications, the main task of sentiment classification is to engineer a suitable set of features.

IV. MACHINE LEARNING TECHNIQUES

We now discuss the various machine learning techniques that have been employed by various researchers over the years for sentiment analysis problem. This section focuses on the unique aspects of the machine learning techniques in sentiment analysis mainly because of the different features involved in case of supervised and semi-supervised techniques. Unsupervised techniques use sentiment driven pattern to obtain labels for words and phrases.

A. *Supervised Learning*

Supervised learning generally functions as follows: in the initial training phase, an inductive process learns the characteristics of a class based on a feature set of pre classified documents (reference corpus) and it then applies the acquired knowledge to categorize unseen documents, during testing. Several classical classifiers like Naïve Bayes,, Maximum Entropy and Support Vector Machines are most commonly used supervised methods used.

Pang et al.[2] experimented with three classifiers(Naive Bayes, maximum entropy, and support vector machines) using features like unigrams, bigrams, term frequency, term presence and position, and Parts-of-speech to classify movie reviews as good or bad. They concluded that SVM classifier works best and that unigram presence information was most effective. Dave et al. [5] although claim that in some situations, bigrams and trigrams produce better product-review polarity classification.

Using supervised learning for predicting the rating scores has also been done (1-5 stars) in [4]. The problem is formulated as a regression problem since the rating scores are ordinal.

Supervised learning methods have been used for subjectivity classification too. Most works focus on adjectives and their effects on subjectivity of sentences [7]. Wiebe et al.[21] used the naive Bayes classifier to develop a gold standard data set for subjectivity classification.

Yu and Hatzivassiloglou [22] developed three approaches to classify opinions from facts at the sentence level. The first approach explored the hypothesis that "within a given topic, opinion sentences will be more similar to other opinion sentences than to factual sentences". The second method trained a Naive Bayes classifier , using sentences in opinion and fact documents as the examples of the two categories. The features included words, bigrams, and trigrams, as well as the parts of speech in each sentence. They also included in their features the counts of positive and negative words in the sentence , as well as counts of the polarities of sequences of semantically oriented words. Third approach involved training separate Naive Bayes classifier for each different subset of the features. The goal was to reduce the training set to the sentences that are most likely to be correctly labeled. They assumed as ground truth the information provided by the document labels and that all sentences inherit the status of their document as opinions or facts. Then they train the first classifier on the entire training set. Then they used the classifier to predict the labels of the training set. The sentences that were labeled incorrectly were removed. The second classifier then trained on the reduced training set and this went on until the training set could no longer be reduced.

Wilson et al. [23] also formulate sentiment detection as a supervised learning task. However, instead of using just text classification, they focus on the construction of linguistic features, and train classifiers using Boostexter [24]. Incorporating background knowledge, in terms of linguistic rules, in such classifiers is an interesting direction for future work.

There has been a growing interest in the use of background, prior or domain knowledge in supervised learning. Most of this work has focused on using such prior class-bias of features to generate labeled examples that are then used for standard supervised learning. Provided with some features associated with each class, Wu and Srihari [25] assigned labels to unlabeled documents, which were then used in conjunction with labeled examples to build a Weighted Margin Support Vector Machine.

Another paper that includes prior knowledge is [26]. They constructed a generative model based on a lexicon of sentiment-laden words, and a second model trained on labeled documents. The distributions from these two models were then adaptively pooled to create a composite multinomial Naïve Bayes classifier that captured both sources of information. By exploiting prior lexical knowledge they dramatically reduced the amount of training data required. In addition, by using some labeled documents they were able to refine the background knowledge, which is based on a generic lexicon, thus effectively adapting to new domains.

Adaption to different domains is crucial as the accuracy of sentiment classification can be influenced by the domain. Thus, classifiers trained in a certain domain give poor results in other domains. This is because phrases can be expressing different sentiments in different domains.

B. *Unsupervised Machine Learning*

There has been shift from using supervised approaches to using unsupervised and semi supervised approaches as the manual effort to annotate a huge corpus is too much. Unsupervised learning approaches first build a sentiment lexicon in an unsupervised manner, and then resolve the strength of sentiment (or subjectivity) of a text using a function based on the orientation (or subjectivity) indicators.

Thus, an important task of applying this technique is the construction of the lexicon by means of unsupervised labeling of words or phrases with their sentiment orientation or subjectivity status.

To create a lexicon Turney [8] suggested comparing whether a phrase was more likely to co-occur with the word "poor" or "excellent". The basic idea was that a phrase has a positive semantic orientation when it has good associations and similarly negative semantic orientations when it has bad associations. The relationship between an unknown word and a set of manually-selected seeds defined by PMI (Point-wise mutual information), was used to place it into a positive or negative subjectivity class.

Kim and Hovy [9] manually created a small seed list of positive and negative words that contained verbs and adjectives. The synonyms and antonyms of the words were extracted from WordNet and then added to appropriate lists (synonyms would have same orientation and antonyms opposite). The seed lists were further developed by using the expanded list to extract another set of words. They then

calculate the sentiment strength of the unseen word by determining how it interacts with the sentiment seed list.

Kamps[10] measured similarity of words by using distance between words based on WordNet lexical relation. They collected all words in WordNet, and related words that could be synonymous, i.e. were part of the same synset. A graph was created with edges connecting each pair of synonymous words. The distance between two words w_i and wj was the length of a shortest path between wi and wj . The orientation of a term was determined by its relative distance from the two seed terms good and bad. The values ranged from [-1, 1] with the absolute value indicating the strength of the orientation.

Gamon et al. [11] used the unsupervised learning technique for identification of aspects or features. They presented an unsupervised aspect identification algorithm that employed clustering over sentences with each cluster representing an aspect. Sentence clusters were labeled with the most frequent non-stop word stem in the cluster.

C. *Semi Supervised Machine Learning*

Semi Supervised Learning models learn from both tagged and untagged data. The untagged data provides no information about subjectivity or sentiment polarity but they contain information about the joint distribution of the classification features. Bootstrapping is usually the technique used in semi supervised learning Bootstrapping is fundamentally to use the output of an existing initial classifier to produce labeled data, to which a supervised learning algorithm is later applied. This method is also called self-training.

Riloff et al.[12] proposed a bootstrapping process to identify subjective patterns. A bootstrapping process is used that learns linguistically rich extraction patterns for subjective (opinionated) expressions. Two high-precision classifiers, Hp-Subj and Hp-Obj, label unannotated data to automatically create a large training set, which is then given to an extraction pattern learning algorithm. The learned patterns are then used to identify more subjective sentences. A set of syntactic templates was needed to represent the space of possible extraction patterns.

Co-training is another semi supervised method that has been applied. Jin et al. [13] created disjoint training sets for building two initial classifiers. The bootstrap document was then tagged using each of the trained HMM(Hidden Markov Model) based classifiers. The opinion sentences that were agreed upon by both classifiers were extracted and saved in the database if it was unique. The newly discovered data was randomly split and added to the training set of the two classifiers. This bootstrap process was continued until no new data could be discovered.

Graph based semi supervised technique has been used in the task of rating inference by Goldberg and Zhu[14].

Given below is a table which compares the accuracy of the different machine learning techniques implemented by researchers (This is not an exhaustive table):

TABLE I. COMPARATIVE RESULTS

Literature and author	***Machine Learning Method***	***Classifier/Training Set***	***Accuracy***
Pang et al. (2002)[2]	Supervised	NB	.815
		ME	.810
		SVM	.829
Dave et al. (2003)[5]	Supervised	SVM	
Turney and Littman (2002)[27]	Unsupervised	SO-PMI-IR using a two billion word corpus	.894
Riloff et al. (2003)[12]	Semi Supervised	News document from FBIS	.733
Pang and Lee (2004)	Supervised	SVM	.872
Kim nd Hovy (2004)[9]	Unsupervised	WordNet	.81
Kamps et al. (2004)[10]	Unsupervised	WordNet	.787
Aue and Gamon (2005)[11]	Supervised	SVM	.905
Jin et al. (2009)[13]	Semi Supervised	Online product review from Amazon	.771

a. .NB: Naïve Bayes
b. .ME: Maximum Entropy
c. SVM: Support Vector Machine.

While machine learning methods have established to generate good results, there are associated disadvantages. Machine learning classification relies on the training set used, the available literature reports detail classifiers with high accuracy, but they are often tested on only one kind of sentiment source, mostly movie review, thus limiting the performance indication in more general cases. Further, gathering the training set is also arduous; the noisy character of input texts and cross-domain classification add to the complexities and thus push the need for continued development in the area of sentiment analysis.

V. CONCLUSION

Web is an ever expanding sea of information and sentiment analysis is one of the ways that can be used to analyse it and confer structure to it. Machine Learning is one of the foremost techniques used to achieve this end. This paper attempted at exploring the union of the two major research fields, Sentiment analysis and Machine Learning. We can conclude by saying that all sentiment analysis tasks are challenging and difficult. Our knowledge

and comprehension of the problems in this field is still developing. The many practical applications of sentiment analysis is urging researchers to make significant improvements to understand and work in the sentiment analysis domain.

REFERENCES

[1] B. Liu . "Sentiment Analysis and Subjectivity". Handbook of Natural Language Processing, Second Edition, (editors: N. Indurkhya and F. J. Damerau), 2010

[2] B. Pang, L.Lee, and S. Vaithyanathan. "Thumbs up? Sentiment classification using machine learning techniques". In Proceedings of the Conference on Empirical Methods in Natural Language Processing (EMNLP), pages 79–86, 2002

[3] B.Pang and L. Lee,"Opinion mining and sentiment analysis". Foundations and Trends in Information Retrieval 2(1-2), pp. 1–135, 2008

[4] Bo Pang and Lillian Lee." Seeing stars: Exploiting class relationships for sentiment categorizationwith respect to rating scales". In Proceedings of the Association for Computational Linguistics (ACL),pages 115–124, 2005.

[5] Dave K., Lawrence S, and Pennock D.M. "Mining the peanut gallery: Opinion extraction and semantic classification of product reviews". In Proceedings of WWW , :519–528,2003

[6] Bo Pang and Lillian Lee. A sentimental education: Sentiment analysis using subjectivity summarization based on minimum cuts. In Proceedings of the Association for Computational Linguistics (ACL), pages 271–278, 2004.

[7] J. Wiebe, "Learning subjective adjectives from corpora," Proceedings of AAAI, 2000

[8] Peter Turney. "Thumbs up or thumbs down? Semantic orientation applied to unsupervised classification of reviews". In Proceedings of the Association for Computational Linguistics (ACL), pages 417–424, 2002.

[9] Soo-Min Kim and Eduard Hovy."Determining the sentiment of opinions". In Proceedings of the International Conference on Computational Linguistics (COLING), 2004.

[10] Jaap Kamps, Maarten Marx, Robert J. Mokken, and Maarten de Rijke. "Using WordNet to measure semantic orientation of adjectives". In LREC, 2004

[11] M. Gamon, A. Aue, S. Corston-Oliver, and E. Ringger. "Pulse: Mining customer opinions from free text". In Proceedings of the 6th International Symposium on Intelligent Data Analysis (IDA), 2005

[12] E. Riloff, J. Wiebe, and T. Wilson, "Learning subjective nouns using extraction pattern bootstrapping," Proceedings of the Conference on Natural Language Learning (CoNLL), pp. 25– 32, 2003

[13] Wei Jin, Hung Hay Ho, and Rohini K.Srihari." OpinionMiner: A novel machine learning system for web opinion mining". In Proceedings of the 15th ACM SIGKDD International Conference on Knowledge Discovery and Data Mining, Paris, France,2009

[14] Andrew B. Goldberg and Jerry Zhu." Seeing stars when there aren't many stars: Graph-based semi-supervised learning for sentiment categorization". In TextGraphs: HLT/NAACL Workshop on Graph-based Algorithms for Natural Language Processing, 2006

[15] Bhatia, MPS. & Kumar, A., "Information Retrieval & Machine Learning: Supporting Technologies for Web Mining Research & Practice", Webology, Vol. 5, No.2 ,2008.

[16] Simon, H. A.. "Why Should Machine Learn?" In R. S. Michalski, J. Carbonell, & T. M. Mitchell (Eds.), Machine learning: An artificial intelligence approach (pp. 25-38). Palo Alto, CA Tioga Press.,1983

[17] Alpaydin E "Introduction to machine learning", vol 452. MIT Press, Cambridge,2004

[18] Vucetic,Slobodan,
http: //www.ist.temple.edu/~vucetic/cis526fall2003/lecture1.pdf

[19] Ana-Maria Popescu and Oren Etzioni."Extracting product features and opinions from reviews". In Proceedingsof the Human Language Technology Conference and the Conference on Empirical Methodsin Natural Language Processing (HLT/EMNLP), 2005

[20] Yejin Choi, Eric Breck, and Claire Cardie. "Joint extraction of entities and relations for opinion recognition".In Proceedings of the Conference on Empirical Methods in Natural Language Processing(EMNLP), 2006

[21] J. Wiebe, R. F. Bruce, and T. P. O'Hara. "Development and use of a gold standard data set for subjectivity classifications." Proceedings of the Association for Computational Linguistics (ACL), pp. 246–253

[22] Hong Yu and Vasileios Hatzivassiloglou." Towards answering opinion questions: Separating facts from opinions and identifying the polarity of opinion sentences". In Proceedings of the Conference on Empirical Methods in Natural Language Processing (EMNLP), 2003

[23] Theresa Wilson, Janyce Wiebe, and Paul Hoffmann. "Recognizing contextual polarity in phrase-level sentiment analysis". In Proceedings of the Human Language Technology Conference and the Conference on Empirical Methods in Natural Language Processing (HLT/EMNLP), pages 347–354, 2005

[24] Schapire, R. E. and Singer, Y. 2000. "BoosTexter: a boosting-based system for text categorization". Machine Learning 39, 2/3, 135–168

[25] X. Wu and R. Srihari." Incorporating prior knowledge with weighted margin support vector machines". In KDD, 2004

[26] Melville, Prem, Wojciech Gryc, and Richard D. Lawrence. 2009. "Sentiment analysis of blogs by combining lexical knowledge with text classification". In KDD. ACM

[27] Turney, P. D., & Littman, M. L." Unsupervised learning of semantic orientation from a hundred-billion-word corpus". Technical Report ERB-1094. National Research Council Canada, Institute for Information Technology,2002.

International Scholarly Research Network
ISRN Electronics
Volume 2012, Article ID 529194, 7 pages
doi:10.5402/2012/529194

Research Article

Multithreshold MOS Current Mode Logic Based Asynchronous Pipeline Circuits

Kirti Gupta,[1] Neeta Pandey,[1] and Maneesha Gupta[2]

[1] *Department of Electronics and Communication Engineering, Delhi Technological University, Delhi 110042, India*
[2] *Department of Electronics and Communication Engineering, Netaji Subhash Institute of Technology, New Delhi 110078, India*

Correspondence should be addressed to Kirti Gupta, kirtigupta22@gmail.com

Received 21 September 2012; Accepted 31 October 2012

Academic Editors: A. Mercha and I. Shubin

Multithreshold MOS Current Mode Logic (MCML) implementation of asynchronous pipeline circuits, namely, a C-element and a double-edge triggered flip-flop is proposed. These circuits use multiple-threshold MOS transistors for reducing power consumption. The proposed circuits are implemented and simulated in PSPICE using TSMC 0.18 μm CMOS technology parameters. The performance of the proposed circuits is compared with the conventional MCML circuits. The results indicate that the proposed circuits reduce the power consumption by 21 percent in comparison to the conventional ones. To demonstrate the functionality of the proposed circuits, an asynchronous FIFO has also been implemented.

1. Introduction

Digital VLSI circuits can be broadly classified into synchronous and asynchronous circuits. A synchronous circuit employs a common clock signal to provide synchronization between all the circuit components. The synchronous circuits suffer from the problems of clock distribution and clock skew which becomes a challenge to overcome as the technology scales down. Asynchronous circuits, on the other hand, are attractive replacements to synchronous designs as they perform synchronization through handshaking between their components. Some other advantages of asynchronous circuits include high speed, low power consumption, modular design, immunity to metastable behavior, and low susceptibility to electromagnetic interference [1].

Traditionally, the asynchronous circuits were implemented by using CMOS logic style but due to the substantial dynamic power consumption at high frequencies, CMOS logic style is usually not preferred. MOS Current Mode Logic (MCML) is found to be an alternative to the CMOS asynchronous circuits in the literature [2–5]. A conventional MCML circuit consists of a differential pull-down network (PDN), a current source, and a load. The PDN implements the logic function, the current source generates the bias current I_{SS}, while the load performs the current to voltage conversion [6]. The circuit has static power consumption given as the product of the supply voltage and the bias current. The power consumption can be lowered by either reducing the bias current or the supply voltage. The reduction in bias current is generally not favored as it degrades the speed [7]. Therefore, lowering the supply voltage of the circuit is preferred. One of the techniques suggested in [8, 9] is multithreshold MOS Current Mode Logic (MT-MCML) which uses multithreshold transistors in conventional MCML circuits. In this paper, MT-MCML technique has been applied to implement low-power multithreshold MCML asynchronous pipeline circuits.

The paper first describes the architecture and the operation of MT-MCML circuits in Section 2. In the next section, a brief introduction to asynchronous pipelines is presented. Thereafter, multithreshold MCML asynchronous pipeline circuits, namely, a double-edge triggered flip-flop and a C-element are proposed in Section 4. In the subsequent Section 5, the proposed circuits are simulated in PSPICE using TSMC 0.18 μm CMOS technology parameters and their performance is compared with existing MCML circuits.

An FIFO is also implemented using the proposed circuit. Finally, the conclusions are drawn in the last section.

2. MT-MCML Circuits

MT-MCML circuits are the modified form of the conventional MCML circuits. They use multithreshold CMOS technology for the realization of the logic functions [8, 9]. The circuit of an MT-MCML AND/NAND gate is shown in Figure 1. It consists of two levels of source-coupled transistor pairs (M2-M5) to implement the logic function and a constant current source M1 to generate bias current I_{SS}. The transistors in the upper level (M4, M5) have lower threshold voltage than the transistors in the lower level (M2, M3). The minimum supply voltage for the circuit is defined as the lowest voltage at which all the transistors in the two levels and the current source operate in the saturation region [8] and is computed as

$$V_{MIN} = 3\ V_{BIAS} - \ 3V_{T1} \ + \ V_{TU}, \tag{1}$$

where V_{T1} and V_{TU} are the threshold voltages of the transistor M1 and the transistors in the upper level (M4, M5), respectively.

As an example, an MT-MCML AND/NAND gate with $V_{BIAS} = 800\,\text{mV}$, $V_{T1} = 500\,\text{mV}$, and $V_{TU} = 200\,\text{mV}$ results in a value of $V_{MIN} = 1.1\,\text{V}$ in comparison to the conventional gate which results in $V_{MIN} = 1.4\,\text{V}$ for $V_{T1} = V_{TU} = 500\,\text{mV}$. Thus, MT-MCML circuits can be used in low-power applications as they can operate at low supply voltage than the conventional one.

3. Asynchronous Pipeline

In asynchronous pipelines, data is communicated between the sender and the receiver modules through a handshaking protocol. A very common protocol is the two-phase bundled-data handshaking protocol [10, 11]. Bundled-data channels connect the sender and the receiver through a data bus consisting of separate requests (Req) and acknowledge signals (Ack) and data signals (Data). The sender initiates the data transfer by placing Data on the bus and raises the Req signal, and the receiver then absorbs the data and acknowledges it by raising the Ack signal. Then, the two signals are reset to zero in the same order.

The block diagram of a typical two-phase bundled-data asynchronous pipeline is shown in Figure 2. It comprise of four-stages wherein each stage consists of a functional unit and a control unit. The functional unit has a combinational stage for computing the result of each stage and a matched delay element inserted in the request line. The control unit employs a double-edge triggered flip-flop (DETFF) and a C-element to control the communication between the successive stages.

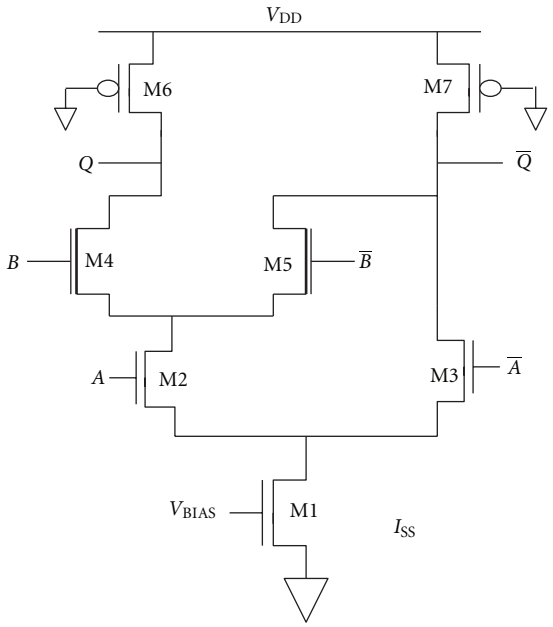

Figure 1: MT-MCML AND/NAND gate.

4. MT-MCML Control Unit

The control unit in asynchronous pipelines consists of two elements, namely, a double-edge triggered flip-flop and a C-element. This section proposes the low-power MT-MCML circuits for both the elements.

4.1. MT-MCML DETFF. A DETFF is an essential element to store the new data produced by the functional unit till the time the successor stage is ready to receive it. It samples the data at the falling and the rising edges of the local clock pulses generated by the C-element.

A block diagram of a DETFF consisting of two opposite level sensitive latches and a multiplexer is shown in Figure 3. When CLK is high, latch L1 becomes transparent and the data stored in the latch L2 is obtained as the output. Similarly, when CLK is low, latch L2 becomes transparent and the data stored in the latch L1 is obtained as the output of the flip-flop. The circuit of the proposed MT-MCML DETFF is shown in Figure 4. It consists of two MT-MCML latches L1, L2 and MCML multiplexer (MUX) with a common source-coupled transistor pair for differential clock input (CLK). The advantage of using common clock source-coupled transistor is the reduction in the routing complexity and the overall area. The transistors in the upper level of latches and the multiplexer (M4-M15) have low threshold voltages values and have been highlighted in the figure.

4.2. MT-MCML C-Element. A C-element is a fundamental component of asynchronous pipelines. It is a state holding element wherein if both inputs are same, that is, low (high), the circuit produces the output which is equal to the input value, that is, low (high), respectively, otherwise the output

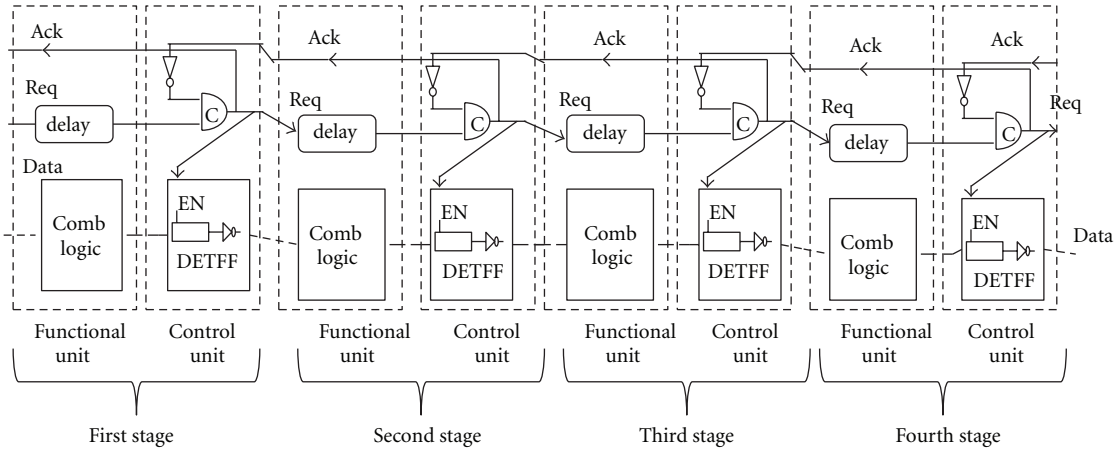

Figure 2: Block diagram of two-phase asynchronous pipeline.

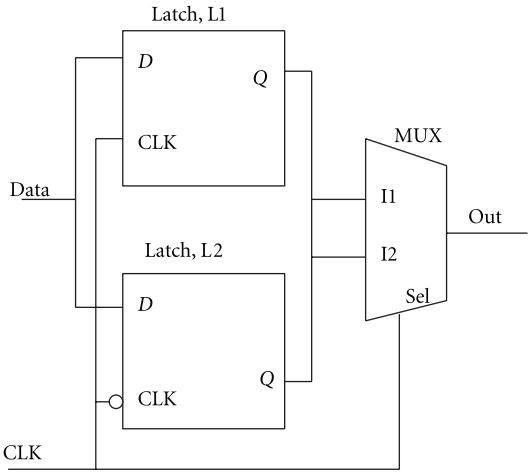

Figure 3: Block diagram of a DETFF.

remains at the previous state value. A state diagram is given in Figure 5 which can be expressed by a Boolean function:

$$C = \left[\hat{C} \cdot (A + B)\right] + (A \cdot B), \tag{2}$$

where A, B are the inputs and $\hat{C}$ is the previous state of the output.

The circuit of the proposed MT-MCML C-element is shown in Figure 6. In circuit, the two stacked transistors (M2, M8) form an AND structure whereas the parallel connection of transistors (M3, M4) performs the OR operation. The cross-coupled transistor pair (M9, M10) forms the latch structure. The transistors in the upper level of the C-element (M8-M11) have low threshold voltages values and have been highlighted in the figure. When both the inputs (A, B) have the same value then the bias current either flows through the two right most branches or the left most branches. This, however, makes the output (C) of the circuit same as the input value. Conversely, when both the inputs (A, B) have different values, the output stores the previous value by making the bias current flow in the latch structure branches only.

5. Simulation Results

This section first presents the simulation results for the proposed control unit elements, namely, DETFF and C-element. Thereafter, the performance of the proposed circuits is compared with the conventional MCML control unit elements. Lastly, the simulation results for an asynchronous FIFO are presented. All the simulations are performed by using TSMC 0.18 μm CMOS technology parameters and load capacitance of 10 fF. The channel length of the transistors is taken as 0.18 μm uniformly. The value of the supply voltage for the MT-MCML and conventional MCML circuits is 1.1 V and 1.4 V, respectively.

5.1. Proposed Control Unit Elements. The proposed MT-MCML control unit elements are implemented with an output voltage swing of 400 mV and a bias current (I_{SS}) of 30 μA and 90 μA for C-element and DETFF, respectively. The bias current of DETFF is taken to be three times the value of bias current in C-element as in DETFF there is a common source-coupled transistor pair that drives the two D-latches and a multiplexer. The aspect ratio of the transistors in the PDN of both the elements is 3 μm/0.18 μm, whereas the aspect ratio for load transistors is 0.46 μm/0.18 μm. The simulation waveforms are shown in Figure 7. In Figure 7(a), it can be observed that in DETFF whenever CLK is low, the previous value stored in L1 is obtained as the output of the DETFF. Similarly, when CLK is high, the previous value stored in L2 is obtained as the output. The simulation waveforms for C-element shown in Figure 7(b) depict that whenever both the inputs (A and B) have the same value an output which is equal to the current vales of the inputs is obtained. Further for different values of the inputs (A and B), the output remains in the previous state value.

The impact of parameter variation on power consumption of the proposed MT-MCML control unit elements is studied at different design corners. It is found that the power consumption of the proposed DETFF varies by a factor of 1.87 between the best and the worst cases. For the proposed

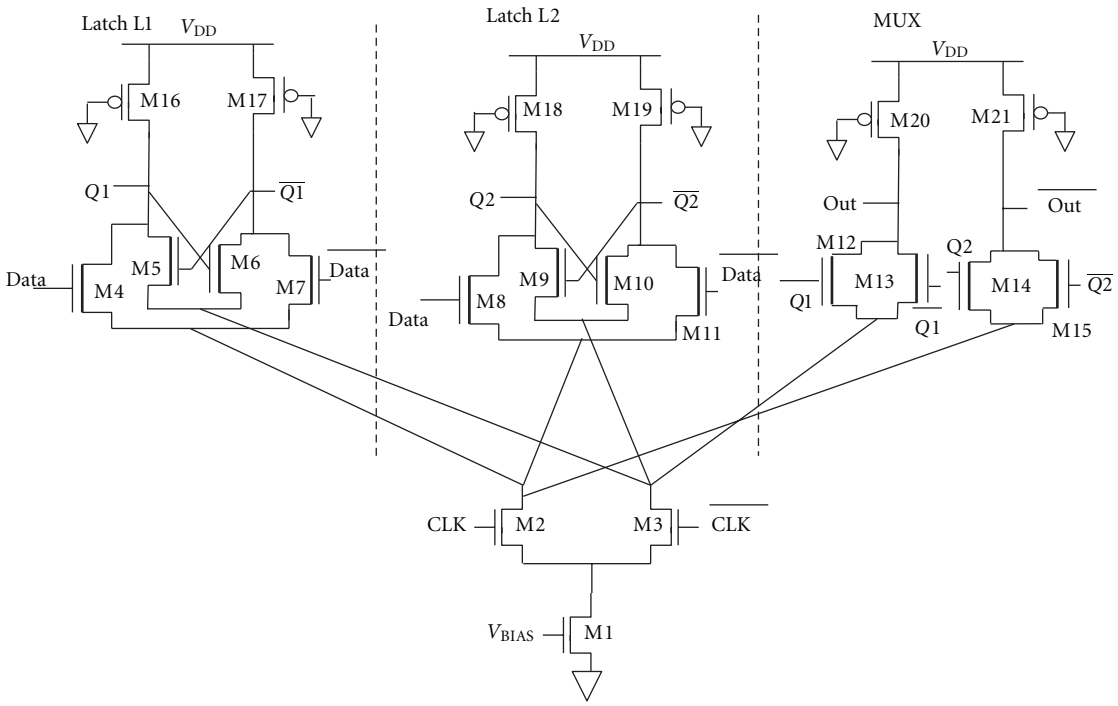

Figure 4: Proposed MT-MCML DETFF.

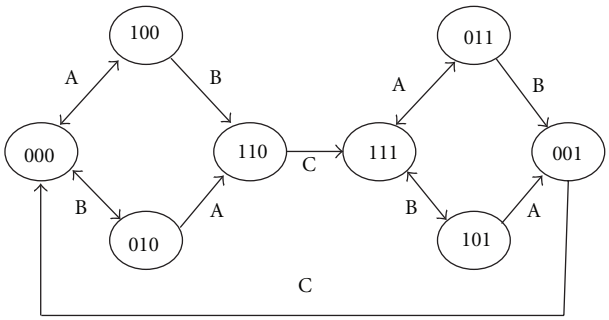

Figure 5: State diagram of the C-element.

C-elements, the power consumption varies by a factor of 1.4 between the best and the worst cases.

5.2. Performance Comparison. The performance of the proposed MT-MCML and the conventional MCML control unit elements has been compared using simulation test benches [3] which are redrawn in Figure 8. The simulation results are listed in Tables 1 and 2. The power result for MCML circuits includes static power due to the presence of the constant current source. The result shows that the proposed MT-MCML circuits reduce power consumption by 21 percent due to the operation at low supply voltage through the use of multiple-threshold voltage transistors. Further, the propagation delay of the proposed MT-MCML control unit elements is slightly higher than the conventional MCML elements due to the increase in transistor sizes in the proposed elements [8]. Thus, the power-delay product (PDP) values for the proposed are reduced accordingly.

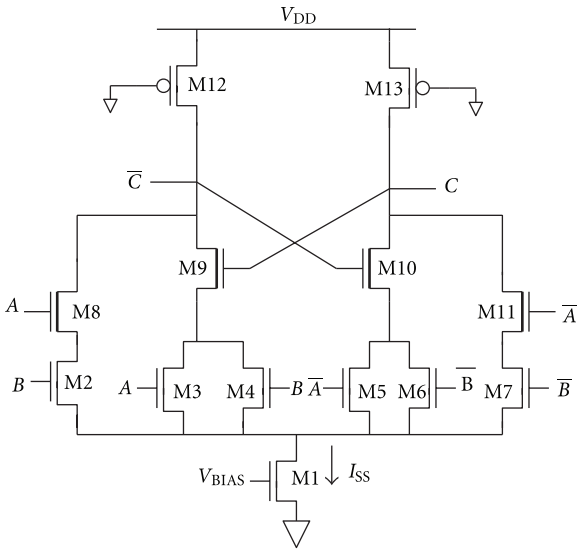

Figure 6: Proposed MT-MCML C-Element.

Therefore, the use of MT-MCML circuits can lead to the design of power-efficient asynchronous pipelines.

5.3. An Application. An asynchronous MT-MCML FIFO is implemented as an application of the proposed control unit elements. The block diagram of a 4-stage FIFO is shown in Figure 9. The handshaking signals shown as Req(in) and Ack(out) communicate the data, Data(in) between sender and the first stage. At the receiver side, the signals Req(out) and Ack(in) are used to synchronize the output

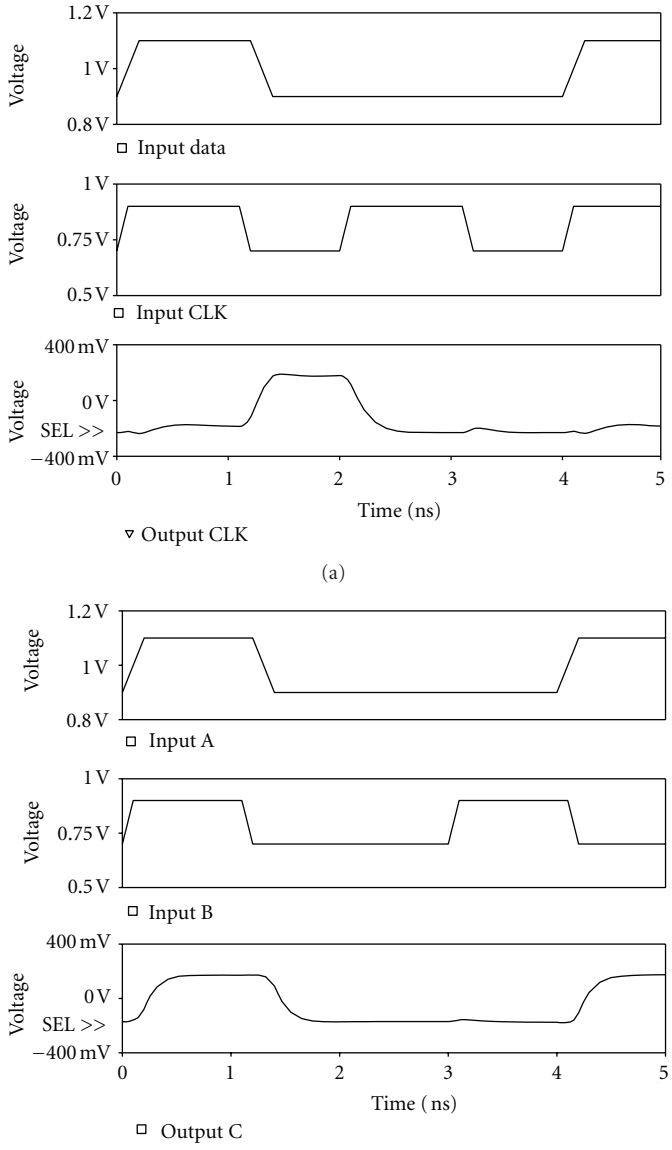

Figure 7: Simulation waveforms of the proposed MT-MCML (a) DETFF and (b) C-Element.

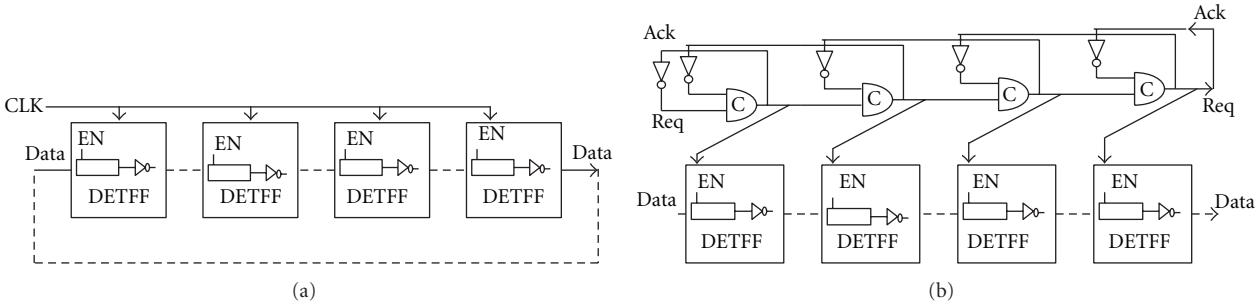

Figure 8: Simulation test bench [3] (a) DETFF and (b) C-element.

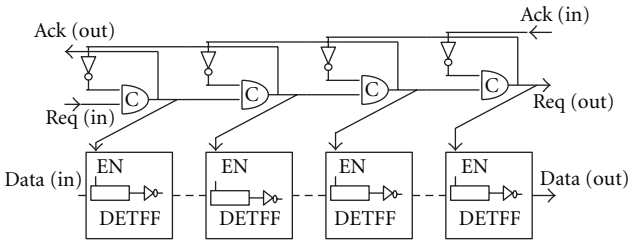

Figure 9: Block diagram of 4-stage asynchronous FIFO.

Table 1: Summary of simulated performance for DETFF.

Parameter	Type of DETFF	
	Conventional MCML	Proposed MCML
Power (μW)	141	111
Propagation delay (ps)	1230	1240
PDP (fJ)	173	138

Table 2: Summary of simulated performance for C-element.

Parameter	Type of C-element	
	Conventional MCML	Proposed MCML
Power (μW)	44	35
Propagation delay (ps)	239	241
PDP (fJ)	11	8

data, Data(out) with the receiver and the last stage. Initially, the input data Data(in) is loaded in the first stage of the FIFO, and the Req(in) is asserted to low to start the data transfer. This results in a transition at the output of a C-element such that the data is stored in the DETFF of the first stage. At the same time an acknowledge signal Ack(out) is given to the sender. The stored data then flows through the different stages in the FIFO. Then, a request signal Req(out) is generated by the last stage to the receiver to enable the receiver to accept the data. This is followed by an acknowledge signal, Ack(in), from the destination to the last stage. The waveforms obtained through the simulation of a four-stage asynchronous FIFO are shown in Figure 10. The first three waveforms correspond to the input data Data(in), request signal (Req(in)), and acknowledge signal (Ack(out)) at the sender section. The last three graphs are the acknowledge signal Ack(in), data Data(out), and request signal Req(out). It can be found that the asynchronous MT-MCML FIFO outputs the sampled data correctly.

6. Conclusions

This paper proposes low-power Multithreshold MOS Current Mode Logic (MT-MCML) asynchronous pipeline circuits. The proposed circuits involve the use of multiple-threshold CMOS technology which helps in reducing the power consumption. The proposed circuits have been simulated using 0.18 μm CMOS technology parameters, and their performance has been compared with the conventional MCML circuits. A performance comparison indicates that

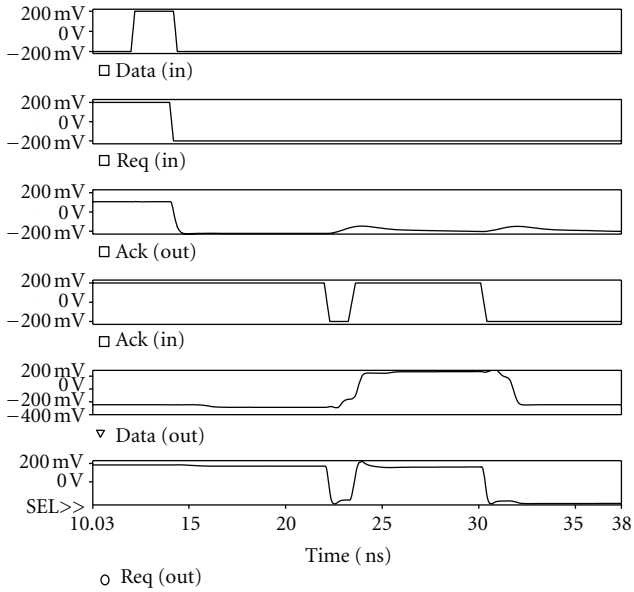

Figure 10: Transient response of the 4-stage multithreshold MCML asynchronous FIFO circuit.

the proposed circuits are power efficient than the conventional ones. An asynchronous FIFO implemented as an application confirms to the functionality of the proposed circuits.

References

[1] C. H. Van Kees Berkel, M. B. Josephs, and S. M. Nowick, "Scanning the technology applications of asynchronous circuits," *Proceedings of the IEEE*, vol. 87, no. 2, pp. 223–233, 1999.

[2] T. W. Kwan and M. Shams, "Design of multi-ghz asynchronous pipelined circuits in MOS current-mode logic," in *Proceedings of the 4th International Conference on Embedded Systems*, pp. 1–6, 2005.

[3] T. W. Kwan and M. Shams, "Design of asynchronous circuit primitives using mos current-mode logic (MCML)," in *Proceedings of the 16th International Conference on Microelectronics (ICM '04)*, pp. 170–173, December 2004.

[4] T. W. Kwan and M. Shams, "Design of high-performance power-aware asynchronous pipelined circuits in MOS Current-Mode Logic," in *Proceedings of the 11th IEEE International Symposium on Asynchronous Circuits and Systems (ASYNC '05)*, pp. 23–32, March 2005.

[5] T. W. Kwan and M. Shams, "Multi-GHz energy-efficient asynchronous pipelined circuits in MOS current mode logic," in *Proceedings of the IEEE International Symposium on Cirquits and Systems*, pp. II645–II648, May 2004.

[6] H. Hassan, M. Anis, and M. Elmasry, "MOS current mode circuits: analysis, design, and variability," *IEEE Transactions on Very Large Scale Integration (VLSI) Systems*, vol. 13, no. 8, pp. 885–898, 2005.

[7] M. Alioto and G. Palumbo, *Model and Design of Bipolar and MOS Current-Mode Logic (CML, ECL and SCL Digital Circuits)*, Springer, Amsterdam, The Netherlands, 2005.

[8] M. Anis and M. Elmasry, "Power reduction via an MTCMOS implementation of MOS current mode logic," in *Proceedings of the IEEE International Conference on ASIC/SOC*, pp. 193–197, 2002.

[9] H. Hassan, M. Anis, and M. Elmasry, "Analysis and design of low-power multi-threshold MCML," in *Proceedings of the IEEE International SOC Conference*, pp. 25–29, September 2004.

[10] M. Shams, J. C. Ebergen, and M. I. Elmasry, *Asynchronous Circuits*, John Wiley's Encyclopedia of Electrical Engineering, 1999.

[11] I. E. Sutherland, "Micropipelines," *Communications of the ACM*, vol. 32, no. 6, pp. 720–738, 1989.

Order Statistics Based Measure of Past Entropy

Richa Thapliyal

Department of Applied Mathematics,
Delhi Technological University,
Bawana Road, Delhi-110042, India.
Email: richa31aug@gmail.com

H.C.Taneja

Department of Applied Mathematics,
Delhi Technological University,
Bawana Road, Delhi-110042, India.
Email: hctaneja@rediffmail.com

Abstract

In this paper we have proposed a measure of past entropy based on order statistics. We have studied this measure for some specific life- time distributions. A Characterization result for the proposed measure has also been discussed and also and an upper bound for this measure has been derived.

Keywords: Order Statistics, Past entropy, Reversed hazard rate, Survival function.

1 INTRODUCTION

Shannon entropy (1948) plays a central role in the field of information theory. For a non-negative continuous random variable X with distribution function $F(.)$ and p.d.f $f(.)$, it is given by

$$H(X) = -\int_0^\infty f(x)\log f(x)dx = -E(\log f(X)). \tag{1}$$

Here $H(X)$ measures the average uncertainty associated with the random variable X. If X is the lifetime of a system and if the system has survived up to time t, then to measure the uncertainty about the remaining lifetime of such a system the measure (1) is not appropriate. Ebrahimi (1996) proposed a measure which measures the uncertainty about the remaining lifetime of a system if it is working at time t, given by

$$H(X;t) = -\int_t^\infty \frac{f(x)}{\bar{F}(t)}\log\left(\frac{f(x)}{\bar{F}(t)}\right)dx\,, t>0. \tag{2}$$

The measure (2) is called the measure of residual entropy. Obviously, when $t = 0$, it reduces to (1). Further by writing $\lambda_F(t) = \frac{f(t)}{\bar{F}(t)}$, (2) can be rewritten as

$$H(F;t) = 1 - \frac{1}{\bar{F}(t)}\int_t^\infty f(x)\log\lambda_F(x)dx, \tag{3}$$

Mathematical Journal of Interdisciplinary Sciences
Vol. 1, No. 2,
January 2013
pp. 63–70

where $\lambda_F(t)$ is the hazard rate function and $\bar{F}(x) = 1 - F(x)$ is the survival function of X.

In many realistic situations uncertainty is not necessarily related to the future but can also refer to the past. For example, a system which is monitored only at certain preassigned inspection times is found to be down at time t, then the uncertainty of the system depends on the past, that is at which instant in $(0, t)$ it has failed. Di Crescenzo and Longobardi (2002) studied this case and introduced a measure of past entropy over $(0, t)$ given by

$$\bar{H}(X;t) = -\int_0^t \frac{f(x)}{F(t)} \log\left(\frac{f(x)}{F(t)}\right) dx, \tag{4}$$

which tends to (1) when $t \to \infty$. They have also discussed properties of past entropy and its relationship with the residual entropy. By writing $\tau_F(t) = \frac{f(t)}{F(t)}$, (4) can be rewritten as

$$\bar{H}(F;t) = 1 - \frac{1}{F(t)} \int_0^t f(x) \log \tau_F(x) dx, \tag{5}$$

where $\tau_F(t) = \frac{f(t)}{F(t)}$ is the reversed hazard rate of X.

Suppose that $X_1, X_2, \cdots, X_n$ are independent and identically distributed observations from cdf $F(x)$ and pdf $f(x)$. The order statistics of the sample is defined by the arrangement of $X_1, X_2, \cdots, X_n$ from the smallest to the largest, denoted as $X_{1:n} \leq X_{2:n} \leq \cdots \leq X_{n:n}$. Order statistics have been used in a wide range of problems like detection of outliers, characterizations of probability distributions, quality control and strength of materials; for more details see Arnold et al.(1992), David and Nagaraja (2003). Several authors have studied the information theoretic properties of an ordered data. Wong and Chen (1990) showed that the difference between the average entropy of order statistics and the entropy of parent distribution is a constant. Park (1995) obtained some recurrence relations for the entropy of order statistics. Ebrahimi et al. (2004) explored some properties of the Shannon entropy of order statistics and showed that the Kullback-Leibler (1959) relative information measure involving order statistics is distribution free. Arghami and Abbasnejad (2011) studied Renyi entropy (1961) based on order statistics.

In this communication we extend the measure of past entropy (4) to order statistics. In Section 2, we propose the measure of past entropy for order statistics. Section 3 focuses on a characterization result that the measure of past entropy of the i^{th} order statistics under some conditions determines the distribution function uniquely and also we study an upper bound for this measure. Some concluding remarks are mentioned in Section 4.

2 PAST ENTROP FOR ORDER STATISTICS

Shannon's measure of uncertainty associated with the i^{th} order statistics $X_{i:n}$ is given by

$$H(X_{i:n}) = -\int_0^\infty f_{i:n}(x)\log f_{i:n}(x)dx, \tag{6}$$

where

$$f_{i:n}(x) = \frac{1}{B(i,n-i+1)}(F(x))^{i-1}(1-F(x))^{n-1}f(x) \tag{7}$$

is p.d.f of i^{th} order statistics, for $i = 1, 2, \cdots, n$, and

$$B(a,b) = \int_0^1 x^{a-1}(1-x)^{b-1}dx, a>0, b>0, \tag{8}$$

is beta function with parameters a and b, refer to Ebrahimi et al. (2004). Note that for $n = 1$, (6) reduces to (1).

Using probability integral transformation $U = F(X)$, where U follows standard uniform distribution, (6) can be expressed as

$$H(X_{i:n}) = H_n(W_i) - E_{gi}[\log(f(F^{-1}(W_i)))], \tag{9}$$

where

$$\begin{aligned} H_n(W_i) = {} & \log B(i,n-i+1) - (i-1)[\psi(i) - \psi(n+1)] - (n-i) \\ & \times [\psi(n-i+1) - \psi(\boldsymbol{n}+1)], \end{aligned} \tag{10}$$

denotes entropy of i^{th} order statistics from standard uniform distribution whose p.d.f is given by

$$g_i(w) = \frac{1}{B(i,\, n-i+1)}w^{i-1}(1-w)^{n-1}, 0<w<1 \tag{11}$$

and $\psi(z) = \dfrac{d\log\Gamma(s)}{dz}$ is the digamma function, refer to Ebrahimi et al. (2004).

Analogous to (4), we propose the past entropy of i^{th} order statistics as

$$\bar{H}(X_{i:n};t) = -\int_0^t \frac{f_{i:n}(x)}{F_{i:n}(t)}\log\left(\frac{f_{i:n}(x)}{F_{i:n}(t)}\right)dx. \tag{12}$$

As in case of (5), (12) can be rewritten as

$$\bar{H}(X_{i:n};t) = 1 - \frac{1}{F_{i:n}(t)}\int_0^t f_{i:n}(x)\log\tau_{F_{i:n}}(x)\,dx, \tag{13}$$

where $\tau_{F_{i:n}}(x)$ is the reversed hazard rate of i^{th} order statistics given by

$$\tau_{F_{i:n}}(x) = \frac{f_{i:n}(x)}{F_{i:n}(x)}. \tag{14}$$

Note that, if we take $t \to \infty$ in (12) and use the probability integral transformation $U=F(X)$ then it reduces to (9).

In reliability engineering $(n - k + 1)$-out-of-n systems are very important kind of structures. A $(n - k + 1)$-out-of-n system functions iff atleast $(n - k + 1)$ components out of n components function. If $X_1, X_2, \cdots, X_n$ denote the independent lifetimes of the components of such system, then the lifetime of the system is equal to the order statistic $X_{k:n}$. The special case of $k = 1$ and n, that is for sample minima and maxima correspond to series and parallel systems respectively.

Next we discuss two specific distributions exponential and Pareto for the case $i = n$, the case $i = 1$ follows on similar lines but a little bit complicated. For $i = n$, from (7) we have $f_{n:n}(x) = nF^{n-1}(x) f(x)$ and $F_{n:n}(x) = F^n(x)$. Using these values and putting $U = F(X)$ in (12), after some simplifications, we get

$$\bar{H}(X_{n:n};t) = n \log F(t) - \frac{1}{F^n(t)} \int_0^t nu^{n-1} \log(nu^{n-1} f(F^{-1}(u)))du \tag{15}$$

Example 2.1 Let X be an exponentially distributed random variable with pdf $f(x) = \theta e^{-\theta x}$, $\theta > 0$, $x \geq 0$. Then $F(x) = 1 - e^{-\theta x}$ and $f(F^{-1}(u)) = \theta(1 - u)$. Using (15) and letting $t \to \infty$, we get

$$\lim_{t\to\infty} \bar{H}(X_{n:n};t) = 1 - \log n\theta + \gamma + \psi(n),$$

where $\gamma = -\psi(1) \approx 0.5772$, which is same as derived by Ebrahimi et al. (2004) using Shannon entropy.

Example 2.2 Let X be a random variable having Pareto distribution with pdf $f(x) = \frac{\theta\beta^{\theta+1}}{x^{\theta+1}}, x \geq \beta, x \geq 0$. It is easy to see that $f(F^{-1}(u)) = \frac{\theta}{\beta}(1-u)^{\frac{\theta}{1+\theta}}$.

Hence using (15) we have

$$\bar{H}(X_{n:n};t) = 1 - \frac{1}{n} + \log F(t) - \log n - \log\left(\frac{\theta}{\beta}\right) - \frac{n(\theta+1)}{\theta F^n(t)} \int_0^{F(t)} u^{(n-1)} \log(1-u)du.$$

As we take limit $t \to \infty$ we obtain

$$\lim_{t\to\infty} \bar{H}(X_{n:n};t) = 1 - \frac{1}{n} - \log n - \log\left(\frac{\theta}{\beta}\right) - \frac{\theta+1}{\theta}\left(-\gamma - \psi(n) - \frac{1}{n}\right).$$

as the entropy of the n^{th} order statistics for Pareto distribution.

3 CHARACTERIZATION RESULT

Several authors have studied characterization results for information theoretic measures using order statistics. Baratpour et.al. (2007,2008) have studied characterization results for Shannon and Ranyi (1961) entropy based on order statistics using Stone-Weistraas Theorm. Continuing with similar kind of approach, in this section we prove a characterization theorem which ensures that under certain condition the proposed measure of past entropy based on order statistics characterizes the distribution function uniquely. To prove this result, we require the following lemma, see Kamps (1998).

Lemma 3.1 *For any increasing sequence of positive integers* $\{n_j, j \geq 1\}$*, the sequence of polynomials* $\{x^{n_j}\}$ *is complete in L(0, 1), if and only if* $\sum_{j=1}^{\infty} n_j^{-1}$ *is infinite.*

Here, $L(0, 1)$ is the set of all Lebesgue integrable functions on the interval (0, 1).

Next, we state the following characterization theorem.

Theorem 3.1 *Let* $X_1, X_2, \cdots, X_n$ *and* $Y_1, Y_2, \cdots, Y_n$ *be n i.i.d random variables with cdf F (x) and G(y), pdf f (x) and g(y) respectively and having finite entropies. Let* $X_{k:n}$ *and* $Y_{k:n}$ *denote their corresponding* k^{th} *order statistics. Assume that* $\exists$ *a constant* t_0 *such that* $F(t_0) = G(t_0)$*. If* $\bar{H}(X_{k:n};t_0) = \bar{H}(Y_{k:n};t_0), 1 \leq k \leq n,$ *then X is identical in distribution with Y.*

Proof: The notations having their usual meanings, the reversed hazard rate is

$$\tau_{F_{k:n}} = \frac{f_{k:n}(x)}{F_{k:n}(x)}.$$

Using (7), the above expression can be written as

$$\tau_{F_{k:n}}(x) = K_{n,k}(F(x))\tau_F(x), \tag{16}$$

where $K_{n,k}(F(t)) = \frac{1}{B(k-1,n-k+1)} \left(\frac{\frac{F(t)^k}{(1-F(t))^k}}{\sum_{i=1}^{n} \left(\frac{(n)!}{(i)!(n-1)!} \right) \left(\frac{F(t)}{(1-F(t))} \right)^i} \right).$

It can be seen easily that

$$\bar{H}(X_{k:n};t) = 1 - E[\log \tau_{X_{k:n}}(X_{k;n}) \,|\, X_{k:n} < t]. \tag{17}$$

Using (16) in (17), we get

$$1-\bar{H}(X_{k:n};t)=E[\log(\tau_X(X_{k:n})K_{n,k}(F(X_{k:n}))\,|\,X_{k:n}<t]. \tag{18}$$

Using probability integral transformation U = F (X) in (18), we get

$$\begin{aligned}1-\bar{H}(X_{k:n};t) &= E[\log(\tau_X(F^{-1}(U_{k:n}))K_{n,k}(U_{k:n}))\,|\,U_{k:n}<F(t)]\\ &=\int_0^{F(t)}\frac{\log\tau_X(F^{-1}(u))K_{n:k}(u)h_{U_{k:n}}(u)}{H_{U_{k:n}}(F(t))}du\end{aligned}$$

where

$$h_{U_{k:n}}(u)=\frac{u^{k-1}(1-u)^{n-k}}{B(k,n-k+1)},0<u<1,$$

is the pdf of k^{th} order statistics of standard uniform distribution and $H_{U_{k:n}}$ is the distribution function of k^{th} order statistics of the standard uniform distribution.

We are given that $\bar{H}(X_{k:n};t_0)=\bar{H}(Y_{k:n};t_0)$. Hence

$$\begin{aligned}&\int_0^{F(t_0)}\log\tau_X(F^{-1}(u))K_{n,k}(u)\frac{h_{U_{k:n}}(u)}{H_{U_{k:n}}(F(t_0))}du\\ &=\int_0^{G(t_0)}\log\tau_X(G^{-1}(u))K_{n,k}(u)\frac{h_{U_{k:n}}(u)}{H_{U_{k:n}}(G(t_0))}du.\end{aligned} \tag{19}$$

Using change of variable $u\to\frac{u}{\mu}$ and $F(t_0) = G(t_0)$ in (19) we obtain

$$\int_0^1\log\left(\frac{\tau_X\left(F^{-1}\left(\frac{u}{\mu}\right)\right)}{\tau_Y\left(G^{-1}\left(\frac{u}{\mu}\right)\right)}\right)h_{U_{k:n}}\left(\frac{u}{\mu}\right)\frac{du}{\mu}=0. \tag{20}$$

It is easy to see that $h_{U_{k:n}}\left(\frac{u}{\mu}\right)$ satisfies the conditions of Lemma 3.1, therefore using this lemma we get

$$\log\left(\frac{\tau_X\left(F^{-1}\left(\frac{u}{\mu}\right)\right)}{\tau_Y\left(G^{-1}\left(\frac{u}{\mu}\right)\right)}\right)=0, \tag{21}$$

which is possible only when

$$\tau_X\left(F^{-1}\left(\frac{u}{\mu}\right)\right)=\tau_Y\left(G^{-1}\left(\frac{u}{\mu}\right)\right),\forall\left(\frac{u}{\mu}\right)\varepsilon\,(0,1)$$

that is, $f\left(F^{-1}\left(\frac{u}{\mu}\right)\right)=g\left(G^{-1}\left(\frac{u}{\mu}\right)\right),\forall\left(\frac{u}{\mu}\right)\varepsilon\,(0,1).$

Note that $\frac{d}{dt}F^{-1}(t)=\frac{1}{f(F^{-1}(t))}$ .Therefore, $F^{-1}\left(\frac{u}{\mu}\right)=G^{-1}\left(\frac{u}{\mu}\right)+d,\forall\left(\frac{u}{\mu}\right)\varepsilon\,(0,1),$

where d is a constant. Using $F(t_0) = G(t_0)$ we get the desired result.

3.1 An upper bound to the past entropy

We prove that, if $f_{i:n}\leq 1$, then

$$\bar{H}(X_{i:n}(t))\leq\frac{H(X_{i:n})}{F_{i:n}(t)}.$$

We have

$$\begin{aligned}\bar{H}(X_{i:n}(t)) &= -\int_0^t\frac{f_{i:n}(x)}{F_{i:n}(t)}\log\left(\frac{f_{i:n}(x)}{F_{i:n}(t)}\right)\\ &= \log F_{i:n}(t)-\frac{1}{F_{i:n}(t)}\int_0^t f_{i:n}(x)\log f_{i:n}(x)\,dx.\end{aligned}$$

For $t > 0$, we have $\log F_{i:n}(t) \leq 0$

$$\begin{aligned}\bar{H}(X_{i:n};t) &\leq -\frac{1}{F_{i:n}(t)}\int_0^t f_{i:n}(x)\log f_{i:n}(x)\,dx\\ &\leq -\frac{1}{F_{i:n}(t)}\int_0^\infty f_{i:n}(x)\log f_{i:n}(x)\,dx.\end{aligned}$$

Hence

$$\bar{H}(X_{i:n}(t))\leq\frac{H(X_{i:n})}{F_{i:n}(t)}.$$

The equality is obtained when $t\to\infty$.

4 CONCLUSION

Information measures are applied widely in different areas of physics, communication theory and economics. Residual and past measures of information have found applications in life testing and reliability theory. The proposed mesure of order statistics based on past entropy characterizes

the underlying distribution uniquely. This can be possibly used further for statistical modeling and reliability analysis.

ACKNOWLEDGEMENT

The first author is thankful to the Center for Scientific and Industrial Research, India, to provide financial assistance for this work.

REFERENCES

Arghami, N.R., Abbasnejad, M. (2011). Renyi entropy properties of order statistics. Communications in Statistics, Vol. 40, 40-52.

Arnold, B. C., Balakrishnan, N., Nagaraja, H. N., 1992. A first Course in Order Statistics. New York: John Wiley and Sons.

Baratpour, S., Ahmadi, J., Arghami, N. R., (2007). Some characterizations based on entropy of order statistics and record values. Communications in Statistics-Theory and Methods 36: 47-57.

Baratpour, S., Ahmadi, J., Arghami, N. R., (2008). Characterizations based on Renyi entropy of order statistics and record values. Journal of Statistical Planning and Inference, 138, 2544-2551.

David, H.A., Nagaraja, H.N., (2003). Order Statistics. New York : Wiley.

Di Crescenzo, A., Lomgobardi, M. (2002). Entropy-based measure of uncertainty in past lifetime distributions. J. App. Prob.39,434-440.

Ebrahimi, N., Soofi, E.S., Zahedi, H., (2004). Information properties of order statistics and spacings. IEEE Trans. Inform. Theor vol 50, 177-183.

Ebrahimi, N., (1996). How to measure uncertainty in the residual lifetime distributions. Sankhya A 58, 48-57.

Ebrahimi, N., Kirmani, S.N.U.A., (1996). A measure of discrimination between two residual lifetime distributions and its applications. Ann. Inst. Statist. Math 48, 257-265.

Ebrahimi, N., Kirmani, S.N.U.A., (1996). A characterization of the propotional hazards model through a measure of discrimination between two residual life distributions. Biometrika 83(1), 233-235.

Kamps, U. (1998). Characterizations of distributions by recurrence relations and identities for moments of order statistics. In: N. Balakrishnan and C. R. Rao, eds. Order Statistics: Theory and Methods. Handbook of Statistics,16, 291-311.

Kullback, S. (1959). Information theory and Statistics. Wiley, New York.

Park, S. (1995). The entropy of consecutive order statistics. IEEE Trans. Inform. Theor. 41, 2003-2007.

Renyi, A. (1961). On measures of entropy and information. Proc. Fourth. Berkley Symp. Math. Stat. Prob. 1960, I, University of California Press, Berkley, 547-561.

Shannon, C.E., (1948). A mathematical theory of communication. Bell syst. Tech. J. 27, 379-423 and 623-656.

Wong, K. M., Chen, S., (1990). The entropy of ordered sequences and order statistics. IEEE Trans. Inform. Theor. 36, 276-284.

Richa Thapliyal is a research scholar in the department of Applied Mathematics, Delhi Technological University, Delhi. She is working for her Ph.D. programme in the broad field of Information Theory and Its Applications.

Dr. H.C. Taneja is a Professor in the department of Applied Mathematics, Delhi Technological University, Delhi. His field of interest includes Information Theory, Stochastic Processes and Applications.

International Journal of Emerging Technology and Advanced Engineering
Website: www.ijetae.com (ISSN 2250-2459, ISO 9001:2008 Certified Journal, Volume 2, Issue 12, December 2012)

Performance Improvement of a Regenerative Gas Turbine Cycle Through Integrated Inlet Air Evaporative Cooling and Steam Injection

Shyam Agarwal[1], S.S. Kachhwaha[2], R.S. Mishra[3]
[1,3]*Department of Mechanical Engineering, Delhi Technological University, Bawana Road, Delhi-110042,*
[2]*Pandit Deendayal Petroleum University, Gujrat, India.*

***Abstract*- Like many developed countries, energy efficiency and environment impact are the most important process in the development of power generation policy in India. A high ambient temperature reduces the air density and makes inlet air cooling (IAC) and steam injection gas turbine (STIG) attractive power augmentation method for existing regenerative gas turbine. With a high back work ratio and a high exhaust temperature, the regenerative cycle gas turbine generation system usually has low generation efficiency particularly in hot ambient weather conditions. From available retrofitting technologies to improve the power generation capacity and efficiency of regenerative cycle gas turbine, IAC through fog cooling and STIG are considered most effective ways to modify an existing simple cycle unit without major description to its original integrity. To evaluate and stimulate the performance of power generation system, a computer program has been developed. The results from computer simulation indicated that the retrofitting of regenerative cycle with IAC and STIG can boost the power output from 30MW to 49.05MW while the generation efficiency can be increased from about 36.99% to 45.21%. The effect of retrofitting techniques on exergy destruction in various system components has also been determined. The exergy destruction rate per MW of power output for different system components (combustion chamber and compressor) reduces while for gas turbine increases for retrofitted cycles.**

***Keywords*- Regenerative gas turbine; Retrofitting, Inlet air cooling, STIG, Exergy destruction**

I. INTRODUCTION

Regenerative gas turbine power generation system are most common powere generation units in entire world. A large number of power generation units in Indaia use regenrative gas turbine in order to utilize the heat energy of exhaust gases from the turbine. Rgenerative units are more efficient and benefitial compare to simple cycle units to fulfill the peak load demand but provide low power output and overall efficiency during summer season. In order to recover lost power output and overall efficiency, the retrofitting techniques have seriously been considered by which increasing demand of electricity can be fulfilled.

The thermodynamic analysis of regenerative gas turbine power generation system results that huge amount of useful energy has wasted along with exhuast gases (which release out from the turbine about at 400 ^{0}C to 500 ^{0}C). However, some amount of heat energy of exhaust gases have been recoverted into the regenerator yet a large amount of heat goes wasted in to the atmosphere along with exhuast gases after regenerator means there is a considerable amount of heat energy remains present into the exhaust gases which has to be recovered in order to make the cycle efficient. Secondly, a large part of turbine work has used to compress the inlet air.

Many well established technologies can be used to enhance the power output and thermal efficiency of the regerative gas turbine. Among those, single or double effect vapour absorption LiBr refrigeration system, spray cooling system may be employed to cool the inlet air to the compressor by which the compressor work-done can be reduced. Along with above mentioned inlet air cooling techniques (IAC) the steam injection gas turbine (STIG) technology may also employed to recover the available energy of exhaust gases . The integration of IAC and STIG technologies can be employed with regenerative gas turbine cycle in order to boost power out and generation efficiency of the power generation unit which consequences the most effective way to use retrofitted techniques.

Recently, the integration of inlet air cooling (IAC) by spray cooling and steam injection gas turbine (STIG) is the most effective strategy to enhance the performance of power generation. Both features can be implemented in the existing basic system without major modification to the original system integration in an economic way. In the spray cooling technique, the water at dry bulb temperature corresponding to ambient conditions has been sprayed in to the air adiabatically by which heat transfer between air and water has been taken place. However, daily requirement of water increases along with demineralization of water reduces the envirno-friendly relationship and economic feasibility.

International Journal of Emerging Technology and Advanced Engineering
Website: www.ijetae.com (ISSN 2250-2459, ISO 9001:2008 Certified Journal, Volume 2, Issue 12, December 2012)

The high pressure steam generated into the heat recovery steam generator (HRSG) has also fed into the combustion chamber in the form of STIG. The injection ratio of the steam has to be maintained according to the manufacture prescribed for the combustion chamber and turbine.

Nishida et al.[1] have analyzed the performance characteristics of two configuration of regenerative steam-injection gas turbine (RSTIG) systems. They concluded that the thermal efficiencies of the RSTIG systems are higher than those of regenerative, water injected and STIG systems. . Hawaj & Mutairi[2] studied a cogeneration system comprising a combined cycle power plant (CCPP) with an absorption chiller used for space cooling. They have also studied the relative advantage of using CCPP with absorption cooling over thermally equivalent mechanical vapor compression (MVC).They found that a cogeneration CCPP with absorption cooling yields significantly less power penalty than a CCPP with a MVC cooling. Pelster et al.[3] studied the combined cycle with advanced options viz. compressor air inter-cooling, water injection and reheating. They studied environmental and economic analysis simultaneously. They have optimized the system for economic and other better operations. Bhargava & Homji[4] have studied parametric analysis of existing gas turbines with inlet evaporative and overspray fogging. Chaker et al.[5] have presented fog droplet sizing analysis, nozzle types, measurement, and testing. The result of extensive experimental and theoretical studies conducted over several years includes coupled with practical aspects learned in the implementation of nearly 500 inlet fogging systems on gas turbines ranging in power from 5 to 250 MW. This study describes the different measurement techniques available, covers design aspects of nozzles, provides experimental data on different nozzles, and provides recommendations for a standardized nozzle testing method for gas turbine inlet air fogging. Bansode[6] have studied the effect of fog cooling system for inlet air cooling. They concluded that performance parameters indicative of inlet fogging effects have a definite correlation with the climate condition (humidity and temperature) and showed improvement in turbine power and heat rate. Alexis[7] has studied the performance parameters for the design of a combined refrigeration and electrical power cogeneration system. A steam power cycle (Rankine) produces electrical power 2 MW and steam is bleeded off from the turbine at 7bar to warm a factor or units of buildings during winter or to supply a steam ejector refrigeration cycle to air-conditioning the same area during the summer. Kumar et al.[8] have been developed design methodology for parametric study and thermodynamic performance evaluation of a gas turbine cogeneration system (CGTS).

Wang & Chiou[9] suggested that application of IAC and STIG technique can boost the output and generation efficiency. They concluded that implementing both STIG and IAC features cause more than a 70% boost in power and 20.4 % improvement in heat rate. Bilgen et al.[10] has developed design and economic methodology for the gas turbine cogeneration system. Ondrays et al.[11] have investigated gas turbine power augmentation in a cogeneration plant using inlet air chilling. Gas turbine power augmentation in a cogeneration plant using inlet air chilling is investigated. Options include absorption chillers, mechanical (electrical driven) chillers, thermal energy storage, Motive energy for the chillers is steam from the gas turbine exhaust or electrical energy for mechanical chillers. Chilled water distribution in the inlet air system is described. The overall economics of the power augmentation benefits is investigated. They concluded that the gas turbine power augmentation via inlet air chilling can be effectively used to boost power during high ambient temperature usually synchronous with the on-peak power generation, allowing leveling of GT power output.

A large number of efforts have been executed to apply either STIG technology or the IAC method to enhance the gas turbine's performance, to our knowledge, no attempt has been made to integrate these techniques in the combined form for the same system. In this study, a regenerative cycle generation unit is considered as base unit and STIG and IAC features are sequentially retrofitted to the system. The relative benefits obtained from either the STIG or IAC can be distinguished and the integrated efforts from the combined STIG and IAC can be quantified for further economic analysis.

II. NOMENCLATURE

AP	Approach point (^{0}C)
PP	Pinch point(^{0}C)
TIT	Turbine Inlet Temperature (K)
wbt	Wet bulb temperature(^{0}C)
M	Molecular weight (kg/kmol)
$\dot{E}$	Exergy rate (kW)
U	Internal energy (kJ)
$\dot{m}$	Mass flow rate (kg/s)

A. Subscripts

sup	superheated
Th	Thermal
HRSG	Heat recovery steam generator
GEN	Heat generator
f	fuel
REG	Regenerator
dbt	dry bulb temperature(^{0}C)

International Journal of Emerging Technology and Advanced Engineering
Website: www.ijetae.com (ISSN 2250-2459, ISO 9001:2008 Certified Journal, Volume 2, Issue 12, December 2012)

B. Superscript

fraction of gas phase at dead state
1 fraction of gas phase before combustion
2 fraction of gas phase after combustion
$\dot{E}$ Exergy rate (kW)
U Internal energy (kJ)
$\dot{m}$ mass flow rate (kg/s)

C. Greek symbol

η efficiency
λ fuel-air ratio
ω steam-injection ratio
ε Exergetic efficiency

D. Acronyms and abbreviations

FCS Fog cooling system
STIG Steam injection gas turbine
EVC Evaporative cooling

III. System Description

The regenerative cycle gas turbine system integrated with both IAC and STIG featuring are shown in Figure 1.

The basic unit includes compressor, combustor, gas turbine and a generator. A heat recovery steam generator (HRSG) was installed at the downstream exit of the turbine (state point 5) in order to recover the heat from the exhaust gases. The fraction of superheated steam generated from the HRSG is used for STIG (state point 9) and the remaining steam is used for process application. An evaporative fog cooling system (FCS) is installed to cool the ambient air (state point $1'$) as shown in Fig. 1. Fog cooling is an active system which uses very fine droplets of high pressure water injected through special atomizing nozzles located at discrete points across the inlet duct at high pressure to create the cooling effect. The amount of fog is to be monitored based on dry and wet bulb ambient conditions to achieve the required cooling A typical fog cooling system consists of a high pressure pump skid connected for feeding to an array of manifolds located at a suitable place across the compressor inlet duct. The manifolds have a requisite number of fog nozzles[6] which inject very fine droplets of water into the inlet air.

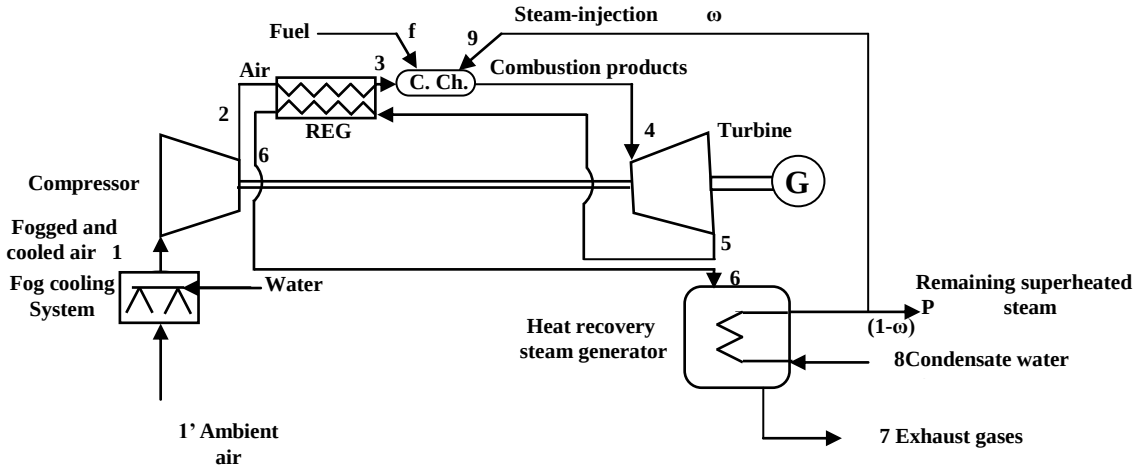

Fig. 1(a)- Regenerated cycle gas turbine with fog cooling and STIG

International Journal of Emerging Technology and Advanced Engineering
Website: www.ijetae.com (ISSN 2250-2459, ISO 9001:2008 Certified Journal, Volume 2, Issue 12, December 2012)

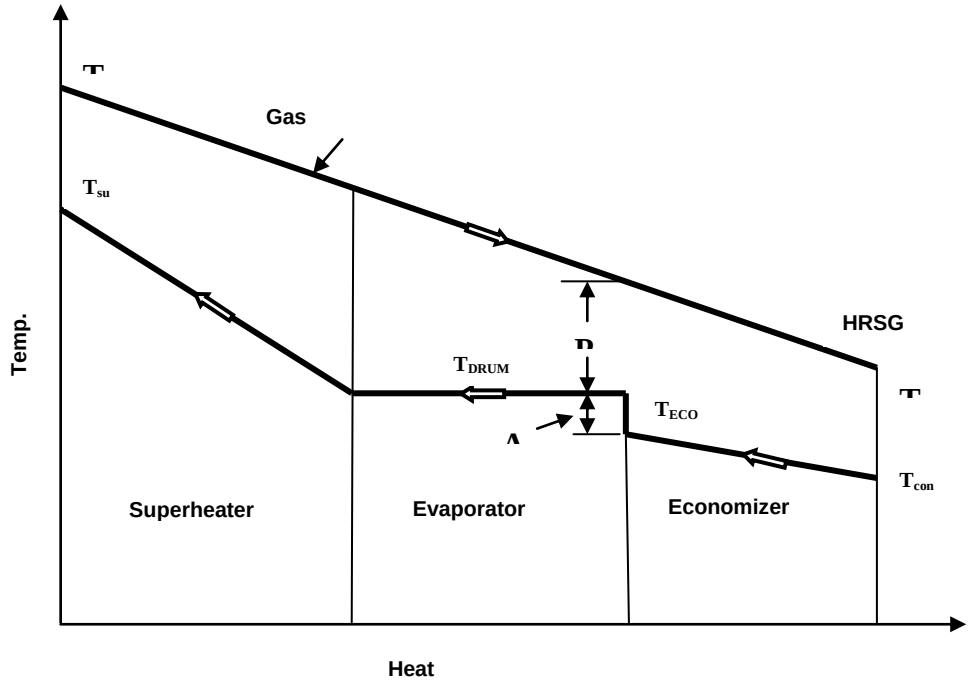

Fig. 1(b)- Temperature / Heat energy diagram for HRSG

The discharge through each nozzle is around 3ml/s and produces 3 billion droplets per second. The fine fog evaporates very fast, thus dropping inlet air temperature.

IV. Thermodynamic Modeling And Computer Simulation

A. Formulation:

The following assumptions have been considered for the present study:

1. The composition of ambient air has been assumed in terms of molar fraction of 1mole of air is: N_2=0.7748, O_2=0.2059, CO_2=0.00030 and H_2O=0.0190.
2. Fog cooling system has been maintained for 100% saturation of ambient air at wet bulb temperature of air.
3. Fog cooling system has been maintained for 100% saturation of ambient air at wet bulb temperature of air.
4. The pressure of water injected from the nozzle into the evaporative cooling chamber has been assumed 138 bar and converts into the fog (fine droplets), absorbs latent heat of air through adiabatic mixing.
5. Combustion chamber has been maintained at constant temperature.
6. The regenerator exchanges heat at constant pressure with fixed effectiveness of 0.6118.

A computer program has been developed to formulate and simulate the retrofitting techniques over simple gas turbine with a set of steady-state governing equations including mass, energy, entropy and exergy balances using control volume analysis sequentially for compressor, combustor, gas turbine and HRSG.

A set of governing equations for a particular component (k) is expressed as-

Mass rate balance

$$\sum_i \dot{m}_{i,k} = \sum_e \dot{m}_{e,k} \qquad (1)$$

Energy rate balance

$$\dot{Q}_{cv,k} - \dot{W}_{cv,k} = \sum_e \dot{m}_{e,k} h_{e,k} + \sum_i \dot{m}_{i,k} h_{i,k} \qquad (2)$$

Exergy rate balance

$$\dot{E}_{D,k} = \sum \dot{E}_{q,k} - \dot{W}_{cv,k} + \sum_i \dot{E}_{i,k} - \sum_e \dot{E}_{e,k} \qquad (3)$$

Where $\dot{E}_D$ denotes the rate of exergy destruction and $\dot{E}_q$ denotes the associated exergy transfer rate due to heat transfer.

If the effect of kinetic and potential energy is ignored, the total exergy rate $\dot{E}_k$ consisting of physical and chemical can be expressed as

$$\dot{E}_k = \dot{E}_k^{PH} + \dot{E}_k^{CH} \qquad (4)$$

International Journal of Emerging Technology and Advanced Engineering
Website: www.ijetae.com (ISSN 2250-2459, ISO 9001:2008 Certified Journal, Volume 2, Issue 12, December 2012)

Regenerator is a type of heat exchangers. The purpose of the heat exchangers is to increase the exergy of the hot stream coming from compressor and entering into the combustion chamber. Preheating the air promotes better combustion.

$$\varepsilon = \frac{T_3 - T_2}{T_5 - T_2} \quad (6)$$

Mass flow rate of air is given by

$$\dot{m}_a = \frac{M_a \dot{W}_{net}}{(1+\lambda+w)(\bar{h}_4 - \bar{h}_5) + (\bar{h}_1 - \bar{h}_2)} \quad (6)$$

and mass flow rate of fuel

$$\dot{m}_f = \lambda \frac{M_f}{M_a} \dot{m}_a \quad (7)$$

Where M_f = Molecular weight of fuel (Methane) (16.043 kg/kmolK), M_a = Molecular weight of air (28.649 kg/kmol), Fuel (methane) is injected in combustion chamber at pressure p_f and temperature T_1.

Exergy destruction in regenerator-

$$\dot{E}_{D,REG} = \sum_i \left(1 - \frac{T_0}{T_1}\right) Q_1 - \dot{W}_C + \dot{E}_2 + \dot{E}_5 - \dot{E}_3 - \dot{E}_6$$

$$\dot{E}_{D,REG} = \dot{E}_2 + \dot{E}_5 - \dot{E}_3 - \dot{E}_6 \quad (8)$$

The heat transfer between exhaust gases and condensate water has been taken place in water heat recovery boiler where superheated steam is generated.

$$m_{exh}(h_6 - h_7) = m_w(h_{sup} - h_{cond}) \quad (9)$$

Where m_{exh} and m_w are mass flow rate of exhaust gases of turbine and condensate water, h_6, h_7, h_{sup} and h_{cond} are enthalpies of exhaust gases at state 6 and 7, super-heated steam and condensate water.

$$T_{PP} = T_{sat} + PP \quad (10)$$

$$T_{AP} = T_{sat} - AP \quad (11)$$

Where T_{pp} , T_{sat} and T_{AP} are pinch point temperature, saturation temperature of water and approach point temperature. PP is the pinch-point difference and AP is the approach point difference from saturation temperature.

The heat transfer takes place in fog cooling system or evaporative cooling system such that:

$$m_w(h_{v1} - h_{w1'}) = m_a(h_{a1'} - h_{a1}) + \omega_1 m_a(h_{v1'} - h_{v1}) \quad (12)$$

Where m_w and $h_{w1''}$ are the mass flow rate and enthalpy of cooling water, m_a is the mass flow rate of dry air, ($h_{a1'} - h_{a1}$) is the enthalpy change of dry air, ($h_{v1'} - h_{v1}$) is the enthalpy change of water vapour during cooling.

1. Thermal Efficiency (η_{Th}): Thermal efficiency of a thermal system is defined as the ratio of net work output ($\dot{W}_{net}$) to the total heat input ($\dot{Q}_f$) of the fuel.

$$\eta_{Th} = \frac{\dot{W}_{net}}{\dot{Q}_f} \quad (13)$$

2. Generation Efficiency (η_{Gen}): Generation efficiency of a thermal system is defined as the ratio of electrical power output (W_{el}) to the total heat input of the fuel(Q_f).

$$\eta_{Gen} = \frac{W_{el}}{Q_f} \quad (14)$$

3. Heat-Rate (HR in kJ/s/kW): Heat rate is defined as the ratio of heat produced by the fuel ($\dot{Q}_f$) to the electrical power output ($\dot{W}_{el}$) of the thermal system.

$$HR = \frac{\dot{Q}_f}{\dot{W}_{el}} \quad (15)$$

4. Power to heat ratio (R_{PH}): The cost effectiveness of any cogeneration system is directly related to the amount of power it can produce for a given amount of process heat added. Hence, another parameter used to assess the thermodynamic performance of such a cogeneration system is R_{PH}, which is defined as:

$$R_{PH} = \dot{W}_{el} / (\dot{Q}_{EVAP} + \dot{Q}_{Pro}) \quad (16)$$

5. Specific Fuel-Consumption (SFC): Specific fuel–consumption of a thermal system is defined as the ratio of mass of fuel to the net work output. It is reciprocal of specific net work (W_{spec}).

$$SFC = \frac{\dot{m}_f}{\dot{W}_{net}} \quad (17)$$

6. First–Law Efficiency (η_I): The ratio of all the useful energy extracted from the system (electricity and process heat) to the energy of fuel input is known as first-law efficiency.

International Journal of Emerging Technology and Advanced Engineering
Website: www.ijetae.com (ISSN 2250-2459, ISO 9001:2008 Certified Journal, Volume 2, Issue 12, December 2012)

First-law efficiency is also known as fuel utilization efficiency or utilization factor or energetic efficiency. By definition,

$$\eta_I = \frac{\left(\dot{W}_{el} + \dot{Q}_{Pro}\right)}{\dot{Q}_f} \qquad (18)$$

Where $\dot{Q}_{Pro}$ is process heat rate.

7. Second–Law Efficiency (η_{II}): Since exergy is more valuable than energy according to the second law of thermodynamics, it is useful to consider both output and input in terms of exergy. The amount of exergy supplied in the product to the amount of exergy associated with the fuel is a more accurate measure of thermodynamic performance of a system, which is called second-law efficiency. It is also called exergetic efficiency (effectiveness or rational efficiency). By definition,

$$\eta_{II} = \frac{\left(\dot{W}_{el} + \dot{E}_{pro}\right)}{\dot{E}_f} \qquad (19)$$

8. Energy utilization factor (EUF): It is defined as the ratio of useful energy (net work output and process heat) to the heat supplied by the fuel.

$$EUF_{COH} = \frac{\dot{W}_{net} + \dot{Q}_{Pro}}{\dot{Q}_f} \qquad (20)$$

9. Fuel energy saving ratio (FESR): It is defined as the net energy output to the total energy output of the power generation system.

$$FESR_{COH} = \frac{\frac{\dot{Q}_{PRO}}{\eta_{HRSG}} + \frac{\dot{W}_{net}}{\eta_{Brayton}} - \dot{Q}_f}{\frac{\dot{Q}_{PRO}}{\eta_{HRSG}} + \frac{\dot{W}_{net}}{\eta_{Brayton}}} \qquad (21)$$

Where $\dot{E}_{PRO}$ is the exergy content of process heat and $\dot{E}_f$ is the exergy content of fuel input.

10. Effectiveness(Exergetic efficiency) of component (ε) : Exergetic efficiency of component is defined as the ratio of exergy rate recovered from the component ($\dot{E}_R$) to the exergy rate supplied to the component ($\dot{E}_S$). Exergetic efficiency gives true measure of useful energy which cannot be obtained from energy criteria.

$$\varepsilon = \frac{\dot{E}_R}{\dot{E}_S} = \frac{\dot{E}_R}{\dot{E}_R + \dot{E}_D} = 1 - \frac{\dot{E}_D}{\dot{E}_R + \dot{E}_D} \qquad (22)$$

11. Exergy-Destruction Rate ($\dot{E}_{DR}$): The component exergy destruction rate can be compared to the total exergy destruction rate within the system.

$$\dot{E}_{DR} = \frac{\dot{E}_D}{\dot{E}_{D,tot}} \qquad (23)$$

V. Results And Discussion

In the present study following three configurations with retrofitting have been studied in comparison to simple gas turbine cycle:

(i) Regenerative gas turbine cycle with inlet air cooling (IAC)
(ii) Regenerative gas turbine cycle with STIG
(iii) Regenerative gas turbine cycle with both IAC and STIG.

The initial conditions for system analysis are as shown in Table 1. In the calculation, the steady state operation is investigated without considering the turbine blade cooling. The performance analysis of these retrofitted gas turbine system is done by preparing a computer program in EES validated with Bilgen et al.[10]. The temperature, pressure and gas concentration in each component are calculated by taking into consideration of the compositions and proportions of gases and consequently, various performance parameters and exergy loss in these systems are estimated. Table 2 represents the comparison of performance parameters of regenerative cycle with other combinations. The net power output and power generation efficiency for regenerative cycle are 30 MW and 36.99% respectively. Attachment of evaporative cooler with regenrative cycle improves the performance parameters (which includes system efficiencies, heat rate and specific power output etc.). Gas turbine inlet air fogging is a commonly used method of cooling the intake air where de-mineralized water is converted into fog droplets by means of special atomizing nozzles operating at approximately 138 bar. The evaporation of small size (5 to 20 microns) droplets in the intake duct cools the air and consequently increases the moist air mass flow rate to improve power performance. This technique allows close to 100% evaporation effectiveness in terms of attaining saturation conditions and wet bulb temperature at the compressor inlet. Thus variation in the ambient temperature influences the exhaust temperature of the compressor, the internal and external temperature of the turbine, the mass flow, the specific work, the specific consumption and power. When the ambient temperature drops, the power supplied by the machine increases. Therefore, it is useful in many cases to cool the compressor inlet air with a view to obtain a greater production of electric power and also the compressor work decreases. Using evaporative cooling, the available air (25^0C and 60% RH) can be cooled up to 19.47^0C.

International Journal of Emerging Technology and Advanced Engineering
Website: www.ijetae.com (ISSN 2250-2459, ISO 9001:2008 Certified Journal, Volume 2, Issue 12, December 2012)

The impact of evaporative cooling will be higher in dry summer season when dry bulb temperature is higher and RH is lower.

TABLE I
Essential input parameters for simple gas turbine cycle and retrofitted systems

Ambient air temperature at state 1′ (K)	298.15
Ambient air pressure at state 1′, (bar)	1.013
Ambient air relative humidity at state1′, (%)	60
Spray water temperature at state1′, (K)	298.15
Spray water pressure at state1′, (bar)	138
Air inlet pressure to compressor (P_1), (bar)	1.013
Air inlet temperature to compressor, (T_1) , (K)	298.15
Relative humidity of inlet air to compressor at 1, (%)	100
Pressure ratio of compressor (r_p)	10:1
Isentropic efficiency of compressor (η_{SC}), (%)	0.86
Isentropic efficiency of Turbine (η_{ST}), (%)	0.86
Lower heating value of fuel (LHV), (kJ/kmol)	802361
Turbine inlet temperature (TIT), (T_4), (K)	1520
Network output for regenerative cycle(W_{output}), (MW)	30
Injection pressure of fuel (methane) (P_f), (bar)	12
Injection temperature of fuel (methane) (T_f), (K)	298.15
Pressure drop in combustion chamber, (%)	5
Pressure drop in regenerator on the gas side, (%)	3
Pressure drop in regenerator on the air side, (%)	5
Effectiveness of regenerator	0.6118
Exhaust pressure of combustion products after HRSG (P_7), (bar)	1.013
Exhaust temperature of combustion products after HRSG (T_7), (K)	403.15
Pressure of steam generation (P_9), (bar)	20
Pressure of condensate water at inlet of HRSG (P_8), (bar)	20
Temperature of condensate water at inlet to HRSG (T_8), (K)	298.15
Pressure drop in HRSG on the gas side, (%)	5
Amount of steam injected (ω), (% of the mass flow rate of the air)	10
Temperature of superheated steam STIG (T_9), (K)	753.15
Approach point , (K)	2
Pinch point, (K)	20

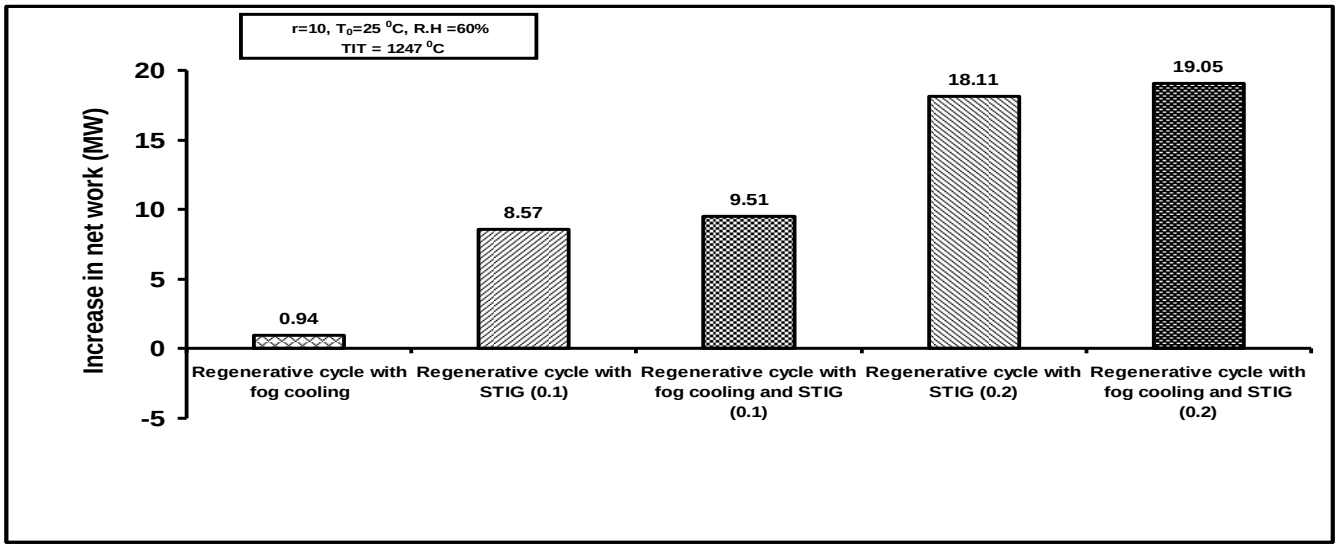

Fig. 2- Net work output for retrofitted cycles in comparison to regenerative cycle

International Journal of Emerging Technology and Advanced Engineering
Website: www.ijetae.com (ISSN 2250-2459, ISO 9001:2008 Certified Journal, Volume 2, Issue 12, December 2012)

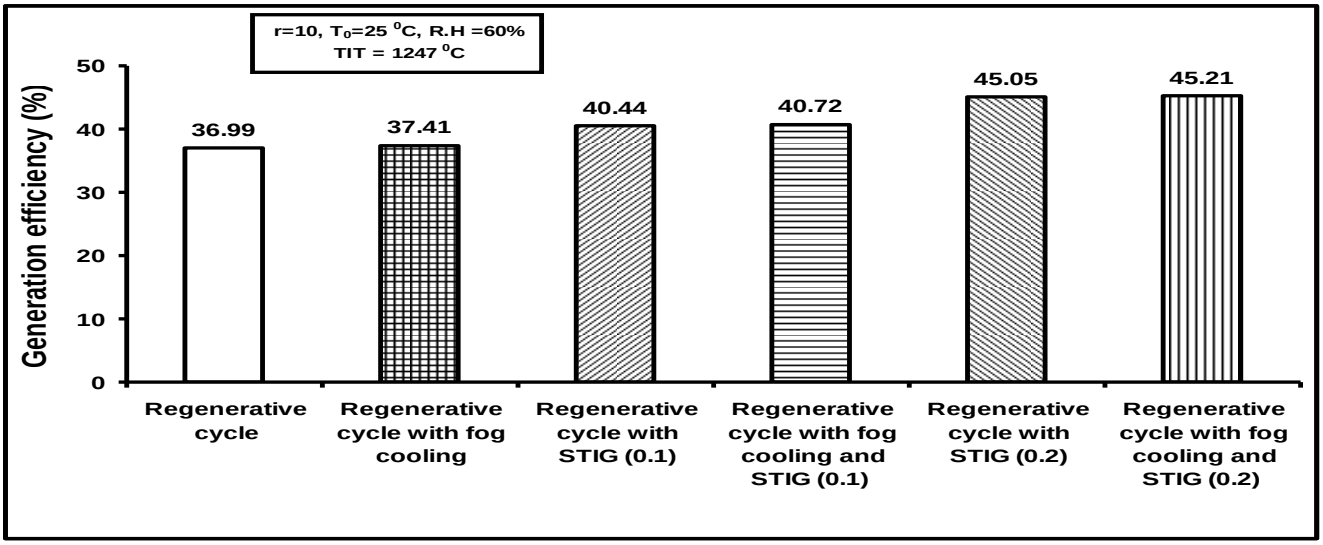

Fig. 3- Comparison of Generation efficiency for different retrofitted

Comparison of regenerative cycle gas turbine with and without fog cooling shows (Table 2) that the net power output increases by 3.1% and various efficiencies increase by 0.44% while the heat rate decreases by 1.1%. Comparison of regenerative cycle gas turbine with and without STIG shows (Table 2) that net power output and thermal efficiency increase by 28.57% and 3.52% respectively while heat rate decreases by 8.5%. In the process of recovering energy from the exhaust gases via the HRSG, the temperature at the outlet of the stack (state point 7 in Fig.1) is usually kept above 127^0C (dew point temperature of acid) in order to prevent condensation of SO_2 and NO_2 which ultimately hydrolyzed into sulphuric acid (H_2SO_4) and nitric acid (HNO_3) and cause scale and corrosion to the air preheater of HRSG. The pinch point and approach point for present analysis are taken as 20^0C and 2^0C respectively. Under these conditions, the maximum flow rate of generated superheated steam at 753.15K and 20bar is about 19.27 kg/s. If all the generated steam is injected into the combustor (STIG only), the maximum injection ratio (m_{steam}/m_{air}) is about 0.2. Therefore, there is a wide range of STIG available to optimize the power cycle. The calculated power output for injection ratio 0.1 shows that the effect of the STIG is quite substantial. The net power output is increased to 38.57MW. The profound effect from STIG alone is obtained from the pump. Since the pumping work is 2 to 3 orders of magnitude smaller than that of compressor, the net power output produced by the steam is, thus, much higher than that of air per unit mass flow rate. Besides this the specific heat of superheated steam is almost double the value of air and the enthalpy of steam is higher than that of air at a certain temperature.

Therefore, the STIG method is a very effective way to boost the net power output and increase the overall efficiency of the gas turbine. Regenerative gas turbine cycle with STIG (for steam injection ratio 0.1) significantly improves the system efficiencies. Comparison of regenerative cycle gas turbine with and without FC (fog cooling) and STIG shows that net power output increases by 31.7% and thermal efficiency increases by 3.81%, while heat rate decreases by 9.2%. Hence, combination of simple cycle with STIG and evaporative (fog) cooling further improves the system performance.

The Fig.2 represents the net increase in work output for different retrofitted cycle in comparison to regenerative cycle. The maximum value of increase in work output obtained is 19.05 for regenerative cycle combined with STIG (injection ratio 0.2) and fog cooling.

Fig.3 represents the comparison of generation efficiencies for regenerative cycle and retrofitted cycles. The maximum generation efficiency achieved is 45.21% for retrofitted combined cycle (fog cooling and STIG) with injection ratio 0.2. The trends show that the combination of fogging and STIG with simple cycle gas turbine cycle is a better approach to enhance the performance of the system on the basis of first law as well as second law.

The benefit of adding the STIG feature can be estimated from Fig. 4, it shows the effect of STIG on generation efficiency, first law efficiency and process heat for fixed inlet air conditions as the air gets saturated up to 100% R.H due to fog cooling. The first law efficiency falls with the increasing amount of steam injection ratio.

International Journal of Emerging Technology and Advanced Engineering
Website: www.ijetae.com (ISSN 2250-2459, ISO 9001:2008 Certified Journal, Volume 2, Issue 12, December 2012)

The reason for decrease in first-law efficiency is that the slope of process heat is sharper than the slope of generation efficiency i.e. the reduction in process heat takes place with much faster rate. The maximum amount of injection steam is limited by the available energy recovered from the HRSG. The maximum injection ratio at 0.2 is still below the allowable injection limit (prescribed by the manufacturer) for the available industrial turbines.

The exergy destruction rate represents the wastage of available energy. Exergy destruction of all components have been calculated to enhance the overall cycle performance. Table 3 presents the exergy destruction of regenerative and retrofitted cycle components. While examine the exergy destruction for all components, the combustor has the largest exergy destruction and shows the major location of thermodynamic inefficiency because of large irreversibility arising from the combustion reaction and heat transfer. Steam injection will increase the exergy destruction due to mixing of high temperature superheated steam (753.15^0C) and compressed air (at 604.95^0C) into the combustor increases the overall temperature of combustor. The exergy-losses at position 7 (see Fig.1) is considered as exergy loss through stack. Since part of exhaust heat is recovered in HRSG, the exhaust exergy out of stack can be reduced substantially after retrofitting. The exergy losses through stack will not only waste the available exergy but also dump the thermal pollution to our living environment.

Exergetic efficiency for each component can be defined as the ratio of $\dot{E}_R$ to $\dot{E}_S$, where $\dot{E}_S$ is the exergy rate supplied to the component and $\dot{E}_R$ is the exergy rate recovered from the component. For a retrofitted cycle with fog cooling and STIG, exergetic efficiencies of compressor, turbine, combustor, regenerator and HRSG are respectively 93%, 94%, 71%, 84% and 79%, among which gas turbine and compressor have higher exergetic efficiency. This implies most of the exergy destruction in combustor and compressor is inevitable. It is interesting to note that the exergy destruction rate of combustor is the highest. Exergy efficiency of regenerator and HRSG is higher than that combustor. Due to maximum injection ratio limitation, there is about 5.5MW heat remain available into superheated steam. Therefore, there is a greater improvement margin exists for HRSG than for combustor.

Comparison of regenerative cycle gas turbine with and without FC (table 2) shows that exergetic efficiency gets also improve by 0.4%. However fuel-air ratio increases by 0.6%. Comparison of regenerative cycle gas turbine with and without STIG shows that exergetic efficiency gets also improved by 23.1% however fuel-air ratio increases by 17.7%.

Exergy destruction increases in each system component except air compressor due to mixing of steam and air. Comparison of regenerative cycle gas turbine with and without FC and STIG shows that exergetic efficiency gets also improve by 23.02% however fuel-air ratio increases by 18%. The exergy destruction gets increased in each system component due to increasing mass flow rate.

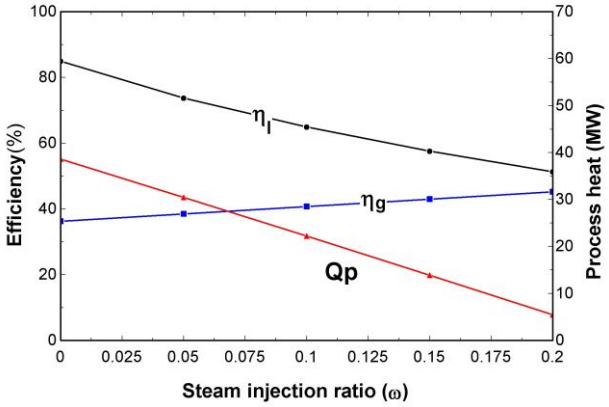

Fig. 4- The effect of steam injection ratio on first-law efficiency, generation efficiency and process-heat for regenerative cycle combined with fog cooling and STIG

However with increasing amount of STIG, exergy destruction rate of each component increases except combustion chamber and compressor.

The exergy destruction rate (MW) for different system components of regenerative and retrofitted cycle has been shown in Fig. 5. The power output increases for large amount of STIG due to increasing mass flow rate of air and steam mixture. While the exergy destruction rate increases into the Combustion chamber, turbine, regenerator and HRSG. The exergy destruction in combustion chamber is highest among all the system components due to highest temperature of combustion chamber.

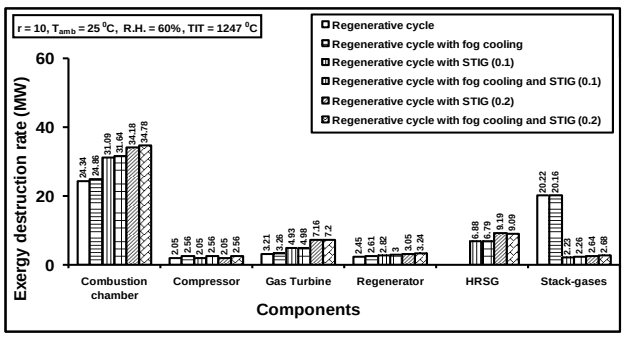

Fig. 5- Comparison of exergy destruction rate of system components for regenerative and retrofitted cycle (fog cooling and STIG)

International Journal of Emerging Technology and Advanced Engineering
Website: www.ijetae.com (ISSN 2250-2459, ISO 9001:2008 Certified Journal, Volume 2, Issue 12, December 2012)

The results predicts that as the steam injection increases the amount of stack-losses reduces appreciably up to some extent (for STIG 0.1) and further increases slightly (for STIG 0.2). The exergy destruction in combustion chamber increases with increasing amount of STIG due increasing amount of air and steam mixture. The exergy destruction rate (MW) per MW of power output for different system components with different amount of STIG has been shown in Fig. 6.

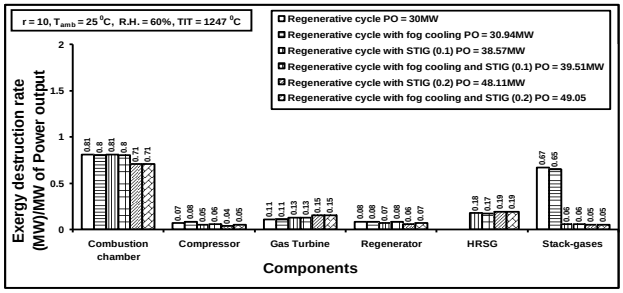

Fig. 6- Comparison of Exergy destruction rate (MW) per MW of output for system components for diggernent retrofitted

Due to significant increase in power output the rate of exergy destruction (MW) per MW of power output reduces for combustion chamber, compressor and stack - gases while increases for gas turbine due to increasing mass flow rate (mass flow rate of air from compressor plus mass flow rate of superheated injected-steam with lower exergy).

VI. CONCLUSIONS

With the rapidly increasing demand for electricity in the developed countries like India, and the expected shortage in power supply due to delays in the major power projects, retrofitting regenerative gas-turbines with inlet air pre-cooling and STIG are attractive investment opportunity. Recovering the energy from the exhaust gas of a regenerative cycle can be used back to the system to improve the system performance. Steam injection and inlet air evaporative cooling are well-proven technology that can effectively improve power output and power generation efficiency for a regenerative cycle gas turbine. In the present work, a regenerative cycle gas turbine has been investigated. An existing regenerative cycle gas turbine was considered as the basic system and has been converted into modified retrofitted system with either the IAC or /and STIG features. The steam needed in the STIG feature is generated from the energy recovered from the system's own exhaust gases.

Under the average local weather conditions (25^0C and 60% RH), the benefit of adding the STIG feature can substantially improve the power output from the 30 MW to 38.57 MW and power generation efficiency from 36.99 to 40.44%. The maximum power that can be reached by the system with both IAC and STIG features is 49.05 MW for steam injection pressure ratio at 0.2. Although the steam injection will increase the total exergy losses, the exergy loss per MW output is much smaller than that of regenerative cycle. It also reveals that the degree of energy wasting and thermal pollution can be reduced through retrofitting.

REFERENCES

[1] Nishida K., Takagi T., Kinoshita S. 2005. Regenerative steam-injection gas turbine systems, Applied Energy **81** (2005) 231-246; Japan.

[2] Hawaj O. M., Mutairi H, A. 2007. combined power cycle with absorption air cooling, Energy **32** (2007) 971-982, Kuwait.

[3] Pelster S., Favrat D.,Von Spakovsky M. R. 2001. The thermo economic analysis and environomic modeling and optimization of the synthesis and operation of combined cycle with advanced options, Engineering for gas turbine and power, transaction of the ASME **123** (2001) 717-26.

[4] Bhargava R. & Meher-Homji C. B. 2005. Parametric analysis of existing gas turbines with inlet evaporative and overspray fogging, Journal of Engineering for gas turbines and power **127** (2005) 145; Houston.

[5] Chaker M., Homji C. B. M., Mee I. I. I. T. 2004. Inlet fogging of gas turbine engines-part II: fog droplet sizing analysis, nozzle types, measurement and testing, Journal of engineering for gas turbines and power **126** (2004) 559, Monrovia.

[6] Bansode S., Sinha R., A. 2010. thermodynamic analysis for gas turbine power optimization by fog cooling system, 20th national and 9th International ISHMT-ASME heat and mass transfer conference (2010).

[7] Alexis G. K. 2007. Performance parameters for the design of a combined refrigeration and electrical power cogeneration system, International journal of refrigeration **30** (2007) 1097-1103, Greece.

[8] Kumar A., Kachhwaha S. S., Mishra R. S. 2010. Thermodynamics analysis of a regenerative gas turbine cogeneration plant, Journal of Scientific & Industrial Research, **69** (2010) 225-231; India.

[9] Wang F. J. & Chiou J. S. 2004. Integration of steam injection and inlet air cooling for a gas turbine generation system, Exergy conversion and Management, **45** (2004) 15-26, Taiwan; ROC.

[10] Bilgen E, Exergetic and engineering analysis of gas turbine based cogeneration systems, Energy **25** (2000) 1215-1229, Canada.

[11] Ondryas I. S., Wilson D. A., Kawamoto M., Haub G. L. 1991. Options in gas turbine power augmentation using inlet air chilling, Journal of Engineering for gas turbines and power **113** (1991) 205.

Shear Strength Parameters for Silty-Sand Using Relative Compaction

Sadanand Ojha
Research Scholar, Department of Civil Engineering
Faculty of Technology, University of Delhi
(Delhi Technological University Campus)
Bawana Road, Delhi-110042, India
e-mail: sadanand_ojha@yahoo.com

AshutoshTrivedi
Professor, Department of Civil Engineering
Delhi Technological University
Bawana Road, Delhi-110042, India
e-mail: prof.trivedi@yahoo.com

ABSTRACT

The strength behavior of silty sand can be interpreted from its relative compaction, mean confining pressure and relative dilatancy. The present work considers triaxial test results on silty sand at different relative compaction and confining pressure. The review of past results on shear testing indicates that strength parameter of clean sand and silts are often considered corresponding to relative density. There are serious problem associated with the estimation of relative density of the soil containing significant percentage of plastic and non-plastic silt. In fact, presence of plastic fines disallows the investigator to interpret relative density. Therefore it is pertinent to use relative compaction of the soil as considered in the present study to interpret the strength parameter of the soil containing fines. This concept is used for an analytic simplicity for generic application. This relative density assumption for the soil containing significant percentage of fines often leads to significant error in overall estimation of strength and deformation properties of silty sands. Previous researchers considered the stress strain response of silty sand based on critical state friction angle Φ_c, peak friction angle Φ_p; maximum and minimum void ratio (e_{max} and e_{min}) and empirical strength parameters Q_b and R_b.The uncertainty in calculating the relative density for silty sands when fine contents is more than a certain limit gives error in computation of strength parameters of silty sand. Hence, the authors in the present study used the relative compaction instead of relative density and obtained the strength parameters Q_{af} and R_{af}. The results are compared with the back calculated values from the previously published studies. It is found appropriate to use the strength parameters Q_{af} and R_{af} for the soils containing significant percentage of fines.It was observed that the Yamuna sand containing silts has comparable values (25 to 40) of empirical shear strength fitting parameters (Q_{af}) at select relative compaction as shown in the present work in terms of Q_{af} and R_{af}. The value of Q_{af} and R_{af} has been analysed with reference to standard errors.

KEYWORDS: Silty sand, relative compaction, relative density, strength parameters, critical and peak friction angle.

INTRODUCTION

The stress-strain response of sand at varied strain levels depends upon soil state variables (the relative compaction of the sand R_c, confining pressure, and soil fabric) and other related factors such as particle shape, particle size distribution, particle surface characteristics, and mineralogy. The factors related to the constitution and general nature of the sand particles are referred to as intrinsic variables [3, 16]. The examples of intrinsic variables are the critical-state friction angle ϕc, the maximum and minimum void ratio e_{max} and e_{min}, and the dilatancy parameters Q_b and R_b of the peak friction angle given by the correlation of Bolton [3].However natural soil deposit of Yamuna sand near Delhi and NCR region contain significant amount of silt and or clayup to a depth of15 meter or greater. It contains fines up to 30 %. It is pertinent to recall that in the same range of grain sizes below water table are significantly vulnerable to liquefaction during earth quakes. The authors have reviewed the work carried out by the previous researcher [1-23] and have addressed the effect of silt sized particles on the stress-strain response of Yamuna sand when silt content is up to 25% by weight. For a safe foundation design of these structures and to ensure that they don't have any structural damage in their life time, the knowledge of strength behaviour of silty Yamuna sand becomes very important. Previous studies published so far in the engineering literature; do not provide a direct relationship for prediction of the shear strength and dilatancy parameters of silty sand obtained from the river Yamuna. As such, the knowledge of the shear strength parameters (Q_{af} and R_{af}) of Yamuna sand would be necessary for the safe design of structures being constructed on the Yamuna basin. In the present work samples were prepared at different relative compaction and were subjected to different level of mean effective confining pressure. The stress-strain response was recorded and shear strength and dilatancy parameters were obtained for each fine percentage. The critical state and peak friction angle were calculated for each soil sample. The various state variables were also calculated for clean sand and sand containing silt in various proportions and a co-relation for shear strength of silty sands was found. The behaviour of silty sand has been compared with the behaviour of materials as published in various literature in relation to the Bolton's empirical shear strength fitting parameter for clean sands (Q_b=10). A plot between relative density and relative compaction has been drawn and empirical co-relation has been established. This co-relation is verified empirically and has been used in the present paper to find out the Q_{af} values. It was observed that the Yamuna sand containing silts has comparable values of empirical shear strength fitting parameters (Q_{af}=25 to 40) at select relative compaction.

RELATIVE DENSITY AND RELATIVE COMPACTION

The relative density is used to define the state condition of silty sand when silt content is approximately less than 15 percent. It is based on the prediction of maximum void ratio; minimum void ratio and natural void ratio. Alternatively it can also be expressed in terms of maximum unit weight, minimum unit weight and natural unit weight of soil. The correct prediction of relative density is not possible since it is difficult to obtain maximum and minimum unit weight values within a definite accurate range. The definition is for the maximum and minimum values but average values are usually used for calculating relative density (R_d). This value range together with the uncertainty in obtaining the in situ value can give a potential error in computing relative density. Due to the above reason the authors has used the term relative compaction (R_c) in this paper instead of relative density which is defined as the ratio of natural unit weight to maximum unit weight ($Rc= \gamma_n/ \gamma_{max}$) which takes care of the uncertainty in computation of unit weight of soil since values of γ_n and γ_{max} can be accurately ascertained. Also the plot between R_d and R_c at different confining pressures has been drawn as shown and an

empirical relation between R_c and R_d has been found which is validated theoretically by substituting in Bolton's equation.

SAMPLE COLLECTION AND SAMPLE PREPARATION

There are vast deposits of silty sand along the banks of river Yamuna which has prominent cities of northern India namely Delhi, Noida, Mathura, Agra and Allahabad. The soil samples were taken from nearby area of Noida and Greater Noida during soil exploration using split spoon sampler. Sieve analysis has been performed on the collected soil sample and the material passing through 4.75mm sieve and retained on 75 micron was collected. The sample was washed with water to remove any amount of silt and or clay. The dried sample was again repeated through the same procedure mentioned above and the clean Yamuna sand is obtained. The specific gravity of the sand particles was 2.67 which were determined by the pycnometer method. The non-plastic fines which passes through IS 75μ sieve size were used. The fines were prepared in the laboratory and wet analysis was carried to know the percentage of particles passing 75μ sieves. After processing, soil was finalized as silt which has a maximum amount of particles passing 75 μ. The material which passes through 75 μ was collected in a container and allowed to settle. Then the passing material is dried in the oven and pulverized. The pulverized material was again sieved through 75 μ sieve. Then a hydrometer analysis was carried out to know the amount of clay particles. The amount of clay particles was found insignificant. The sample of sand and silt thus obtained is used for triaxial testing. The samples were prepared by first estimating the weights of sand and silt needed for fines content. These amounts of silt and sand were then mixed in a cylindrical Plexiglas tube completely filled with desired water. The silt and sand are thoroughly mixed by vigorous shaking of the Plexiglas tube for approximately 20 minutes to achieve sample uniformity. Afterward, the rubber cap is removed, a very small amount of desired water is added to raise the water level back to the top of the tube, and the tube is topped with the pieces of high-density polyethylene film. The contents of the tube are then released into the membrane by raising the tube. Densification of the sample is accomplished by carefully and symmetrically tapping the sides of the sample mould immediately after slurry deposition. Because the mass of sand and silt used in sample preparation can be accurately estimated, it is possible to obtain a relative compaction that is reasonably close to a target value by measuring the height of the sample as it gets compacted. The samples had heights of the order of 76 mm and diameters of the order of 38 mm. The confining pressures of 100kPa, 200 kPa and 400 kPa were applied to the samples and the rate of strain was kept slow enough at 1.25 per minute to ensure uniformity of results. The volume change of the sample was measured using a sensitive differential pressure technique. The stress-strain data was recorded. The details of the sample preparation and testing procedures were followed as recommended by IS 2720.

EXPERIMENTAL PROGRAM

A series of tri-axial tests were performed to assess how the shear strength of sand changes with an increasing percent of silt. In order to explain the effect of silt on the behaviour of clean sand, a series of tests was carried out for silt content in the range of up to 25% atvaried relative compaction. The effect of fine content on the values of angle of internal friction, the minimum and maximum void ratios, the effective size (D_{10}), the mean grain size (D_{50}), coefficient of uniformity (Cu), and unconfined compressive strength of silty sands are also evaluated. The schedule of tests are given in Table 1(a) and Table 1(b). The index properties, grain size characteristics and intrinsic properties are given in Table (2, 3) and (4).The relative compaction

corresponding to various relative densities is shown in Fig.5. The dilatancy properties of some other silty sand by previous researcher are given in Table (5). The results obtained from present study are presented in Table (6). Maximum and minimum void ratio of clean sand e_{max} and e_{min} are 0.78 and 0.50. The specific gravity of silt and sand is calculated as 2.63 & 2.67.

BASIC CONCEPTS

The data of a typical drained compression test on a dense, cylindrical sample with frictionless end is required to interpret preliminary stress - dilatancy relations. Strains were inferred from boundary displacements and volume changes, and they therefore under estimate the strains in the rupture zone which was developed between points [16]. The stress-dilatancy relationship is predicted with standard error analysis due to non-uniformity of the sample and the uncertainty regarding membrane correction following the formation of a rupture plane. Nevertheless existing research indicates that soil in rupture zones will dilate fully to achieve a critical state, at which shear deformation can continue even in the absence of a volume change. The point of peak strength is normally associated with the maxima of ($d\varepsilon1$ / $d\varepsilon3$) [1-3, 16, 19, 20]. A typical result of triaxial testing on silty sand showing plot between deviator stress and axial strain is shown in Fig.2a-2e. The corresponding volume change vs. axial strain plots can be obtained from the details of the out-put captured by the first author [15] and is shown in Fig.3a-3e. Bolton [3] reviewed a large number of tri-axial and plane-strain test results for 17 clean sand and proposed a much simpler relationship between Φ, Φ_c and ψ which Salgado et al [] found to be operationally equivalent [16] as shown in the following Eqs.

$$\Phi = \Phi_c + 0.8\psi \tag{1}$$

The relationship between the peak friction angle Φ_p and the critical-state friction angle Φ_c can be written for tri-axial test, so that the dilatancy angles are expressed in terms of the same quantity I_R, defined as dilatancy index, for tri-axial conditions,

$$\Phi_p = \Phi_c + 3I_R \tag{2}$$

Using the Bolton's [3] relation, the relative dilatancy index I_b can be expressed in terms of relative density as,

$$I_b = R_d\ (Q_b - \ln 100P`_p / P_A) - R_b \tag{3a}$$

For silty sand R_d cannot be precisely estimated according to ASTM [9] therefore, the Eqs.3(a) is proposed in terms of relative compaction.

$$I_{af} = R_c\ (Q_{af} - \ln 100\ P`_p / P_A) - R_{af} \tag{3b}$$

where, R_c is relative compaction defined as a ratio of natural unit weight to maximum unit weight, P'_p is the mean effective stress at peak strength in kPa, P_A is reference stress (100 kPa) in the same units as P'_p, Q_{af} and R_{af} are fitting parameters as per present work and Eqs. (2a) and Eqs.(3a) are valid for $0 \leq I_R \leq 4$ as per Bolton [3].

Comparing equation (2) and equation (3b)

$$R_c\,(Q_{af} - \ln 100P`_p / P_A) - R_{af} = [\Phi_p - \Phi_c]/3 \quad (4)$$

Rearranging Eqs. (4)

$$[\Phi_p - \Phi_c]/3 + R_c \ln 100P`_p / P_A = Q_{af}R_c - R_{af} \quad (5)$$

Further the authors defines a relationship among relative dilatancy, relative compaction and mean confining pressure in terms of a new term I_{na} as,

$$I_{na} = [\Phi_p - \Phi_c]/3 + R_c \ln 100\,(P`_p / P_A) \quad (6)$$

Substitution of Eq. (6) in Eq. (5) gives

$$I_{na} = R_c Q_{af} - R_{af} \quad (7)$$

A typical variation of I_{na} with relative compaction is shown in Fig. 4a-4f. Using the relationships of Eqs (7), we obtained the values of Q_{af} and R_{af} and results are presented in Table (6) for best fit and with R=25, 30, 40. Hence the estimate of I_R, I_{na}, and dilatancy angle can be made for wide ranging granular materials namely sands, silty sands[1-3, 5-6, 10, 16], coal ashes [20], and even rock masses[19].

VALIDATION OF BOLTON'S DILATANCY PARAMETERS USING RELATIVE COMPACTION

For soils a relationship among relative compaction can be defined in parametric form

$$Rc = m\,R_d + n \quad (8)$$

Using Fig.5 for clean sand, m= 0.217 and n=0.789

A relationship between relative compaction and Ina can be defined in parametric form as

$$Ina = Q_{af}R_c - R_{af} \quad (9)$$

Hence from Fig. 4a for clean sand Q_{af}=49.883 and R_{af}= 40.105

Substituting values of R_c in Eq. (9)

$$Ina = Q_{af}R_d - R_{af} \quad (10)$$

where Q_{af}=10.77 and R_{af}=1.19

From Eqs. (10) value of dilatancy parameter Q_{af} is10.77 corresponding to R_{af} value of 1.19. It isvery close to Bolton's fitting parameters (Q_b=10 corresponding to R=1). Hence it is recommended to use R_c instead of R_d since the deficiency involved in estimation of Rd is eliminated without affecting the results.

Table 1 (a): Test Schedule for Index Properties

Sample Type	Total Test/ Accepted Result	Grain Size Analysis	Atterberg's Limits
Clean sand	10/10	Mechanical Sieve Analysis	-
Silty sand	25/20	Hydrometer Analysis	Liquid Limit/ Plastic Limit

Table 1 (b): Test Schedule and Limits inTriaxial Tests

Sample Type	Total Test/ Accepted Result	Relative Compaction (%)	Silt (%)	σ_3 (kPa)	P'_p (kPa)
Clean sand and silty sand	105/90	0.92-0.96	0 to 25	100 to 400	147-524

Table 2: Plasticity Characteristics of Silty Sand

S.No.	Sample Description	Liquid Limit	Plastic Limit	Plasticity Index
1	Silt	22.4%	10%	12.4%
2	Clean Sand	-	-	-
3	Clean Sand + 5% Silt	-	-	-
4	Clean Sand + 10% Silt	15.0%	Non Plastic	-
5	Clean Sand + 15% Silt	18.0%	Non Plastic	-
6	Clean Sand + 20% Silt	20.0%	Non Plastic	-
7	Clean Sand + 25% Silt	22.0%	Non Plastic	-

Table 3: Grain Size Characteristics of Silty Sand

S.No.	Sample Description	D_{10}	$D_m = D_{50}$	C_c	C_u	q_u
1	Clean Sand	0.135	0.225	1.070	1.852	--
2	Clean Sand + 5% Silt	0.125	0.224	1.136	1.992	0.23
3	Clean Sand + 10% Silt	0.075	0.222	1.840	3.307	0.24
4	Clean Sand + 15% Silt	0.018	0.215	7.317	13.667	0.25
5	Clean Sand + 20% Silt	0.0099	0.213	11.915	24.747	0.27
6	Clean Sand + 25% Silt	0.0067	0.208	14.941	35.821	0.42

Table 4: Peak Friction Angle for Clean and Silty Sand

S.No.	Sample Description	Confining Pressure (kPa)	Relative Compaction (%)				
			0.92	0.93	0.94	0.95	0.96
1	Clean Sand	100	24.40	27.98	26.37	32.51	32.79
		200	24.28	26.30	25.63	26.37	26.84
		400	22.32	26.14	24.30	24.56	24.99
2	Clean Sand + 5% Silt	100	26.89	32.39	31.14	34.15	34.81
		200	24.38	24.61	26.34	26.84	27.15
		400	20.31	19.59	23.75	24.13	24.73
3	Clean Sand + 10% Silt	100	33.92	31.87	35.42	36.21	36.72
		200	25.79	27.95	29.51	29.78	30.59
		400	27.05	22.32	21.99	22.48	23.02
4	Clean Sand + 15% Silt	100	20.19	17.55	19.80	30.15	31.38
		200	24.39	22.81	25.91	26.07	26.68
		400	23.24	24.24	25.34	25.67	26.06
5	Clean Sand + 20% Silt	100	20.21	24.25	24.71	26.98	28.61
		200	20.37	22.14	22.88	23.03	25.06
		400	15.92	17.32	17.40	21.01	21.90
6	Clean Sand + 25% Silt	100	24.46	26.94	28.62	30.40	31.01
		200	22.04	23.99	24.80	25.90	26.98
		400	17.11	20.39	21.12	21.84	22.85

Table 5: Data for Silty Sand compiled from published work[7] and present work

Sand type	% Fines	e_{min}	e_{max}	ϕ_c	G_s	D_m
Ham river	0	0.92	0.59	33	-	0.22
Monterey Sand	0	0.57	0.86	37	-	-
Toyoura Sand	0	0.61	0.99	35.1	2.65	0.16
Ottawa Sand	0	0.48	0.78	29	-	-
Yamuna Sand	0	0.5	0.78	27	2.67	0.225
Yamuna Sand	5	0.46	0.76	25.1	2.668	0.224
Yamuna Sand	10	0.42	0.72	29.8	2.666	0.222
Yamuna Sand	15	0.38	0.68	24.5	2.664	0.215
Yamuna Sand	20	0.33	0.63	25.4	2.662	0.213
Yamuna Sand	25	0.31	0.62	30.7	2.66	0.208
Banding 1	0	0.54	0.82	32	-	0.18
Banding 5	0	0.55	0.87	30	-	0.11
Banding 6	0	0.52	0.82	28.6	-	0.16
Banding 9	0	0.53	0.8	26.8	-	0.14
Brenda	0	0.688	1.06	36	-	0.1
Chiba	3	0.839	1.271	34	-	0.17

Chiba	18	0.685	1.307	34	-	0.15
ChonanSilty	18	0.69	1.31	34	-	0.15
Dune	6	0.59	1.08	32	-	0.21
Erksak 330	0.7	0.527	0.753	31	-	0.33
Fort Peck	2	-	1.01	32	-	-
Fraser River	0	0.6	1	34.5	-	0.25
HostunRF	0	0.655	1	33.5	-	0.32
Kiyosu	0	0.745	1.206	30	-	0.31
Kogyuk 350	0	0.523	0.783	31	-	0.35
Kogyuk 350	2	0.47	0.829	31	-	0.35
Kogyuk 350	5	0.487	0.866	31	-	0.36
Kogyuk 350	10	0.465	0.927	31	-	0.34
Lagunillas	70	0.766	1.389	31	-	0.05
Leighton Buzzard	5	0.665	1.023	30	-	0.12
Likan	0	0.756	1.239	34.5	-	0.24
Lornex	0	0.68	1.08	35	-	0.3
Mailiao	5	0.739	1.279	-	-	0.25
Mailiao	10	0.739	1.279	-	-	0.22
Mailiao	15	0.44	1.031	-	-	0.21
Massey tunnel	3	0.71	1.102	39.5	-	0.25
Monterey	0	0.53	0.86	33	-	0.38
Monterey	16	0.49	0.71	33	-	1.3
Nerlerky	0	0.66	0.89	30	-	0.23
Nerlerky	2	0.62	0.94	30	-	0.23
Nevada fine	5	0.57	0.87	29	-	0.12
Sacramento	0	0.53	0.87	33.2	-	0.3
Sydney	0	0.565	0.855	31	-	0.3
Syncrude	12	0.55	0.93	30	-	0.17
Tar Island Dyke	5	-	1.005	-	-	-
Tia Juana Silty	12	0.62	1.099	30.5	-	0.16
Toyoura	0	0.597	0.977	31	-	0.17
Unimin 2010	0	0.646	1.027	33	-	0.87

Table 6: Dilatancy Parameters with reference to Relative Compaction for Silty Yamuna Sand [Present Work]

Silt (%)	D_{50} (mm)	Best Fit		Tread line with R_{af} = 40	Tread line with R_{af} = 30	Tread line with R_{af} = 25
		Q_{af}	R_{af}	Q_{af}	Q_{af}	Q_{af}
0	0.225	49.883	40.105	49.77	39.14	33.83
5	0.224	38.091	29.115	49.64	39.03	33.72
10	0.222	33.863	24.821	49.99	39.36	34.05
15	0.215	34.700	25.977	49.63	38.98	33.66
20	0.213	10.689	4.372	48.71	38.03	32.70
25	0.208	5.023	1.094	48.73	38.09	32.77

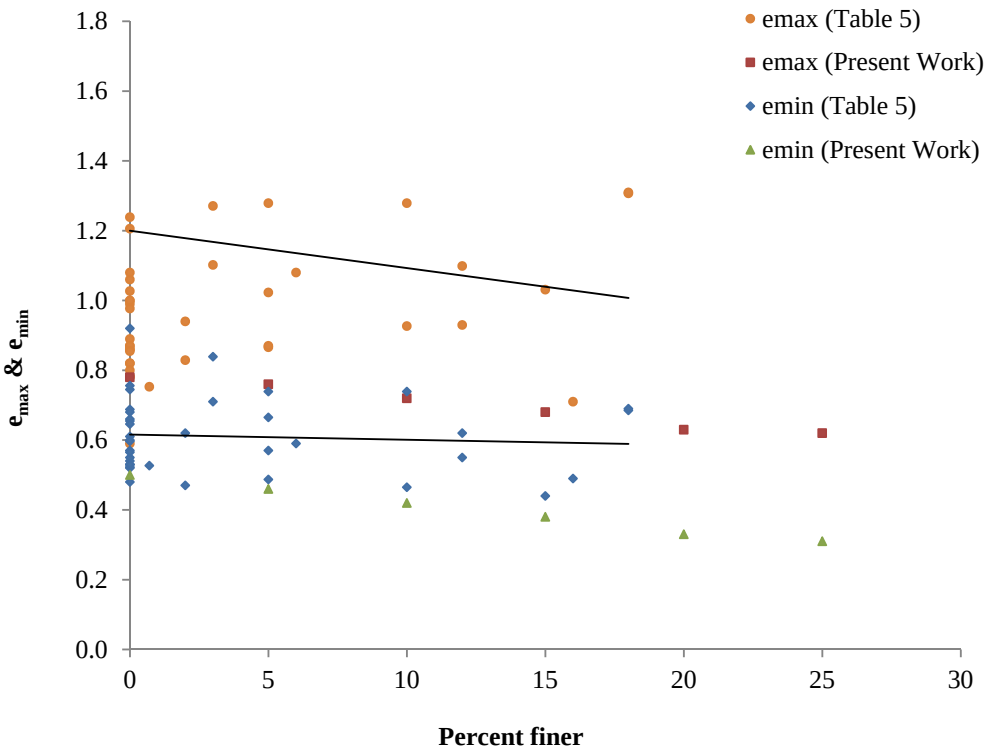

Figure 1 (a): e_{max} & e_{min} v/s. Percent Finer

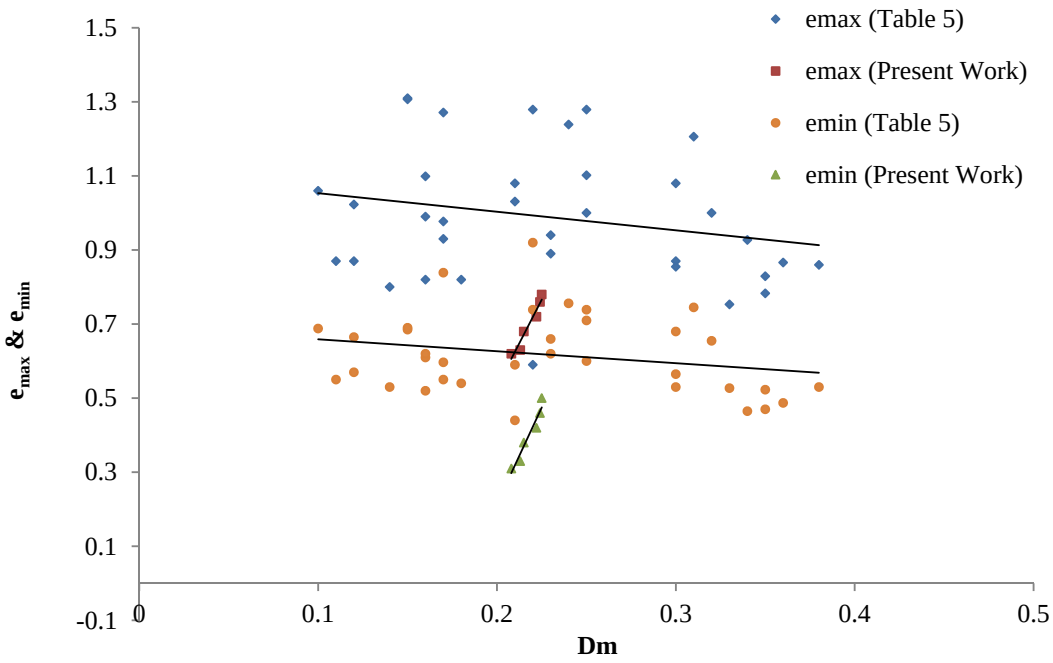

Figure 1 (b): e_{max} & e_{min} v/s. Mean Diameter of Particles

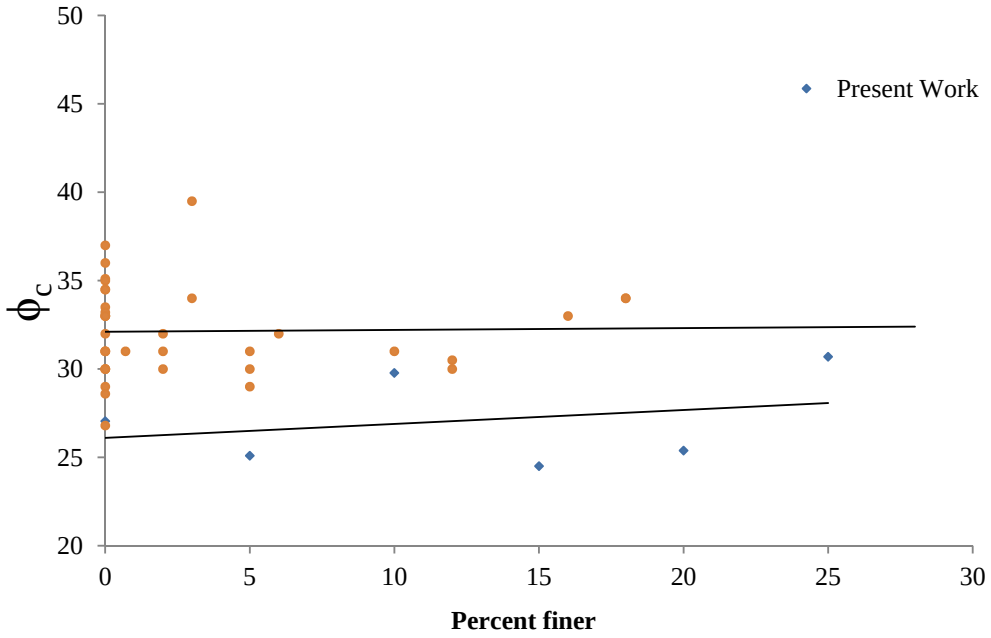

Figure 1 (c): Critical Friction Angle v/s. Percent Finer

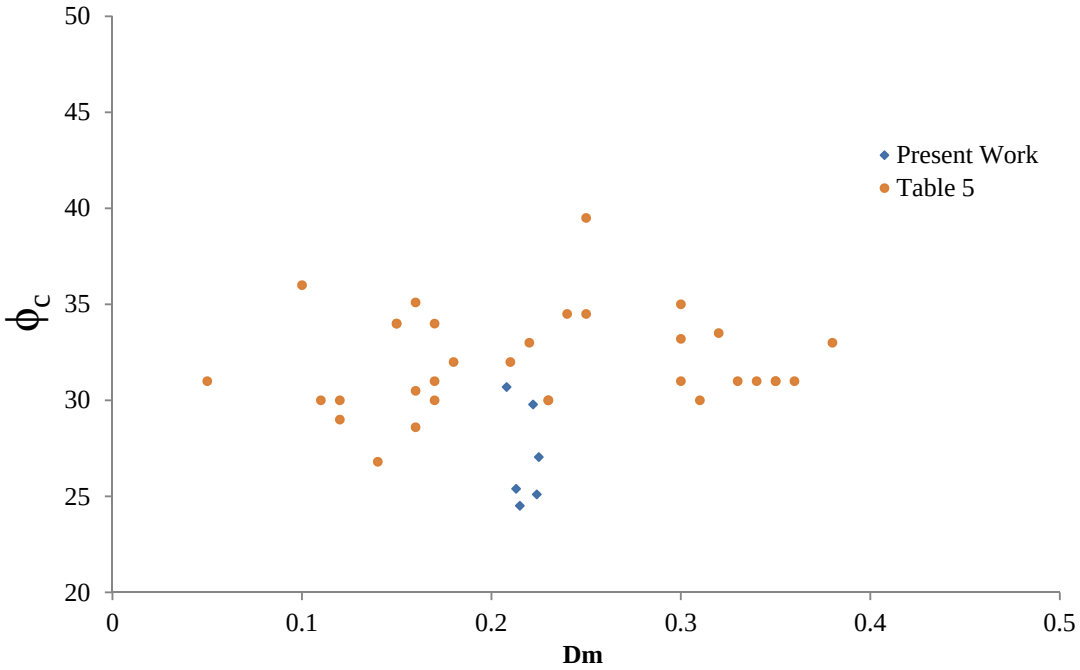

Figure 1 (d): Critical Friction Angle v/s. Mean Diameter of Particles

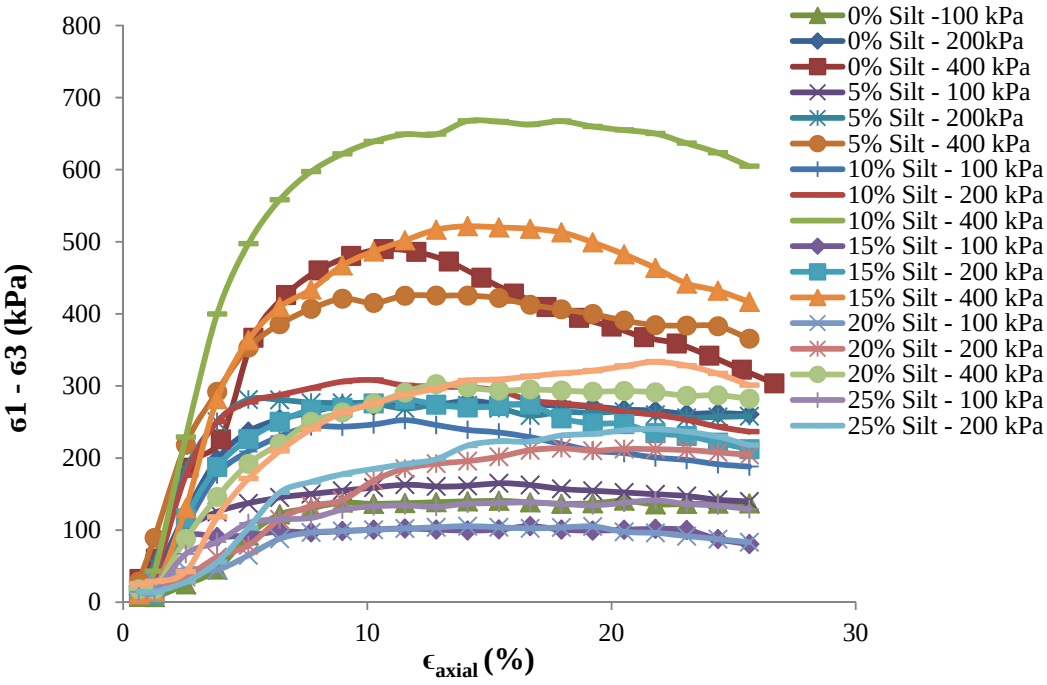

Figure 2 (a): Typical Deviator Stress v/s Axial Strain at Rc =

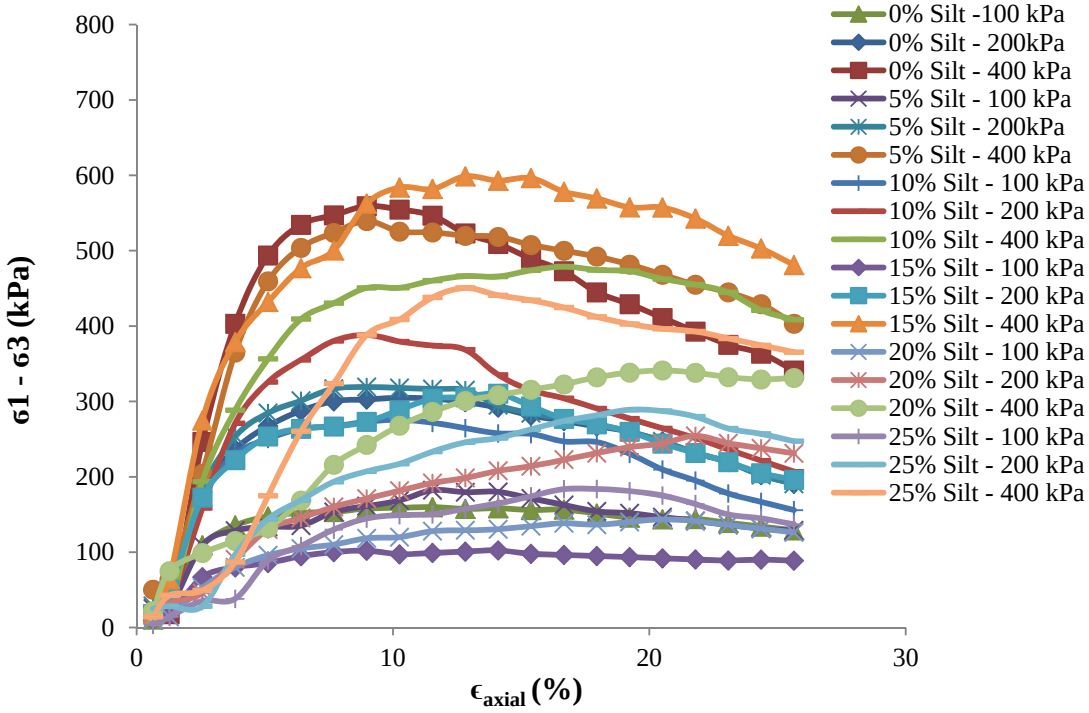

Figure 2 (b) Typical Deviator Stress v/s Axial Strain at R_c = 0.94

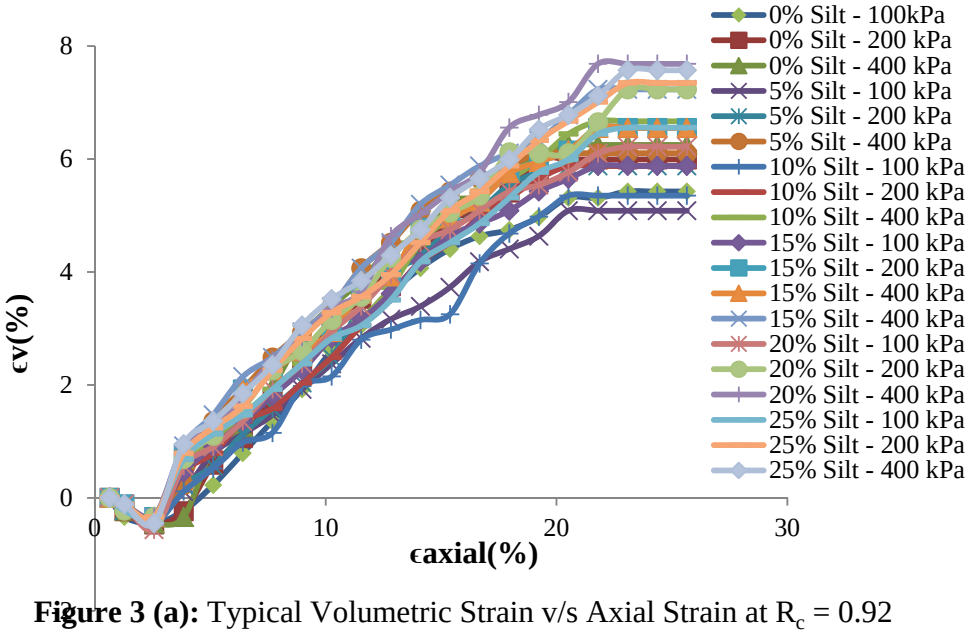

Figure 3 (a): Typical Volumetric Strain v/s Axial Strain at R_c = 0.92

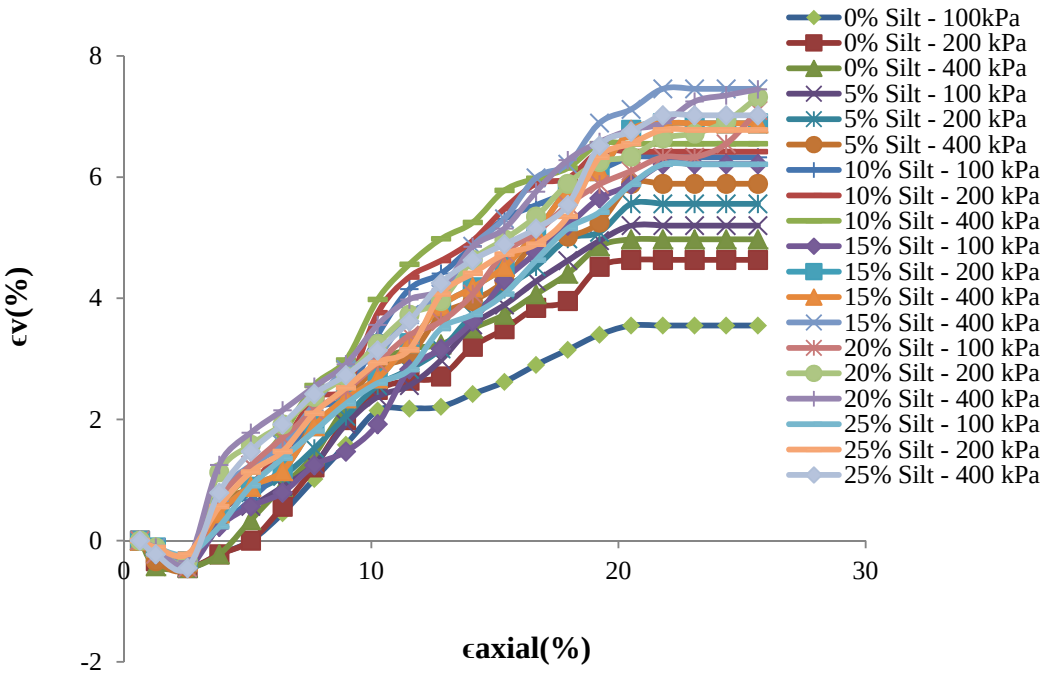

Figure 3 (c): Typical Volumetric Strain v/s Axial Strain at $R_c = 0.94$

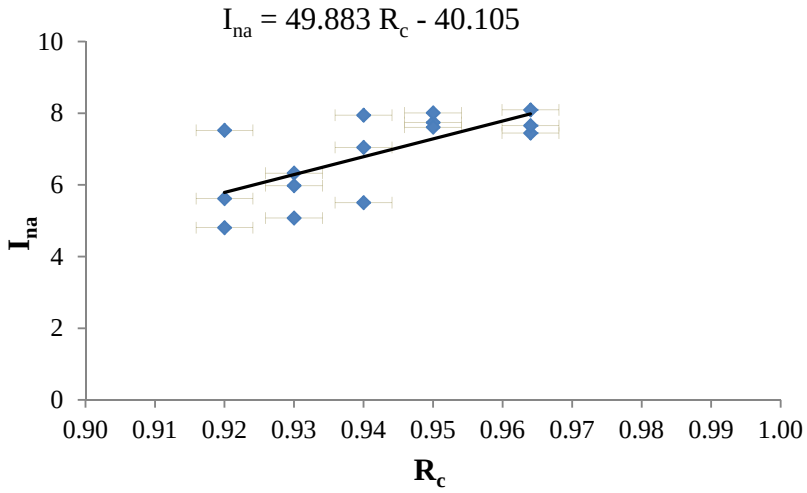

Figure 4 (a): I_{na} v/s R_c for clean sand ($Dm^{0.225}$)

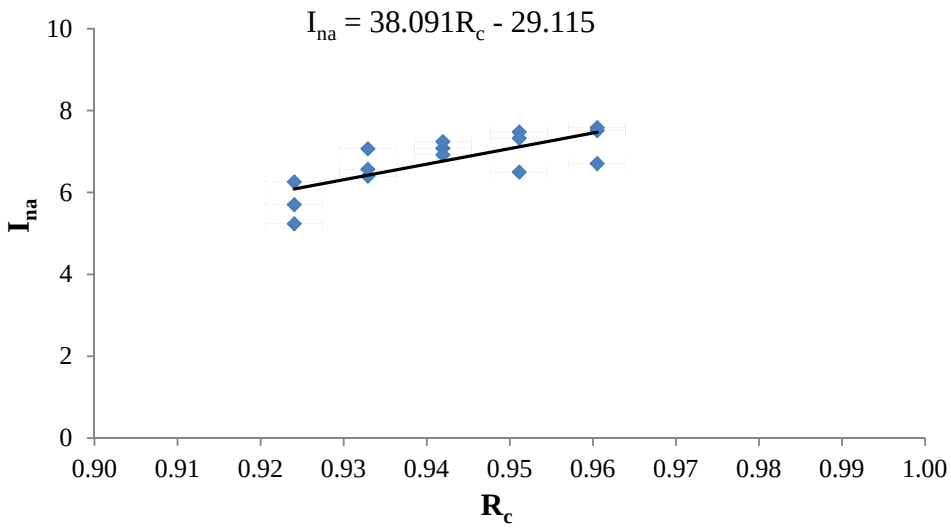

Figure 4 (b): I_{na} v/s R_c for clean sand + 5% fines ($Dm^{0.224}$)

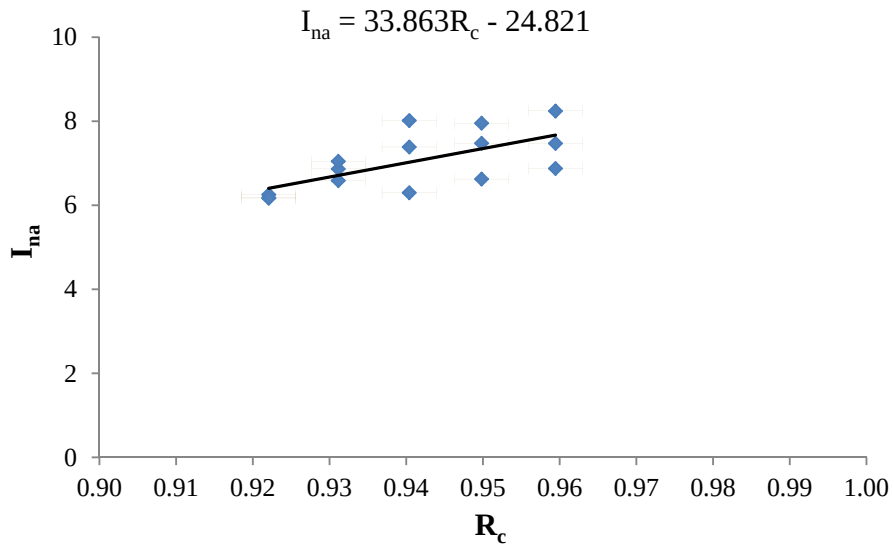

Figure 4 (c): I_{na} v/s R_c for clean sand + 10% fines ($Dm^{0.222}$)

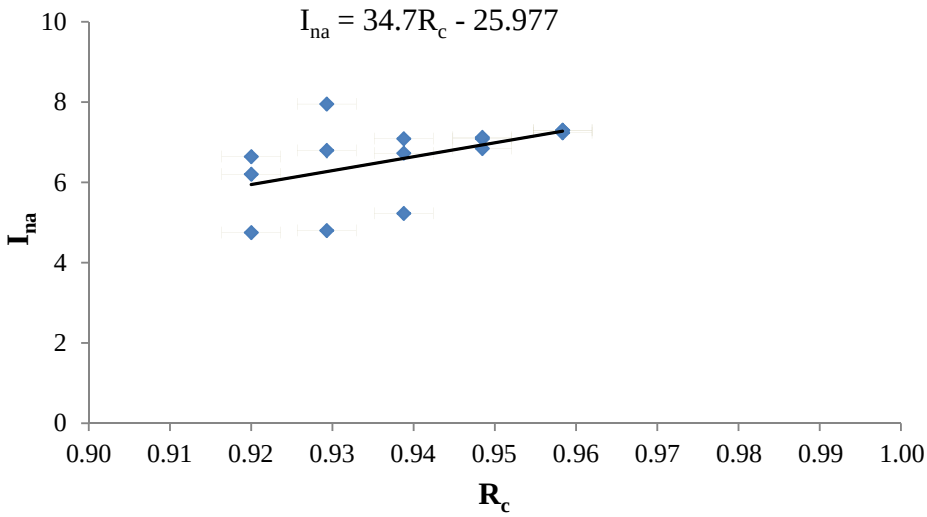

Figure 4 (d): I_{na} v/s R_c for clean sand + 15% fines ($Dm^{0.215}$)

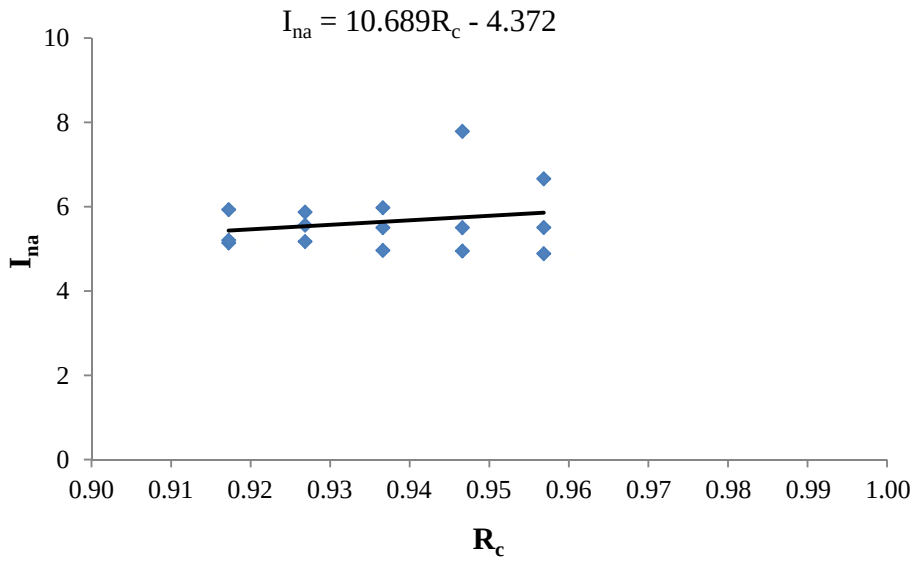

Figure 4 (e): I_{na} v/s R_c for clean sand + 20% fines ($Dm^{0.213}$)

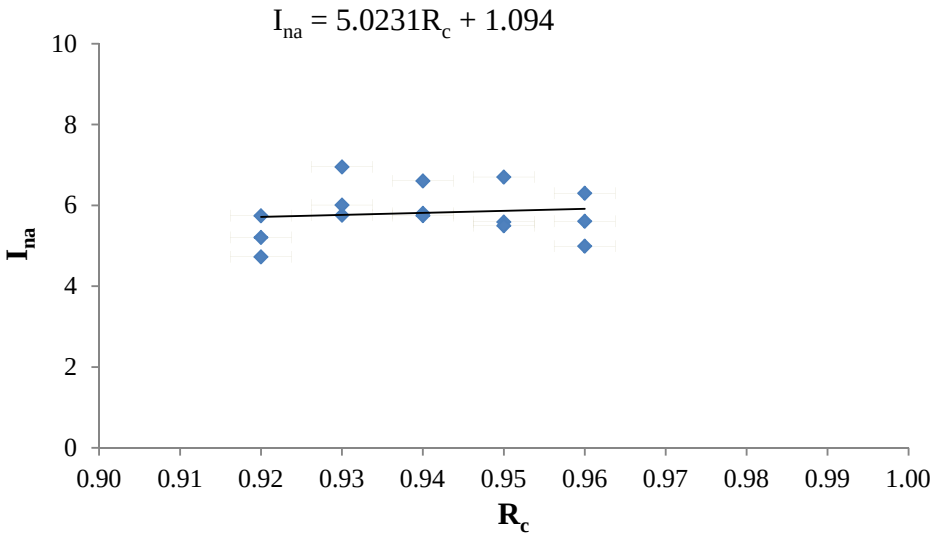

Figure 4 (f): I_{na} v/s R_c for clean sand + 25% fines ($Dm^{0.208}$)

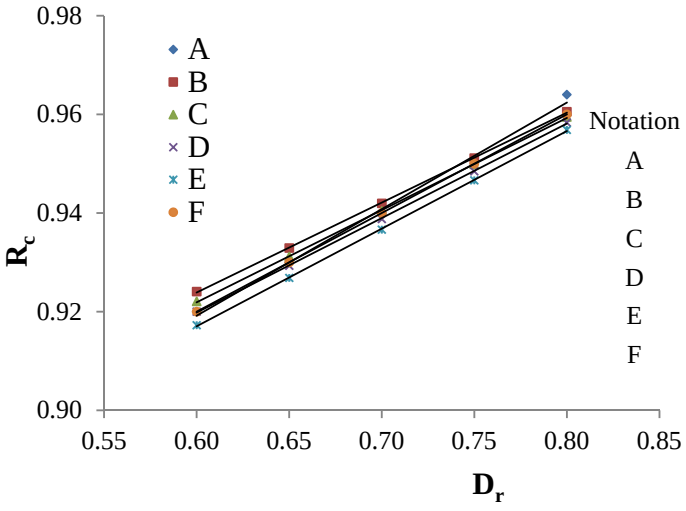

Notation	Description	m	n
A	clean sand	0.216	0.789
B	clean sand + 5% fines	0.182	0.814
C	clean sand + 10% fines	0.186	0.809
D	clean sand + 15% fines	0.191	0.804
E	clean sand + 20% fines	0.198	0.798
F	clean sand + 25% fines	0.200	0.800

Figure 5: R_c v/s D_r

RESULTS AND DISCUSSION

The test schedule for the index properties and triaxial test for the clean sand and silty sand is described in Table (1). The liquid and plastic limit of the various samples considered in this study are given in Table (2).The grain size characteristics as presented in Table (3) indicate that the silty sands considered in this study may be classified as SM as per the standard soil classification system. The peak friction angle is shown in Table (4).The data for intrinsic parameters of the selected sands and silts along with that of present work is shown in Table (5). In the present

study for silty Yamuna sand we have calculated the values of dilatancy parameters for fines up to a range of 25% and relative compaction based on Eq. (7-10) [see Table (6)]. The variation of maximum and minimum void ratio with percent finer and mean diameter of silty sand is shown in Fig.1 (a, b). The critical angle of internal friction was also calculated and its variation with mean size and percent finer is drawn in Fig.1(c).The result shows that maximum and minimum void ratio decreases with increase in silt content and critical angle of internal friction increases with increase in percent silt. Typical Variation of deviatric stress with axial strain corresponding to relative compaction (among0.92 and 0.94) is shown in Fig.2 and corresponding variation of volumetric strain with axial strain is shown in Fig.3. On the basis of Fig.3 (a, b) the peak angle of internal friction was calculated for varied values of relative compaction and confining pressure. Variation of I_{naf} with Rc along with error analysis is shown in Fig.4.The values of Q_{af} and R_{af} are calculated from Fig.4.

CONCLUSIONS

As a result of present work, the dilatancy of silty sand based on relative compaction is evaluated. The values of shear strength parameters (Q_{af} and R_{af}) of silty sand calculated based on the concept of relative compaction is more appropriate as compared to that based on relative density due to the inherent limitation associated with the correct determination of relative density for silty soils. The values thus obtained for Q_{af} and R_{af} are comparable with that calculated by Bolton (Q_b and R_b). The outcome of present study indicates that the values of Q_{af} & R_{af} are sensitive to the mean sizes, relative compaction and extent of confinement. Such a sensitivity of the shear strength parameters Q_{af} & R_{af} significantly contributes to the evaluation of strength behaviour of silty sand obtained from the catchment of river Yamuna.

LIST OF SYMBOLS

The following symbols are used in this paper:

CS	Clean Sand
C_u	Coefficient of uniformity
SP	Poorly graded sand
C_c	Coefficient of curvature
S	Shear strength
б	Normal stress on the plane of shearing
$б_1$	Principal stress
$б_3$	Confining stress
Φ	Friction angle
$Φ_p$	Peak friction angle
$Φ_c$	Critical friction angle
Ψ	Dilatancy angle
G_s	Specific gravity
$б_d$	Deviator stress
$ϵ_{axial}$ $ϵ_v$	Axial and volumetric strain
e_{max} and e_{min}	Maximum andminimumvoid ratio
$γ_w$	Unit weight of water
$γ_{min}$ and $γ_{max}$	Minimum and maximumdry density
$(б_1 / б_3)_c$	Effective principal stress ratio at critical state
$(б_1 / б_3)_p$	Effective principal stress ratio at peak state

$(б`_1 / б`_3)$	Effective principal stress ratio or stress obliquity
$d\epsilon_v$	Volumetric strain increment
$d\epsilon_1$	Major principal strain increment
R_D	Relative density
$P`_p$	Mean effective stress at peak strength
P_A	Reference stress
$Q_b R_b, Q_{af} R_{af}$	Fitting parameters
R_c	Degree of compaction
D_{10}, D_{30},D_{60}	Diameter of particle corresponding to 10,30, 60% finer
D_m	Mean diameter of particles
$б`_{3p}$	Lateral confining pressure
$б`_{mp}$	Mean pressure = $(б_1 + 2\ б_3)/3$
I_R	Dilatancy index

REFERENCES

1. Ayadat, T, Hanna, A. (2007) Prediction of collapse behaviour in soil, Revue Europeans de Genie Civil, 11 (5), 603-619.
2. Been, K., Jefferies, M. G., and Hachey, J.(1991). “The critical state of sands.” *Geotechnique*, 41(3), 365–381.
3. Bolton, M. D. (1986). “The strength and dilatancy.” *Geotechnique*, 36(1), 55–78.
4. Bui, M. and Priest, J. (2007). ”Discussion of “Particle Shape Effects on Packing Density, Stiffness, and Strength: Natural and Crushed Sands” by Gye-Chun Cho, Jake Dodds, and J. Carlos Santamarina.” J. Geo-tech. Geo-environ. Eng., 133(11), 1473–1474.
5. Chakraborty T. and Salgado R. (2010). “Dilatancy and Shear strength of sand at low Confining Pressure”, Journal of Geotechnical and Geo-Environmental Engineering, ASCE, 136(3), 527-534.
6. Chen, Y. C., and Liao, T. S. (1999). “Studies of the state parameter and liquefaction resistance of sands.” *Earthquake Geotechnical Engineering: Proc., 2nd Int. Conf.*, Lisbon, Portugal, [P. S. Seco e Pinto, ed.,].
7. ChoG, Dodds J, and SantamarinaJ., (2006) “Particle Shape Effects on Packing Density, Stiffness, and Strength: Natural and Crushed Sands”, Journal of Geotechnical and Geo-environmental Engineering, ASCE, 132, (5), 591-602
8. Chu, J., and Lo, S. C. R. (1993). “On the measurement of critical state parameters of dense granular soils.” *Geo-tech. Test. J.*, 16(1), 27–35.
9. Diego C.F. Lo Presti, Pedroni S. and Crippa V. (1992). ‘‘Maximum dry density of cohesion less soil by pluviation and by ASTM D 4253-83: A comparative study.’’ Geotech. Testing J., 15(2), 180–189.
10. Gupta R. and Trivedi A. (2009). “Effects of non-plastic fines on the behaviour of loose sand an experimental study”, *Electronic Journal of Geotechnical Engineering*, 14, (B), 1-14.

11. Gupta, R., and Trivedi, A. (2009). "Bearing Capacity and Settlement of Footing Resting on Confined Loose Silty Sands." *Electronic Journal of Geotechnical Engineering*, 14, (B).

12. IS: 2720 (Part3/Sec2)-1980 Methods of tests for soils: Part 3 Determination of specific gravity, Section 2 Fine, medium and coarse grained soils.

13. Konrad, J. M. (1990). "Minimum undrained strength versus steady-state strength of sands." *J. Geotech. Eng.*, 116(6), 948–963.

14. Lee, C. J. (1995). "Static shear and liquefaction potential of sand." *Proc., 3rd Int. Conf. on Recent Advances in Geotechnical Earthquake Engineering and Soil Dynamics*, St. Louis, Vol. 1, 115–118.

15. Ojha S., Goyal P., Trivedi A., (2012) "Non linearbehavior of silty sand from catchment area of Yamuna river" Proceeding of IGC conference Dec 13-15,2012 Delhi, paper no. B211.

16. Salgado R., Bandini P. and Karim A. (2000). "Shear Strength and Stiffness of Silty Sand", Journal of Geotechnical and Geo-environmental Engineering, ASCE,126(5), 451–462.

17. Simoni, A., and Houlsby, G., (2006). "The direct shear strength and dilatancy of sand–gravel mixtures." *Geotechnical and Geological Engineering*, 24, 523–549.

18. SladenJ.A. (1989) problem with interpretation of sand state from cone penetration test, Geotechnique *39*, 323–332.

19. Trivedi A. (2010). "Strength and dilatancy of jointed rocks with granular fill", ActaGeotechnica, 5(1), 15-31.

20. Trivedi, A., and Sud, V. K. (2007). "Settlement of compacted ash fills." *Geotechnical and Geological Engineering*, 25(2), 163–176.

21. Usmani, A., Ramana, G., and Sharma, K. (2012) Stress-Strain-Volume Change Modelling of Delhi Silt in Triaxial Compression and Extension, International Journal of Geo-mechanics, , 12 (3), 323-326.

22. Vesic, A.S.(1973) "Analysis of loads of shallow foundations". J. Soil Mechanics Found.Div., ASCE, Vol.99:No.SM-1, 45-69.

23. Zhang, H., and Garga, V. K. (1997). "Quasi-steady state: A real behaviour" *Can. Geotech. J.*, 34, 749–761.

American Journal of Electrical Power and Energy Systems
2012; 1(1) : 1-8
Published online December 30, 2012 (http://www.sciencepublishinggroup.com/j/epes)
doi: 10.11648/j.epes.20120101.11

SPV based water pumping system for an academic institution

Majid Jamil[1], Ahmed Sharique Anees[1], M. Rizwan[2,*]

[1]Department of Electrical Engineering, Jamia Millia Islamia, New Delhi, India
[2]Department of Electrical Engineering, Delhi Technological University, Delhi, India

Email address:
rizwaniit@yahoo.co.in (M. Rizwan)

To cite this article:
Majid Jamil, Ahmed Sharique Anees, M. Rizwan. SPV Based Water Pumping System for an Academic Institution, *American Journal of Electrical Power and Energy Systems.* Vol. 1, No. 1, 2012, pp. 1-8. doi: 10.11648/j.epes.20120101.11

Abstract: This paper presents the water pumping system based on solar photovoltaic (SPV) to cater the need of water in an academic institution for various applications like irrigation, drinking, washing etc. In this paper a case study of Faculty of Engineering and Technology (FET), Jamia Millia Islamia, New Delhi, India is carried out. Presently water is pumped with the help of grid power supply resulting huge energy consumption. As solar water pumping has several advantages over conventional water pumping systems, apart from economical advantages, therefore an attempt has been made to develop SPV based water pumping system to meet daily water needs of the institute. A techno-economic analysis of SPV based water pumping system and comparison of proposed system with the conventional one is also discussed in this work.

Keywords: SPV System; Water Pumping System; Decentralized Application; Environmental Benefit

1. Introduction

Photovoltaic pumping systems provide a welcome alternative to grid power supply based water pumping systems or hand pumps. They provide the most water precisely when it is needed the most that is when the sun shines the brightest. The generation of solar electricity coincides with the normal peak demand during daylight hours in most places, thus justifying peak energy costs, brings total energy bills down, and obviates the need to build as much additional generation and transmission capacity as would be the case without PV Solar pumps. Advantages of using PV-powered pumps include low maintenance, ease of installation, reliability and scalability. A SPV water pumping system consist of a DC / AC surface mounted / submersible / floating motor pump set, electronics if any, interconnect cables, a on-off switch and a PV array mounted on a suitable structure with a provision of tracking. A SPV water pumping system is expected to deliver a minimum of 65000 liters per day for a 900 watts panel and 135000 liters per day for an 1800 watts panel from a suction head of 7 meters and total head of 10 meters on a clear sunny day. In case of deep well submersible pumps, the water shall be a minimum of 45000 liters from 1200 Wp. The discharge from the pump would vary with the intensity of the sunrays from morning till evening. India being a tropical country receives adequate solar radiation for 300 days, amounting to 3,000 hours of sunshine equivalent to over 5,000 trillion kWh. Almost all the regions in India receive 4-7 kWh of solar daily radiation per sq meters depending upon the location. In India there is an acute shortage of power. The per capita annual energy consumption of the country is hardly 779 kWh whereas world average is 2600 kWh. During last decade, a lot of industrialization took place in the country but growth suffered due to lack of power [1]-[2]. To bridging the gap between demand and supply, use of renewable resources is becoming important keeping in mind the environmental benefits. Major types of renewable energy sources include solar, wind, hydro and biomass, all of which have huge potential in India to meet future energy challenges. Solar power is one of the most promising and more predictable than other renewable sources and less vulnerable to changes in seasonal weather. Generation of power from other renewable sources is limited to sites where these resources exist in sufficient quantities whereas solar energy can produce power at the point of demand in both rural and urban areas [3].

A review of solar water pumping systems is presented for Palestine [4]. Feasibility analysis is carried out for solar water pumping systems. In this paper the water pumping system is proposed at low cost. In addition, the information about the conventional pumps is also presented.

PV water pumping systems for energy conservation is also presented [5]. Two pumps of 7.5 kW total 15 kW were

replaced by solar PV pump to lift the water. Operating the PV pump for only 10 hours in a day yielded a net saving of 3000 units which is 7.5% of the total consumption of 40000 units in an industry. However, the solar PV pumps are expensive but the cost would be reduced in near future.

An experimental agricultural structure has been implemented to overcome factors affecting the valorization of new technologies for irrigation in dry season such as the lack of modern technological knowledge by farmers, the lack of affordable means by farmers, the lack of interface between the researchers and the users of research results [6]. Convincing results revealed that the farmers could afford to invest in the photovoltaic water pumping projects for irrigation, the incomes being better than the ones in raining season.

Several types of pumps and motors are available in the market based on the PV pumping [7]-[8]. The commonly employed pumps are the single-stage centrifugal and helical rotor type. The most commonly utilized motor for PV pumping systems is the permanent magnet (PM) brush less direct current (BLDC) motor. However, induction motors and brushless dc motors are generally used in bore-hole and deep well pumping applications because of less maintenance. Since BLDC consumes less power in comparison with induction motor therefore it is preferred in SPV based water pumping system [9]. In addition there is no requirement of inverter assembly in BLDC based SPV system. In this paper, a techno-economic analysis of SPV based water pumping system is proposed and compared with the existing system.

The proposed study is carried for an academic institute at faculty of engineering and technology, Jamia Millia Islamia, New Delhi, India, having more than 5000 students and employs at the campus daily. Heavy payments towards electricity bills and shortage of power resulting power cuts for many hours in a day particularly during peak seasons encouraged to provide an alternative option to replace the grid operated pumping system with the SPV based pumping system to ensure reliable, economical and environment friendly supply. The paper is organized as follows: Section 2 presents the brief description of existing water pumping systems. A design analysis of the proposed system based on AC drive and DC drive is discussed in Section 3 and Section 4 respectively. Techno-economic analysis of the proposed system is discussed in Section 5. Results and discussions are presented in Section 6. A conclusions followed by the references is presented in Section 7.

2. Description of Existing AC Drive Based Grid Connected Water Pumping System

The existing water pumping system of the proposed site supply water to many neighbouring buildings of the campus such as faculty of engineering building, dean's office, canteen, faculty of architecture, department of management, faculty of third world studies and many parks located in the premises. The total water requirement of proposed site is around 1.1 million litres per day. Out of which 50,000 litters are used in wash rooms, 10000 litres for drinking and 50000 litres for irrigation. To fulfil this requirement, the existing system comprises one water pumping station which consists of various electric water pumps like submersible pump, induction motor type pump. These pumps lift the water from the ground to the overhead tanks placed on the top of the buildings.

As mentioned above, the daily water requirements for irrigation at FET premises is 50,000 litters. To meet this demand, two booster pumps of 10 HP each are installed. These motor-pump are operating for 5 hours daily. Water is supplied from the round tank which is situated nearby the pumping station to the lawns of the campus at a horizontal distance of around 400 meters from pumping station. Another important requirement of water is in washrooms that is around 50,000 litters per day. Since availability of water in washrooms is essential all twenty four hours, therefore facility of water storage is required. One circular storage tank of the capacity 40000 liters placed on the ground level is provided to store water and it is pumped through one 10 HP submersible pump, extracting water from 100 feet below the ground level. Further the water is also pumped to 8 neighboring buildings of the campus by another 10 HP pump. Maximum horizontal and vertical distances from the water tank placed on the ground to the overhead tanks placed on the roof top of different buildings are 300 meters and 25 meters respectively.

To meet drinking water needs of around 10000 litres per day a water tank of one lack litre capacity is provided at ground level. Further, the water is pumped to overhead tanks by two induction motors of 5 HP each. These motors are operated for one hour per day for the aforesaid application.

The details of different motors operation used in the existing system are presented in Table 1 and the description of storage tanks are presented in Table 2.

Table 1. *Ratings of various pumps and their duration of operation.*

S. No.	Items	Ratings in HP	Total time of Operation	Duration of Operation	Purpose
1	Submersible Pump 1	7.5	7 hr.	9:00 AM to 1:00 PM 3:00 PM to 6:00 PM	Lifts the water from underground to circular tank
2	Submersible Pump 2	10	5 hr.	9:00 AM to 12:00 PM 3:00 PM to 5:00 PM	Supply water from circular tank to different buildings

3	Booster Pump 1	10	3 hr.	9:00 AM to 12:00 PM	Irrigation
4	Booster Pump 2	10	2 hr.	3:00 PM to 5:00 PM	Irrigation
5	Pump 1	5	1 hr.	8:00 AM to 9:00 AM	Supply the MCD water from rectangular tank to different buildings
6	Pump 2	5	1 hr.	8:00 AM to 9:00 AM	Supply the MCD water from rectangular tank to different buildings

Table 2. *Description of various storage tanks.*

S.No.	Description	Size (L*B*D) in ft	Tank size (ft^3)	Tank capacity in Litres
1.	MCD rectangular Tank	22.5*16.5*10	3712.5	105000
2.	Ground water circular tank	12.7 Diameter, Depth 12	1519.3518	43000
3.	Over head tank on each building			100000

The block diagram of existing pumping system is shown in Figure 1.

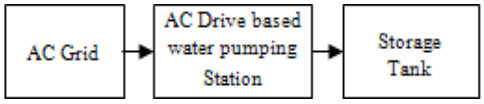

Figure 1. *AC Driven based grid connected water pumping system.*

3. SPV Based Water Pumping System

In the proposed study two options are suggested based on solar power generation. One is AC driven motor pump set feed from SPV plant and the other is DC drive based SPV array connected water pumping system. Here technical and economical feasibility of both options are discussed and compared with the existing system.

3.1. AC Driven Based SPV Plant Connected Water Pumping System

Here existing motor pump set is used to pump the water. Only grid power is replaced by solar power. The block diagram of proposed AC driven based SPV water pumping system is shown in Figure 2.

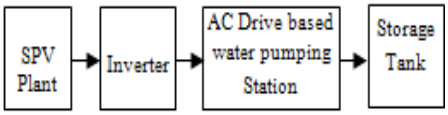

Figure 2. *AC driven based SPV array connected water pumping system.*

3.2. DC Drive based SPV Array Connected Water Pumping System

It is the other option in which existing ac motor-pump sets are replaced by dc motor-pump sets. Here dc generated power from solar system is fed directly to dc motor-pump sets eliminating need of converting dc into ac that minimizing the cost. Three different water pump sets are to be installed for different applications to meet the water need. The description of proposed system is shown in Figure 3.

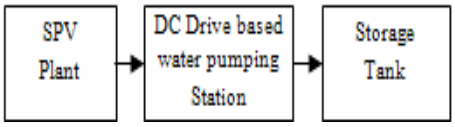

Figure 3. *DC drive based SPV array connected water pumping system.*

In this scheme, the centrifugal water pump sets are connected with d.c drive based motor. The power generated by PV array is feed to dc motors as shown in Figure 4 [7]. For each pump set separate solar array is provided. A separate boring is also required at nearby place for this system. In SPV based water pumping system a 2 pole brush less synchronous DC motor for driving the centrifugal pump is used. A layout of the proposed system is shown in Figure 4.

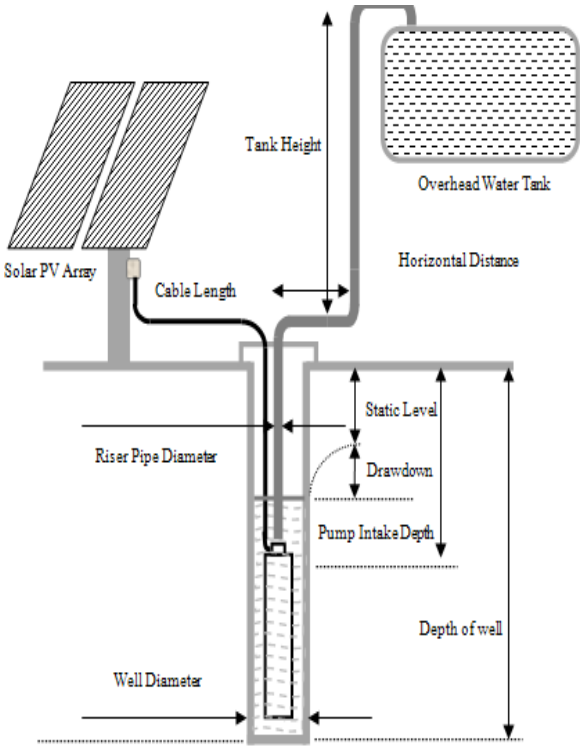

Figure 4. *Layout of the proposed system.*

4. Techno-Economic Analysis

A techno economical analysis of existing and proposed methods is carried out to identify the better and viable option. The better option means the system be reliable, efficient and economical. Further the techno economic analysis is done keeping in view of electricity tariff appreciation in the existing water pumping system and government policies in the proposed SPV based water pumping system.

4.1. Existing AC Drive based Grid Connected Water Pumping System

As the existing system does not require any new installation, the running and maintenance cost only is involved. The running and maintenance cost includes electricity bills and maintenance of the system. For calculating the electricity charges, the study of load cycle curve or energy consumption per day is required. Therefore the load curve of the existing water pumping system is drawn and shown in Figure 5. The energy consumption of different pump sets which are used in the existing grid connected water pumping system is presented in Table 3.

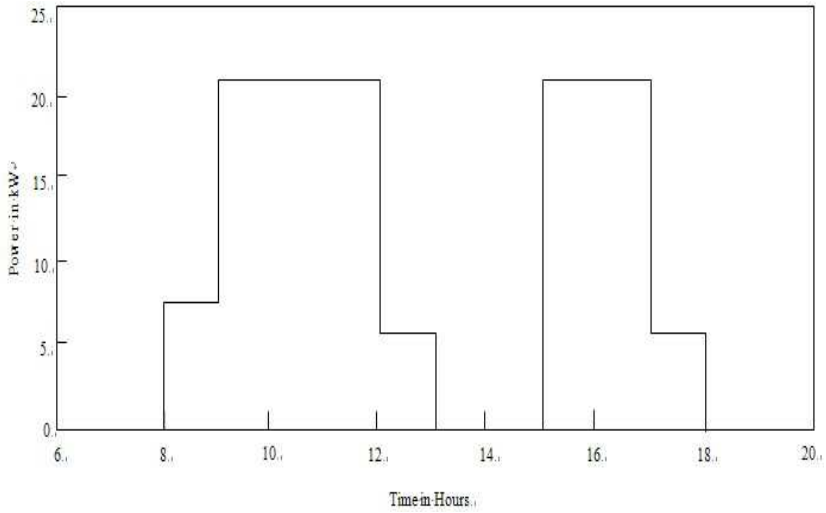

Figure 5. *Daily load cycle for the existing water pumping station.*

Table 3. *Annual energy consumption in the existing system.*

S. No.	Items	Ratings in (kW)	Total time of Operation (Hours)	Energy Consumed per Day (kWh)	Energy Consumed per Year (kWh)
1	Submersible Pump1	5.595	7	39.165	14295.225
2	Submersible Pump2	7.46	5	37.3	13614.5
3	Booster Pump1	7.46	3	22.38	8168.7
4	Booster Pump2	7.46	2	14.92	5445.8
5	Pump1	3.73	1	3.73	1361.45
6	Pump2	3.73	1	3.73	1361.45
7	Total Electrical Energy Consumption in kWh			121.225	44247.125

For the existing system, sanctioned load of 25 kW is used for water pumping purposes. This water pumping system is operating at 0.8 power factor lagging. The cost associated with the existing grid connected water pumping system is shown in Table 4. The cost of electricity is calculated by two different tariff plans. First one is the old tariff plan which was applicable till June 30, 2012 and the second tariff plan that is the recently revised plan applicable from July 1, 2012

[10]. This exercise is done just to show how frequently the cost of electricity is varying even it increased during the proposed duration of study. It can be easily seen from the Table 4 that the cost of electricity gets increased by 1.5 times of the older tariff plan during this period.

Table 4. *Cost of Energy for the existing grid connected water pumping system.*

S. No.	Existing Systems 25 kW @ 0.8 p.f.	Old Tariff Plan		New Tariff Plan	
		Tariff Rate @ Rs.	Amount in Rs.	Tariff Rate @ Rs.	Amount in Rs.
1.	Fixed Charges	50/kW/ Month	15000	115kVA/Month	34500
2.	Variable Energy Charges	4.92/kVAh	272120	7.25/kVAh	400990
3.	Electricity Tax	5%	13600	5%	20050
4.	Surcharge on Fuel	8%	21770	8%	32080
5.	Total Annual Electricity Bill		322490/-		487620/-

4.2. AC Drive based SPV Plant Connected Water Pumping System

In AC drive based system power is fed from SPV plant. The installation cost of this system include only SPV system however same motor pump sets as used with the grid are used. The capacity of SPV system is determined with the help of load duration curve as shown in Figure 5. From Figure 5, it is observed that the peak power requirement for water pumping system is around 21 kW. To meet peak power requirement, an SPV plant of around 35 kWp would be required considering the 60% capacity factor. Such system would be quite costly and requires huge space for installation. Therefore, the load cycle is adjusted by changing the operating timings of the pumps. The peak load is distributed during the different hours of the day time when solar power is available. The energy requirement for water pumping is 121 kWh per day. To meet this energy requirement of 121 kWh, 15.15 kW plant would be sufficient considering 8 hours sunshine. The modules available in the market are calibrated at an irradiance of 1000 W/m^2 and 25 ^{0}C [11-12]. However the solar insolation received on earth is varying and not available more than 900 W/m^2 with very low irradiance intensity in early morning and evening hours. The solar insolation varies almost in a sinusoidal way. Therefore the power generated from PV modules is less than the rated value. To fulfil the peak power requirement of 15.15 kW, it is required to install a plant of 26.5 kWp. Hence by adjusting load cycle the plant capacity of the SPV based plant is reduced from 35kWp to 26.5 kWp that minimizing the cost. In India, the solar irradiance available is almost same throughout the year during clear sky. However, the water required for irrigation is also reduced in winter therefore, the same water pumping system is sufficient to fulfill the requirements.

Table 5. *Cost for the 26.5 kW SPV based water pumping system.*

S.No.	Major Component of the SPV plant	Unit Rate in Rupees	Total Cost in Rupees (approximate Cost)
1	Solar PV Array of 26.5 kW	100 per watt	27,00,000
2	Inverter of 15.153 kW	6000 per kW	1,00,000
3	Installation and accessories charge		5,00,000
4.	Total Cost of the SPV plant		33,00,000

4.3. DC Drive based SPV Array Connected Water Pumping System

In DC drive based system the power generated from the SPV array is directly used to operate the DC motor pump set. In this scheme modern brushless dc motor based submersible pumps are used which are low power consuming and have higher efficiency as compared to the conventional motor pump sets.

For the same water requirement for different purposes such as irrigation, drinking and utilities, three different DC motor pumps are used. These pumps are to be installed nearby the existing pumping stations. Therefore the additional cost of boring is required. The types of solar water pumps selected to fulfill the water requirements for different applications are presented in appendix I. The cost involved in DC drive based system is presented in Table 6.

Table 6. *Total Cost of the DC drive based solar water pumping system.*

S. No.	Items	Cost in Rupees
1.	Drinking Water pump set	1,11,000
2.	Irrigation Water pump set	2,17,000
3.	Utility/Wash Room pump set	3,02,000
4.	Installation charge and others	3,70,000
	Total cost of Installation	10,00,000

In this paper three different options of water pumping system for the given site are discussed. The proposed system is compared with the existing system. The economical benefits of the proposed study are compared with the existing one. Recently in Delhi state tariff is revised by the government and during last three years it has been revised many times and it is increased more than double during past two years. This effect is also considered in the proposed study. According to old tariff plan, the cost of the proposed ac driven based SPV system was recovering in 12 years and the cost associated with dc drive based SPV system would be recovering in less than 4 years. As per the new tariff plan the same will be recovering in 8 years and 2.5 years respectively. Here the cost of electrical energy receiving from grid was assumed constant over the study period of the proposed system, but in actual practice it increased significantly during study period too. Since the cost of energy is a dependent parameter of the international market, therefore the payback period of the initial investment on the proposed system will be reducing further [10].

Now the proposed system based on AC drive has higher initial investment than the proposed DC drive. But there are certain technical drawbacks in the proposed AC drive based system like lower efficiency because of inverter which has their own conversion loss and at the time of starting it draws dangerously high inrush current from the SPV plant. Further, it is important to provide certain back up scheme during the cloudy weather condition, as the output of the proposed system depends on the solar irradiance level. To meet out the water requirement during the cloudy weather, it is either to increase the water storage capacity or some alternate electrical supply arrangements. So large power is required for proposed AC drive based system but for proposed DC drive based system it is required just to install a rectifier unit which convert the grid power from AC to DC and this DC power will be directly fed to the proposed DC system. DC drive based system requires only around 4 kW powers which is quite less as compared to the existing AC drive based system as shown in appendix I.

Hence it is concluded that the proposed system based on DC drive is more efficient and cost effective. As the payback period is much less than the total life of the proposed system, so it is highly recommended to install the proposed system based on DC drive. A comparative study of the proposed system with the existing system is presented in Table 7.

Table 7. *Comparative study of different water pumping systems.*

S. No.	Different methods	Equipment and Installation Cost	Running and maintenance cost for 1 year	Running and maintenance cost for 20 years	Total Investment For 20 years
1.	Existing AC drive based grid connected water pumping system by Old Tariff plan	Already installed	3,22,000	64,40,000	64,40,000
	Existing AC drive based grid connected water pumping system by New Tariff plan	Already installed	4,87,000	97,40,000	97,40,000
2.	AC drivebased SPV plant connected water pumping system	33,00,000	25,000	5,00,000	38,00,000
3.	DC drive based SPV array connected water pumping system	10,00,000	10,000	2,00,000	12,00,000

6. Conclusions

In this paper a solar water pumping system is proposed to meet the water requirements of an academic institution. A case study at faculty of engineering and technology, Jamia Millia Islamia, New Delhi is carried out. Techno-economic analysis of SPV based water pumping system is presented and compared with the existing system. Further a comparative study is also carried out between the existing motor pump sets, if fed by SPV systems in place of grid supply and if the complete existing water pumping system is replaced by the proposed one. The installation cost of the proposed

system is around Rs 10 lac that would be recovered in less than 4 years. If the life of the proposed system is considered 20 years, then it would supply power at free of cost for 16 years that is huge savings, where institute is paying around Rs 3 lac per year as electricity bill for this purpose which is a substantial amount for an academic institute in a developing country like India. Apart from economical benefits, the proposed system is environment friendly. Likewise, such a system can be utilized to reduce the grid dependency of the existing systems and to make them more cost effective. This system can also be considered as a potential alternative in areas having deficient power or in areas inaccessible to the main supply grid.

Appendix I

Description of proposed Systems:

Washroom water.

S. No.	Description	Unit rate	Qty	Amount
1	Lorentz Submersible Pump Systems (complete system pump end, motor and controller). Lorentz (PS1800 CS J 5-12)-for wash water Lifting from Bore	95,600.00	1	95600.00
2	Dry run switch for above	3,200.00	1	3200
3	Cable jointing Kits (2 nos)	750.00	2	1500.00
4	Submersible cable.3core x 4mm2 copper to IS	120.00	42	5040.00
5	Cable for dry run switch- 2 core 0.5 sq.mm	29.00	42	1218.00
6	Solar Modules--250Wp-72cells make Green Brilliance.IEC,UL approved.	22,000.00	8	176000.00
7	Module mounting structure-fixed tilt type for 2 Modules. Out of 50x5 mm Aluminum angles. Sshardware	4,980.00	2	9960.00
8	Pump suspension assembly-Polyester riopes, SS barrel nipple-clips, tie wraps, Dshackles etc for suspending pump from existing well head/cap-approx 46 metere below ground.	4,500.00	1	4500.00
9	DC MCB 250V 15A-In suitable MS powder coated enclosure.	2,580.00	1	2580.00
10	Array JB- for string interconnections.	1,890.00	1	1890.00
	Sub Total			**301488.00**

Drinking water.

s/n	Description	Unit rate	Qty	Amount
1	Lorentz Submersible Pump Systems (complete system pump end, motor and controller).Lorentz (PS200 HR07)-for drinking water Lifting from Bore	78,900.00	1	78900.00
2	Dry run switch for above	3,200.00	1	3200
3	Cable jointing Kits (2 nos)	750.00	2	1500.00
4	Submersible cable.3core x 4mm2 copper to IS	120.00	15	1800.00
5	Cable for dry run switch- 2 core 0.5 sq.mm	29.00	15	435.00
6	Solar Modules--210Wp-60 cells make Green Brilliance.IEC,UL approved.	18,900.00	1	18900.00
7	Module mounting structure-fixed tilt type for 2 Modules. Out of 50x5 mm Aluminum angles. Sshardware	2,780.00	1	2780.00
8	Pump suspension assembly-Polyester riopes, SS barrel nipple-clips, tie wraps, Dshackles etc for suspending pump from existing well head/cap-approx 46 metere below ground.	1,200.00	1	1200.00
9	DC MCB 250V 15A-In suitable MS powder coated enclosure.	2,580.00	1	2580.00
10	Array JB- for string interconnections.	1,890.00	0	0.00
	Sub Total			**111295.00**

Irrigation water.

s/n	Description	Unit rate	Qty	Amount
1	Lorentz Submersible Pump Systems (complete system pump end, motor and controller). Lorentz (PS1800 CSJ 5-8)-for wash water Lifting from Ground water Tank	95,600.00	1	95600.00
2	Dry run switch for above	3,200.00	1	3200
3	Cable jointing Kits (2 nos)	750.00	2	1500.00
4	Submersible cable.3core x 4mm2 copper to IS	120.00	30	3600.00
5	Cable for dry run switch- 2 core 0.5 sq.mm	29.00	30	870.00
6	Solar Modules--280Wp-72 cells make Green Brilliance.IEC,UL approved.	24,360.00	4	97440.00
7	Module mounting structure-fixed tilt type for 2 Modules. Out of 50x5 mm Aluminum angles. Sshardware	4,950.00	2	9900.00
8	Pump suspension assembly-Polyester riopes, SS barrel nipple-clips, tie wraps, Dshackles etc for suspending pump from existing well head/cap-approx 46 metere below ground.	2,500.00	1	2500.00
9	DC MCB 250V 15A-In suitable MS powder coated enclosure.	2,580.00	1	2580.00
10	Array JB- for string interconnections.	1,890.00	0	0.00
	Sub Total			**217190.00**

References

[1] Directorate of Economics & Statistics (DES), Department of agriculture and cooperation, Ministry of agriculture, Government of India.

[2] S. N. Kaplanis, New methodologies to estimate the hourly global solar radiation: comparison with existing models, Renewable Energy, vol. 31, pp. 781–790, 2006.

[3] M. Rizwan, Majid Jamil and D. P. Kothari, "Solar energy estimation using REST model for PV-ECS based distributed power generating system", Solar Energy Materials & Solar Cells, vol. 94, pp. 1324-1328, 2010.

[4] Tamer Khatib, " Design of photovoltaic water pumping systems at minimum cost for Palestine: A review", Journal of Applied Sciences, vol. 10, no. 22, pp. 2773-2784, 2010.

[5] V. A. Kulkarni1 and P. K. Katti, "Energy conservation in industries by PV solar pump as renewable energy source", International Journal of wind and Renewable Energy, vol. 1, Issue 1, pp. 44-47, 2011.

[6] M. Kamta and O. Bergossi, "Factors affecting the valorization of photovoltaic water pumping projects for irrigation in the Adamawa Province (Cameroon)", International Scientific Journal for Alternative Energy and Ecology, vol. 62, no. 6, pp. 49-52, 2008.

[7] T. S. Surendra and S. V. V. Subbaraman, "Solar PV water pumping comes of age in India", Twenty-Ninth IEEE Conference on Photovoltaic Specialists, pp. 1485–1488, 19-24, May 2002.

[8] R. E. Katan, V. G. Agelidis and C. V. Nayar, "Performance analysis of a solar water pumping system", International Conference on Power Electronics, Drives and Energy Systems for Industrial Growth, pp. 81 – 87, vol.1, 8-11 Jan 1996.

[9] http://www.lorentz.de/en/products/submersible_solar_pumps/ps1800.html.

[10] Delhi Electricity regulatory commission. http://www.derc.gov.in/ordersPetitions/orders/Tariff/Tariff%20Order/201213/Press%20Release_26.06.2012/BRPL.pdf.

[11] A. Mukherji, Photovoltaic Analysis and Design, PHI publication, New Delhi,2011.

[12] B. H. Khan, Non Conventional Energy Resources, 2nd edition, Tata McGraw-Hill pg no. 424.

Defence Science Journal, Vol. 63, No. 1, January 2013, pp. 63-68

Subpixel Target Enhancement in Hyperspectral Images

Manoj K. Arora* and K.C. Tiwari#

Indian Institute of Technology Roorkee, Roorkee–247 667, India
#Delhi Technological University, New Delhi–110 042, India
**E-mail: manojfce@iitr.ernet.in*

ABSTRACT

Hyperspectral images due to their higher spectral resolution are increasingly being used for various remote sensing applications including information extraction at subpixel level. Typically whenever an object gets spectrally resolved but not spatially, mixed pixels in the images result. Numerous man made and/or natural disparate targets may thus occur inside such mixed pixels giving rise to subpixel target detection problem. Various spectral unmixing models such as linear mixture modeling (LMM) are in vogue to recover components of a mixed pixel. Spectral unmixing outputs both the endmember spectrum and their corresponding abundance fractions inside the pixel. It, however, does not provide spatial distribution of these abundance fractions within a pixel. This limits the applicability of hyperspectral data for subpixel target detection. In this paper, a new inverse Euclidean distance based super-resolution mapping method has been presented. In this method, the subpixel target detection is performed by adjusting spatial distribution of abundance fraction within a pixel of an hyperspectral image. Results obtained at different resolutions indicate that super-resolution mapping may effectively be utilized in enhancing the target detection at sub-pixel level.

Keywords: Super-resolution mapping, mixed pixel, subpixel target detection, hyperspectral data, linear mixture modeling

1. INTRODUCTION

The hyperspectral imaging has paved the way to uncover targets which used to remain uncovered while analyzing data from multispectral sensors. In most cases, however, the spatial resolution for many satellite based hyperspectral sensors is still too coarse in comparison to their spectral resolution[1]. Thus, a target of interest may get spectrally resolved but may not spatially due to small size. Such a target may partly occupy one pixel or several pixels and may manifest itself in several ways, as can be seen from Fig. 1. For example, a target may lie completely within a pixel or it may cover one pixel fully and also simultaneously exist partially in all the eight pixels in the neighbourhood. In both the cases, the problem is referred to as subpixel target detection. In subpixel target detection, the goal is to recover the target, which due to its smaller size than the spatial resolution is completely embedded in the pixel.

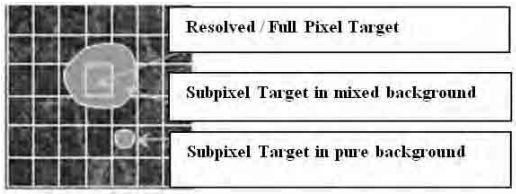

Figure 1. Full and subpixel targets.

Determination of individual components and their abundance fractions inside a pixel is known as mixed pixel classification and is the first step towards subpixel target detection using hyperspectral data. Further, while multipixel target detection can exploit both the spatial and the spectral properties, subpixel target detection can be achieved only by exploiting spectral properties[2]. Since the spectrum of the subpixel target is mixed with the spectrum of the background in a given pixel, it requires unmixing of both the spectrum as well as the proportion of the constituent material (i.e., the abundance fraction). Amongst various unmixing models, linear mixture model (LMM) is the most widely used one for its simplicity[3] despite the fact that it is not guaranteed to produce non-negative abundances and hence there always exists a requirement of a more robust model such as constrained linear mixing model or a nonlinear mixing model for estimating abundance fractions within a pixel. Alternatively, multilayer perceptron neural network and neuro-fuzzy methods[4,5] have also been used to recover the components. These models generally use a priori target information drawn from spectral libraries or from the image scene itself and output both the endmember spectrum and their corresponding abundance fractions inside the pixel. However, abundance fractions thus obtained indicate only their relative proportions and not their spatial distribution within the pixels.

The effective subpixel target detection depends on appropriate spatial distribution of these abundance fractions via super resolution mapping. A number of techniques based on several theories for super resolution mapping have been reported in the literature. These include linear optimization techniques, Markov Random Field models[6], Hopfield neural network[7,8], pixel swapping, etc[9,10] . Most of these techniques

Received 24 September 2012, revised 15 December 2012, online published 24 January 2013

are still under evolution and testing. These have mostly been applied for land cover mapping with very few implemented for subpixel target detection. In this paper, a new inverse Euclidean distance based super resolution mapping technique for subpixel target detection has been introduced and discussed.

2. EXPERIMENTAL DATA

First set of experiments have been conducted on synthetically generated data with known subpixel abundance fractions, which have been used as reference data to test the proposed technique. Thereafter, the experiments have been repeated on hyperspectral data collected from AVIRIS sensor to detect aircrafts as targets.

Figure 2. 30x30 pixels image approximating shape of an aircraft. (Fractions ranging from 0.25 to 0.9).

2.1 Synthetic Data

A synthetic dataset approximating the shape of an aircraft and of similar complexity as an actual aircrafts in terms of shape and size has been considered. Further, a number of synthetic images at different scales, namely, 3x3, 5x5, 7x7, 9x9 and 11x11 pixels corresponding to scale factors 3, 5, 7, 9, and 11 respectively have been generated to account for difference in spatial resolutions.

2.2 AVIRIS Data

An archived hyperspectral image (size: 400 x 400 pixels, 224 bands) from AVIRIS sensor acquired over a naval air station in San Diego, California has been used (Fig. 3(a)). The image is available as example data in ENVI image processing software. After removal of water absorption and bad bands, 189 bands of this hyperspectral image already available as reflectance spectra have been considered. The image contains five aircrafts (Fig. 3 (a)) centered at pixel coordinates (row, column), (244, 145), (232,137), (199,158), (89, 11), (70, 22). These have been given reference IDs, P1 to P5. From this data, an image of size 40 x 40 pixels has been extracted containing two aircrafts, P3 and P5 (Fig. 3 (b)). It may be noticed that these two targets fall under shadow and may be treated as difficult targets to detect. For the set of experiments in this study, regions containing both full and partially full pixels have been extracted.

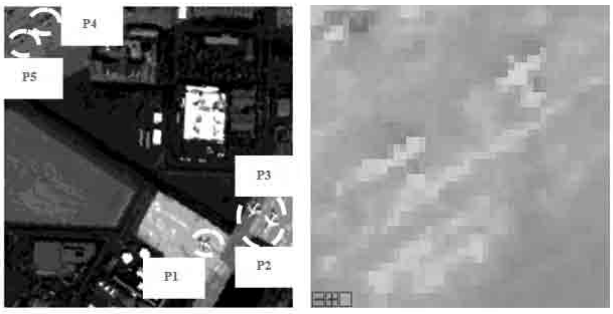

(a) **(b)**

Figure 3. (a) a 200x200 pixels true colour image of AVIRIS data. (b) 40x40 pixels region of segmented image AVIRIS data with two aircrafts (referred AVIRIS - i).

3. EUCLIDEAN DISTANCE BASED SUPER RESOLUTION

Spectral unmixing is the process by which fractions of various constituents within a pixel (in this case, fraction and the background, also known as abundance fractions) are estimated[11,12]. On the other hand, super resolution may be defined as optimization of abundance fractions within or between the pixels to derive a subpixel map at a spatial resolution finer than that of the coarse spatial resolution input image[6,7,8]. It may be carried out at different scale factors depending upon the spatial resolution required to be achieved. However, developing a model that accurately captures the spatial distribution of abundance fractions within a pixel requires understanding of how natural features get translated into an image.

3.1 Super Resolution Using Abundance Fractions

In nature, all earth surface features exhibit spatial contiguity in their layout and composition. They also appear to hover around a centre of mass. This spatial contiguity also gets retained in the images depicting these features which appear centered around a centre of mass. Thus, all the pixels belonging to that feature (also referred to as class or object or target) are assumed to be attracted towards the pixel in the centre. In other words, the central pixel exerts some attractive influence on all the surrounding pixels of the same class. This attractive influence can be expressed in terms of an attractive function. In a similar way, all subpixels for a given target/class inside a pixel (which can be determined from the knowledge of its abundance fraction) can be assumed to experience an attraction towards the centermost subpixel. Naturally, this attractive influence can be expected to be a function of the distance of any given subpixel from the centermost subpixel and hence can be modeled using an appropriate distance measure. Thus, the attractive influence can be quantified knowing the number of subpixels (expressed in terms of abundance fractions) and the distance of any given subpixel from the centermost subpixel. The genesis of super resolution techniques lies in quantification of this attractive influence.

Modeling the above attractive influence for each pixel to be super resolved requires an appropriate distance function, the number of subpixels for each class and a pixel neighbourhood scheme.. The number of subpixels is calculated based on the scale factor corresponding to the pixel in the coarse spatial resolution image. For example, a scale factor of 5 implies that abundance fractions in a pixel are mapped into five rows and five columns of subpixels. Thus, a total of 25 subpixels are created within each pixel. Further, if a target (or a class) is estimated to have a value of 0.6 as its abundance fraction in a pixel and the scale factor is 5, it implies that 60% of the total

subpixels (*i.e*, 25 x 0.6 = 15 subpixels) belong to that target. The next requirement for modeling is the selection of appropriate neighbourhood scheme. Pixel neighbourhood constitutes the group of pixels that exert or experience attraction on/from the central pixel/subpixel. There are several different types of pixel neighbourhood schemes such as 2 x 2 pixels, 4 x 4 pixels and 8 x 8 pixels neighbourhood schemes etc. Each of these pixel neighbourhood schemes also includes the pixel at which the object/class centre is located. Both, the pixel neighbourhood scheme and the object/class centre concepts shall be used in estimation of subpixel distances for modeling attractive influence.

Consider an n x m pixel image, as shown in Fig. 4, to be used for super resolution mapping. It may be noticed that the pixels at the corners are surrounded by other pixels only on three sides while those at the centre are surrounded by eight pixels from different sides. A clique is defined as a subset of an image array whose two distinct elements are mutual neighbours[6]. Thus, for an image array, it is necessary to consider all the possible cliques separately. C1 to C9 are the various possible cliques. Cliques marked as C1 through C8 do not have an 8 x 8 pixel neighbourhood but clique C9 has an 8 x 8 pixel neighbourhood. These cliques are the backbones of super resolution as these decide the number of pixels that directly influence the pixel being super resolved.

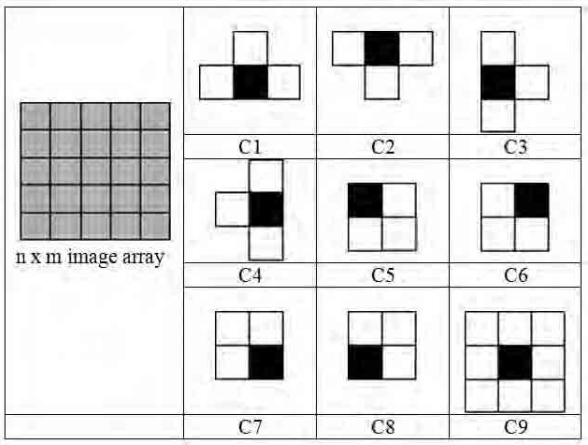

Figure 4. An n x m pixel image array for super resolution and corresponding cliques.

3.2 Modeling the Attractive Influence based on Inverse Euclidean Distance

To understand, modeling of the attractive influence in the case of the proposed inverse Euclidean distance based method, consider an n x m array as shown in Fig. 5 (a) (note that it is the same n x m pixel array as shown in Fig. 4). For super resolution, let a 3 x 3 pixel array be extracted from this pixel array as in Fig. 5(b). Further, consider that the central pixel is the pixel to be super resolved (Fig. 5(c)). This presents a case of clique C9 as shown in Fig. 4. Let all the pixels in this clique be denoted by P1 through P9 (Fig. 5 (c)). Assuming that super resolution is being performed at a scale factor of 5, a 5 x 5 subpixel grid has been created at the central pixel. Thus, there are 25 subpixels which need to be spatially distributed. In other words, there are 25 subpixel locations which are occupied by either of the binary classes but their exact locations are yet to be ascertained. To do this, we need to know the fractions of the binary classes. Let one of the binary classes in the entire 8-pixel neighbourhood be referred as CL-1 and let abundance fractions for this class in each of the pixels, identified as P1 to P9, be a1 to a9 as shown in Fig. 6(b). Once these fractions are known, the number of subpixels for each binary class can be calculated. Consider for example that the fraction for CL-1 in the central pixel is 0.8. Then the number of subpixels of class, CL-1, present in the central pixel is 0.8 x 25= 20 subpixels and rest belong to the other class. Similarly, number of subpixels for each of the binary class inside all the pixels P1 through P9 can be found. The requirement now is to spatially distribute the subpixels of each of the binary classes. In the preceding example, 20 subpixels of Cl-1 and balance 5 subpixels of other class have to be assigned a unique location amongst the total 25 subpixel locations available in the central subpixel. It can be expected that the distribution of these subpixels of say CL-1 (and of the other class) would depend upon two things, namely the abundance fractions of the same class in all the neighbouring pixels of the clique and the distance of each subpixel from the neighbouring pixel. For example, refer to Fig. 6. Assume that there are 20 subpixels of Cl-1 in the central pixel P5. First, the number of subpixels experiencing attraction from each of the neighbouring pixels P1, P2, P3, P4, P6, P7, P8, P9 (*i.e*, excluding P5 which is the pixel being

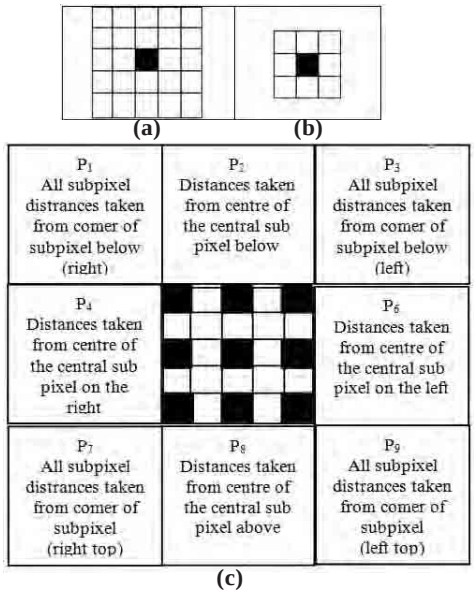

Figure 5. (a) An n x m image array for super resolution, (b) 8 x 8 pixel neighbourhood, and (c) 8 x 8 pixel neighbourhood with central pixel for super resolution mapping.

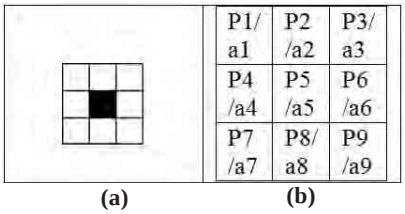

Figure 6. (a) 3 x 3 pixel array, and (b) abundance fractions of Cl-1 in the image.

super resolved) and getting aligned at locations closer to it, will depend upon the abundance fraction of CL-1 in these pixels. In other words, a pixel with higher abundance fraction of CL-1 would attract larger number of subpixels from the pixel being super resolved (*i.e* P5). Second, the attraction experienced by each of the subpixels will be in inverse proportion to its distance from any of the neighbouring pixels. Modelling these two aspects together leads to assigning a unique location to each of the subpixels of both the classes. For the proposed Inverse Euclidean Distance based technique, these aspects have been discussed in the following paragraphs,

3.2.1. Number of Subpixels Getting Attracted Towards Each of the Neighbourhood Pixel

For ease of explanation, assume that the abundance fractions for CL-1 in each of the pixel P1 to P9 (*i.e*, values assigned to a1 to a9 in Fig. 6 (b)) are 0.3, 0.3, 0.3, 0.3, 0.6, 0.2, 0.2, 0.2, 0.2 respectively. Further let the central pixel, P5 be the pixel being super resolved at a scale factor of 5. This means that pixel P5 which is being super resolved has 25 x 0.6=15 subpixels of CL-1 which get attracted towards the class/object centre. During the process of super resolution, it is assumed that the target centre can be located in any of the neighbouring pixels (*i.e*, P1 to P9 except P5 which is under super resolution), and hence each is considered separately in turn as the target centre. Now, the number of subpixels (out of these total 15 subpixels) getting attracted towards each of the neighbourhood pixels P1 to P9 (except P5 which is under super resolution) can be determined. It may, however, be noted that while calculating the number of subpixels getting attracted towards a pixel, the values are always rounded off to the next higher value and the deficiency of subpixels, if any, is accounted towards the pixel having the least abundance fraction.

3.2.2. Estimation of Attractive Influence

In the previous section, the number of subpixels (of pixel P5 under super resolution) getting aligned with each of the neighbourhood pixels (*i.e*, pixels P1 to P9 except pixel P5 which is under super resolution) have been determined. Now, each of these subpixels needs to be assigned a specific location in an array of pixels, the size of the array being determined by the scale factor (as discussed earlier). It is obvious that a subpixel nearer to any given neighbouring pixel will experience greater attractive influence and therefore the relative attractive influence experienced by different subpixels can be used to assign them a specific location. This, however, requires that the attraction being experienced by each of these subpixels from the corresponding neighbourhood pixel is to be determined. Further, it is easy to estimate this attractive influence as a function of the inverse of the distance between the subpixel and any given pixel. Next, for estimating the attractive influence using inverse Euclidean distance, two definite locations are needed namely the start and the finish. The start location is always the class/object centre which is expected to exert attractive influence on the subpixels being super resolved. The finish location is the subpixel of the array on which the attractive influence is being estimated. Since any of the neighbourhood pixel can be the class/object centre, each of the neighbourhood pixel is assumed to be the class/object centre in turn and treated as start location for estimation of the attractive influence. Now, to calculate the Euclidean distance between the two locations, these need to be defined in terms of certain coordinates. To do this, first the pixel to be super resolved is decided and subdivided into a grid of subpixels depending upon the scale factor (in this example, P5 is the pixel being super resolved and the scale factor is 5). All the subpixels can thus be referred to in the form of their row and column coordinates (*i.e* (1,1), (1,2) etc). Next, the locations of all the neighbourhood pixels are also defined in terms of row and column coordinates of the subpixels of the pixel under super resolution. Thus, in Figure 5 (c), the start location in respect of all the corner pixels (P1, P3, P7, P9) are defined as (1,1), (1,5), (5,1), (5,5). Similarly, the start location in respect of all middle subpixels (P2, P4, P6, P8) are defined as (1,3), (3,5), (5,3), (5,1). In the above computations, the inverse Euclidean distance from this class/object centre is defined as,

$$A_{ij} = \left(\frac{1}{d_{ij}}\right) \quad (1)$$

where Euclidean distance is given by,

$$d_{ij} = \sqrt{(i - x_c)^2 + (j - y_c)^2} \quad (2)$$

where d_{ij} is the Euclidean distance, i and j represent row and column coordinates of the neighbourhood pixel assumed to be start location (class/object centre), x_c and y_c are the row and column coordinates of the the subpixel on which the attractive influence is being ascertained

3.2.3. Achieving Super Resolution.

Once the attractive influence experienced by different subpixels from each of the neighbourhood pixels has been estimated, subpixel locations can be ranked in the order of descending attractive influence and these rankings are stored for their subsequent reference during the spatial distribution. At this stage, the number of pixels attracted towards each of the neighbourhood pixels and the ranking of the attractive influence experienced by each of the subpixels are known. It is now assumed that the pixel with the highest abundance fraction for CL-1 shall have the highest attractive influence on the subpixels, therefore the super resolution is commenced with the pixel having the highest abundance fraction. All the subpixels getting attracted to this pixel are considered first and assigned a fixed location as per the stored ranking for this pixel. The process is repeated for the pixel having the next highest abundance fraction for CL–1 and so on until all the pixels of the clique have been processed. During this process, it is ensured that the attractive influence experienced by any single subpixel from any two neighbourhood pixels is never the same. If so, the pixel having higher abundance fraction is assigned higher ranking. The advantages of this ranking procedure are, the attractiveness values for different scale factors can be ranked and stored initially itself and there is no computational requirement at the run time thus making the super-resolution process faster. It considers subpixels of a given class together and hence there is no iterative clustering involved and that it considers the fractions of binary class both in the pixel being super resolved as well as in the neighbouring

clique pixels; hence it may be possible to extend the method for various multi-class problems.

4. IMPLEMENTATION OF PROPOSED TECHNIQUE

The implementation of proposed technique can be summarized in the form of an algorithm as,

(a) Obtain the image to be super resolved and estimate the abundance fractions for various classes/targets using spectral unmixing or any other technique.

(b) Decide the scale factor for super resolution. Since there are no heuristics which guide us on the maximum extent to which the input image can be superesolved. This judgement is usually based on trial and error through experiments for a given dataset and the definition of the classes being mapped. In the instant case, scale factor of 3, 5, 7, 9, and 11 were chosen as they were considered sufficient to give adequate enhancement of the target under study.

(c) Calculate attractiveness for each subpixel towards object/class centre.
- Obtain object/class centre points at a given scale factor for all neighbouring pixels in all the cliques.
- Calculate A_{ij} using d_{ij} as given in Eqns (1) and (2).
- Arrange A_{ij} in descending order and store it separately for each of the clique pixels.

(d) Consider the pixel to be super resolved. Obtain abundance fraction for a given class CL-1 in all the clique pixels associated with this pixel and calculate the number of subpixels to be associated to each of the clique pixels.

(e) Commence super resolution,
- Commence super resolution starting with the clique pixel having the highest abundance fraction for any given class.
- Recall the stored rankings for this clique pixel estimated at *step (c)* (iii) and spatially distribute the number of subpixels associated with this pixel.
- Repeat *steps (a) to (e)* till all the clique pixels have been considered. In case of any overlap of subpixel position at any stage, use the next vacant location.

5. RESULTS AND DISCUSSION

5.1 Accuracy of Subpixel Target Detection in Synthetic Data

The classification accuracy and CPU time obtained for the Synthetic image is given in Table 1. It can be seen from the table that classification accuracy achieved using inverse Euclidean distance technique at a scale factor of 11 is as high as 82.22%. The classification accuracy increases marginally from scale factor 3 to scale factor 11 despite the increase in complexity. This suggests that the technique may be more suitable at higher scale factors. On the other hand, the CPU time taken for the proposed technique increases only marginally with the increase in the scale factor. The near constant CPU time for the Euclidean distance technique across all the scale factors demonstrates the effectiveness of the proposed technique in sub-pixel target detection at any given spatial resolution. The main reason for this higher computational efficiency in the proposed technique is the fact that or, it does not involve any iteration as the attractive influence experienced by subpixels for each scale factor is stored *ab initio* itself and are simply recalled at the run time for super resolution process. The targets, recovered using this technique for the synthetic image (shape approximating an aircraft) are shown in Fig. 7. On focusing on the shape of the target (i.e., the aircraft), these figures depict marginal improvement with increase in scale factors. This suggests that there may be improvement in classification accuracy with increase in scale factor without any substantial increase in the CPU time.

Table 1. Classification accuracy and efficiency in case of synthetic dataset

Scale factor	Proposed technique	
	Classification accuracy (%) (s)	CPU Time
3	75.94	09.25
5	81.85	09.25
7	81.65	09.28
9	81.98	09.54
11	82.22	09.59

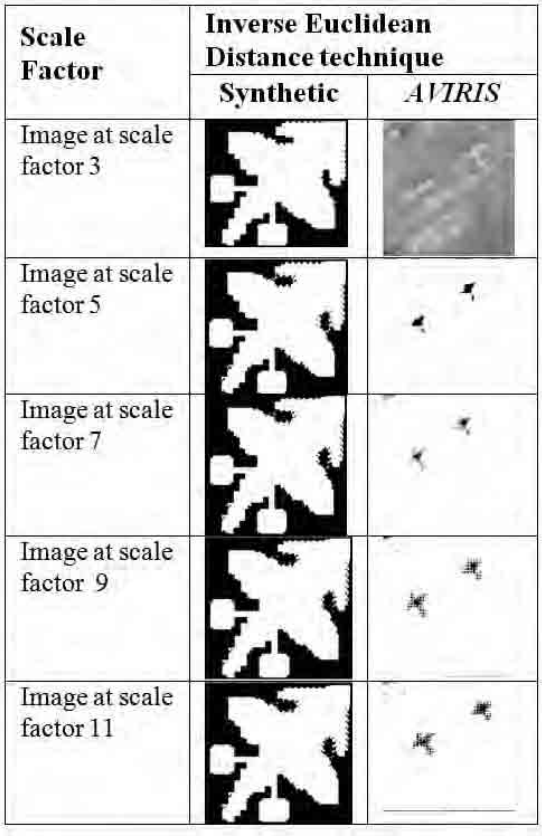

Figure 7. Super resolved images.

5.2 Subpixel Target Detection in AVIRIS

In order to further evaluate the performance of the technique, an AVIRIS has been considered. The dataset consists of two aircrafts as targets. First, the abundance fractions of each pixel in these images have been obtained using the unsupervised spectral unmixing method available as part of ENVI software. It is pertinent to point out here that simple

LMM is not guaranteed to produce non-negative abundances and hence there always exists a requirement of a more robust unmixing model such as constrained linear mixing model or a nonlinear mixing model may for obtaining an accurate estimate of abundance fractions within a mixed pixel. However, for reasons of computational simplicity and to maintain the focus of the study, simple LMM has been used here. Thereafter, the proposed technique has been applied to perform super resolution. However, due to non-availability of reference data, the super resolved images have been evaluated visually and not quantitatively. The super resolved significant increase in CPU time. Images of targets detected across different scale factors are shown in Fig. 7. As is evident from this figure, the proposed inverse Euclidean distance technique produces satisfactory results across all scale factors. The reason for success of this method lies in the fact that it does not involve any iterative convergence and is based on the stored rankings of attractiveness values of the super resolved subpixels. The major advantage of the proposed technique has been the near constant CPU processing time despite increase in scale factor or in complexity (*i.e* synthetic *vs* AVIRIS data).

6. CONCLUSIONS

Spectral unmixing methods such as linear mixture modeling (LMM) are used to recover abundance fractions of the components occurring inside a mixed pixel, There are two main limitations of LMM. The simple LMM is not guaranteed to produce non-negative abundances and hence there always exists a requirement of a more robust unmixing model such as constrained linear mixing model or a nonlinear mixing model may for obtaining an accurate estimate of abundance fractions within a mixed pixel. The second limitation of LMM is its incapability to provide spatial distribution of the abundance fractions within a pixel. These limitations, in particular its incapability to provide spatial distribution severely restricts the applicability of hyperspectral data for subpixel target detection. In this paper, a new inverse Euclidean distance based super-resolution technique has been proposed. The technique achieves subpixel target detection in hyperspectral images by adjusting spatial distribution of abundance fraction within a pixel. The experiments have been conducted using synthetic as well as AVIRIS dataset. The performance of the proposed technique measured in terms of classification accuracy and CPU time for both the datasets have been found be satisfactory and encouraging. The major advantage of the proposed technique has been the near constant CPU processing time despite increase in scale factor or in complexity (i.e synthetic *vs* AVIRIS data).Though the technique produces good results, one of the limitation of the proposed technique lies in the use of a linear Euclidean distance as a measure of attractiveness. Future studies may consider the use of a non-linear measure for ranking subpixels for spatial distribution, particularly in case of multi-class problems.

REFERENCES

1. Chang, C.I. Hyperspectral imaging-techniques for spectral detection and classification. Plenum Publishers, New York, USA, 2003. pp.101-300.
2. Manolakis, D.; Sircausa, C. & Shaw, G. Hyperspectral subpixel target detection using linear mixing model. *IEEE Trans. Geosci. Remote Sens.*, 2001, **39**(7) 1392-409.
3. Keshva, N. A survey of spectral unmixing algorithms. *Lincoln Lab. J.*, 2003, **14**(1), 55-78.
4. Baralde, A.; Binaghi, E. & Bloda, P. Comparison of multilayer perception with neuro fuzzy techniques in estimation of cover class mixture in remotely sensed data. *IEEE Trans. Geosci. Remote Sens.*, 2001, **39**(5), 994-1005.
5. Foody, G.M. Estimation of subpixel land cover composition in the presence of untrained classes. *Comput. Geosci.*, 2000, **26**(4), 469-478.
6. Kasetkasem, T.; Arora, M.K. & Varshney, P.K. Super resolution land cover mapping using a Markov Random field based approach. *Remote Sens. Environ.*, 2005, **96**(3-4), 302-14.
7. Tatem, A.J.; Lewis, H.G.; Atkinson, P.M. & Nixon, M. S. Super resolution target identification from remotely sensed images using a hopfield neural network. *IEEE Trans. Geosci. Remote Sens.*, 2001, **39**(4), 781-96.
8. Tatem, A.J.; Lewis, H.G.; Atkinson, P.M. & Nixon, M. S. Super resolution land cover pattern prediction using a hopfield neural network. *Remote Sens. Environ.*, 2002, **79**(1), 1-14.
9. Atkinson, P.M. Sub pixel target mapping from soft classified remotely sensed imagery. *Photogrammetric Engg. & Remote Sens.*, 2005, **71**(7), 839-46.
10. Thornton, M.W.; Atkinson, P.M. & Holland, D.A. Sub-pixel mapping of rural land cover objects from fine spatial resolution satellite sensor imagery using super-resolution pixel-swapping. *Int. J. Remote Sens.*, 2006, **27**(3), 473-91.
11. Rosin, P.L. Robust pixel unmixing. *IEEE Trans. Geosci. Remote Sens.*, 2001, **39**(9), 1978-983.
12. Vikhamar, D. & Solberg, R. A constrained spectral unmixing approach to snow-cover mapping in forests using MODIS data. *In* Proceedings of IEEE International Symposium on Geoscience and Remote Sensing, 2003. IGARSS, 2003, **2**, pp.833-35.

Contributors

Prof. Manoj K. Arora

(Brief Biodata available on page no. 63)

Dr K C Tiwari (Retd. Colonel) graduated from NIT Allahabad and then completed his ME CAD (Civil) and PhD from IIT Roorkee. currently a Professor in the Department of Civil Engineering, Delhi Technological University, Delhi, India. He has published more than 40 papers in International/National Journals and Conferences. His research interests include: Detection of small and buried objects using microwave and hyperspectral remote sensing.

Title: Synthesis and characterization of nanocrystalline ferroelectric $Sr_{0.8}Bi_{2.2}Ta_2O_9$ by conventional and microwave sintering: A comparative study

Authors: Sugandha Miglani, A.K. Jha

PII: S0025-5408(12)01022-7
DOI: doi:10.1016/j.materresbull.2012.12.049
Reference: MRB 6379

To appear in: *MRB*

Received date: 11-4-2012
Revised date: 6-10-2012
Accepted date: 22-12-2012

Please cite this article as: S. Miglani, A.K. Jha, Synthesis and characterization of nanocrystalline ferroelectric $Sr_{0.8}Bi_{2.2}Ta_2O_9$ by conventional and microwave sintering: A comparative study, *Materials Research Bulletin* (2010), doi:10.1016/j.materresbull.2012.12.049

Synthesis and characterization of nanocrystalline ferroelectric $Sr_{0.8}Bi_{2.2}Ta_2O_9$ by conventional and microwave sintering: A comparative study

Sugandha[1] and A. K. Jha[1, 2]
[1]Thin Film and Material Science Laboratory, Department of Applied Physics,
Delhi Technological University (Formerly Delhi College of Engineering),
Delhi-110042, India.
[2]Department of Applied Sciences, A.I.A.C.T.R.
Geeta Colony, Delhi 110092, India.
[2]Corresponding author email: prof.akjha@gmail.com
Ph. No: +9198 68 24 21 50, Fax no: +91 11 27 87 10 23

Abstract

In recent years mechanical activation technique has been utilized to synthesize the nanocrystalline form of compounds resulting in enhancement in the properties. Also, microwave sintering is being preferred over conventional sintering due to rapid processing and uniform temperature distribution throughout the specimen. In the present work, nanocrystalline non-stoichiometric strontium bismuth tantalate (SBT) of the composition $Sr_{0.8}Bi_{2.2}Ta_2O_9$ ferroelectric ceramics were synthesized by microwave sintering process (with sintering temperatures of 1000°C and 1100°C) and conventional solid state reaction process (with sintering temperature of 1100°C) with an objective of comparing the properties of the synthesized specimens by the two processes. X-ray diffraction analysis shows the formation of single phase layered perovskite structure formation by both the processes. Scanning electron microscopy reveals the formation of a finer granular microstructure in the specimen synthesized by microwave sintering compared to that in the specimen prepared by conventional sintering. The specimen prepared by microwave sintering process exhibits improved electrical properties with higher dielectric constant, higher piezoelectric and pyroelectric coefficients and lower dielectric loss.

KEYWORDS: A. Ceramics, A. Nanostructures, C. X-ray diffraction, D. Dielectric properties, D. Piezoelectricity.

Introduction

Recently nanocrystalline $SrBi_2Ta_2O_9$ has emerged as a potential material for scientific and industrial applications such as high capacitance capacitors, piezoelectric transducers, pyroelectric sensors, non volatile ferroelectric random access memories, etc [1, 2]. SBT belongs to the aurivillius family of mixed bismuth layered perovskites having the general formula $(Bi_2O_2)^{2+}$ $(A_{m-1}B_mO_{3m+1})^{2-}$ where m denotes the number of corner sharing octahedral forming the perovskite like slabs [3, 4]. It is well known that characteristics of any material are closely related to its synthesization process. The method of synthesis of ferroelectric materials plays a significant role in determining their microstructural, electrical and optical properties [5-7]. Conventionally, these ceramics are synthesized by solid state reaction process. Although significant progress has been achieved, there are certain problems associated with above technique. These include compositional inhomogeneity resulting from the incomplete reaction of the starting oxides, abrupt increase of grain size, volatilization of bismuth oxide due to high processing temperatures, longer soaking durations, etc [8, 9]. Nowadays, microwave processing of ceramics has emerged as a successful alternative to conventional processing technique [10-13]. This is due to the fact that microwave sintering has significant advantages over the conventional sintering technique in material processing. These are rapid and volumetric heating leading to enhanced microstructure, controlled grain growth, higher

densification at comparatively lower processing temperature and shorter soaking durations, substantial energy saving, etc. Detailed literature survey shows that even though this process has been used to synthesize many ferroelectric ceramics [14-18], hardly any work has been reported on the synthesis of nanocrystalline non-stoichiometric SBT compound. It has been reported that the introduction of non-stoichiometry to the starting composition by varying Sr/Bi ratio enhances the dielectric and ferroelectric properties [19, 20]. This is due to the fact that $(Bi_2O_2)^{2+}$ layer in SBT significantly alters electrical properties including the transition temperature(T_c), dielectric constant, dielectric loss, leakage current etc. However, strontium deficient samples facilitate large atomic displacements resulting into enhanced polarization and hence higher remnant polarization [20]. This prompted the authors to synthesize and characterize a non stoichiometric composition $Sr_{0.8}Bi_{2.2}Ta_2O_9$ (SBT) by this novel technique and compare its structural and electrical properties with the specimen prepared by the conventional solid state reaction technique.

2. Experimental

Highly pure powders of $SrCO_3$, Bi_2O_3, Ta_2O_5 (all from M/s Aldrich) were mixed in proportions to get $Sr_{0.8}Bi_{2.2}Ta_2O_9$ compound. This mixture of powders was milled in a high-energy planetary ball mill (Retsch, PM 100) for 20 hours at a milling speed of 300 rpm to yield nanocrystalline SBT. Milling was carried out in toluene medium with a high wear-resistant 10mm zirconium oxide balls in a zirconium oxide vial with a ball-to-powder weight ratio of 10:1. The mixture was then admixed with 2wt% polyvinyl alcohol as a binder and then pressed at 200MPa into a disk shaped pellet. The specimen was divided into two sets. One set of pellet was sintered in conventional furnace at 1100°C

for 2h at a heating rate of 5°C/min. Another set of pellets were sintered in microwave furnace (V.B.Ceramics, Eurotherm 2404) at 1000°C and 1100 °C for 20 min at a heating rate of 50°C/min.

Phase development in the synthesized compound was monitored using an X-ray diffractometer (Bruker, D8 Advance) with CuK_{α} radiation (λ= 1.5405Å) at a scanning rate of 1°/min. Transmission electron microscopy (TEM) (Jeol, 2100-F) was used to confirm nanocrystalline nature of the synthesized compound. Scanning electron microscopy (Hitachi, S-3700N) was used to study the grannular morphology of the synthesized samples. The sintered pellets were polished and silver pasted on both sides and cured at 500°C for 1h. Dielectric measurements were carried out using a precision LCR meter (Agilent 4284A) at an oscillation amplitude of 1 V. The measurement of the pyroelectric coefficient was performed using the Byer-Roudy technique. The sample was first poled at an elevated temperature (~150°C) for 4 h in silicon oil. The poled sample was then placed in a programmable furnace, and the temperature was increased at a rate of 2°C/min. The current generated in the specimen was measured using a high precision electrometer (Keithley 6517A). Piezoelectric coefficient, d_{33} values, was measured using a piezometer system (PiezoTest PM300).

3. Results and Discussions

3.1 Microstructural studies

The X-ray diffractograms of the studied samples are shown in Fig. 1. It is observed that the samples prepared by both the conventional sintering (CS) and microwave sintering (MW) exhibit single phase layered perovskite structure. The peaks

are well defined and are observed to shift slightly towards higher angle in the specimen prepared by the microwave sintering (1000°C) as compared to that in the specimen prepared by conventional sintering (1100°C). The lattice parameters were calculated using the observed interplanar spacing, d-values, obtained from the diffractograms and refined using the least square refinement method by the computer program package Powder X [21]. The obtained lattice parameters are listed in Table 1. It is observed that the values of the lattice parameters are slightly lower in the sample prepared by the microwave sintering compared to that in the sample prepared by the conventional sintering process. The strain parameter, orthorhombic strain [2(a-b)/ (a+b)], has been calculated and the values are presented in table 1. It is observed that sample sintered by microwave sintering technique at 1000°C exhibit highest orthorhombic distortion as compared to conventionally sintered sample.

It is likely that when the specimen is milled for longer duration like 20 hours using zirconium balls and vial, it is possible that some zirconium atoms enter the perovskite structure [22]. However, no extra peaks corresponding to ZrO_2 or any compound involving zirconium are seen in the XRD diffractograms which is possibly due to the high wear resistant balls and vial used in the present work [23, 24]. However, the introduction of some zirconium atoms in the lattice cannot be ruled out and possibly the number of zirconium atoms entering the structure is below the sensitivity of the X-ray diffractometer.

The images obtained from transmission electron microscopy (TEM) and electron diffraction (ED) of the studied specimen milled for 20 h is shown in Fig. 2. The average particle size is seen to be in the range of 30-50nm. The formation of particles of nano

dimensions is also confirmed by diffraction rings consisting of discrete diffraction spots in the electron diffraction pattern.

The SEM micrographs of the sintered specimen are shown in Fig. 3. It is known that variation in sintering temperature, material processing techniques, compositions, etc. influences the microstructure such as grain growth and densification of the specimen, which in turn controls other properties of the material [25-27]. It can be seen that the average grain size in the specimen prepared by the microwave sintering is lower (~0.5μm, 1000°C) than that in the specimen prepared by the conventional sintering technique (~0.8μm, 1100°C). However, sample sintered at higher temperature (1100°C) by the microwave sintering technique exhibit comparatively larger grain size (~1-2μm) with porous and loosely packed morphology. This is due to the fact that the sintering mechanism in microwave furnace is fundamentally different from sintering in the conventional furnace. Thermal conduction in the conventional sintering takes place through radiation and/or convection heating followed by 'transfer' of thermal energy inside the specimen. However, microwave sintering involves the absorption and/or linear coupling of the microwave field followed by the 'conversion' of electromagnetic energy into thermal energy. In this technique, there is no thermal conduction process involved. This is due to the fact that heat is generated internally within the specimen. Hence, there is an inverse heating profile i.e. 'inside-out' profile unlike the 'outside-in' profile in the conventional sintering process [28-30]. This results in rapid and volumetric heating of the sample resulting into fine microstructure at comparatively lower sintering temperature (1000°C), which is indeed observed (Fig. 3b). It is worth noting that rapid heating and

shorter soaking duration in the microwave sintering inhibits the grain growth in finally sintered sample thus preserving the nanocrystalline nature of the synthesized specimen [31- 35].

3.2 Dielectric properties

Fig. 4 shows the temperature dependence of dielectric constant (ε_r) for all the samples at different frequencies (1, 10 and 100 KHz). It is observed that all the samples exhibit dielectric anomaly at the Curie temperature (T_c) indicating the occurrence of ferroelectric-paraelectric phase transition. It is also observed that all the samples have the same T_c at all the above mentioned frequencies, suggesting that the samples do not show any relaxor behavior [36]. Further, at low temperatures the dielectric constant values are the same regardless of the signal frequencies used for the measurements. However, at higher temperatures dielectric constants vary markedly with varying frequencies. This is possibly due to the fact that bismuth layered ferroelectric materials contains inherent defects such as oxygen vacancies resulting from the volatilization of Bi_2O_3 during sintering. It has been established through X-ray photoemission spectroscopy studies that the oxygen ions in $(Bi_2O_2)^{2+}$ layers are less stable than those in $(SrTa_2O_7)^{2-}$ perovskite slabs [37]. Many investigations of $Pb(Zr,Ti)O_3$ have indicated that the defects such as oxygen vacancies, $Vo^{\cdot\cdot}$, act as space charge and plays an important role in the electrical polarization of perovskite materials [38]. The oxygen vacancy induced polarization becomes dominant at higher temperatures and at lower frequencies [39]. This explains the significantly enhanced dielectric constant at low frequency and high temperatures.

Fig. 5 compares the variation of dielectric constant with temperature for all the samples at 1 KHz frequency. A close observation shows that the dielectric constant of the

sample prepared by the microwave sintering process (1000°C) is much higher than that in the sample synthesized by the conventional solid-state reaction process (1100°C). This can be understood as follows. It is known that in the fine grained ferroelectric ceramics, the dielectric constant increases due to an increase in residual internal stress [40-42] which is higher in a fine grained specimen. The higher value of the dielectric constant in the sample prepared by microwave sintering process can therefore be attributed to its finer grain size (Fig. 3b). The reduction of unit cell volume (Table 1) is another possible reason for the increase in dielectric constant in this specimen as obvious from Clausius-Mossotti relation [43]:

$$\varepsilon_r = \frac{3V_m + 8\Pi\alpha_D}{3V_m - 8\Pi\alpha_D} = 1 + \frac{12\Pi(\alpha_D / V_m)}{3 - 4\Pi(\alpha_D / V_m)}$$

where V_m ($=V_{unit\ cell}/Z$) is the molar volume and α_D is the net dielectric polarizibility. However, comparatively lower dielectric constant is observed in the sample sintered at higher temperature (1100°C) by the microwave sintering technique. This is possibly due to poorly developed microstructure, as observed in Fig. 3c [44].

Fig. 6 shows the temperature variation of dielectric loss (tan δ) for all the samples at different frequencies (1, 10 and 100 KHz). It is observed that the sample synthesized by the microwave sintering (1000°C) has comparatively lower dielectric loss (tan δ) values than that in the conventionally sintered sample (1100°C). However, sample sintered at higher sintering temperature (1100°C) by the microwave sintering technique exhibit maximum dielectric loss values. It is well known that the dielectric loss in these materials depends on many factors such as morphology of the specimen, dipolar loss, dc

conductivity, domain wall relaxation, etc [45]. As discussed above, poorly developed microstructure resulted in higher dielectric loss in the microwave sintered (1100°C) sample [46-48]. It is also observed that in all the samples dielectric loss remains nearly independent with temperature up to ~ 300°C and increases rapidly with temperature thereafter. Also, the variation in tan δ values at low frequency (1 KHz) is significantly faster than that at higher frequency (100 KHz). As discussed earlier, these samples have inherent defects or vacancies (like oxygen vacancies) which act as space charges and these space charges are active at lower frequencies and higher temperatures [39]. The sharp increase of dielectric loss in the higher temperature region is attributed to the increased mobility of space charges in the sample [49, 50]. Also, at lower frequencies, the dipoles are able to follow the applied alternating field resulting in higher values of dielectric constant and dielectric loss while at higher frequencies the dipoles are unable to follow the rapidly changing electric field leading to the reduction in the values of dielectric loss [51].

3.3 Piezoelectric and Pyroelectric studies

Fig, 7 shows the variation of pyroelectric coefficient for both the studied samples by Byer and Roundy technique [52]. It is well known that the variation of temperature causes changes in the spontaneous polarization. This variation produces a displacement current *I* parallel to the polar axis. The pyroelectric coefficient (P_T) was calculated using the relation [53]:

$$P_T = (P_I A\ )/\ (dT/dt)$$

where P_I is the pyroelectric current, *A* the area of the conducting surface of the sample and d*T* /d*t* is the rate of change in temperature. It is observed that for both the samples,

pyroelectric current as well as pyroelectric coefficient remains nearly independent of temperature up to nearly 200°C and thereafter it increases with the increase in temperature. Further, a peak at a temperature lower than the ferroelectric phase transition temperature (T_c) is observed in all the samples. As it can be seen, sample prepared by the microwave sintering technique (1000°C) exhibit higher pyroelectric coefficient as compared to that in conventionally sintered sample (1100°C). The maximum pyroelectric coefficient at transition temperature is observed to be 107.62μCcm^{-2}°C^{-1} in the microwave sintered sample compared to 104.21μCcm^{-2}°C^{-1} in the conventionally sintered sample. However, the sample sintered at higher sintering temperature (1100°C) by microwave sintering technique exhibit very low pyroelectric coefficient (13.35 μCcm^{-2}°C^{-1}). This is possibly due to difference in the poling efficiency of the sintered samples. It is worth mentioning here that sample sintered at 1100°C by microwave sintering technique was observed to have lower poling efficiency or breakdown potential (1.2 KV) as compared to sample sintered at 1000°C (1.8 KV). The sample sintered by conventional sintering technique (1100°C) was also poled at 1.8 KV. The observed behavior is possibly due to the difference in the microstructure of the sintered samples [54]. The obtained values of pyroelectric coefficient are comparable with the reported values of other members of the Aurivillius family of layered perovskites [55, 56].

Table 1 lists the pyroelectric figure of merit for infrared detectors (R_v) calculated from the pyroelectric coefficients and dielectric constant at 100 kHz by using the following formula [57]:

$$R_v = P_T / \varepsilon_r$$

Where P_T is the peak pyroelectric coefficient and ε_r is the permittivity at T_c

Table 1 also lists the measured values of piezoelectric coefficient (d_{33}) for both the samples. The observed variation of piezoelectric coefficient is consistent with the variation of pyroelectric coefficient. The d_{33} value is also observed to be higher in the sample synthesized by the microwave sintering technique (1000°C), which can be understood in terms of its smaller grain size. Small grains have larger number of grain boundaries, which would result in the increase of internal electric fields generated by space charge layers at the grain boundaries [58]. Moreover, enhanced microstructure and high poling efficiency resulted in higher pyroelectric and piezoelectric coefficients in the microwave sintered sample as compared to that in the conventionally sintered sample. However, poorly developed microstructure in the sample sintered at higher temperature (1100°C) by the microwave sintering technique results in lower piezoelectric coefficient.

3.4 Conductivity Studies

Fig. 8 shows the variation of dc conductivity ($\sigma_{dc}=1/\rho$) with inverse of temperature ($10^3/T$) of the studied specimens. For all the studied samples, conductivity is constant in the lower temperature region and thereafter increases considerably with temperature. This indicates negative temperature coefficient of resistance (NTCR) type behavior. As seen in the figure, there are two predominant types of conduction mechanism, one is the lower temperature region in which dc conductivity remains invariant with temperature and the other is higher temperature region in which dc conductivity increases sharply with temperature. In the lower temperature region from room temperature to approximately ~300°C the electrical conduction is dominated by extrinsic defects. Whereas, in higher

temperature region ~ 300°C to ~700°C the conduction is dominated by intrinsic defects such as oxygen vacancies [59, 60].

Conclusion

$Sr_{0.8}Bi_{2.2}Ta_2O_9$ compound was synthesized by both conventional and microwave sintering processes. X-ray diffractograms confirm the formation of single phase layered perovskite structure in SBT compound prepared by both the processes. Microstructural studies reveal the formation of smaller grains in the sample synthesized by the microwave sintering process compared to that in the sample prepared by the conventional sintering technique. Sample synthesized by microwave sintering process exhibit enhanced dielectric constant, piezoelectric coefficient, pyroelectric coefficient and lower dielectric loss at comparatively lower sintering temperature and shorter soaking duration. Thus microwave sintering technique is superior to conventional solid state reaction technique for synthesizing nanocrystalline SBT samples in which better properties can be obtained at comparatively lower sintering temperature.

Acknowledgement

Authors acknowledge and thanks to the University Grants Commission (UGC), India for the grant of research project (F. No. 39-469/2010 (SR)).

References

[1] F. Jacob, Y. Gagou, E. Elkain, J. Appl. Cryst. 36 (2003) 880-89.

[2] A. B. Panda, A. Pathak, M. Nandagoswami, P. Pramanik, Mater. Sci. & Eng. B B97 (2003) 275- 282.

[3] R. E. Newhan, R. W. Wolfe, R. S. Horsey, F. A. D. Colon, M. I. Kay, Mater. Res. Bull. 8 (1973) 1183.

[4] J. F. Scott, C. A. P. De Araujo, Science 246 (1989) 1400-5.

[5] K. Kiezer, E. H. Janssen, A. J. Mater. Res. Bull. 8 (1973) 533.

[6] T. Yamamoto, Am. Ceram. Soc. Bull. 71 (1992) 978.

[7] G. Arlt, Ferroelectrics 104 (1990) 217.

[8] M. V. Ramana, S. R. Kiran, N. R. Reddy, K. V. Siva Kumar, V. R. K. Murthy, B. S. Murthy, Mater. Chem. Phys. 126 (2011) 295-300.

[9] Y. T. Chen, C. I. Sheu, S. C. Liu, S. Y. Cheng, Ceramics Inter. 34 (2008) 621-624.

[10] P. K. Sharma, Z. Quanais, V.V.Varadan, V.K. Varadan, Smart Mater. Struct. 10 (2001) 878.

11] V. K. Sankaranrayan, C. Sreekumar, Curr. Appl. Phys. 3 (2003) 205.

[12] A.C. Metaxas, J. G. P. Binner, Advance Ceramic Processing Technologies, Noyes publications, NJ, USA, 1990, pp-285.

13] S. Rhee, D. Agrawal, T. Shrout, M. Thumm, Ferroelectrics, 261 (2001) 15.

14] S. Mahajan, O. P. Thakur, D. K. Bhattacharya, K. Sreenivas, Mater. Chem Phys. 112, (2008) 858-862.

[15] S. M. Zanetti, J. S. Vasconcelos, N. S. L. S. Vasconcelos, E. R. Leiti, E. Longo and J.A. Varela. J. Europ. Ceram. Soc. 24 (2004) 1597-1602.

[16] C. S. Chen, P. Y. Chen, C. C. Chou, C. S. Chen, Ceram. Inter. Doi: 10.1016/ Ceram. Int. 2011.04.063, (2011).

[17] J. D. Katz, Ann. Rev. Mater. Sci. 22 (1992) 153-70.

[18] R. Peelamedu, A. Badzian, R. Roy, R.P. Martukanitz, J. Am. Ceram. Soc. 87 (2004) 1806.

[19] T. Noguchi, T. Hase, M. Myasaka, Jpn. J. Appl. Phys.; 35 [1] (1996) 4900.

[20] Y. Shimakawa, Y. Kubo, Y. Nakagawa, H. Asano and F. Izumi, Appl. Phys. Lett. 74 (1999) 1904-1906.

[21] C. Dong, J. Appl. Cryst. 32, (1999) 838.

[22] P. Ganguly, A.K. Jha, J. Am. Ceram. Soc. Doi : 10.1111/j.1551-2916.2010.04321.x, 1-6 (2011).

[23] A.R. James, J. Subrahmanyam, J. Mater. Sci: Mater. Electron. 17 [7] (2006) 529.

[24] Sugandha and A. K. Jha, Mater. Charact. 65 (2012) 126-132.

[25] T. Atsuki , N. Soyama, T. Yonezawa, K. Ogi. Jpn. J. Appl. Phys. 34, (1995) 5096.

[26] M.Noda, M. Matsumuro and M. Okuyama, Jpn. J. Appl. Phys. 38 (1999) 2275.

[27] A. K. Jha and Sugandha, Ferroelectrics 421 (2011) 1-8.

[28] P. Thomas, L. N. Sathapathy, K. Dwarakanath,. K. B. R. Varma. Bull. Mater. Sci. 30[6] (2007) 567-570.

[29] S. Das, A. Mukhopadhyay, S. Datta, D. Basu. Bull. Mater. Sci. 31[7] (2008) 943-956.

[30] M. Oghbaei, O. Mirzaee, J. Alloys & Cmpds., 494 (2010) 175-189.

[31] Z. Xie, Z. Gui, L. Li, T. Su, Y. Huang, Mater. Lett. 36 (1998) 191.

[32] Z. Xie, J. Yang, X. Huang, Y. Huang, J. Eur. Ceram. Soc. 19 (1999) 381.

[33] B. Vaidhyanathan, D. KAgrawal, T. R.Shrout, Y. Fang Mater. Lett. 42 (2000) 207.

[34] X. H. Wang, X. Y. Deng, H. L. Bao, H. Zhou, I. W. Chen, J. Am. Ceram. Soc. 89 (2006) 438.

[35] R. Chaim, M. Levin, A. Shlayer and C. Estournes. Adv.Appl. Ceram. 107[3] (2008) 159.

[36] P. R. Das, R. N. P. Choudhary, B. K. Samantray, Alloys and Comp. 448 (2008) 32-37.

[37] B. H. Park, S. J. Hyun, S. D. Bu, T. W. Noh, J. Lee, H. D. Kim, T. H. Kim, W. Jo, Appl. Phys. Lett. 74 (1999) 1907–1909.

[38] I. Coondoo, A. K. Jha, S. K. Agarwal, J. Europ. Ceram. Soc. 27 (2007) 253.

[39] W.R. Buessem, L.E. Cross, A.K. Goswami, J. Am. Ceram. Soc. 49 (1966) 33-36.

[40] W. Kanzig, Phys. Rev. 98 (1955) 549-550.

[41] K. Uchino, E. Sadanaga, T. Hirose, J. Am. Ceram. Soc. 72 (1989) 1555-58.

[42] J. Li, X.M. Chen, Y. Wu, J. Eur. Ceram. Soc. 22, (2002) 87-91.

[43] Y. Wu, C. Nguyen, S. Seraji, M.J. Forbess, S.J. Limmer, G. Cao, J. Am. Ceram. Soc. 12 (2001) 2882-88.

[44] Sonia, R.K. Patel, P. Kumar, C. Prakash, D.K. Agarwal,Ceram Int. 32 (2002) 1585-89.

[45] A. Chen, Y. Zhi, L.E. Cross, Phys. Rev. B 62 (2008) 228.

[46] K. Raju and P.V. Reddy, Curr. App. Phys. 10 (2010) 31.

[47] Y. N. Huang, Y. N. Wang, Phys. Rev. B, 46 (1992) 3290.

[48] S. Su, J. E. Holmes. J. Electroceram. 9, (2002) 11-116.

[49] P. Ganguly, A.K. Jha, J. Alloys. Cmpd. 495 (2010) 7-12.

[50] T. Friessnegg, S. Aggarwal, R. Rames, B. Nielson, E.H. Poindexter and D.J. Keeble, Appl. Phys. Lett. 77 (2000) 127-29.

[51] A. K. Jha and P. Ganguly, Ferroelectrics 420 (2011) 71-79.

[52] C.B. Roundy and R.L. Byer, J. Appl. Phys. 44, (1973) 929–931.

[53] S.B. Lang, Source Book of Pyroelectricity (Gordan and Breach Science Publishers, New York, 1974).

[54] Y. H. Xu, Ferroelectric Materials (Elsevier Science Publisher, Amsterdam, 1991).

[55] T. Takenaka and K. Sakata, Ferroelectrics 118 (1991) 123.

[56] G.S. Murugan and K.B.R. Varma, J. Electroceram. 8 (2002) 37-48.

[57] B. M. Jin, S. Erdei and A.S. Bhalla, Proceedings of the Ninth IEEE International Symposium on Applications of Ferroelectrics. 825–828 (1994).

[58] Z. Zhang. and R. J. Raj, Am. Ceram. Soc. 78 (1995) 3363.

[59] D. Dhak, P. Dhak, P. Pramanik, Appl Surf Sci 254 (2008) 3078–92.

[60] H. S. Shulman, M. Testorf, D. Damjanovic, N. Setter, J. Am. Ceram. Soc. 79 (1996) 3124.

Parameters	Sample preparation method		
	Conventional Sintering Technique	Microwave Sintering Technique	
	1100°C	1000°C	1100°C
a (Å)	5.4772	5.4675	5.4746
b (Å)	5.5089	5.5069	5.5081
c (Å)	24.8451	24.7536	24.8396
V (Å^3)	749.659	745.3055	749.029
$\varepsilon_{r\ max}$ at 100 kHz	856.325	1013.782	350.258
P_T (μC/cm^{-2}°C^{-1})	104.206	107.620	13.351
R_v	0.121	0.106	0.038
d_{33} (pC/N)	16	17	5
2(a-b)/(a+b)	0.0067	0.0071	0.0057

Table 1: Comparison of different parameters between conventionally sintered and microwave sintered samples.

Figure Caption

Figure 1 X-ray diffraction patterns of $Sr_{0.8}Bi_{2.2}Ta_2O_9$ compound prepared by (a) conventional sintering (CS) (1100°C) and microwave (MW) sintering (b) 1000°C (c) 1100°C technique.

Figure 2 TEM micrograph and Electron diffraction pattern of 20 hours ball milled $Sr_{0.8}Bi_{2.2}Ta_2O_9$ powder.

Figure 3 SEM micrographs of $Sr_{0.8}Bi_{2.2}Ta_2O_9$ compound prepared by (a) conventional sintering (CS): (1100°C) and microwave (MW) sintering: (b) 1000°C (c) 1100°C technique.

Figure 4 Temperature variation of dielectric constant (ε_r) for sample prepared by (a) conventional sintering: (1100°C) and microwave: (b) 1000°C (c) 1100°C sintering technique.

Figure 5 Comparison of temperature variation of dielectric constant of the studied samples prepared by different sintering techniques at 1 kHz.

Figure 6 Temperature variation of dielectric loss (tan δ) for sample prepared by (a) conventional sintering (1100°C) and microwave sintering: (b) 1000°C (c) 1100°C technique.

Figure 7 Temperature variation of pyroelectric coefficient for sample prepared by (a) conventional sintering (1100°C) and microwave sintering: (b) 1000°C (c) 1100°C technique.

Figure 8 Temperature variation of dc conductivity for sample prepared by (a) conventional sintering (1100°C) and microwave sintering: (b)

1000°C (c) 1100°C technique.

Table 1: Comparison of lattice parameters, unit cell volume, dielectric constant ($\varepsilon_{r\,max}$), figure of merit (R_v), pyroelectric (P_T), piezoelectric coefficients (d_{33}), orthorhombic strain in $Sr_{0.8}Bi_{2.2}Ta_2O_9$ compound prepared by conventional solid-state reaction (1100°C) and microwave sintering (1000°C and 1100°C) techniques.

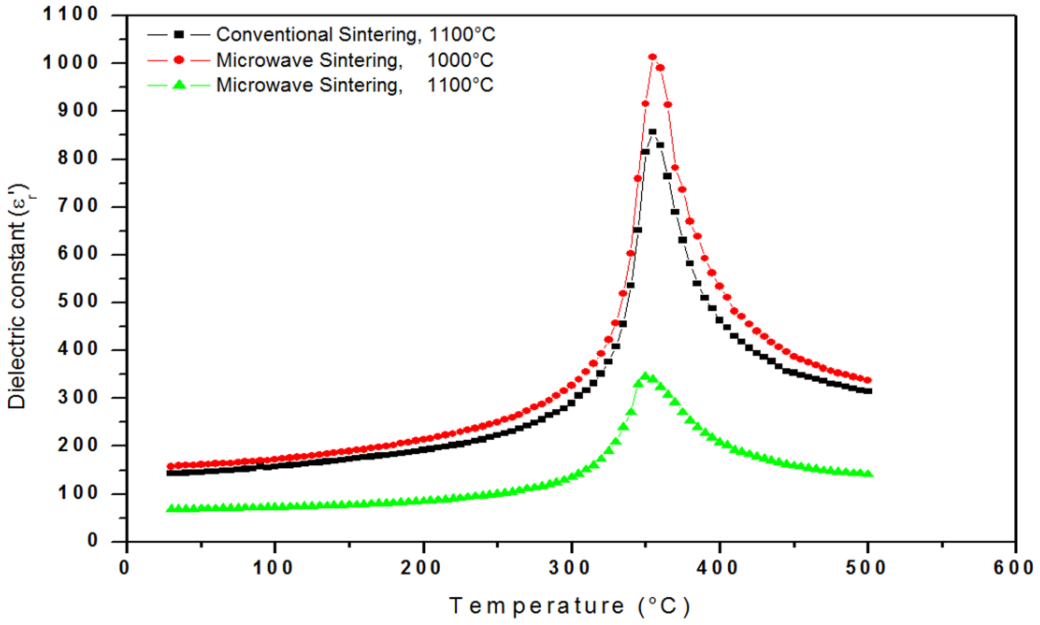

Comparison of Dielectric constant with sintering temperature for conventional sintered (1100°C) sample and Microwave sintered (1000 °C and 1100°C) sample.

Highlights

In this report $Sr_{0.8}Bi_{2.2}Ta_2O_9$ compounds have been synthesized.

Synthesis was carried out by Microwave sintering and solid-state reaction processes.

The synthesized specimens were characterized for their structural and electrical properties.

A comparative study reveals that microwave sintered specimen possesses superior properties.

Figure 1
Click here to download high resolution image

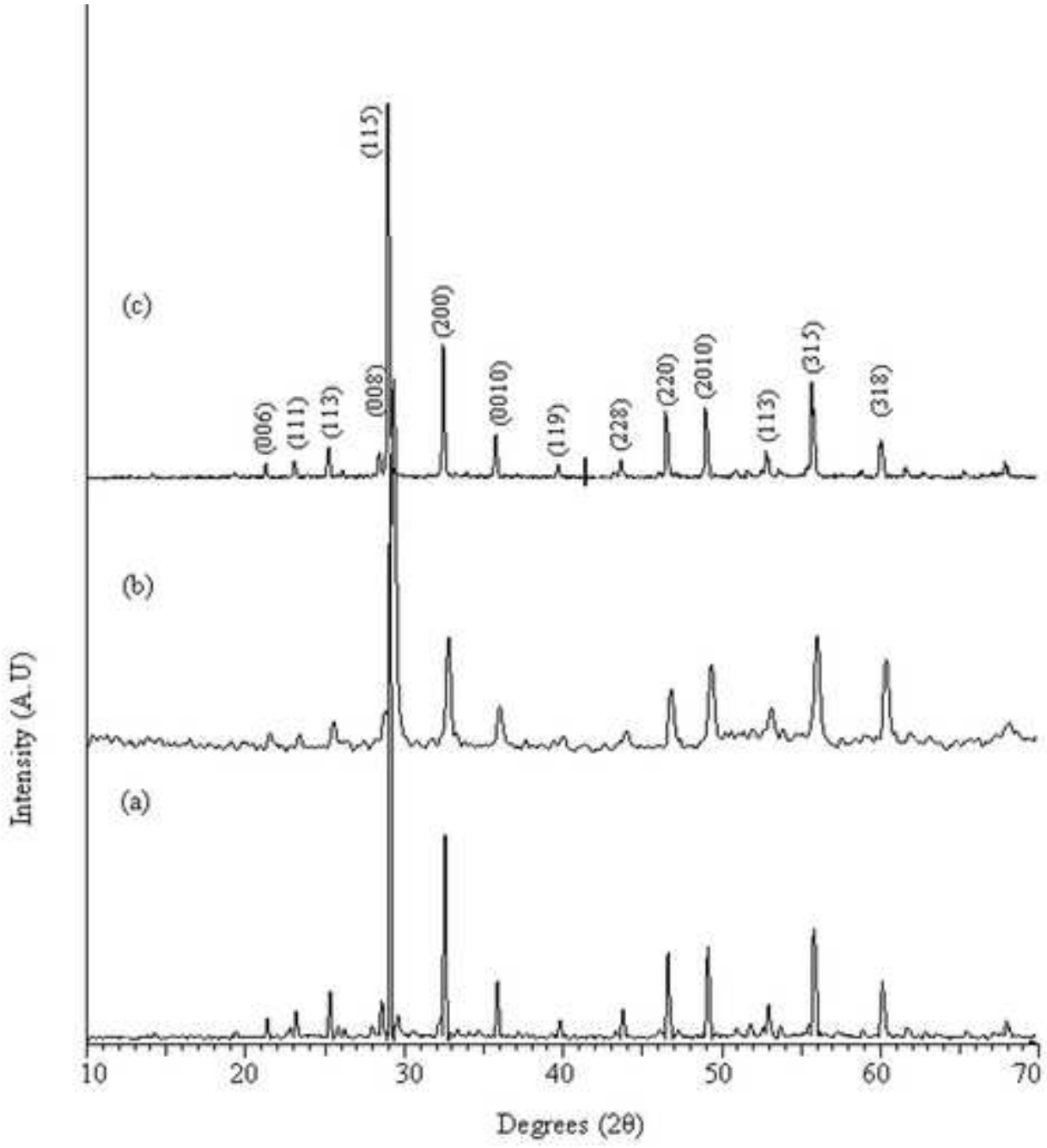

Figure 1

Figure(2)
Click here to download high resolution image

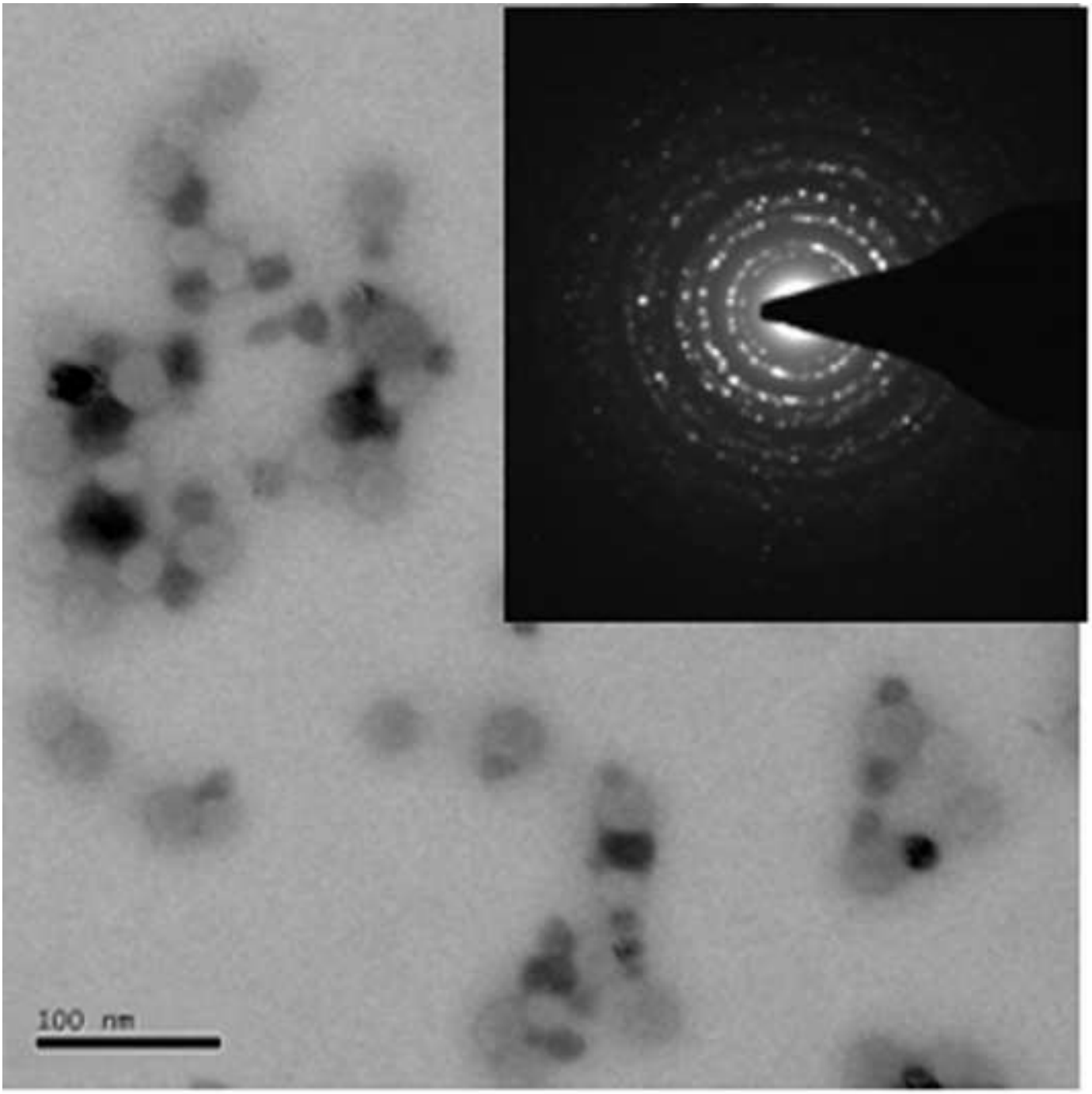

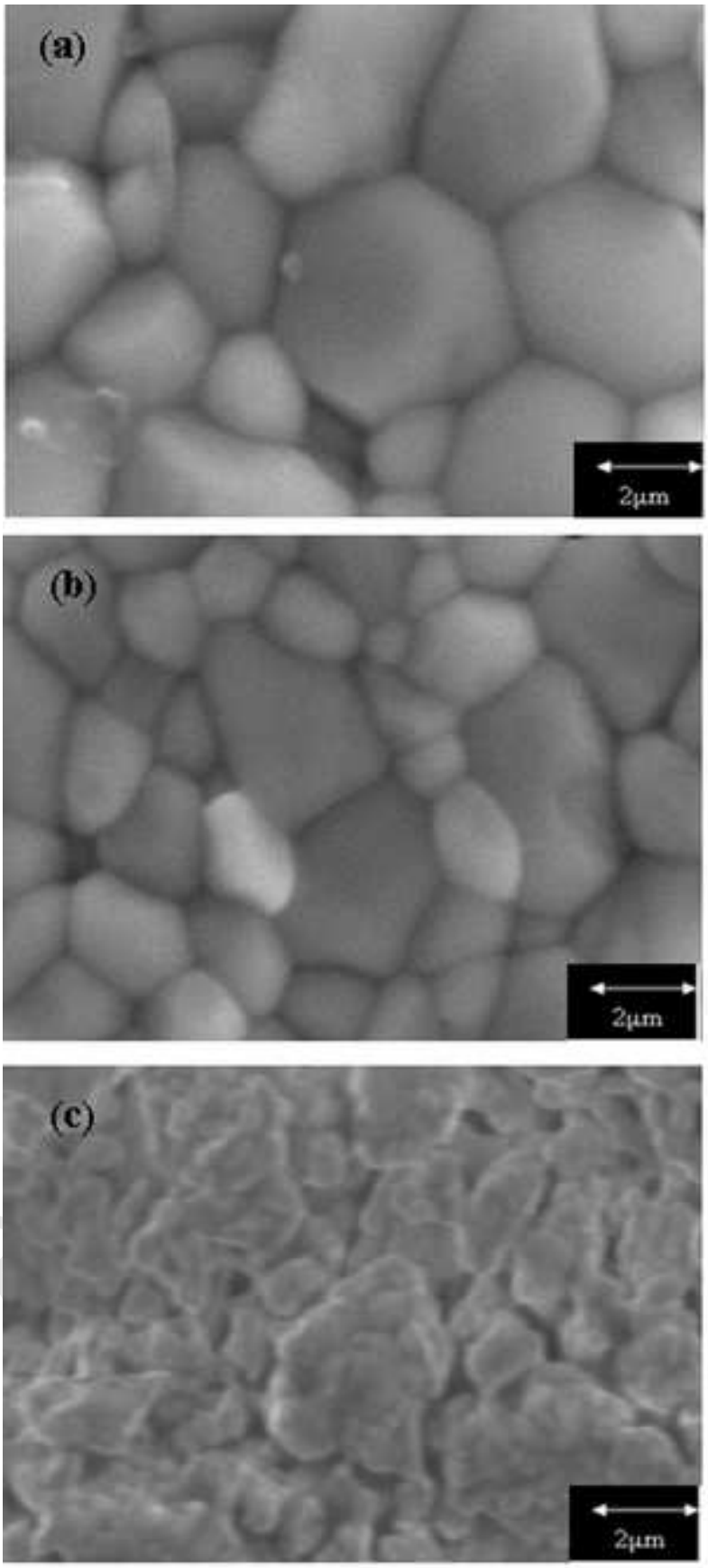

Figure 3

Figure(4a)
Click here to download high resolution image

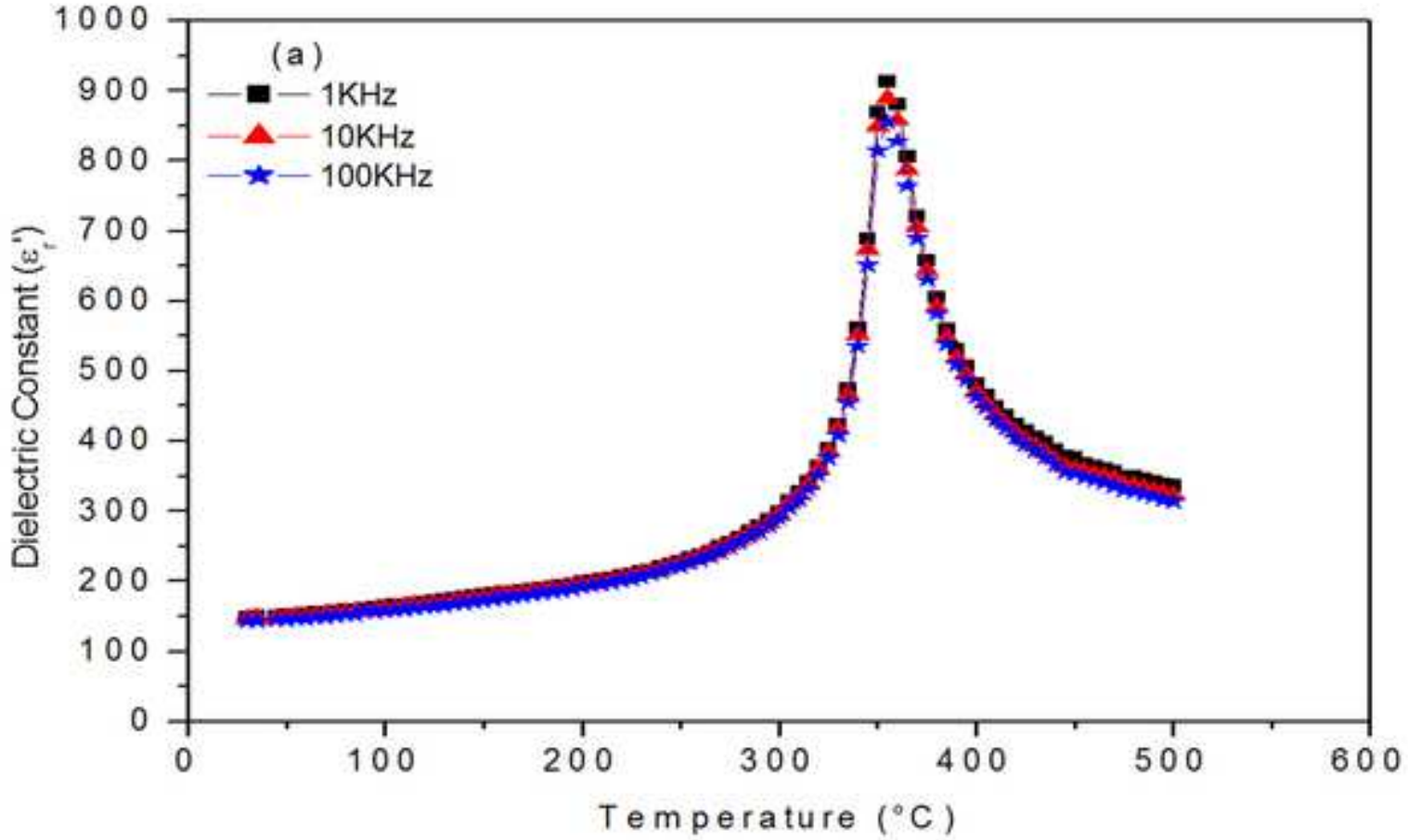

Figure(4b)
Click here to download high resolution image

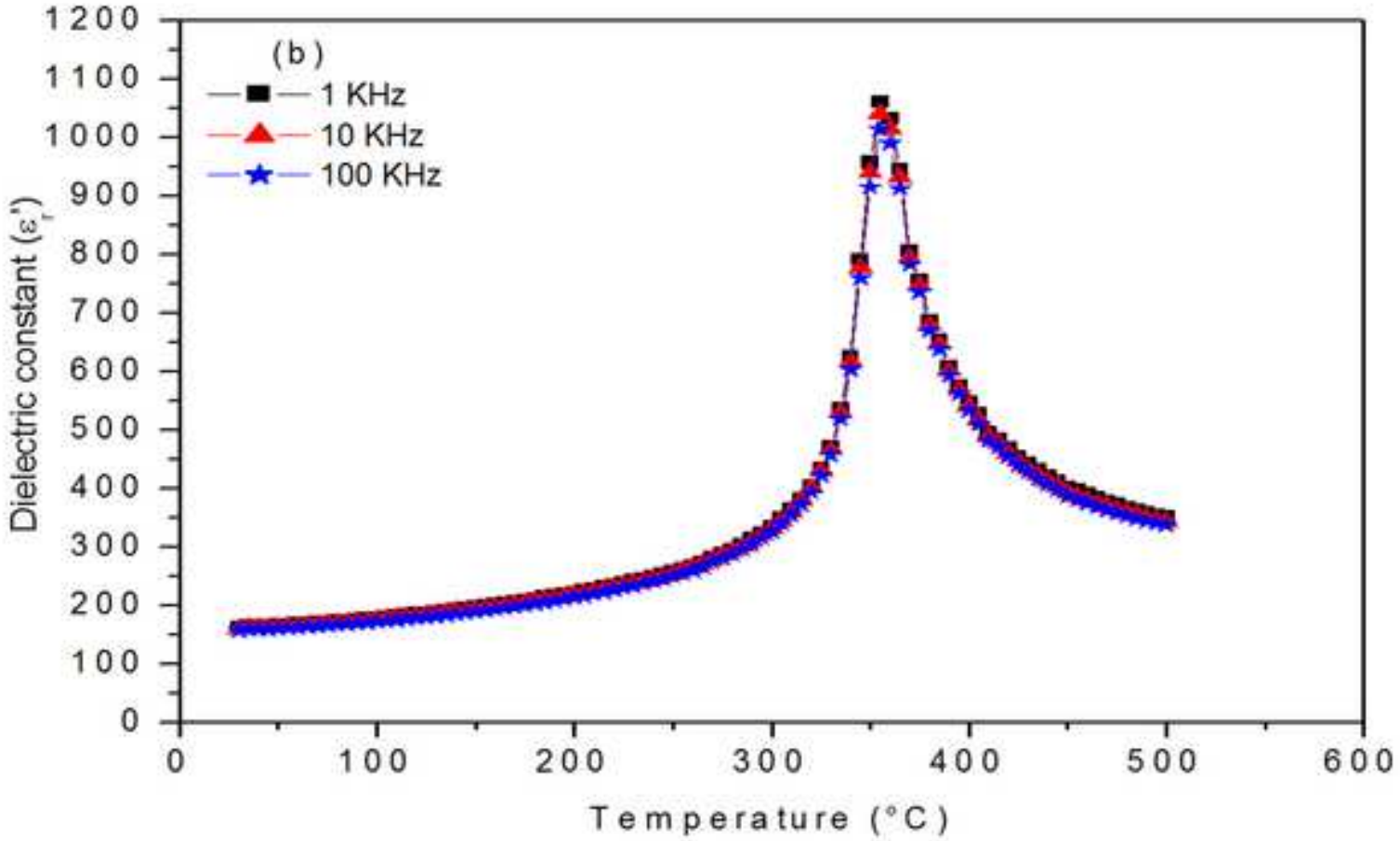

Figure(4c)

Click here to download high resolution image

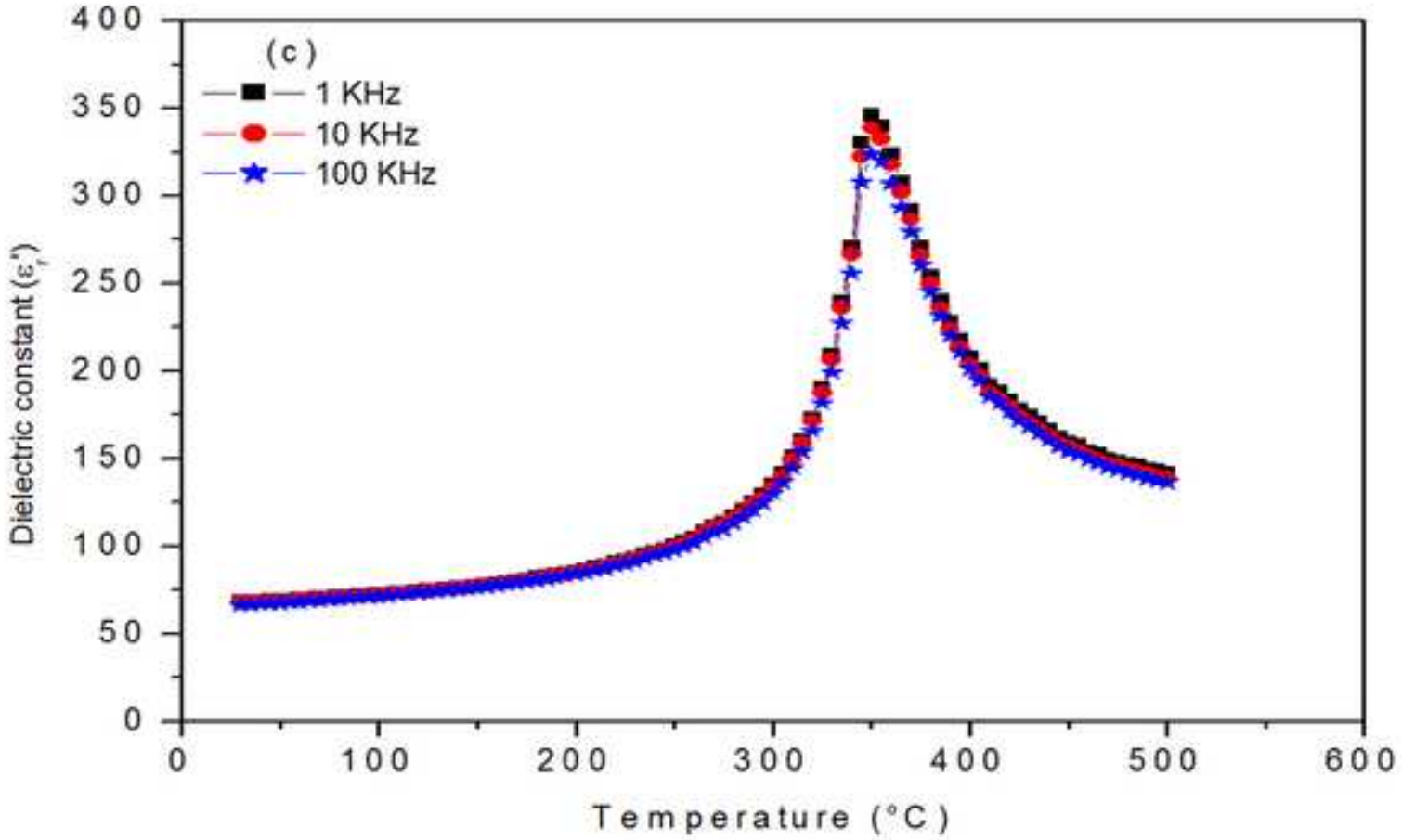

Figure 5
Click here to download high resolution image

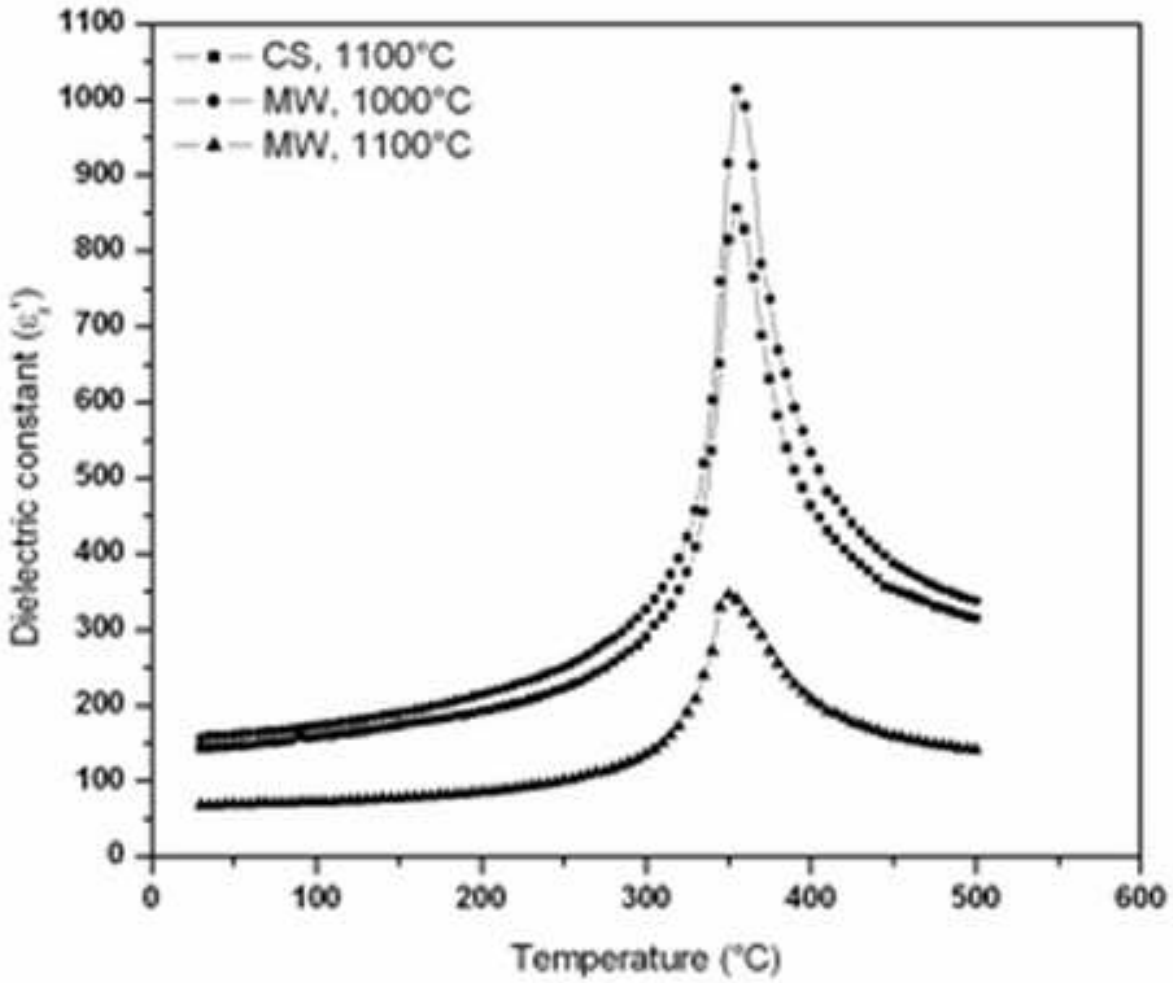

Figure 5

Figure(6a)
Click here to download high resolution image

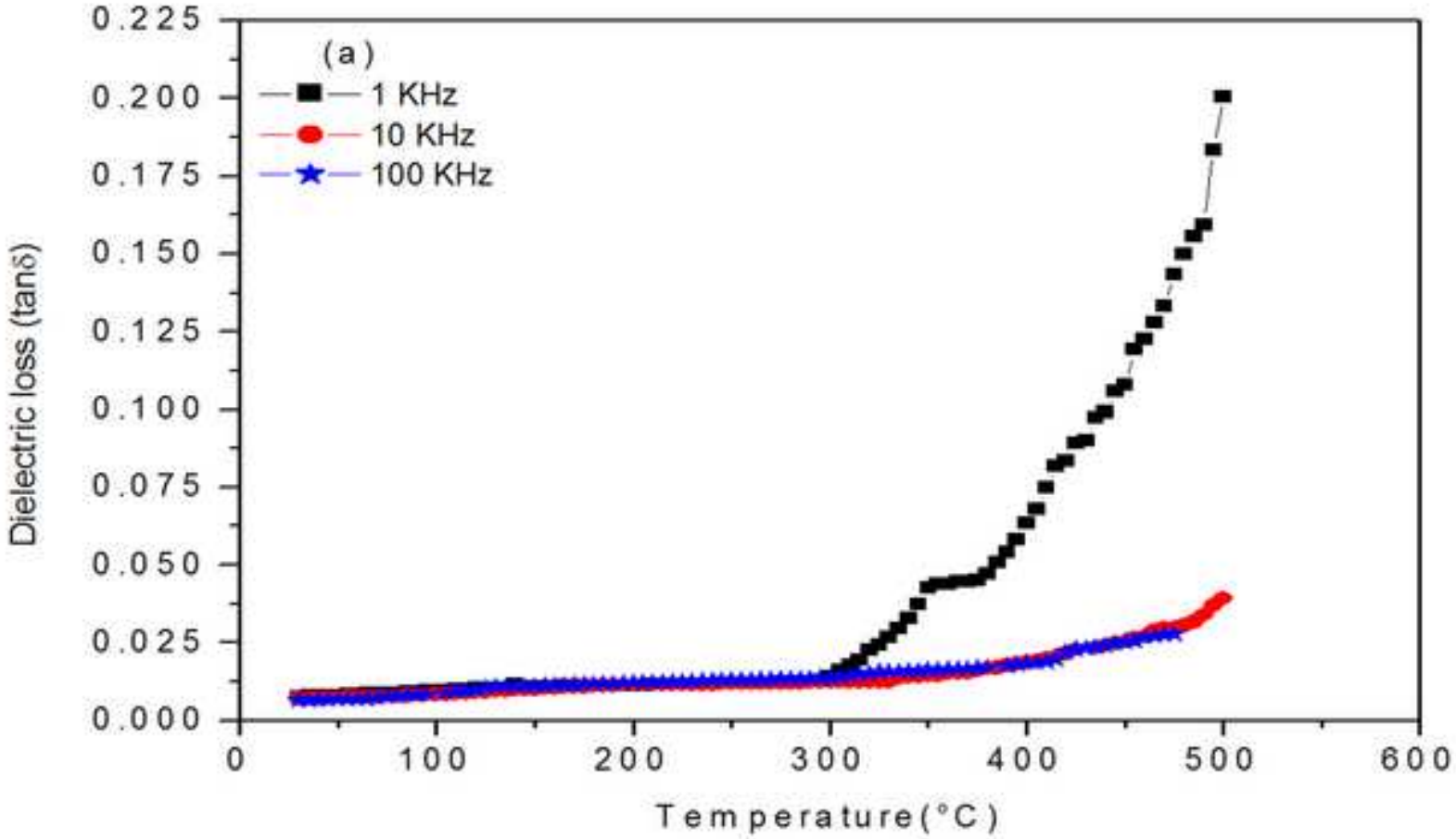

Figure(6b)
Click here to download high resolution image

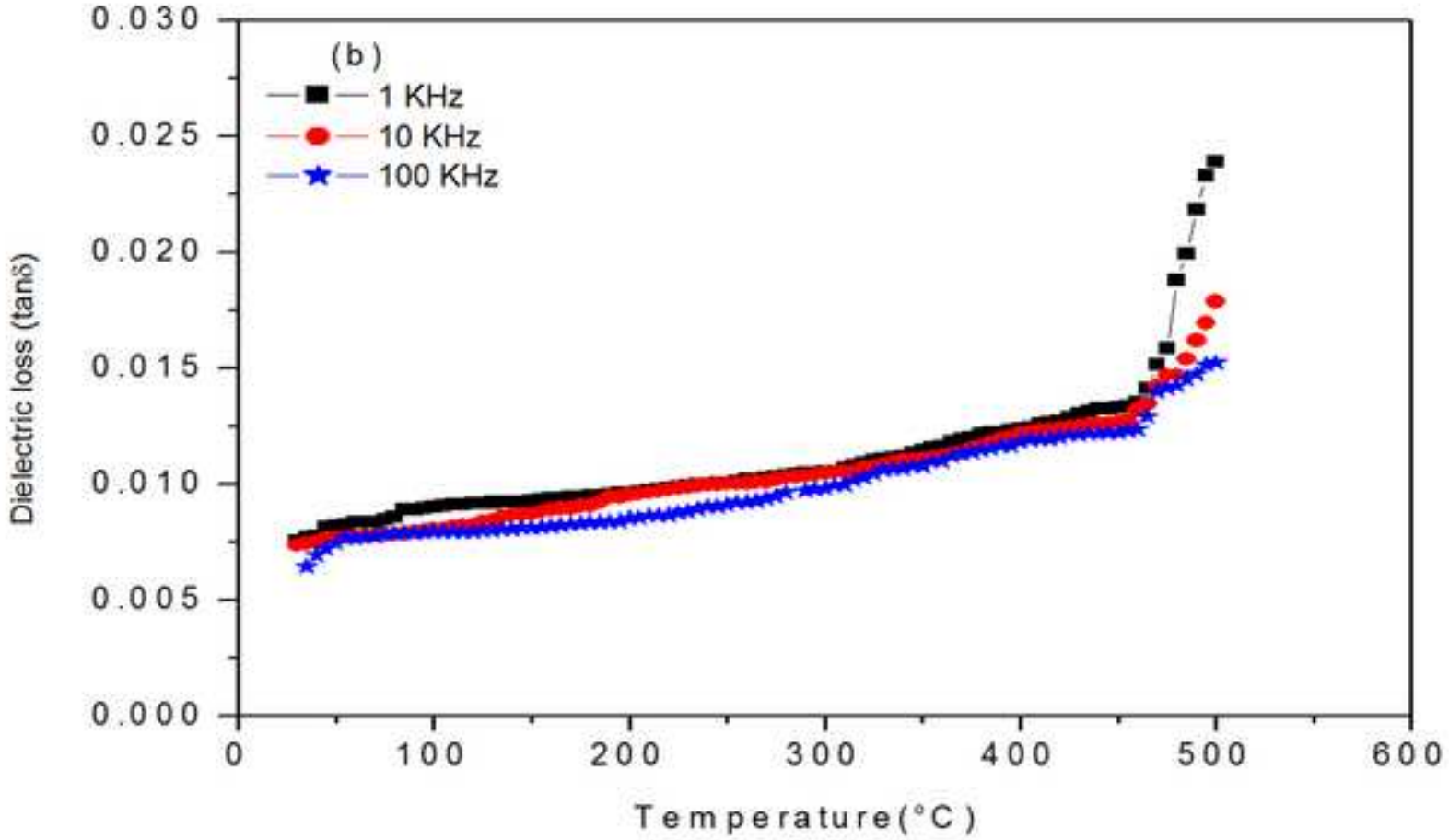

Figure(6c)
Click here to download high resolution image

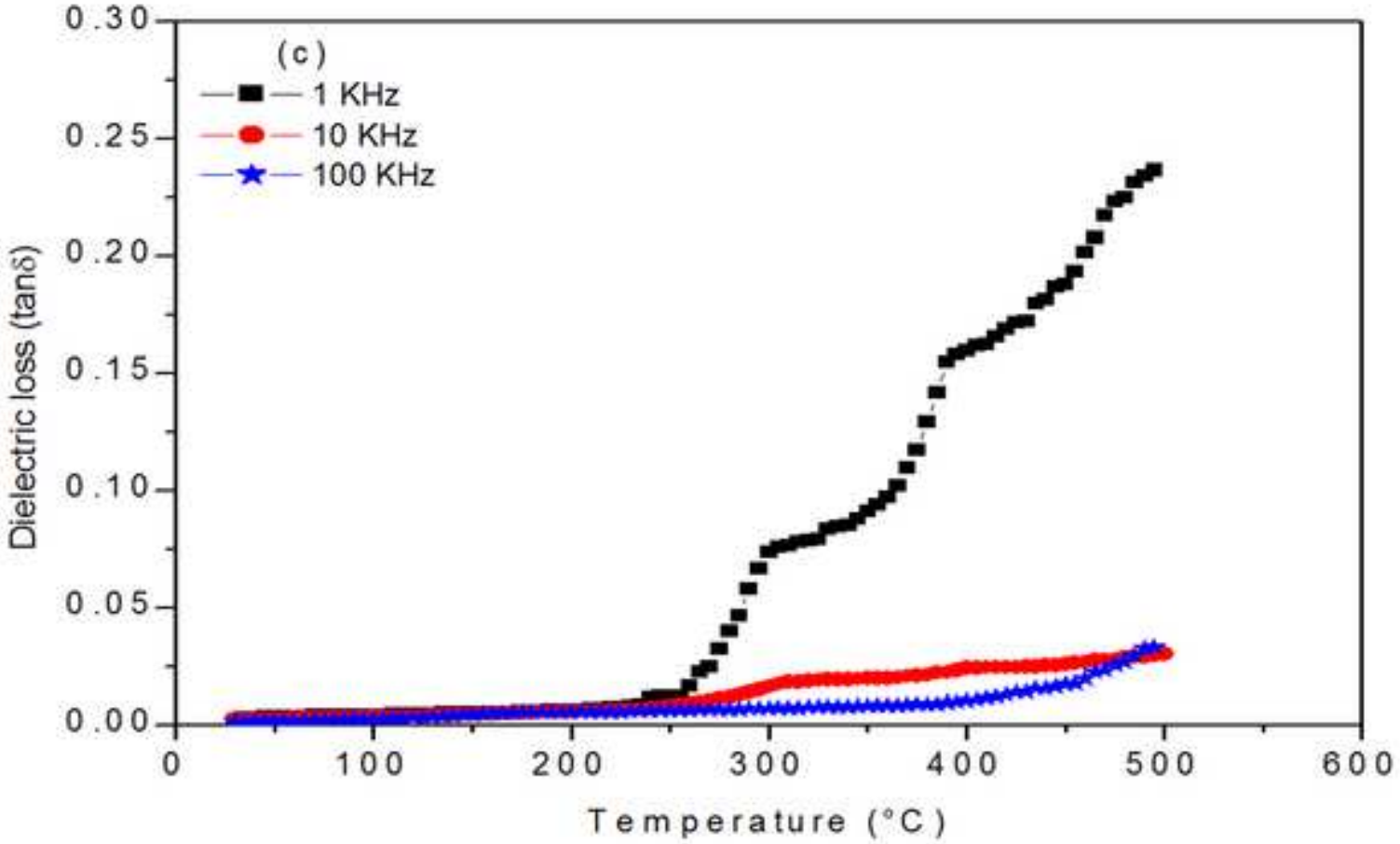

Figure 7
Click here to download high resolution image

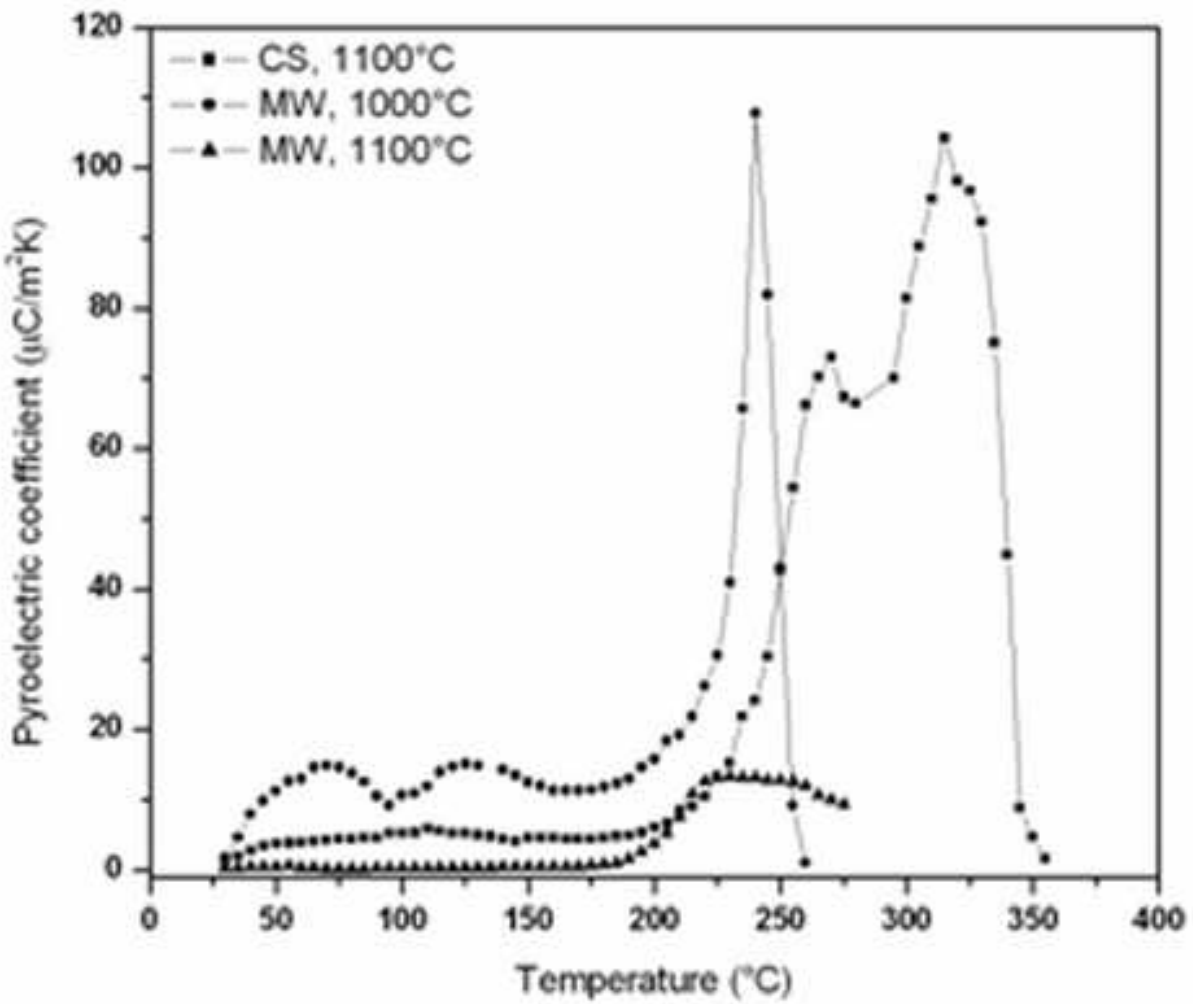

Figure 7

Optics Communications ▮ (▮▮▮▮) ▮▮▮–▮▮▮

Contents lists available at SciVerse ScienceDirect

Optics Communications

journal homepage: www.elsevier.com/locate/optcom

Synthesis and characterization of novel $K_2La_{2-x}Eu_xTi_3O_{10}$ phosphor for blue chip white LEDs

Bhaskar Kumar Grandhe [a,*], Vengala Rao Bandi [a], M Jayasimhadri [b], Kiwan Jang [a], Ho-Sueb Lee [a], Dong-Soo Shin [c], Soung-Soo Yi [d], Jung-Hyun Jeong [e]

[a] Department of Physics, Changwon National University, Changwon, South Korea
[b] Department of Applied Physics, Delhi Technological University, Delhi, India
[c] Department of Chemistry, Changwon National University, Changwon, South Korea
[d] Department of Photonics, Silla University, Busan, South Korea
[e] Department of Physics, Pukyong National University, Busan, South Korea

ARTICLE INFO

Article history:
Received 16 October 2012
Received in revised form
29 November 2012
Accepted 10 December 2012

Keywords:
Optical materials
Sintering
Optical properties

ABSTRACT

Eu^{3+} doped $K_2La_2Ti_3O_{10}$ (KLT) phosphors were prepared by means of conventional solid state reaction method. It has exhibited an intense excitation band at around 466 nm, which matches well to the popular emission line from a GaN based blue light-emitting diode (LED) chip. Using this as an excitation wavelength the Eu^{3+} doped KLT phosphors yielded two strong orange-red emission bands at 595 nm ($^5D_0 \rightarrow {}^7F_1$) and 616 nm ($^5D_0 \rightarrow {}^7F_2$) respectively. The obtained results suggest that Eu^{3+}doped KLT phosphors are useful for blue chip white LEDs. Besides we have studied its dielectric properties along with the other significant characterizations like XRD, SEM and Tg-DTA.

1. Introduction

The increasing demand for fossil fuels and the environmental impact of their use are continuing to exert pressure on an already stretched world energy infrastructure. Energy security is the most important challenge of the 21st century. Lighting is a large fraction of energy consumption. About 22% of electricity consumption is consumed for general illumination. Hence, Lighting is a highly attractive target for reducing energy consumption. Solid-state lighting technology has attracted attention because it offers the potential to save energy and protect the environment by producing light more efficiently. Light Emitting Diodes have been researched as a means to reduce global energy costs due to their efficiency in converting electrical energy into light. LEDs use up to 90% less energy than incandescent bulbs because they emit light by passing electrons across a semiconductor rather than by heating a filament. Conventional incandescent and fluorescent lamps rely on either heat or discharge of gases. Both phenomena are associated with large energy losses that occur because of the high temperatures and large Stokes shifts involved [1–3].

Phosphor-converted white light-emitting diodes (pc-WLEDs) are emerging as an indispensable solid state light source for the next generation lighting industry and display systems due to their unique properties including but not limited to energy savings, environment-friendliness, small volume, and long persistence. The major techniques for fabricating semiconductor-based white-light devices use phosphors to convert UV or blue LED output into longer-wavelength colors to mix to form white light. Nowadays, most commercially available white LEDs are produced on the basis of the combination of yellow phosphor and blue GaN chip. However, the YAG: Ce^{3+} yellow phosphors lack a sufficient red emission component. Therefore, the obtained white light displays a poor color rendering index (CRI) and the efficiency of light conversion is also low. As may be expected, the CRI and light conversion can be greatly improved by combining a small amount of red phosphors with YAG: Ce^{3+} [4,5]. Accordingly, it is an attractive and challenging research task to develop novel, stable, and inorganic RE ions doped red phosphors that can be excited effectively by the near UV or blue LEDs

Ion-exchangeable layered perovskites made up of NbO_6, TiO_6, or TaO_6 octahedra have gained interest in recent years, because of their ion-exchange ability as well as their excellent two-dimensional physical properties, viz., catalytic, ion conductive and luminescence properties. The synthesis of $M_2La_2Ti_3O_{10}$ (M=Li, Na, K) was reported for the first time by Vallino et al. in 1985. $K_2La_2Ti_3O_{10}$ belongs to the Ruddlesden–Popper family having the general formula, A_2' [$A_{n-1}B_nO_{3n+1}$] (A', A=alkali, alkaline

* Corresponding author. Tel.: +82 55 213 3425; fax: +82 55 267 0263.
E-mail addresses:
gncbaskar@gmail.com, gncbaskar@hotmail.com (B.K. Grandhe),
kwjang@changwon.ac.kr (K. Jang).

0030-4018/$ - see front matter © 2012 Elsevier B.V. All rights reserved.
http://dx.doi.org/10.1016/j.optcom.2012.12.020

earth, or rare earth; B=transition metal), has attracted considerable attention due to their unique properties, for example, optical properties, and electrical transport properties and especially its excellent photocatalytic activity [6–9]. As far as our knowledge is concerned, there exists no detailed report on the photoluminescent properties of Eu^{3+} doped $K_2La_2Ti_3O_{10}$ phosphor. Hence, in the present work, Europium ion doped $K_2La_2Ti_3O_{10}$ phosphors were prepared by using conventional solid state reaction method and its structural, micro structural, dielectric and photoluminescent properties were studied and explained appropriately.

2. Experimental

Highly pure and reagent grade chemicals, such as K_2CO_3, La_2O_3, TiO_2 and Eu_2O_3 were used as starting materials. Required chemicals were weighed based on the calculated composition. They were then collected into an agate mortar and grinded with acetone in order to obtain a homogeneous precursor. It was then transferred to an alumina crucible and heated in an electrical furnace from room temperature to different requisite temperatures and with different sintering duration.

The prepared phosphors were characterized by means of a XRD 3003 Seifert diffractometer with a CuK_α line of $\lambda=1.5406$ Å. The data were collected in the 2θ range from 10° to 90° at the rate of 0.05°/s. Their morphology was examined on a JEOL JSEM 840 A Scanning Electron Microscope. The elemental analysis of the synthesized product was carried out using the EDAX attachment to the SEM system. Dielectric properties were carried out on a Phase Sensitive Millimeter (PSM 1700) LCR meter. Photoluminescence spectra of the prepared phosphors were recorded on a Jobin YVON Fluorolog-3 Fluorimeter with a Xe-arc lamp (450 W) as an excitation source.

3. Results and discussion

Fig. 1 shows the XRD profiles of $K_2La_2Ti_3O_{10}$ phosphors sintered at different temperatures and different sintering time. It is well known that the pure phase is favorable for luminescent properties of phosphors. Among all the samples prepared, the XRD pattern of the $K_2La_2Ti_3O_{10}$ phosphor that is sintered at 1000 °C for 24 h is in good agreement with the tetragonal structure reported for the $K_2La_2Ti_3O_{10}$ (JCPDS Card No.82-0209). Hence sintering at 1000 °C for 24 h has been chosen as optimal sintering conditions for preparing europium ions doped $K_2La_2Ti_3O_{10}$ phosphors. The crystallite size of the prepared ceramic powders has been estimated from the Scherer's equation, $D=0.89\,\lambda/\beta\cos\theta$, where D is the crystallite size, λ is the X-ray wavelength (0.15405 nm),θ and β are the diffraction angle and full width at half maximum (FWHM) of an observed peak respectively [10]. Intense diffraction peaks have been selected to compute the crystallite size and it is found to be in an average size of 135 nm. To analyze the effect of europium ion doping on the crystal structure of $K_2La_2Ti_3O_{10}$ host lattice, we have also shown the XRD patterns of 10 mol% Eu^{3+} doped $K_2La_2Ti_3O_{10}$ phosphor. No impurity phase due to Eurpoium ions can be detected in the 10 mol% Eu^{3+} doped $K_2La_2Ti_3O_{10}$ phosphors indicating that the Eu^{3+} ions are completely dissolved in the La^{3+} sites of KLT host lattice. Due to the similar valence and close ionic radii of La^{3+} and Eu^{3+}, it is expected that Eu^{3+} ions would easily occupy the La^{3+} ions sites in the $K_2La_2Ti_3O_{10}$ host lattice.

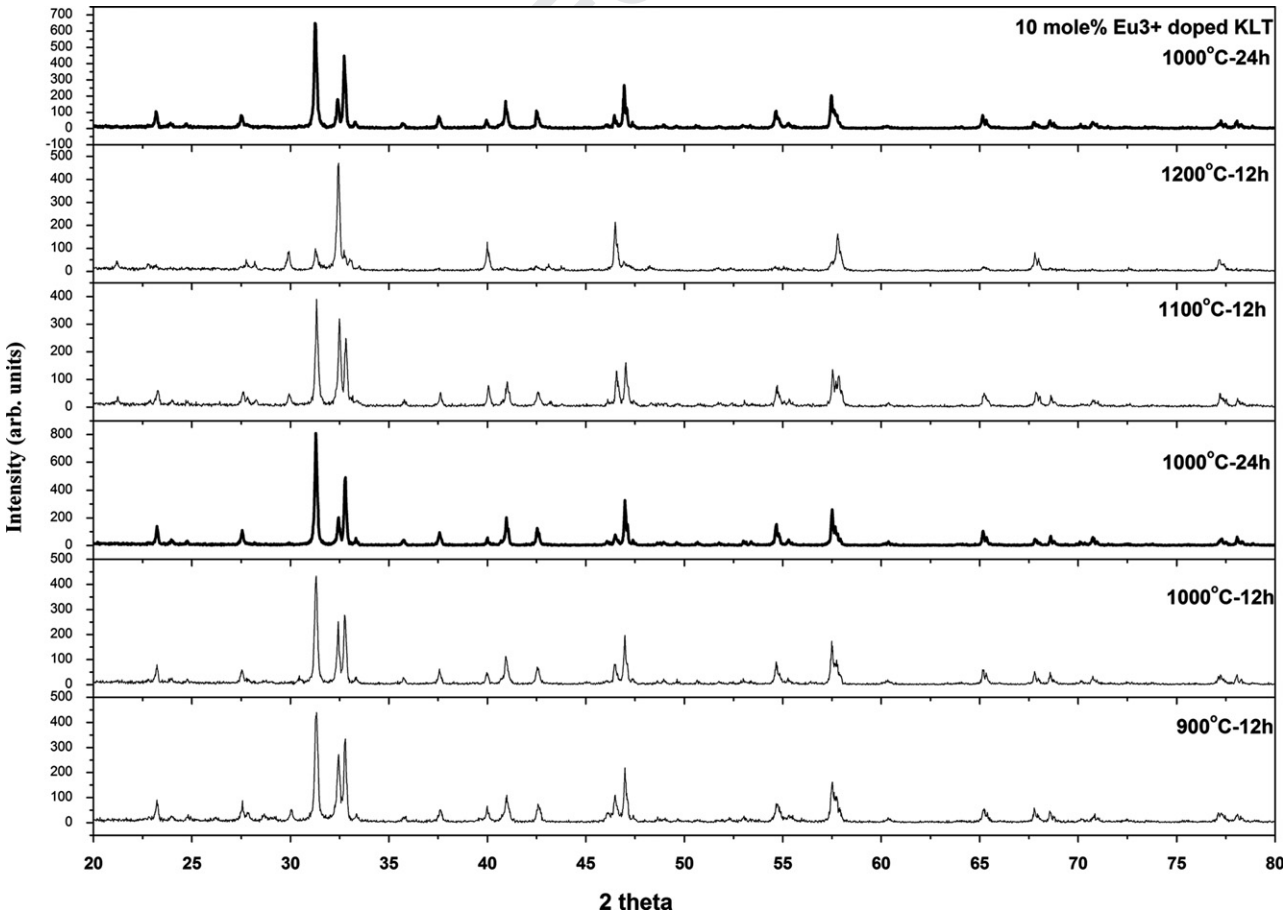

Fig. 1. XRD patterns of $K_2La_2Ti_3O_{10}$ at different sintering criterions.

Please cite this article as: B.K. Grandhe, et al., Optics Communications (2013), http://dx.doi.org/10.1016/j.optcom.2012.12.020

SEM micrograph of the 10 mol% Eu^{3+} doped $K_2La_2Ti_3O_{10}$ sintered at 1000 °C for 24 h is shown in Fig. 2. The obtained micrograph shows that the particles are agglomerated and irregular in shape. Therefore, the average diameter of the grain size has approximately been measured and it is in the range of 1 μm. The narrow widths of the diffraction peaks also indicate that the prepared phosphor powders possess large sized grains [11]. It may be mentioned that crystalline powders in micrometer dimension could display high luminescent intensities [12]. Fig. 3 shows the EDS profile of the 10 mol% Eu^{3+} doped $K_2La_2Ti_3O_{10}$ phosphors sintered at 1000 °C for 24 h. EDS spectrum was measured to confirm the presence of potassium and europium ions in the prepared phosphors and the results revealed its existence. The occurrence of the unassigned carbon peak at 0.2 keV in the EDS spectrum does not belong to the prepared sample, it is due to the carbon tape that was used to hold the specimen during the measurement [11].

For measuring the dielectric constant, pressed cylindrical pellets of 10 mol% Eu^{3+} doped $K_2La_2Ti_3O_{10}$ sintered at 1000 °C for 24 h and later on it was coated on its surface with Silver paste, thereby forming a parallel plate capacitor geometry. The dielectric measurements were performed in the frequency range from 1 Hz to10 MHz. The value of the dielectric constant (ε') of 10 mol% Eu^{3+} doped $K_2La_2Ti_3O_{10}$ was calculated from

$$\varepsilon' = Cd/(\varepsilon_o A)$$

where ε_o is permittivity in vacuum equal to 0.0885 pF/cm^2, C is the capacitance of the specimen, t is the sample thickness and A is the area of the specimen in sq.cm. The dc conductivity was evaluated from the impedance spectroscopy measurement. Fig. 4 shows the variation of dielectric constant (ε') and dielectric loss (tanδ) of the 10 mol% Eu^{3+} doped $K_2La_2Ti_3O_{10}$ powders with frequency at room temperature. It shows that the value of dielectric constant is very high at lower frequency and decreases with increasing frequency which indicates the normal behavior of a dielectric/ferroelectric [13]. The higher values of dielectric constant at lower frequency suggest the presence of all types of polarizations (i.e. interfacial, atomic, dipolar, ionic and electronic) [14]. At higher frequencies, the main contribution of dielectric constant comes from electric polarization, as some of the polarizations become ineffective, and thus, the value of dielectric constant decreases with increasing frequency [15]. The dielectric loss (tanδ) curve a peak was observed at 33.5 KHz indicating the presence of some relaxation species even at room temperature [16]. The complex impedance spectrum (Z′ vs. Z″) was analyzed using Cole–Cole plots. Fig. 5 shows the complex impedance

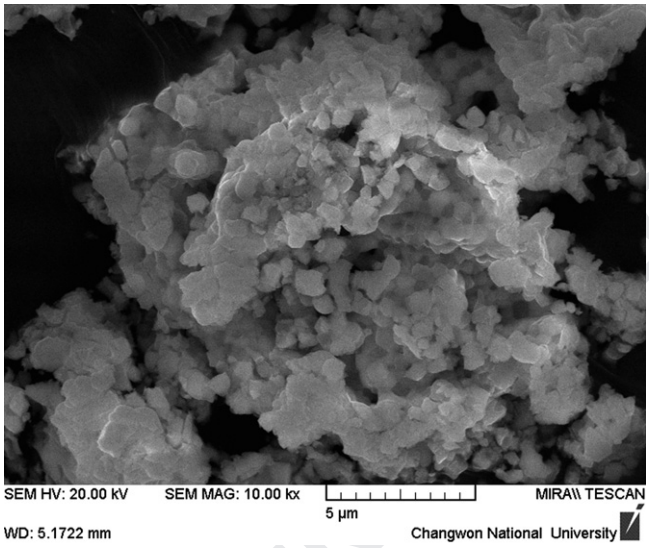

Fig. 2. SEM photograph of 10 mol% Eu^{3+} doped $K_2La_2Ti_3O_{10}$ phosphor sintered at 1000 °C for 24 h.

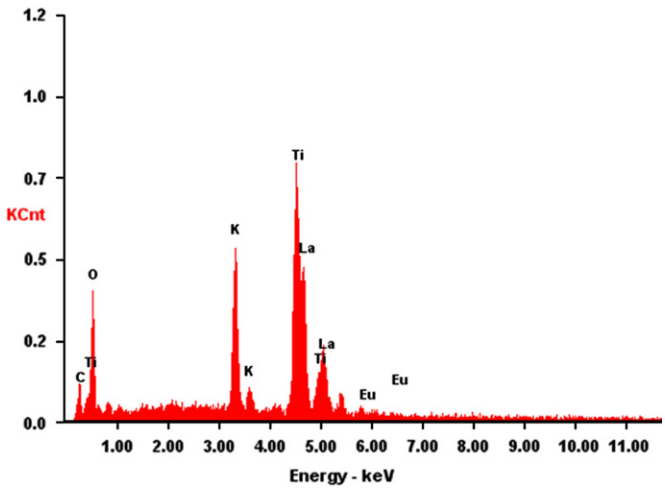

Fig. 3. EDS profile of 10 mol% Eu^{3+} doped $K_2La_2Ti_3O_{10}$ phosphor sintered at 1000 °C for 24 h.

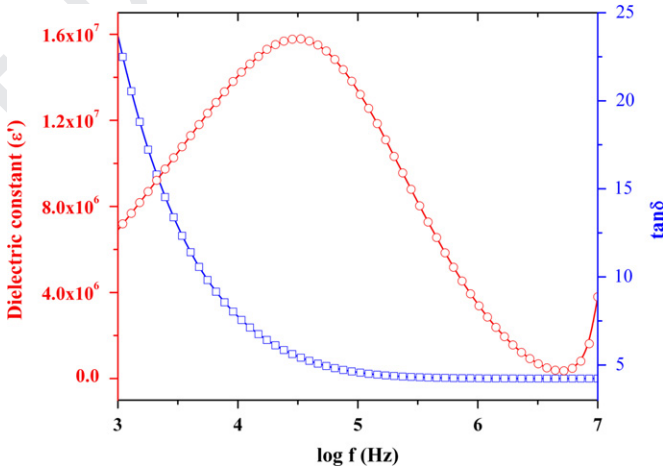

Fig. 4. Variation of dielectric constant (ε') and dielectric loss (tanδ) of the 10 mol% Eu^{3+} doped $K_2La_2Ti_3O_{10}$ phosphor with frequency at room temperature.

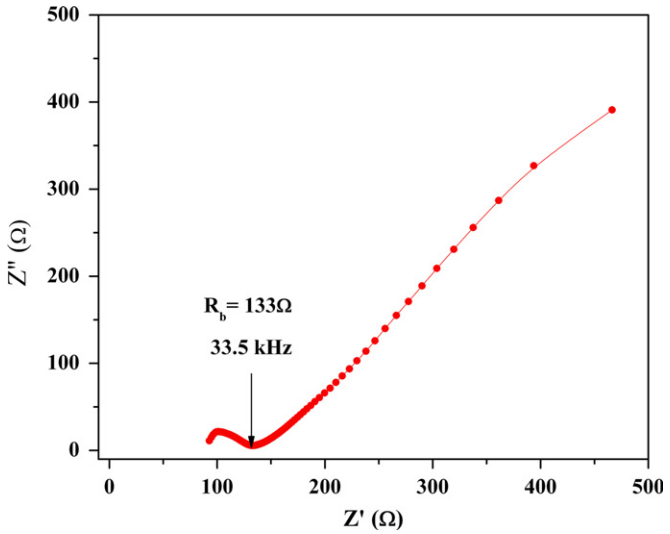

Fig. 5. Complex impedance spectrum (Z′ vs. Z″) of 10 mol% Eu^{3+} doped $K_2La_2Ti_3O_{10}$ phosphor at room temperature.

spectrum (Z′ vs. Z″) of 10 mol% Eu^{3+} doped $K_2La_2Ti_3O_{10}$ at room temperature. Single arc have been observed in a wide frequency range (1 kHz–10 MHz). This indicates that the electrical properties of the material arise mainly due to the bulk effects. The dc conductivity of the 10 mol% Eu^{3+} doped $K_2La_2Ti_3O_{10}$ ceramic powder was determined from the bulk resistance (the diameter of the semicircle) and geometrical factors (the thickness and the electrode area) using the formula $\sigma_{dc}=d/(R_bA)$. Where d is thickness of the sample, R_b is the bulk resistance of the material and A is area of the electrode. The calculated dc conductivity of the $K_2La_2Ti_3O_{10}$ was 3.07×10^{-6} Scm^{-1}. No significant diversifications were noticed in the case of other samples prepared and hence for the sake of clear understanding, we have only shown and discussed the FE-SEM images, EDS and dielectric spectral profiles of 10 mol% Eu^{3+} doped $K_2La_2Ti_3O_{10}$ phosphors alone.

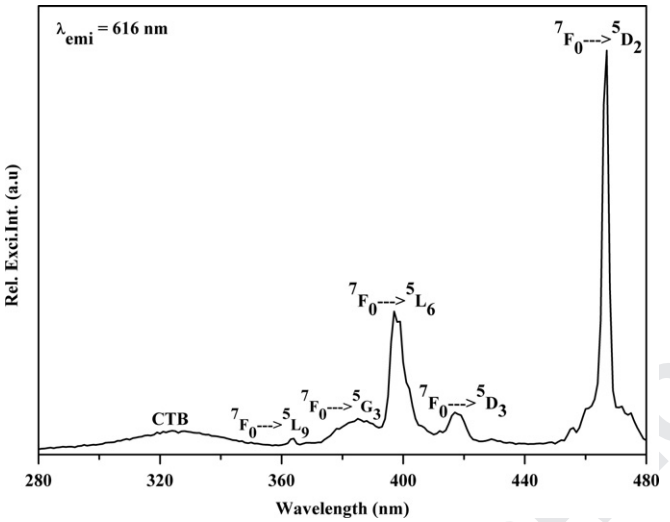

Fig. 6. Excitation spectrum of 10 mol% Eu^{3+} doped $K_2La_2Ti_3O_{10}$ phosphor sintered at 1000 °C for 24 h.

The excitation spectrum of 10 mol% Eu^{3+} ions doped $K_2La_2Ti_3O_{10}$ phosphors (KLT: Eu^{3+}) by monitoring $^5D_0\rightarrow{}^7F_2$ (λ_{em}=616 nm) emission is shown in Fig. 6. It can be seen clearly that the excitation spectrum consists of a tiny broad band and a group of sharp peaks in the visible and UV region. The broad band aroused between 280 nm and 350 nm can be ascribed to the charge transfer (CT) band of Eu^{3+}–O^{2-}, which also usually appears in the range 225–350 nm. The CT band corresponds to the electronic transition from the 2p orbital of O^{2-} to the 4f orbital of Eu^{3+} and is related to the covalency of O^{2-}–Eu^{3+} and coordination environment around Eu^{3+} [17,18]. The other bands that are located at 363 nm, 383 nm, 398 nm, 417 nm and 467 nm are assigned to the electronic transitions of $^7F_0\rightarrow{}^5L_9$, $^7F_0\rightarrow{}^5G_3$, $^7F_0\rightarrow{}^5L_6$, $^7F_0\rightarrow{}^5D_3$ and $^7F_0\rightarrow{}^5D_2$ transitions respectively [19]. Among all the excitation bands that occurred for KLT: Eu^{3+} phosphor, the excitation band at 466 nm is dominant and more intense. The energy levels of trivalent lanthanides are weakly affected by ligand ions in the crystals because their 4f electrons are shielded by the external electric fields of the outer $5s^25p^6$ electrons. Therefore, the optical spectra of most phosphors with the same lanthanide doping are similar. However, some transitions are hypersensitive to the crystal environment. The emission spectra of 10 mol% Eu^{3+} ions doped $K_2La_2Ti_3O_{10}$ phosphors measured with excitation wavelengths namely (a) 466 nm and (b) 398 nm were shown in Fig. 7. The intense emission bands in the range of 570–700 nm are assigned to the electronic transitions of ($^5D_0\rightarrow{}^7F_{J=1,2,3,4}$) and the transitions such as $^5D_0\rightarrow{}^7F_{2,4,6}$ transitions are electric dipole (ED) transitions. Among them, $^5D_0\rightarrow{}^7F_2$ has been a hypersensitive transition that follows the selection rule of $\Delta J=2$ and hence it demonstrates a bright red emission from Eu^{3+} doped $K_2La_2Ti_3O_{10}$ phosphors. The other emission bands at 579 nm, 590 nm, 650 nm and 704 nm are assigned to $^5D_0\rightarrow{}^7F_0$, $^7F_1$, $^7F_3$ and $^7F_4$ transitions respectively [20]. The electric dipole transition $^5D_0\rightarrow{}^7F_2$ is strongly influenced by the coordination environment; whereas the magnetic dipole transition $^5D_0\rightarrow{}^7F_1$ is insensitive to that. The electric dipole emission around 610–630 nm, much stronger than the magnetic dipole transition centered at 595 nm, is induced by the lack of inversion symmetry at the Eu^{3+} site. In the present study we had prepared six different concentrations

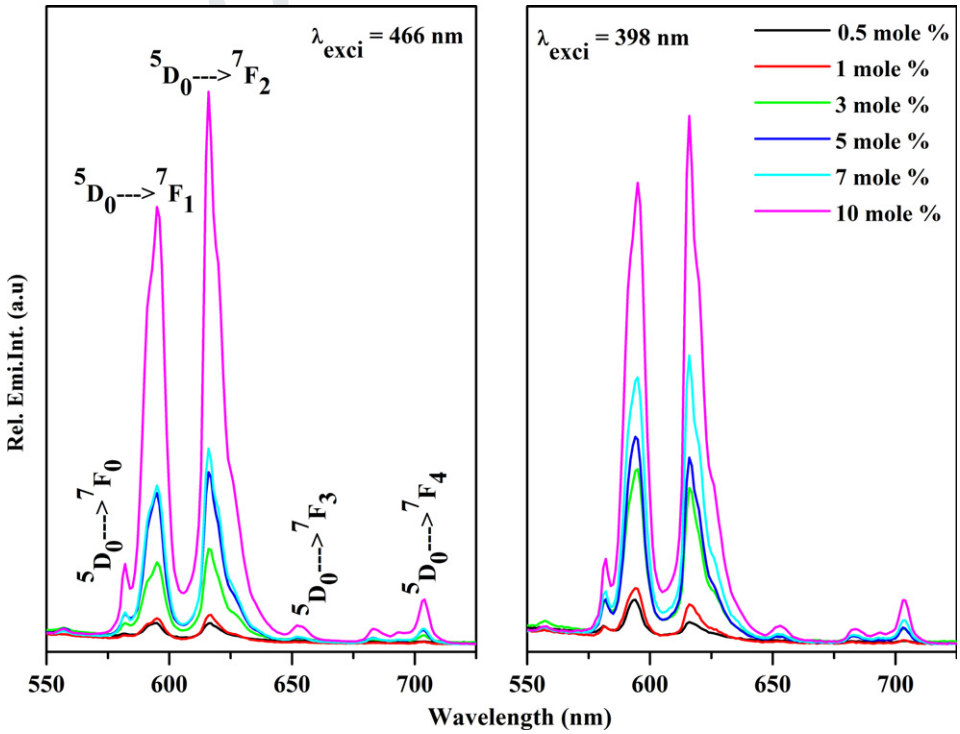

Fig. 7. Emission Spectra of Eu^{3+} doped $K_2La_2Ti_30_{10}$ phosphors sintered at 1000 °C for 24 h with varying europium ion concentrations.

Please cite this article as: B.K. Grandhe, et al., Optics Communications (2013), http://dx.doi.org/10.1016/j.optcom.2012.12.020

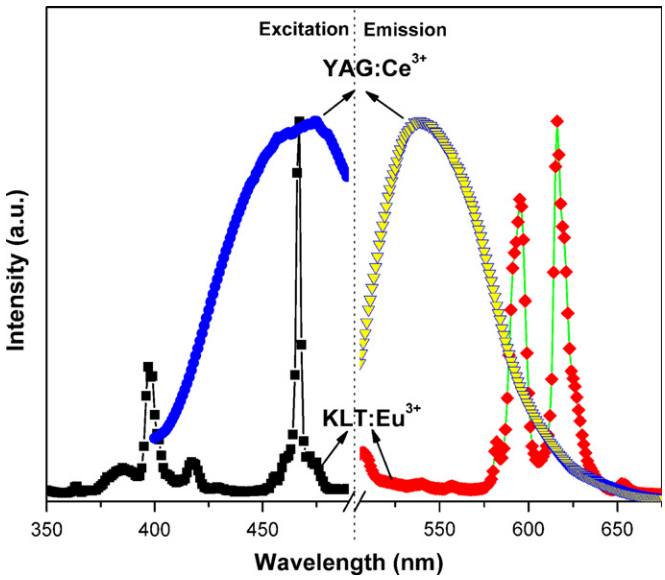

Fig. 8. Typical photoluminescence spectra of Eu^{3+} doped $K_2La_2Ti_3O_{10}$ and standard YAG: Ce^{3+} phosphors.

starting from 0.05 mol% to 10 mol%. But we did not observed the concentration quenching phenomenon when the europium ion concentration was up to 10 mol%.

The Photoluminescence spectra of the optimized KLT: Eu^{3+} phosphor with that of standard YAG: Ce^{3+} have been shown in Fig. 8. The YAG: Ce^{3+} phosphor can be effectively excited by the 470 nm blue light and emits strong yellow emission at 540 nm. However, YAG: Ce^{3+} does not almost absorb n-UV ($\approx$ 400 nm), and its emission is silent under the 400 nm light irradiation. The white light realized by the combination with a blue LED exhibits a poor color rendering index due to the lack of red color component. Hence, the orange or red color objects appear dim or color less under this light. In the present investigation, the emission of KLT: Eu^{3+} phosphor occurs at a fairly longer wavelength in the orange and red spectral region under the excitation wavelength of 468 nm, which perfectly matches with the emission wavelength of blue LEDs. These results suggest that the KLT: Eu^{3+} phosphor can efficiently absorb the emission of blue GaN LED and it can also emit strong orange reddish color. Thus, the prepared KLT: Eu^{3+} phosphor can be used to compensate the red color deficiency of YAG: Ce^{3+} based white LEDs. In general, color is represented by means of color coordinates. The chromaticity diagram established by the Commission Internationale de l'Eclairage (CIE) in 1931 is a two dimensional graphical representation of any color perceivable by the human eye on an x–y plot. Hence, in our present work, the chromaticity coordinates of 10 mol% Eu^{3+} ions doped $K_2La_2Ti_3O_{10}$ phosphors with blue light excitation has been calculated from the emission spectrum and its color coordinates are found to be having a numerical value of (x=0.642, y=0.356).

4. Conclusion

In summary, a novel red phosphor namely $K_2La_{2-x}Eu_xTi_3O_{10}$ phosphors were prepared by conventional solid state reaction method. Optimal sintering criterion was determined to be 1000 °C for 24 h. The synthesized phosphors showed intense orange reddish emission in the region 580–710 nm corresponding to the $^5D_0 \rightarrow {}^7F_{0,1,2,3,4}$ transitions of Eu^{3+} with 468 nm and 398 nm excitations. We have thoroughly characterized the prepared material by means of XRD, FE-SEM, EDS and dielectric measurements. Based on the obtained results, it can be concluded that the Eu^{3+}doped KLT phosphors are useful for blue chip based WLED applications.

Acknowledgments

This work was supported by the Priority Research Centers Program through the National Research Foundation of Korea funded by the Ministry of Education, Science and Technology (NRF-2010-0029634) and also this work was partially supported by the National Research Foundation of Korea funded by the Korean government (NRF-2010-0023034).

References

[1] X. Fang, M. Roushan, R. Zhang, J. Peng, H. Zeng, J. Li, Chemistry of Materials 24 (2012) 1710.
[2] S. Ye, F. Xiao, Y.X. Pan, Y.Y. Ma, Q.Y. Zhang, Materials Science & Engineering 71 (2010) 1.
[3] E.F. Schubert, J.K. Kim, H. Luo, J. Xi, Reports on Progress in Physics 69 (2006) 3069.
[4] V.R. Bandi, M. Jayasimhadri, J. Jeong, K. Jang, H.S. Lee, S.S. Yi, J.H. Jeong, Journal of Physics D: Applied Physics 43 (2010) 395103.
[5] X. Zhang, A. Marathe, S. Sohal, M. Holtz, M. Davis, L.J. Hope-Weeks, J. Chaudhuri, Journal of Materials Chemistry 22 (2012) 6485.
[6] K. Todal, J. Watanabe, M. Sate, Materials Research Bulletin 31 (1996) 1427.
[7] Y. Huang, J. Wu, Y. Wei, J. Lin, M. Huang, Journal of Alloy Compound 456 (2008) 364.
[8] Y. Yang, Q. Chen, Z. Yin, J. Li, Journal of Alloys and Compounds 488 (2009) 364.
[9] A. Kudo, T. Sakata, The Journal of Physical Chemistry 99 (43) (1995) 15963.
[10] B.K. Grandhe, V.R. Bandi, K. Jang, S. Kim, D. Shin, Y. Lee, J. Lim, T. Song, Journal of Alloys and Compounds 509 (2011) 7937.
[11] B.K. Grandhe, S. Ramaprabhu, S. Buddhudu, K. Sivaiah, V.R. Bandi, K. Jang, Optics communications 285 (2012) 1194.
[12] V.R. Bandi, B.K. Grandhe, M. Jayasimhadri, K. Jang, H.S. Lee, S.S. Yi, J.H. Jeong, Journal of Crystal Growth 326 (2011) 120.
[13] M.A. Gabal, S.A. Hameed, A.Y. Obaid, Materials Characterization 71 (2012) 87.
[14] R. Palai, R.N.P. Choudhary, H.S. Tewari, Journal of Physics and Chemistry of Solids 62 (2001) 695.
[15] A. Shukla, R.N.P. Choudhary, A.K. Thakur, D.K. Pradhan, Physica B-Condensed Matter 405 (2010) 99.
[16] B. Tiwari, R.N.P. Choudhary, Physica B-Condensed Matter 404 (2009) 4111.
[17] C. Zhao, X. Yin, F. Huang, Y. Hang, Physica B-Condensed Matter 406 (2011) 4608.
[18] H.K. Yang, J.H. Jeong, Journal of Physical Chemistry C 114 (2010) 226.
[19] V.R. Bandi, B.K. Grandhe, K. Jang, H.S. Lee, D.S. Shin, S.S. Yi, J.H. Jeong, Journal of Alloys and Compounds 512 (2012) 264.
[20] V.R. Bandi, B.K. Grandhe, H. Woo, K. Jang, D. Shin, S.S. Yi, J. Jeong, Journal of Alloys and Compounds 538 (2012) 85.

VOLTAGE MODE OTRA MOS-C SINGLE INPUT MULTI OUTPUT BIQUADRATIC UNIVERSAL FILTER

Rajeshwari PANDEY[1], *Neeta PANDEY*[1], *Sajal Kumar PAUL*[2], *Ajay SINGH*[1], *Balamurali SRIRAM*[1], *Kaushlendra TRIVEDI*[1]

[1]Department of Electronics and Communication Engineering, Delhi Technological University, Main Bawana Road 42, Delhi, 110 042, India
[2]Department of Electronics Engineering, Indian School of Mines, Dhanbad, 826 004, Jharkhand, India

rajeshwaripandey@gmail.com, neetapandey06@gmail.com, sajalkpaul@rediffmail.com, ajaysingh1990.ece@gmail.com , sriram1990dce.ec@gmail.com , kaushaltr.dce@gmail.com

Abstract. *In this paper, an Operational transresistance amplifier (OTRA) based MOS-C voltage mode single input multi output (SIMO) biquadratic universal filter configuration is proposed. The configuration is made fully integrated by implementing the resistors using matched transistors operating in the linear region. It exhibits the feature of orthogonal controllability of angular frequency and quality factor through gate bias voltage. The non-ideality analysis of the circuit is also given. Workability of the universal filter is demonstrated through PSPICE simulations using 0,5 μm CMOS process parameters provided by MOSIS (AGILENT).*

Keywords

Analog signal processing, OTRA, SIMO, universal filter.

1. Introduction

Recently the OTRA has emerged as an alternate analog building block since it inherits all the advantages offered by current mode techniques. The OTRA is a high gain current input voltage output device. The input terminals of OTRA are internally grounded, thereby eliminating response limitations due to parasitic capacitances and resistances at the input. Several high performance CMOS OTRA topologies have been proposed in literature [1], [2], [3], [4], [5] leading to growing interest in OTRA based analog signal processing circuits. In the recent past, OTRA has been extensively used as an analog building block for realizing a number of analog signal processing and generation circuits such as immittance simulators [6], [7], [8], [9], oscillators [10], [11] multivibrators [12], [13] and filters [1], [14], [15], [16], [17], [18], [19], [20], [21], [22]. Many voltage-mode biquadratic filters using OTRA were proposed in the literature that can be classified as single input and single output (SISO) [1], [13], [14], [15], [16] multi-input single output (MISO) [17], [18], [19], and single input multi output (SIMO) [1], [20]. However, only one standard filter function can be obtained at a time in each filter realization of SISO and MISO category. In SIMO configuration with only one input, multiple filter functions may be obtained simultaneously. A detailed comparison of these structures is given in Tab. 1 which reveals that no OTRA based SIMO structure is available in the literature that provides all five standard responses simultaneously. In this paper, a voltage-mode OTRA MOS-C universal biquadratic SIMO filter based on ref. [1] is presented which realizes all the standard filter functions; namely lowpass, highpass, bandpass, notch and allpass, simultaneously. The proposed structure puts no restriction on the input signal in contrast to the structures reported in [18], [19], [20]. Additionally the earlier reported structures require either change of component type [14], [17]or removal of components [1], [22] for realizing various filter responses. However, the proposed circuit does not require a change in component type/ removal of components. It simply poses matching condition on component values for notch and all pass responses. The proposed OTRA MOS-C universal biquadratic SIMO filter employs five OTRAs, twelve resistors and two capacitors. It also enjoys the feature of orthogonal controllability of angular frequency, quality factor and filter gain. All resistors are implemented using MOS transistors operating in the linear region. This not only makes filter electronically tunable but also consumes less chip area. The function of proposed filter has been confirmed by SPICE simulations.

2. Circuit Description

OTRA is a three terminal device, shown symbolically in Fig. 1. Its port relations are characterized by the

Tab.1: Comparison of the proposed work with the previously reported work.

Ref.	No. of inputs	Simultaneous Outputs	Standard filter functions available	Condition		No. of OTRA	No. of passive components (C/R)
				On Input Signal	On component Selection		
[1]	One	Two Three One	LP,BP LP,HP,BP LP,HP,BP,NF,AP	No No No	No No Yes	Two Three Two	Two / Four Two / Six Two / Five
[14]	One	One	LP,HP,BP,NF,AP	No	Yes	One	LP: Two /Three HP: Three/ Two BP: Two / Two NF,AP: Three/ Three
[15]	One	One	LP, BP	No	No	Two	Two / Four
[16]	One	One	AP	No	No	One	First order AP: One/Three Second order AP: Two / Four
[17]	One	One	AP,BR	No	Yes	One	1st order AP: One/three or Two/Two; 2nd order AP,NF: Three / Three
[18]	four	One	LP,HP,BP,NF,AP	Yes	Yes	Two	Topology1:Five/Four Topology2:Six/Four
[19]	Three	One	LP,HP,BP,NF,AP	Yes	Yes	One	Four/Four
[20]	Two	One	LP,HP,BP,NF	Yes	No	Two	Three/Four
[21]	One	Three	LP,HP,BP	No	No	Three	Two/Six
[22]	One	One	LP,HP,BP,NF,AP	No	Yes	Three	Two/Eight
Proposed work	One	Five	LP,HP,BP,NF,AP	No	Yes	Five	Two/Twelve

following matrix.

$$\begin{bmatrix} V_p \\ V_n \\ V_O \end{bmatrix} = \begin{bmatrix} 0 & 0 & 0 \\ 0 & 0 & 0 \\ R_m & -R_m & 0 \end{bmatrix} \begin{bmatrix} I_p \\ I_n \\ I_O \end{bmatrix}. \quad (1)$$

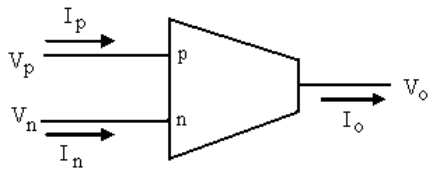

Fig. 1: OTRA circuit symbol.

For ideal operations, the transresistance gain R_m of OTRA approaches infinity and forces the input currents to be equal. Thus, OTRA must be used in a negative feedback configuration. The proposed filter is shown in Fig. 2. Routine analysis of the circuit of Fig. 2 results in the following transfer functions:

$$\frac{V_{01}}{V_{in}} = \frac{s^2 G_1 C_1 C_2}{D(s)}, \quad (2)$$

$$\frac{V_{02}}{V_{in}} = \frac{sG_1 G_4 C_2}{D(s)}, \quad (3)$$

$$\frac{V_{03}}{V_{in}} = \frac{G_1 G_4 G_6}{D(s)}, \quad (4)$$

$$\frac{V_{04}}{V_{in}} = \frac{\frac{G_7}{G_9} s^2 G_1 C_1 C_2 + \frac{G_8}{G_9} G_1 G_4 G_6}{D(s)}, \quad (5)$$

$$\frac{V_{05}}{V_{in}} = \frac{G_1}{D(s)} \cdot \left(\frac{G_{11}}{G_{12}} \left(\frac{G_7}{G_9} s^2 C_1 C_2 + \frac{G_8}{G_9} G_4 G_6 \right) - \frac{G_{10}}{G_{12}} s G_4 C_2 \right), \quad (6)$$

where $D(s) = s^2 G_3 C_1 C_2 + s G_4 G_5 C_2 + G_2 G_4 G_6$.

Equations (2)–(4) clearly indicate that high pass, band pass, low pass responses are available at V_{01}, V_{02}, and V_{03} respectively. Band reject response is available at V_{04} as given in (5), with BR gain (G_{BR}) =G_1/G_3, if

$$G_7 = G_9, \; G_1 G_8 = G_2 G_9. \quad (7)$$

An allpass response is available at V_{05}, as expressed in (6) with allpass gain (G_{AP}) = G_1/G_3, if

$$G_1 G_{10} = G_5 G_{12}, G_7 G_{11} = G_9 G_{12}, G_1 G_8 G_{11} = G_2 G_9 G_{12}. \quad (8)$$

The high pass gain (G_{HP}), band pass gain (G_{BP}) and the low pass gain (G_{LP}) are respectively given by

$$G_{HP} = G_1 / G_3, G_{BP} = G_1 / G_5, G_{LP} = G_1 / G_2. \quad (9)$$

The resonant angular frequency (ω_0) and the quality factor (Q_0) are given by:

$$\omega_0 = \sqrt{\frac{G_2 G_4 G_6}{C_1 C_2 G_3}}, \quad (10)$$

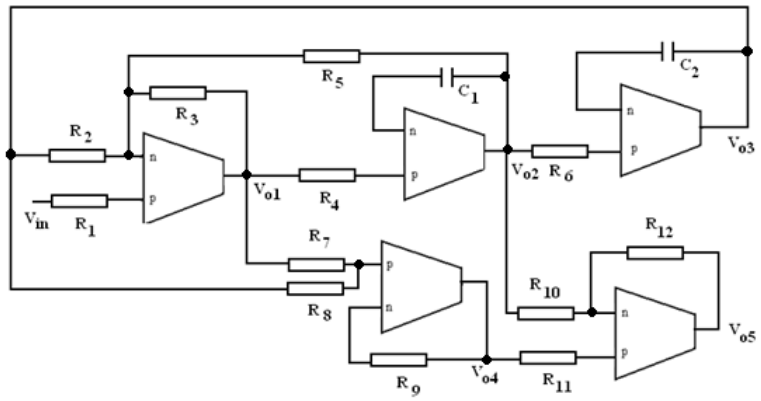

Fig. 2: Proposed biquadratic universal filter.

$$Q_0 = \frac{1}{G_5}\sqrt{\frac{G_2G_3G_6C_1}{C_2G_4}}\,. \tag{11}$$

This suggests that the Q_0 can be independently controlled by varying R_5 without affecting the ω_0. It can be noted from (10) that simultaneous adjustment of R_2 and R_4 results in orthogonal tuning of ω_0. Also, the filter gain can be controlled through R_1 without affecting ω_0 and Q_0.

The sensitivities of ω_0 and Q_0 with respect to each passive component are low and obtained as

$$S_{R2}^{\omega_0} = S_{R4}^{\omega_0} = S_{R6}^{\omega_0} = \frac{1}{2}, S_{R3}^{\omega_0} = S_{C1}^{\omega_0} = S_{C2}^{\omega_0} = -\frac{1}{2}\,. \tag{12}$$

$$S_{R5}^{Q_0} = -1, S_{R2}^{Q_0} = S_{R3}^{Q_0} = S_{R6}^{Q_0} = S_{C1}^{Q_0} = \frac{1}{2},$$

$$S_{C2}^{Q_0} = S_{R4}^{Q_0} = -\frac{1}{2}\,. \tag{13}$$

It is well known that the linear passive resistor consumes a large chip area as compared to the linear resistor implementation using transistors operating in the linear region. The differential input of OTRA allows the resistors connected to the input terminals of OTRA to be implemented using MOS transistors with complete non-linearity cancellation [1]. Figure 3 shows a typical MOS implementation of resistance connected between negative input and output terminals of OTRA. The resistance value may be adjusted by appropriate choice of gate voltages thereby making filter parameters electronically tunable. The value of resistance so obtained is expressed as

$$R = \frac{1}{\mu_n C_{ox}(W/L)(V_a - V_b)}\,, \tag{14}$$

where μ_n, C_{ox}, W and L are electron mobility, oxide capacitance per unit gate area, effective channel width, and effective channel length of MOS respectively which may be expressed as

$$\mu_n = \frac{\mu_0}{1+\theta(V_{GS} - V_T)}\,, \tag{15}$$

$$C_{ox} = \varepsilon_{ox}/T_{ox}\,, \tag{16}$$

$$W = W_{drawn} - 2WD\,, \tag{17}$$

$$L = L_{drawn} - 2LD\,. \tag{18}$$

V_a and V_b are the gate voltages and other symbols have their usual meaning. Figure 4 shows the MOS-C implementation of the circuit of Fig. 2.

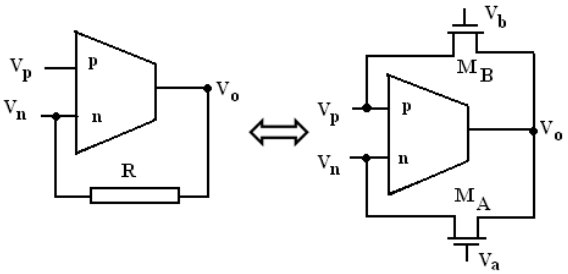

Fig. 3: MOS implementation of a linear resistance connected between negative terminal and the output.

3. Non-Ideality Analysis

The response of the filter may deviate due to non-ideality of OTRA in practice. Ideally the trans-resistance gain R_m is assumed to approach infinity. However, practically R_m is a frequency dependent finite value. Considering a single pole model for the trans-resistance gain, R_m can be expressed as

$$R_m(s) = \left(\frac{R_0}{1+s/\omega_0}\right), \tag{19}$$

where R_0 is low frequency transresistance gain. For high frequency applications, the transresistance gain, $R_m(s)$ reduces to

$$R_m(s) \approx \frac{1}{sC_p} \quad where \quad C_p = \frac{1}{R_0\omega_0}\,. \tag{20}$$

Taking this effect into account the transfer functions of the circuit of Fig. 3 modify to

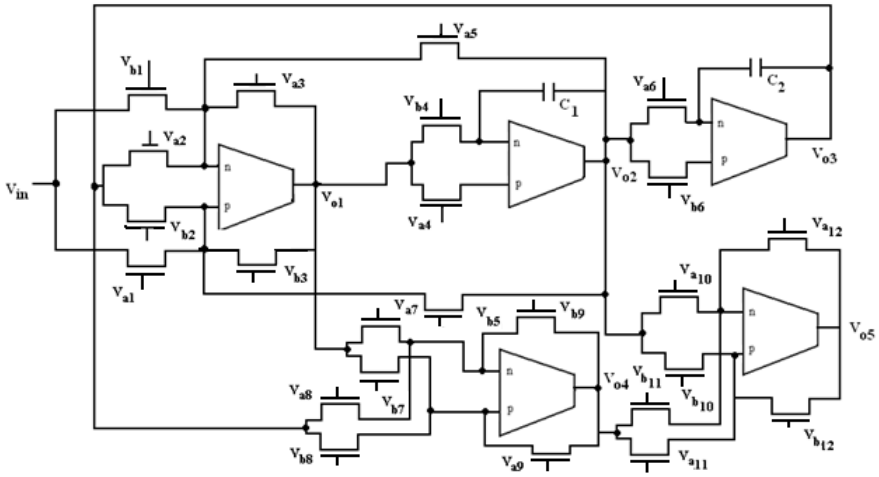

Fig. 4: OTRA MOS-C universal filter.

$$\left.\frac{V_{01}}{V_{in}}\right|_n = \frac{s^2 G_1 (C_1 + C_p)(C_2 + C_p)}{D_n(s)}, \quad (21)$$

$$\left.\frac{V_{02}}{V_{in}}\right|_n = \frac{sG_1 G_4 (C_2 + C_p)}{D_n(s)}, \quad (22)$$

$$\left.\frac{V_{03}}{V_{in}}\right|_n = \frac{G_1 G_4 G_6}{D_n(s)}, \quad (23)$$

$$\left.\frac{V_{04}}{V_{in}}\right|_n = \frac{G_1}{D_n(s)(G_9 + sC_p)} * \frac{}{(s^2 G_7 (C_1 + C_p)(C_2 + C_p) + G_4 G_6 G_8)}, \quad (24)$$

$$\left.\frac{V_{05}}{V_{in}}\right|_n = \frac{G_1}{D_n(s)(G_{12} + sC_p)} * \left((C_2 + C_p)(As^2 (C_1 + C_p) - G_4 G_{10}) + \frac{G_4 G_6 G_8 G_{11}}{(G_9 + sC_p)} \right), \quad (25)$$

where $A = \frac{G_7 G_{11}}{G_9 G_1}$ and

$$D_n(s) = s^2 (G_3 + sC_p)(C_1 + C_p)(C_2 + C_p) + sG_4 G_5 (C_2 + C_p) + G_2 G_4 G_6. \quad (26)$$

The effect of C_p can be eliminated by pre-adjusting the value of capacitors C_1 and C_2 and thus achieving self-compensation. The sC_p term appearing in parallel to G_i for i = 3, 9, 12 will result in the introduction of another pole having radian frequency as $\omega = 1/R_i C_p$. The smallest frequency of this newly introduced pole would occur for the largest value of R_i. The effect of this additional pole can be ignored by selecting the operating frequency range of the SIMO biquadratic universal filter much lower than pole frequency.

4. Simulation Results

The proposed SIMO biquadratic universal filter is verified through simulations using the CMOS implementation of the OTRA [3] as given in Fig. 5. The SPICE simulation was performed using 0,5 µm CMOS process parameters provided by MOSIS (AGILENT). Supply voltages taken are ±1,5 V. Aspect ratios for different transistors used in OTRA are given in Tab. 2. For simulations L_{drawn} and W_{drawn} are taken as 5 µm for all transistors used for resistance realization.

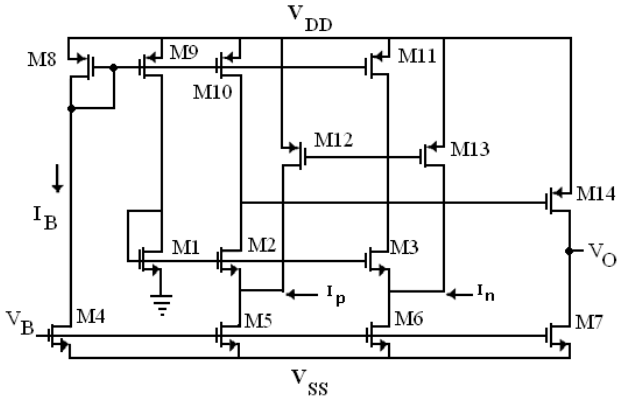

Fig. 5: CMOS implementation of OTRA [3].

Tab.2: Aspect ratio of transistors used in OTRA.

Transistor	W(µm)/L(µm)
M1-M3	100/2,5
M4	10/2,5
M5,M6	30/2,5
M7	10/2,5
M8-M11	50/2,5
M12,M13	100/2,5
M14	50/0,5

The proposed SIMO biquadratic universal filter as given in Fig. 4 is designed for the resonant frequency (f_0) of 120 kHz and Q_0=1 with component values C_1=C_2=100 pF and $R_i \approx 10{,}5$ kΩ for i = 1, 2, . . . 12.

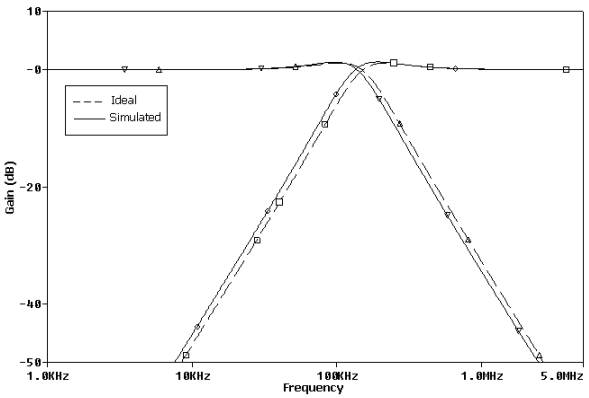

(a)

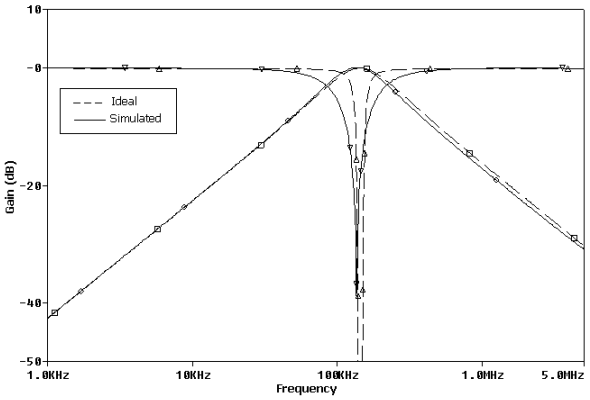

(b)

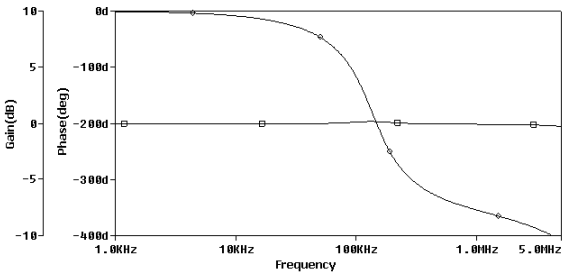

(c)

Fig. 6: Simulated frequency responses of the proposed circuit (a) low-pass and high-pass, (b) band-pass and notch, (c) all pass.

The value of R_i was set by taking the gate voltages as $V_{ai} = 1{,}4$ V and $V_{bi} = 0{,}75$ V for all i = 1, 2,. . . , 12. Figure 6 shows the simultaneously available frequency responses for low-pass, high-pass, band-pass, notch and allpass. The simulated resonant frequency is found to be in close agreement to the theoretical value. The orthogonal tunability of Q_0 with R_5 at $f_0 = 11{,}5$ kHz is shown in Fig. 7. This is obtained by selecting $C_1 = C_2 = 50$ pF, and $R_i = 272$ kΩ for i = 1,…, 4, 6,…,12 for different values of R_5. The values of Q_0 as obtained and gate bias voltages used for tuning of R_5 are listed in Tab. 3.

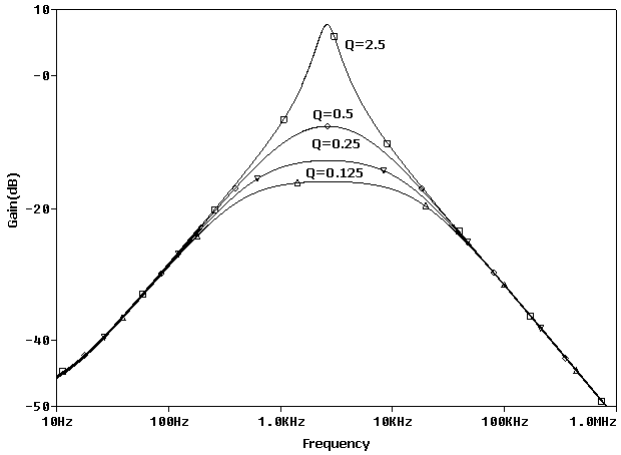

Fig. 7: Band-pass response for different Q_0 values.

Tab.3: Component values used for orthogonal tunability of Q_0.

S. No.	BiasVoltage V_{a5}(V)	Bias Voltage V_{b5}(V)	R_5(kΩ)	Q_0
1.	0,76	0,75	≈680	2,5
2.	0,80	0,75	≈136	0,5
3.	0,85	0,75	≈68	0,25
4.	0,95	0,75	≈34	0,125

The f_0 is electronically tunable by varying the gate voltage and is verified through simulations as depicted in Fig. 8. Values of f_0, for C_1=C_2 = 50 pF and $R_i \approx 23$ kΩ for i = 1,…3, 5,. . . , 12, along with different gate voltages chosen for varying R_4 are listed in Tab. 4.

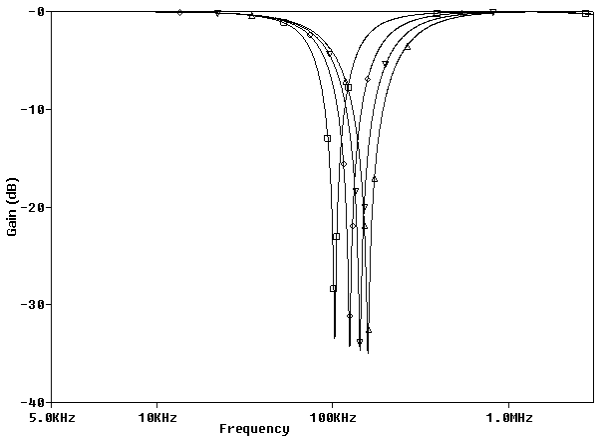

Fig. 8: Notch response for different ω_0 values.

Tab.4: Component values used to make f_0 electronically tunable.

S. No.	BiasVoltage V_{a4}(V)	Bias Voltage V_{b4}(V)	R_4(kΩ)	f_0 (kHz)
1.	1,1	0,9	≈34	113,8
2.	1,2	0,9	≈23	138,4
3.	1,3	0,9	≈17	160,0
4.	1,4	0,9	≈14	179,0

To study the time domain behavior of the BP filter three sinusoidal frequency components, a low frequency signal of 1 kHz, a high frequency component of 100 kHz and the third component is 11,5 kHz which is f_0 of the BP filter, are applied. The transient response of the filter circuit is shown in Fig. 9. It may be noted that the

frequency components other than f_0 are significantly attenuated.

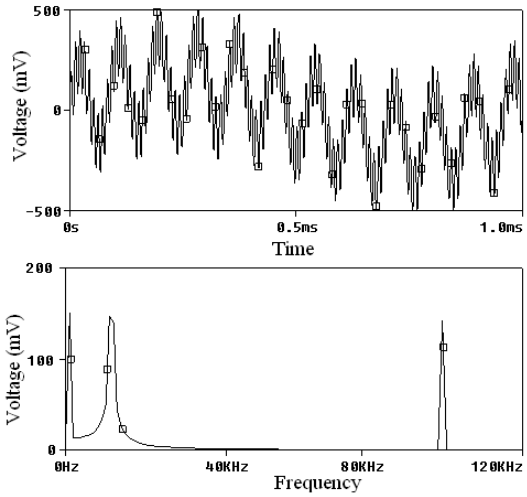

(a)

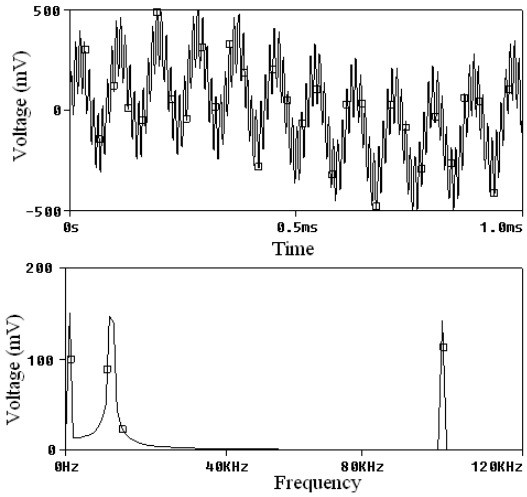

(b)

Fig. 9: Simulated transient response of BP filter. (a) Input signal and its frequency response (b) Output transient response and frequency spectrum.

To check the quality of the output of BP filter, the percentage total harmonic distortion (%THD) with the sinusoidal input signal is obtained as shown in Fig. 10. It is observed that the %THD remains considerably low [23] for input signal values till 70 mV. Simulated power consumption for the proposed universal filter is 4,04 mW.

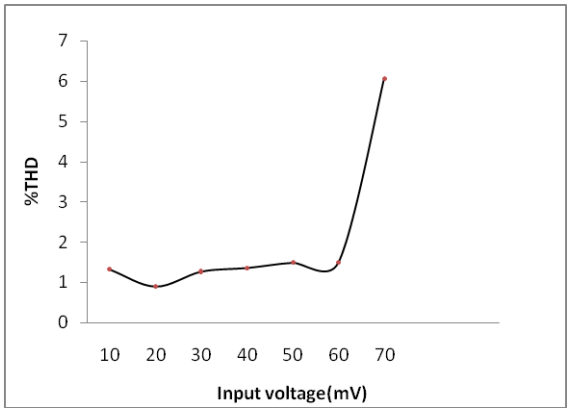

Fig. 10: THD variation with the input signal amplitude.

5. Conclusion

A new voltage-mode OTRA MOS-C universal biquadratic filter is presented which realizes all the standard filter functions simultaneously. The proposed circuit employs five OTRAs, two capacitors and twelve resistors. The filter possesses orthogonal and electronic tunability of filter parameters through MOS implemented resistors. The theoretical proposition is verified using PSPICE simulations.

References

[1] SALAMA, Khaled N. and Ahmed M SOLIMAN. CMOS operational transresistance amplifier for analog signal processing. *Microelectronics Journal*. 1999, vol. 30, iss. 3, pp. 235–245. ISSN 0026-2692. DOI: 10.1016/S0026-2692(98)00112-8.

[2] CHEN, J.-J., H.-W. TSAO and C.-C. CHEN. Operational transresistance amplifier using CMOS technology. *Electronics Letters*. 1992, vol. 28, iss. 22, pp. 2087-2088. ISSN 0013-5194. DOI: 10.1049/el:19921338.

[3] MOSTAFA, H. and A. M. SOLIMAN. A modified CMOS realization of the operational transresistance amplifier. *Frequenz*. 2006, vol. 60, iss. 3-4, pp. 70-77. ISSN 2191 -6349. DOI: 10.1515/FREQ.2006.60.3-4.70.

[4] ABEDELRAHMAN, K. K. and A. M. SOLIMAN. A modified CMOS differential OTRA. *International Journal of Electronics and Communication (AEU)*. 2009, vol. 63, iss. 12, pp. 1067-1071. ISSN 1434-8411. DOI: 10.1016/j.aeue.2008.08.003.

[5] DURUK, A., E. O. GUNES and H. KUNTMAN. A new low voltage CMOS differential OTRA for sub-micron technologies. *International Journal of Electronics and Communications (AEU)*. 2007, vol. 61, iss. 5, pp. 291-299. ISSN 1434-8411. DOI: 10.1016/j.aeue.2006.05.009.

[6] CAM, U., F. KACAR, O. CICEKOGLU, H. KUNTMAN and A. KUNTMAN. Novel grounded parallel immittance simulator topologies employing single OTRA. *International Journal of Electronics and Communications (AEU)*. 2003, vol. 57, iss. 4, pp. 287-290. ISSN 1434-8411. DOI: 10.1078/1434-8411-54100173.

[7] KILINC, S., K. N. SALAMA and U. CAM. Realization of fully Controllable negative Inductance with single operational Transresistance Amplifier. *Circuits Systems Signal Processing*.

2006, vol. 25, iss. 1, pp. 47-57. ISSN 1531-5878. DOI: 10.1007/s00034-004-0706-y.

[8] CAM, U., F. KACAR, O. CICEKOGLU, H. KUNTMAN and A. KUNTMAN. Novel two OTRA-based grounded immittance simulator topologies. *Analog Integrated circuit and Signal Processing*. 2004, vol. 39, no. 2, pp. 169-175. ISSN 0925-1030. DOI: 10.1023/B:ALOG.0000024064.73784.58.

[9] SALAMA, K.N. and A. M. SOLIMAN. Novel oscillators using operational transresistance amplifier. *Microelectronics Journal*. 2000, vol. 31, iss. 1, pp. 39-47. ISSN 0026-2692. DOI: 10.1016/S0026-2692(99)00087-7.

[10] CAM, U. A Novel Single-Resistance-Controlled Sinusoidal Oscillator Employing Single Operational Transresistance Amplifier. *Analog Integrated Circuits and Signal Processing*. 2002, vol. 32, no. 2, pp. 183-186. ISSN 0925-1030. DOI: 10.1023/A:1019586328253.

[11] PANDEY, R., N. PANDEY, M. BOTHRA and S. K. PAUL. Operational Transresistance Amplifier based Multiphase Sinusoidal Oscillator. *Journal of Electrical and Computer Engineering*. 2011, vol. 2011, ID 586853, pp. 1-8. ISSN 2090-0147. DOI: 10.1155/2011/586853.

[12] HOU, C.L., H. C. CHIEN and Y. K. LO. Squarewave generators employing OTRAs. *IEE proceedings.-Circuits Devices Systems*. 2005, vol. 152, no. 6, pp.718-722. ISSN 1350-2409. DOI: 10.1049/ip-cds:20045167.

[13] LO,Y. K., H. C. CHIEN and H. G. CHIU. Switch Controllable OTRA Based Bistable Multivibrator. *IET Circuits Devices Syst*. 2008 vol. 2, no. 4, pp. 373–382. ISSN 1751-8598. DOI: 10.1049/iet-cds:20080011.

[14] GOKCEN, A. and U. CAM. MOS-C single amplifier biquads using the operational transresistance amplifier. *International Journal of Electronics and Communications (AEU)*. 2009, vol. 63, iss. 8, pp. 660-664. ISSN 1434-8411. DOI: 10.1016/j.aeue.2008.05.008.

[15] SALAMA, K. N. and A. M. SOLIMAN. Active RC applications of the Operational Transresistance Amplifier. *Frequenz*. 2000, vol. 54, iss. 7-8, pp. 171-176. ISSN 2191-6349. DOI: 10.1515/FREQ.2000.54.7-8.171.

[16] CAKIR, C., U. CAM, U. and O. CICEKOGLU. Novel allpass filter configuration employing single OTRA. *IEEE Transactions on circuits and systems II: Express Briefs*. 2005, vol. 52, iss. 3, pp. 122-125. ISSN 1549-7747. DOI: 10.1109/TCSII.2004.842055.

[17] KILINC, S. and U. CAM. Cascadable allpass and notch filters employing single operational transresistance amplifier. *Computers and Electrical Engineering*. 2005, vol. 31, iss. 6, pp. 391-401. ISSN 0045-7906. DOI: 10.1016/j.compeleceng.2005.06.001.

[18] CHEN, J.-J., H.-W. TSAO and S.-I. LIU. Voltage -mode MOSFET–C filters using operational transresistance amplifiers (OTRAs) with reduced parasitic capacitance effect. *IEE Proceedings-Circuits Devices Systems*. 2001, vol. 148, iss. 5, pp. 242-249. ISSN 1350-2409. DOI: 10.1049/ip-cds:20010523.

[19] KILINC, S., A. U. KESKIN and U. CAM. Cascadable Voltage-Mode Multifunction Biquad Employing Single OTRA. *Frequenz*. 2007, vol. 61, iss. 3-4, pp.84-86. ISSN 2191-6349. DOI: 10.1515/FREQ.2007.61.3-4.84.

[20] CHANG, C.-M. KO, Y.-J.GUO, Z.-Y.LIN, Y.-T.HOU, C.-L. and HORNG, J.-W. Generation of voltage-mode OTRA-R/MOS-C LP, BP, HP, and BR biquad filter. In: *Proceedings of the 10th WSEAS international conference on Instrumentation, measurement, circuits and systems IMCAS'11*. Wisconsin: World Scientific and Engineering Academy and Society, 2011, pp. 28-34. ISBN 978-960-474-282-0.

[21] CHANG, C.-M. LIN, Y.-T.HSU, C.-K.HOU, C.-L. and HORNG, J.-W. Generation of Voltage-Mode OTRA-Based Multifunction Biquad Filter. In: *Proceedings of the 10th WSEAS international conference on Instrumentation, measurement, circuits and systems IMCAS'11*. Wisconsin: World Scientific and Engineering Academy and Society, 2011, pp. 21-27. ISBN 978-960-474-282-0.

[22] GOKCEN, A., S. KILINC and U. CAM. Fully integrated universal biquads using operational transresistance amplifiers with MOS-C realization. *Turkish Journal of Electrical Engineering and Computer Sciences*. 2011, vol. 19, no. 3, pp. 363-372. ISSN 1300-0632. DOI: 10.3906/elk-1002-416.

[23] ERDOGAN, E. S., R. O. TOPALOGLU, H. KUNTMAN and O. CICEKOGLU. New Current Mode Special Function Continuous - Time Active Filters Employing only OTAs and OPAMPs. *International Journal of Electronics*. 2004, vol. 91, no. 6, pp.345-359. ISSN 0020-7217. DOI: 10.1080/00207214041000169523 7.

About Authors

Rajeshwari PANDEY did B.Tech. (Electronics and Telecommunication) from University of Allahabad in 1988 and received her M.E (Electronics and Control) from BITS, Pilani, Rajasthan, India in 1992. Currently, she is Associate Professor in Department of Electronics and Communication Engineering, Delhi Technological University, Delhi. Her research interests include Analog Integrated Circuits, and Microelectronics.

Neeta PANDEY did M. E. in Microelectronics from Birla Institute of Technology and Sciences, Pilani, Rajasthan, India and Ph.D. from Guru Gobind Singh Indraprastha University Delhi, India. At present she is Associate Professor in Department of Electronics and Communication Engineering, Delhi Technological University, Delhi. A life member of ISTE, and member of IEEE, USA, she has published papers in International, National Journals of repute and conferences. Her research interests are in Analog and Digital VLSI Design.

Sajal Kumar PAUL did B.Tech., M.Tech., and Ph.D. in Radio Physics and Electronics from the Institute of Radio Physics and Electronics, University of Calcutta. He has served Webel Telecommunication Industries, Kolkata; Indira Gandhi National Open University (IGNOU), Kolkata; Advanced Training Institute for Electronics &Process Instrumentation (ATI-EPI), Hyderabad; North Eastern Regional Institute of Science & Technology (NERIST), Nirjuli and Delhi College of Engineering (DCE), Delhi in various capacities. He has served the Department of Electronics Engineering, Indian School of Mines, Dhanbad as Head of the Department and at present professor of the same department. His research interest includes Microelectronic Devices, Electronic Properties of Semiconductor and Bipolar and MOS Analog Integrated Circuits. He has more than 60 research publications in International and National journals of repute and conferences.

Ajay SINGH completed B. E. degree in June 2012 from Delhi Technological University, Delhi, India. His main research Interests include the field of analog circuit design and Signal processing. He has published few papers in National and International conferences/

journals.

Balamurali SRIRAM completed B. E. degree in June 2012,from Delhi Technological University, Delhi, India. His research interests include mixed signal circuit design and analog signal processing. Has also co-authored a journal and conference papers.

Kaushalendra TRIVEDI completed B. E. degree in June 2012 from Delhi Technological University, Delhi, India. His research interests include mixed signal circuit design and signal processing. Has also co-authored a journal and conference papers in current mode circuits.